Optimal Usage of Multiple Energy Carriers in Residential Systems

Unit Scheduling and Power Control

Laura M. Ramírez Elizondo

Optimal Usage of Multiple Energy Carriers in Residential Systems

Unit Scheduling and Power Control

Proefschrift

ter verkrijging van de graad van doctor
aan de Technische Universiteit Delft,
op gezag van de Rector Magnificus Prof.ir. K.C.A.M. Luyben,
voorzitter van het College voor Promoties,
in het openbaar te verdedigen op dinsdag 26 maart, 2013 om 15:00 uur
door

Laura María RAMÍREZ ELIZONDO,
elektrotechnisch ingenieur,
geboren te San José, Costa Rica.

Dit proefschrift is goedgekeurd door de promotor:
Prof.ir. L. van der Sluis

Samenstelling promotiecommissie:

Rector Magnificus	Voorzitter
Prof.ir. L. van der Sluis	Technische Universiteit Delft, promotor
Prof.dr. F. Munteanu	Gheorghe Asachi Technical University of Iaşi
Prof.dr. C.M. Franck	ETH Zürich
Prof.dr.ir. B.J. Boersma	Technische Universiteit Delft
Prof.dr. C. Witteveen	Technische Universiteit Delft
Prof.ir. P.G. Luscuere	Technische Universiteit Delft
Dr.dr.h.c.ir. G.C. Paap	Technische Universiteit Delft, heeft als begeleider in belangrijke mate aan de totstandkoming van het proefschrift bijgedragen.

Dit onderzoek werd uitgevoerd in het kader van het onderzoekprogramma “Innovatiegerichte Onderzoekprogamma’s - Elektromagnetische Vermogenstechniek” (IOP-EMVT), dat financieel wordt ondersteund door SenterNovem, een agentschap van het Nederlandse Ministerie van Economische Zaken.

Published and distributed by: Laura M. Ramírez Elizondo
E-mail: laura.ramirezelizondo@gmail.com

ISBN 978-94-6203-295-8

Cover design: Carolina Ramírez Elizondo
All illustrations included in this thesis: Oscar Calderón

Printed by Wöhrmann Print Service B.V., Zutphen, the Netherlands.

To José, Mami, Papi, Tita, Carolina and Eduardo, who I deeply love.

Summary

The world's increasing energy demand and growing environmental concerns have motivated scientists to develop new technologies and methods to make better use of the remaining resources of our planet. The main objective of this dissertation is to develop a scheduling and control tool at the district level for small-scale systems with multiple energy carriers and to apply exergy-related concepts for the optimization of these systems. The tool is based on the *energy hub approach* and provides insights and techniques that can be used to evaluate new district energy scenarios. The topics that are presented include the *multi-carrier unit commitment framework*, the *multi-carrier exergy hub approach*, a *hierarchical multi-carrier control architecture*, a comparison of *multi-carrier power applications* and the implementation of a *multi-carrier energy management system* in a real infrastructure.

The dissertation consists of seven chapters. Chapter 1 includes the project framework, motivation, problem definition and research questions. Chapter 2 describes the model behind the scheduling tool that was developed for this PhD project, which is used to optimize systems containing multiple energy carriers. Later in Chapter 3 the optimization tool is adapted to include exergetic efficiency as assessment parameter of such systems. Chapter 4 presents the control architecture that was designed to cope with the dynamic behaviour of the systems under study. In Chapter 5 the optimization tool is used to analyze the impact of different emerging trends in district-level power systems, such as the active participation of micro-CHP technologies, the incorporation of renewable sources and the application of the *virtual power plant* concept. Chapter 6 provides insights regarding the implementation of the optimization and control tool in real systems. Finally, Chapter 7 presents the conclusions and recommendations of this dissertation.

The main contributions of this dissertation are listed below:

- A general *multi-carrier unit commitment* framework for energy systems that contain multiple energy carriers was developed. The framework can be used with any kind of energy carrier and for different possible couplings and power scales (Chapter 2).
- A technique to include storage was developed and implemented as part of the optimization tool. The results show that this technique can be valuable for peak-shaving purposes at the generation side (Chapter 2).
- The *exergy hub approach* was introduced. The exergy hub provides a visual indication of the exergetic efficiency of the units. In Section 3.4 both the energy hub and the exergy hub are depicted next to each other in order to reveal that a unit that is considered to be very efficient from an energy point of view can be considered to be very inefficient from an exergy perspective.

- A comparison between the results for the optimal dispatch obtained from an exergetic efficiency optimization and from an energetic efficiency optimization is performed for the first time for multiple energy carriers (Chapter 3).
- The results of the scheduling optimization tool are compared to identify which configuration gives the best energy and exergy performances for specific loads. A sensitivity analysis is performed in which the ratio between heat and electricity consumption is varied to observe the influence of the type of load in the scheduling (Chapter 3).
- A two-level control strategy was designed for the application in systems with multiple energy carriers. Most of the control strategies found in the literature only focus on electricity flows, thus the strategy proposed is valuable for multi-carrier systems (Chapter 4).
- The optimization tool was extended in order to study the benefits of having an *aggregator* in charge of the optimization (Chapter 5).
- A comparison among three micro-CHP technologies was presented to show that different benefits can be obtained by using combined heat and power technologies with different electricity-to-heat efficiency ratios (Chapter 5).
- An example was presented in which the influence of incorporating electric vehicles at a neighbourhood was analyzed (Chapter 5).
- Several practical considerations were presented regarding the implementation of the tool in real systems. A partial implementation in the renewable energy laboratory DENlab was performed, which provides an added value to the theoretical results that were accomplished in this dissertation (Chapter 6).

Laura M. Ramírez Elizondo

Samenvatting

De toenemende wereldwijde vraag naar energie en de groeiende zorg voor het milieu hebben wetenschappers gemotiveerd om nieuwe technologieën en methoden te ontwikkelen om beter gebruik te maken van de resterende grondstoffen van onze planeet. Dit proefschrift vloeit voort uit deze bezorgdheid. De belangrijkste doelstelling van dit proefschrift is het ontwikkelen van een planningsprogramma gebruikmakend van de energy-hub-aanpak voor kleinschalige, (woon)wijkniveau-systemen bestaand uit meerdere energiedragers en het evalueren van het gebruik van een exergie-analyse als assessmentinstrument voor dergelijke systemen. Het proefschrift biedt inzichten en reikt technieken aan die kunnen worden toegepast bij het optimaliseren van systemen met meerdere energiedragers. De gepresenteerde onderwerpen zijn: een raamwerk voor *multi-carrier unit commitment*, de *multi-carrier exergy-hub-aanpak*, een hirarchische *multi-carrier besturingsarchitectuur*, een vergelijking van *multi-carrier toepassingen* en de implementatie van een *multi-carrier energy management system* in bestaande infrastructuur.

Dit proefschrift bestaat uit zeven hoofdstukken. Hoofdstuk 1 omvat het projectkader, de motivatie, de probleemstelling en onderzoeksvragen. Hoofdstuk 2 beschrijft het model achter het planningsprogramma dat is ontwikkeld gedurende dit promotieonderzoek. Dit programma wordt gebruikt voor de optimalisatie van systemen bestaand uit meerdere energiedragers. Een uitbreiding die de exergetische efficiëntie als regelparameter opneemt in de optimalisatieprogramma wordt in hoofdstuk 3 uitgewerkt. Hoofdstuk 4 presenteert de regelarchitectuur die ontworpen is om om te gaan met het dynamische gedrag van de bestudeerde systemen. In hoofdstuk 5 wordt het ontwikkelde optimalisatieprogramma gebruikt om de invloeden van verschillende opkomende trends in wijkniveau-energiesystemen te analyseren. Voorbeelden hiervan zijn de actieve participatie van micro-WKK-technologieën, de integratie van hernieuwbare energiebronnen en de toepassing van het *virtual power plant*-concept. In hoofdstuk 6 wordt vervolgens ingegaan op de verworven inzichten met betrekking tot de implementatie van het optimalisatieprogramma en het regelprogramma gebaseerd op de regelarchitectuur. Tot slot worden er in hoofdstuk 7 de conclusies en aanbevelingen van dit proefschrift gepresenteerd.

De belangrijkste bijdragen van dit proefschrift zijn:

- De ontwikkeling van een algemeen *multi-carrier unit commitment* kader voor energiesystemen bestaand uit meerdere energiedragers. Dit kader kan worden toegepast bij ieder type energiedrager en voor verschillende koppelingsmogelijkheden en vermogens schalen (hoofdstuk 2).

- Een techniek om opslag mee te nemen is ontwikkeld en geïmplementeerd als onderdeel van het optimalisatieprogramma. De resultaten tonen aan dat deze techniek waardevol is voor het afvlakken van pieken aan de generatie kant (hoofdstuk 2).
- De introductie van de exergy-hub-aanpak. De exergy-hub geeft een visuele indicatie van het exergetisch rendement van de eenheden. In hoofdstuk 3 worden zowel de energy-hub als de exergy-hub naast elkaar afgebeeld om aan te geven dat een eenheid die wordt beschouwd als zeer efficiënt vanuit energetisch oogpunt kan worden beschouwd als zeer inefficiënt uit exergieperspectief (hoofdstuk 3).
- Een vergelijking van de resultaten voor de optimale inzet verkregen uit een exergetisch - rendement - optimalisatie en van een energetisch - rendement - optimalisatie. In de literatuur is een dergelijke vergelijking niet eerder uitgevoerd binnen de context van energievoorzieningssystemen met meerdere energiedragers (hoofdstuk 3).
- De resultaten van het optimalisatieprogramma worden vergeleken om te bepalen welke configuratie de beste energie- en exergieprestaties geeft bij specifieke belastingen. Een gevoeligheidsanalyse wordt toegepast waarin de verhouding tussen warmte en elektriciteit wordt gevarieerd om te observeren hoe het type belasting de planning beïnvloedt (hoofdstuk 3).
- Een gecascadeerde regelstrategie is ontworpen voor toepassing in systemen met meerdere energiedragers. De meeste regelstrategieën in de literatuur zijn alleen gericht op elektriciteitsstromen, dus de voorgestelde strategie is waardevol voor multi- dragersystemen (hoofdstuk 4).
- Verscheidene opkomende trends zijn gesimuleerd om inzicht te krijgen in hun gevolgen voor energievoorzieningssystemen op woonwijkniveau. Het optimalisatieprogramma werd uitgebreid om de voordelen van een *aggregator* die verantwoordelijk is voor de optimalisatie te bestuderen (hoofdstuk 5).
- Een vergelijking van drie micro-WKK-technologieën is gemaakt om aan te tonen dat verschillende voordelen kunnen worden verkregen door gebruik te maken van warmtekrachtkoppelingstechnologieën met verschillende elektriciteit-warmteverhoudingen (hoofdstuk 5).
- Een voorbeeld waarin de gevolgen van elektrische voertuigen op het systeem op wijkniveau werd geanalyseerd (hoofdstuk 5).
- Verscheidene praktische overwegingen met betrekking tot de implementatie van het programma in echte systemen. De gedeeltelijke implementatie in het duurzame energie lab DENlab voorziet in toegevoegde (praktische) waarden aan de theoretische resultaten die werden bereikt in dit proefschrift (hoofdstuk 6).

Laura M. Ramírez Elizondo

Contents

List of Tables

List of Figures

Nomenclature

Acronyms

AC	alternating current
ACE	area control error
AFR	air-to-fuel ratio
AIMMS	Advanced Interactive Multidimensional Modeling System
BTU	British Thermal Units
CHP	combined heat and power
CO_2	carbon dioxide
DC	direct current
DEMS	district energy management systems
DENlab	renewable energy laboratory at Delft University of Technology
DHC	district heating and cooling
ECN	Energy Research Centre of the Netherlands
EMS	energy management system
EMVT	electro-magnetic power technology
ETH	Eidgenössische Technische Hochschule Zürich
HEMS	home energy management systems
HHV	higher heating value
HMI	human-machine interface
ICT	information and communication technology
IEA	International Energy Agency
IEEE	Institute of Electrical and Electronics Engineers

IOP	innovation-oriented research programs
IPCC	Intergovernmental Panel on Climate Change
LHV	lower heating value
MSc	master of science
p.u.	per unit
PhD	doctor of philosophy
PID	proportional integral derivative
PLC	programmable logic controller
PQ	active power - reactive power
PV	photovoltaic
SCADA	supervisory control and data adquisition
SEPATH	Simulatie van Energievraag Patronen van Huishoudens
sms	short message service
US	United States of America
VoFEN	Vision of Future Energy Networks
VPP	virtual power plant
WADE	World Alliance for Decentralized Energy

Functions

$\mathscr{F}_{\beta_j}^{k_p}(P_{\alpha_i})$	function decribing the conversion from carrier α_i to carrier β_j
$\mathscr{F}_{\mathrm{obj}}$	objective function

Sets and Subsets

$\mathcal{C}_{\alpha_i} = \{A, B, \ldots\}$ set of converter elements inside the energy/exergy hub

$\mathcal{E}_{\mathrm{in}} = \{\mathrm{e}, \mathrm{g}, \mathrm{q}, \ldots\}$ set of carriers at the input side of the energy/exergy hub

$\mathcal{E}_{\mathrm{out}} = \{\mathrm{e}, \mathrm{g}, \mathrm{q}, \ldots\}$ set of carriers at the output side of the energy/exergy hub

Subscripts

0	reference state/ initial state
e	electricity
g	natural gas

q	heat
act	actual
afr	air fuel ratio
air	air
amb	ambient
col	cold
des	desired
dif	difference
ele	electrical
exc	exchange
exh	exhaust
exp	export
flu	flue gases
fue	fuel
fur	furnace
gen	generation
grd	public electricity grid
hex	heat exchanger
hhd	household
hot	hot
hub	individual hub
imp	import
in	in/inside
max	maximum
mec	mechanical
min	minimum
out	out/outside/output
pip	pipeline

rad	radiator	
rec	recuperator	
ref	reference	
ren	renewable sources	
rof	roof	
rot	rotor/rotational	
rtd	rated	
sch	scheduled	
sur	surroundings	
swh	service water heating	
tnk	storage tank	
tot	total	
tur	turbine	
veh	electrical vehicles	
wal	wall	
wat	water	
wdw	window	
wnd	wind	

Variables and Constants Introduced in Chapter 1

λ_j	power-frequency characteristic of control area j	[MW/Hz]
f	frequency	[Hz]
P_i	active power of generator i	[MW]
P_j	active power export of control area j	[MW]

Variables and Constants Introduced in Chapter 2

$\overline{P}_{\alpha_i}$	upper power limit at the energy hub's input	[kW]
$\overline{P}_{\alpha_i}^{k_p}$	upper power limit at the input of converter k_p	[kW]
$\underline{P}_{\alpha_i}$	lower power limit at the energy hub's input	[kW]
$\underline{P}_{\alpha_i}^{k_p}$	lower power limit at the input of converter k_p	[kW]

F_{cost}	least total cost to arrive at a state	[€/(time period)]
F_{prod}	production costs	[€/(time period)]
F_{tran}	transition cost	[€/(time period)]
I_{dp}	combination of commited units	[-]
J_{dp}	combination of commited units	[-]
N_{dp}	number of strategies that are saved at each period	[-]
t	time	[s]
T_{dp}	time interval for the forward dynamic programming algorithm	[-]
X_{dp}	number of states that are evaluated within each period	[-]
$\dot{E}_{\alpha_i}$	energy change per time period	[kW]
K_{1,α_i}	cost coefficient associated with input carrier α_i	[€/(time period)]
K_{2,α_i}	cost coefficient associated with input carrier α_i	[€/(time period · kW)]
K_{3,α_i}	cost coefficient associated with input carrier α_i	[€/(time period · kW^2)]
$\mathrm{K}_{4,\alpha_i}^{k_p}$	cost coefficient of coverter k_p associated with input carrier α_i	[€/(time period)]
$\widetilde{L}_{\beta_j}$	active power carried by β_j out of the hub's internal cluster	[kW]
$\widetilde{P}_{\alpha_i}$	active power carried by α_i to the hub's internal cluster	[kW]
D_{α_i}	power that flows to a storage element located at the hub's input side	[kW]
$e_{\alpha_i}^{+}$	charge/stand-by storage efficiency	[-]
$e_{\alpha_i}^{-}$	discharge storage efficiency	[-]
e_{α_i}	charge/discharge storage efficiency	[-]
$M_{\beta_j}^{\text{eq}}$	equivalent storage element of the equivalent storage vector	[kW]
M_{β_j}	power that flows to a storage element located at the hub's output side	[kW]
$w_{\alpha_i}^{k_p}$	status variable of converter k_p	[-]
w_{α_i}	status variable of all converter associated with carrier α_i	[-]
$E_{\alpha_i}^{\text{stb}}$	stand-by energy losses per time period	[kW·(time period)]
α_i	energy/exergy carrier at the hub's input	[-]
β_j	energy/exergy carrier at the hub's output	[-]
$\eta_{\alpha_i\beta_j}^{k_p}$	energy conversion efficiency from carrier α_i to carrier β_j of converter k_p	[-]

$c_{\alpha_i\beta_j}$	coupling factor	[-]
k_p	converter inside the energy/exergy hub	[-]
L_{β_j}	active power carried by β_j out of the energy hub	[kW]
$L_{\beta_j}^{k_p}$	active power carried by β_j out of converter k_p	[kW]
$P_{\alpha_i}^{k_p}$	active power carried by α_i to converter k_p	[kW]
P_{α_i}	active power carried by α_i to the energy hub's input	[kW]
$\nu_{\alpha_i}^{k_p}$	dispatch factor of carrier α_i at converter k_p	[-]

Variables and Constants Introduced in Chapter 3

$\overline{\Xi}_{\alpha_i}$	upper limit at the exergy hub's input	[kW]
$\overline{\Xi}_{\alpha_i}^{k_p}$	upper limit at the input of converter k_p	[kW]
$\underline{\Xi}_{\alpha_i}$	lower limit at the exergy hub's input	[kW]
$\underline{\Xi}_{\alpha_i}^{k_p}$	lower limit at the input of converter k_p	[kW]
μ_{che}	chemical potential	[J/mole]
n_{che}	quantity of moles per unit mass	[mole/kg]
v	velocity	[m/s]
w	work per kg	[J/kg]
ϕ_{m}	mass flow	[kg/s]
$\varepsilon_{\alpha_i\beta_j}^{k_p}$	exergy conversion efficiency from carrier α_i to carrier β_j of converter k_p	[-]
ε	exergetic efficiency	[-]
η	energetic efficiency	[-]
ζ_{α_i}	exergy factor of carrier α_i	[-]
$\Upsilon_{\mathrm{LHV},\alpha_i}$	lower heating value of carrier α_i	[kJ/kg]
Γ_{β_j}	exergy flow carried by β_j to the hub's output	[kW]
Γ_{out}	sum of exergy flow used by the loads at the hub's output	[kW]
L_{out}	sum of power used by the loads at the hub's output	[kW]
Ξ_{α_i}	exergy flow carried by α_i to the hub's input	[kW]
Ξ_{inp}	sum of exergy flow brought to the system by the input fuels	[kW]
P_{inp}	sum of power brought to the system by the input fuels	[kW]

a	specific exergy	[J/kg]
$b_{\alpha_i\beta_j}$	coupling factor	[-]
g	gravity	[m/s^2]
h	specific enthalpy	[J/kg]
m	mass	[kg]
p	pressure	[Pa]
Q	heat	[J]
S	entropy	[J/(K)]
s	specific entropy	[J/(K·kg)]
T	temperature	[K]
u	specific internal energy	[J/kg]
v	specific volume	[m^3/kg]
z	height	[m]

Variables and Constants Introduced in Chapter 4

ϵ_{fur}	furnace parameter that is based on experimental data	[-]
κ	thermal conductivity	[W/(m·K)]
ρ	density	[kg/m^3]
$\mathrm{\tau}$	time constant	[s]
ξ_{fur}	factor representing the losses of the furnace	[-]
$p^{k_p}_{\mathrm{f},\beta_j}$	participation factor	[-]
λ	tip speed ratio	[-]
ω	rotational speed	[rad/s]
θ	pitch angle	[-]
ι_{fur}	factor related to the excess air in the furnace	[-]
Φ_{q}	heat flow	[W]
τ	torque	[N·m]
A	area	[m^2]
c_{p}	performance coefficient	[-]

c	specific heat capacity	[J/(K· kg)]
d	thickness	[m]
E	energy	[J]
J	moment of inertia	[kg·m^2]
r_{aft}	stoichiometric air fuel ratio	[-]
U	heat transfer coefficient	[W/(m^2· K)]
V	volume	[m^3]
C	constant related to the performance coefficient of the wind turbine	[-]

Variables and Constants Introduced in Chapter 5

h_d	households	[-]

Variables and Constants Introduced in Chapter 6

σ_t^2	conditional variance of ϱ_t	[-]
ϱ_t	innovations or residuals of the time series	[m/s]
ς_t	standardized residuals	[-]

Vectors and Matrices Introduced in Chapter 2

$\mathbf{M^{eq}}$	equivalent storage vector
$\dot{\mathbf{E}}$	vector containing the energy change during one time period
$\mathbf{S}$	storage coupling matrix
$\mathbf{D}$	vector containing the power that flows to storage elements located at the hub's input side
$\mathbf{M}$	vector containing the power that flows to storage elements located at the hub's output side
$\widetilde{\mathbf{L}}$	output power vector of the hub's internal cluster
$\widetilde{\mathbf{P}}$	input power vector of the hub's internal cluster
$\mathbf{C}$	energy hub's coupling matrix
$\mathbf{L}$	energy hub's output power vector
$\mathbf{P}$	energy hub's input power vector

Vectors and Matrices Introduced in Chapter 3

$\mathbf{\Gamma}$	exergy hub's output vector
$\mathbf{\Xi}$	exergy hub's input vector
$\mathbf{B}$	exergy hub's coupling matrix

Acknowledgements

First of all, I would like to thank my daily supervisor Dr.dr.h.c.ir. Bob Paap for inviting me to work on his project and for all the enriching conversations we have had over the past years. Bob retired two years ago and for that reason he was not allowed to be my co-promotor, however his involvement in this project continued during all this time and for this I am deeply grateful. I would also like to thank his wife, Rietje Paap for making me feel welcome at their home each time I visited Bob to discuss the results of my simulations, particularly during the final year of my PhD. It was a great pleasure to have Bob as my supervisor and I am sure that we will continue to have only pleasant meetings in the future. I, of course, still look forward to seeing his sailing boat one day!

Secondly, I would like to thank my promotor Prof.ir Lou van der Sluis for his good advice and for introducing me to his network of colleagues. As a result of his contacts, I am currently conducting a research project in which the results of my PhD project are realized in practice. In addition, I am currently drawing up some very interesting research proposals with colleagues from other disciplines. I sincerely appreciate his continued support.

This PhD project was financed by SenterNovem. I would like to thank the members of the IOP-EMVT program for all the interesting discussions that we had during our periodical meetings. I would like to thank Prof.ir. M. Antal and Ir. G.W. Boltje for their involvement at these gatherings. I would also like to thank Ir. Hans Buitenhuis, director of DWA, for his input during the project.

During my PhD I had the opportunity to complete an internship at ABB Corporate Research in Västerås, Sweden. I would like to thank Dr. Muhamad Reza and Dr. Georgios Demetriades for giving me the opportunity to spend three months conducting research in their group. This was a very valuable experience from a research point of view, but it also gave me the chance to meet interesting people that I continue to keep in touch with today.

Due to the interdisciplinary nature of my topic I have had the opportunity to collaborate with colleagues from other fields. I have been able to co-author publications with a few colleagues and with others, draw up proposals that we look forward to working on in the near future. I want to thank Ir. Alicja Lojowska, Ir. Sabine Jansen, Dr. Rudy Negenborn, Dr.ir. Richard Toonssen, Ballard Asare-Bediako, MSc., Dr. Matthijs Spaan and Dr. Stefan Witwicki for the joint-collaborations and Dr. Mathijs de Weerdt and Dr. Matthijs Spaan for the collaborations to come. I would also like to thank Dr. Martin Geidl for the valuable contact that we had at the beginning of my PhD and Dr.ir. Madeleine Gibescu for introducing me to the software AIMMS by means of an illustrative example. I also want to thank Dr.ir. Michiel Houwing, Dr. Kas Hemmes, Dr. Poppong Sakulpipatsin, Ir. Theo Woudstra and Dr.ir. Nico Woudstra for the valuable conversations we had about this research topic.

I would like to thank Croon Elektrotechniek, especially Ir. IJsbrand Ponsioen for giving me the opportunity to conduct research on one of their current projects. It has been very enriching to work with the entire Zero-Watt team.

It has been a great pleasure for me to work at the Power Systems Group at the Delft University of Technology. I want to thank my colleagues for all the memorable moments we shared during lunch time and during the coffee breaks. Special thanks to Alicja Lojowska for the joint-collaborations and for being such a great officemate and Ana Ciupuliga for the interesting conversations on nutrition, yoga and music :). During my PhD I supervised several MSc students. Some of them worked on topics related to this thesis and others did not, but they all contributed to my development as research supervisor. Thanks Eva Usó, Victor Vélez, Remco Ammerlaan, Bernardo Valladares, Pradeep Jayakumar, Hugo Cruz and Naoual Oukira. I want to especially thank Remco and Victor for their participation in the papers we published and Bernardo for his work at DENlab.

I would like to thank my colleagues at the Amsterdam University of Applied Sciences for making me feel welcome from the beginning. I am very grateful that I have had the opportunity to be able to combine teaching and research and I would like to especially thank the education manager Jorien Schreuder, Cleantech's project manager Katrien de Witte, and the two *Lectoren* of Cleantech, Dr. ir. Robert van den Hoed and Ir. Inge Oskam for allowing me to change a few working hours in order to finalize the details of my PhD. I would also like to thank my colleagues at the School of Electrical Engineering of the Universidad de Costa Rica, especially Prof.dr. Jorge Romero, its Director, for supporting me with my studies abroad and for the collaborations to come.

There are two very important colleagues that I would like to thank: Dr.ir. Barry Rawn and Dr.ir. Dhiradj Djairam. We started a "Journal Club", consisting of periodical meetings to generate new research ideas and support the publication of journal entries and papers. Their support and interest encouraged me to choose them as my *paranimfs*. Thank you Barry and Dhiradj for accepting! I am grateful for all your support.

In order to keep things in perspective during a PhD, it is important to continue to do the things one loves. A very important activity that I was able to continue to do the entire duration of my PhD was to teach piano. I would like to deeply thank Marleen and Pieter van Rijckevorsel, Anne and Tim van Wingerde, María Sofía Clercx Lao, their parents and family for not only giving me the opportunity to teach them to play the piano but also the opportunity to enjoy making wonderful music with them. Being able to witness their significant progress has given me energy and inspiration during all this time. I am very thankful for all the special moments that we have shared during our periodic concerts. You really fill my heart with joy.

I would not have been able to teach piano if it was not for my piano teacher Prof. Flora Isabel Elizondo, who accepted me as her undergraduate piano student whilst I was completing my bachelor's degree in engineering. Completing a bachelor's degree in music, was a very important achievement in my life. Attending her nice and motivating lessons was always a favourite activity for me. I want to thank her for her support and encouragement in my decision to come to the Netherlands and for having travelled from Costa Rica to be able to attend my PhD defense. I would like to give very special thanks to Prof. Emilio Alpízar (electrical engineering professor at my home university), who motivated me to start a PhD abroad and who also supported me on my decision to follow both engineering and music.

Surrounding yourself with nice people fills you with energy and brings so much pleasure. For this reason I would like to thank all the friends that I have met here, for their continued support and appreciation. I want to deeply thank Milena Markova, Johan Wolmarans, Taryn Bonnette, Marco Álvarez, Mónica Morales, Marcelo Ackermann, Neslihan Parmaksizoğlu, Adolfo Chaves, Marcelo Gutiérrez, Jodi Kooijman, Coralie Selin, Antoine Ripol, Ana Lao, Luud Clercx, Barry Lennon, Natalie Kretzschmar, Julian Schmied, Mustafa Ibrahim, Alon Yehezkely, Shelly Nevo, Miriam ter Brake and Marieke Nekeman for all the dinners/concerts/coffee breaks/movies/activities and all the time that we have spent together. You all have a very important place in my heart. I would also like to thank all my good friends who live in Costa Rica, with whom I meet every year when I go home to visit. It is wonderful to be able to maintain our friendship even though there is such a great distance between us. Even though I do not have a list with their names on here, they know who they are :) I look forward to seeing you all in December to celebrate the completion of my PhD! Finally, I want to thank my friends Taryn Bonnette, Barry Lennon, Barry Rawn and Stefan Witwicki for helping me with last-minute revisions as well as Jodi Kooijman and Arjen van der Meer for assisting me with the Dutch translations. Furthermore, I want to deeply thank Oscar Calderón for the amazing illustrations he contributed to my thesis.

A loving family is one of the most valuable treasures a person can have. I cannot describe how much I love and cherish my family. My Mom and Dad have been my greatest inspiration. I have always looked up to their perseverance and multiple talents. They gave my brother, my sister and me the best opportunities possible to develop our abilities and they always encouraged us to follow our passions. I love them from the bottom of my heart! My brother Eduardo and sister Carolina are wonderful! Their creativity is something I really admire, my brother creates meaningful and fun videogames and my sister wonderful paintings, besides working as industrial engineer. I am proud of them for their unique talents and for the goodness in their hearts. Pi and Ami, you are awesome! I want to thank my Mom for the beautiful dress she made for my defense and my sister for the great painting she made for the cover of this thesis and that she designed based on the *energy hub* representation. Thanks to the rest of my family, including my dearly beloved grandparents Lucila (Tita), Dulia† and Jorge† and my family in law for their constant support, their constant thoughts and for the special moments we always share every time we go to Costa Rica.

And finally José. My true soulmate. Thank you for the unconditional love and support that you have given me during all these years. You supported me from the very beginning with the idea of coming to the Netherlands and starting an MSc, the idea to continue and complete a PhD, followed by the idea of pursuing my love for yoga in completing a teacher training :) It is awesome to have found someone with whom I can feel free to do the things I love and be supported whilst doing them. It is wonderful to share time with a person with whom life is so full of love and enjoyment and to live with someone who every single day puts a smile on my face ♡.

Laura M. Ramírez Elizondo
Delft, March 2013.

Chapter 1

The Project

Introduction

The world's increasing energy demand and growing environmental concerns have motivated scientists to develop new technologies and methods to make better use of the remaining resources of our planet. This dissertation emerges in response to these concerns as it investigates different scenarios in which the implementation of a scheduling and control tool for the optimization of small-scale systems with multiple energy carriers at district level proves to be beneficial. Furthermore, it analyzes the application of exergy-related concepts for the optimization of such systems.

This first chapter describes the research framework and serves as theoretical background for the other chapters. The chapter is organized in the following way. Section 1.1 introduces the research program under which the project was performed. In Section 1.2 some of the main aspects that have motivated the study and implementation of decentralized generation are discussed. Section 1.3 describes the evolution of power systems due to the integration of cogeneration and renewable energy sources. Section 1.4 presents the problem definition of this thesis. In Section 1.5, the objectives and research questions are formulated. Finally Section 1.6 contains the outline of this dissertation and a summary of the main contributions. Parts of this chapter have been published in [1–3].

1.1 Project Framework

This PhD project was performed within the "Intelligent Power Systems" research framework of the IOP-EMVT program "Innovation-Oriented Research Programs - Electro - Magnetic Power Technology", financed by SenterNovem, a former agency of the Dutch Ministry of Economic Affairs. The project "Intelligent Power Systems" was initiated by the Electrical Power Systems Group and the Electrical Power Processing Group of Delft University of Technology and by the Electrical Energy Systems Group and the Control Systems Group of Eindhoven University of Technology. The project focuses on the effects caused by the introduction of distributed (renewable) generators on existing power systems. A large implementation of decentralized technologies leads to *horizontally-operated power systems* consisting of a large number of small to medium-sized distributed generators [4].

The project “Intelligent Power Systems” consists of 4 parts, in which more than 10 PhD students were involved. Figure 1.1 shows a schematic representation of the research project. Each part is briefly described below:

- **Inherently Stable Transmission Systems** In this part, the influence of uncontrolled decentralized generation on the stability and dynamic behavior of the transmission network is investigated. The topics of research include the control of decentralized and centralized power plants and the application of power electronics and monitoring systems to allow their control.

- **Manageable Distribution Networks** This part focuses on how to use power electronic interfaces to support the electrical grid and on how to make the distribution network more *active*. Moreover, the stability of the distribution network and the effect of the stochastic behavior of certain decentralized generators on the voltage level is studied.

- **Self-Controlling Autonomous Networks** This part of the project is focused on the development of control techniques to operate autonomous networks in an optimal and secure way. The local networks studied are operated autonomously, but they can remain connected to the electrical grid for security reasons.

- **Optimal Power Quality** The goal of this part is to provide elements for discussion between the polluter and the electrical grid operator, who has to apply measures in order to comply with the standards and electrical grid codes.

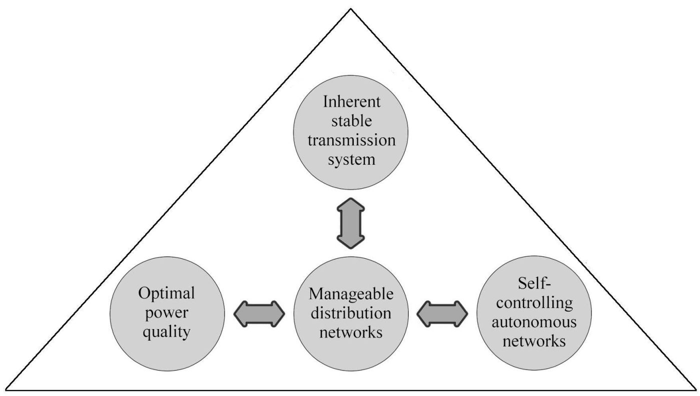

Figure 1.1: Four parts of the “Intelligent Power Systems” research project

This dissertation falls under the topic “Self-Controlling Autonomous Networks”. The title of the PhD project under which this dissertation was performed is “Intelligent Energy Supply at Household and District Level”. The project is divided into two parts: the part that focuses on the *household level* is being performed at the Electrical Energy Systems Group of Eindhoven University of Technology, while the part that focuses on the *district level* was performed at the Electrical Power Systems Group of Delft University of Technology. This dissertation corresponds to the second part of the project, entitled “Intelligent Energy Supply at District Level”.

1.2 Motivations to Integrate Decentralized and Renewable Generation

Due to the economic and industrial development that took place during the twentieth century, the need for electricity has become crucial in our society. Nowadays, the availability of electricity has a strong influence in the way we live, not only in aspects related to the way we accomplish our tasks, but also in aspects related to the way we interact and communicate with others. It is for this reason that scientists are strongly encouraged to look for ways to provide a long-term energy supply.

The interest in decentralized energy systems with high penetration of combined heat and power technologies (CHP) and renewable sources has increased during the last years. Decentralized generation systems are systems in which the electricity production occurs at or near the point of use, irrespective of the size or technology [5]. They can be connected to the electrical grid (on-grid) or they can operate autonomously with no connection to the grid (off-grid).

The energy sector is facing unprecedented challenges in relation to the world's energy supply. The International Energy Agency (IEA) estimates that between 2009 and 2035 the total primary energy demand will increase by 48,5% if current policy scenarios are kept unchanged, and by 22,8% if a post-2012 climate policy framework is applied to stabilize the concentration of global greenhouse gases at 450 ppm CO_2 equivalent [6]. The IEA indicates that developing countries may play an important role in the increase of energy demand.

The predicted depletion of fossil fuels and the need to reduce carbon dioxide emissions have stimulated the quest for more sustainable options. In 2007, the European Council adopted ambitious energy and climate change objectives for 2020. Furthermore, the European Council has stated a long-term commitment to reduce the carbon dioxide emissions in a margin of 80% to 95% by 2050. The objectives are presented below as published in [7]:

- To reduce greenhouse gas emissions by 20%, rising to 30% if the conditions are right.
- To increase the share of renewable energy to 20%.
- To make a 20% improvement in energetic efficiency.

Four main reasons have served as motivation to look for more efficient and sustainable energy technologies:

- There is a continuous increase in energy demand due to the growing population and to the adoption of more electricity-consuming devices.
- There is a high dependency on fossil fuels and a predicted depletion of their reserves.
- There is an uneven distribution of fossil fuel reserves over the world.
- The environmental concerns are increasing due to the global warming phenomenon.

These four aspects motivate new technologies and policies to emerge. In each of the following subsections, a general description of each of these aspects is given and a brief description is provided about how decentralized renewable generation can help to improve each of the aspects.

1.2.1 Increasing Global Energy Demand

Three of the main challenges that emerge from the forecasted increase in energy demand are: to ensure sufficient energy supplies, to reduce the dependency on fossil fuels, and to tackle the environmental impact of our consumption habits [8]. Renewable sources can be used to ensure sufficient energy supplies and to reduce the dependency on fossil fuels since they are abundant and they are spread all over the planet. On the other hand, decentralized energy systems can contribute to supply energy to new consumers in developing countries, where in many cases the existing infrastructure is not suitable to supply remote areas with electricity. Because of the fact that in decentralized systems the production is carried out at the point of use, no costs are associated with electricity transmission at high voltage levels; this makes these technologies appropriate and attractive.

In order to tackle the environmental impact of our consumption habits, we are forced to stop placing economical revenues above environmental conservation and to make considerable changes in our life-style. This does not only apply at societal level, but at individual level as well. We can progressively substitute products that we regularly buy with eco-friendly products. Moreover, not turning off the lights when we are not using them and not bringing a reusable bag to the supermarket to put in our groceries should be unacceptable in this day and age. We are responsible of preventing the following saying from holding true:

> *Only when the last tree has died, the last river has been poisoned and the last fish has been caught will we realize that we cannot eat money.*
> Cree Indian saying

1.2.2 High Dependence on Fossil Fuels

Fossil fuels have traditionally been the most important energy sources to supply both the primary energy and the electricity demand. According to the World Energy Statistics of the International Energy Agency about 86,6% of the primary energy demand was supplied by fossil fuels in 1973; this percentage was reduced to 80,9% in 2009 [6]. A reason for that decrease was the higher participation of nuclear and hydro energy, which increased from 2,7% in 1973 to 8,1% in 2009. Alternative technologies such as geothermal, solar, wind and heat increased from a 0,1% to a 0,8% in the same period of time. According to the same statistics report, in the case of the fuel shares of electric generation, fossil fuels occupied 75,1% of the total shares in 1973. Later in 2009, this percentage was reduced to 67,1%. In this case, the participation of alternative sources increased from 0,6% in 1973 to 3,3% in 2009. Even though some reduction in the total shares of fossil fuels has been achieved, the energy scenario is still strongly dominated by these sources.

There is an ongoing controversy about the forecasted depletion of fossil fuels, however actions should be taken in a short term to reduce the existing high dependency. Renewable energy sources have the potential to relieve fossil fuels from being the major energy sources, in this way their remaining lifetime can be extended. Moreover, decentralized systems with combined heat and electricity technologies can attain higher efficiencies than conventional systems, which also reduces fossil fuel consumption. In the near future, the adoption of alternative sources and more efficient technologies will be crucial for our further development. The remaining fossil fuels could better be reserved for the production of other important products, such as plastics.

1.2.3 Uneven Distribution of Fossil Fuel Reserves

The fossil fuel reserves are unevenly distributed throughout the planet; this produces tension among countries. The proven oil and gas reserves are concentrated in a reduced number of countries; for example, over half of the global proven gas reserves are concentrated in three countries: the Russian Federation (27%), Iran (15%) and Qatar (14%) [9]. An increasing number of nations are relying on gas imports to meet their energy demands [10]. According to the International Energy Agency, the concentration of fossil fuel resources is the most enduring energy security risk [9, 11]. The dependence on global oil consumption is expected to increase, moreover prices are expected to fluctuate due to the short-term demand and supply shifts [12]. This means that tensions among countries are likely to increase in the coming years even more.

By introducing renewable energy, a wider range of sources can be used to cover the national energy demand. Renewable sources are more evenly distributed than fossil fuels. Therefore, in order to take advantage of this favorable characteristic, a country must first identify the sources that are available and consequently encourage policies for their integration. By doing this, the country will not only be able to supply its own energy demand, but also to reduce import costs, create local jobs and open the door to new investments.

1.2.4 Growing Environmental Concerns

The Intergovernmental Panel on Climate Change (IPCC) concluded that the global mean temperature has increased by 0,6°C during the 20th century [13, 14]. They argue that this increase is likely to have resulted from a rise in the amount of greenhouse gases in the atmosphere. Moreover, they indicate that there are strong evidences to infer that this warming effect is a consequence of human activities. A excerpt from [10], in which the effects associated with climate change are listed, is cited below:

> *Climate change has been linked to increased temperatures causing droughts, famines, insect infestations, the witness of new diseases, surges in existing maladies, and fires; floods and widespread human displacements; violent storms resulting great human suffering; unseasonable blizzards and cold temperatures and almost every other type of weather imaginable. The inefficient generation of electricity in centralized plants is therefore a major cause of climate change and the resulting conflict and insecurity that is resultant from it.*

According to the World Alliance for Decentralized Energy (WADE), approximately one third of the global CO_2 emissions in 2005 resulted from heating, cooling and power supply systems in residential and commercial sectors [14]. WADE estimated that in the United States of America, 20% of the total growth of CO_2 emissions can be displaced by integrating decentralized combined heat and power technologies in buildings due to the increased thermal efficiency of these systems. Similarly, renewable energy technologies utilize sources that are continuously replenished, abundant and do not produce extra CO_2 emissions, therefore they are suitable to complement both conventional and new technologies.

It can be concluded from this section that the inclusion of renewable and (decentralized) combined heat and power technologies in energy supply systems has the potential to promote a more efficient and sustainable use of resources.

1.3 Changes that Trigger the Evolution of Power Systems

The power system's evolution that is taking place at this moment is driven by different factors. First, the expected depletion of fossil fuels and environmental concerns have encouraged society to look for a more sustainable development path. Second, new technical developments have allowed scientists to aim for more *intelligent* and efficient ways to control and operate power systems. Third, international agreements set around the Kyoto Protocol in 1997 have stimulated governments to pursue a new direction towards sustainability.

One of the main differences encountered by integrating decentralized and renewable technologies in relation to traditional systems is that the power flow direction in the network is not predictable anymore: one-way traffic becomes two-way traffic [15]. This has a significant impact in protection systems but also in the way power systems are optimized and controlled. Traditionally, networks had a vertical structure with a single power flow direction. Power systems consisted of large centralized power plants connected to transmission networks that fed distribution networks, from which the load was supplied. Due to the introduction of decentralized generation, power systems are becoming horizontally-operated systems in which power is not only produced at the traditional *generation level*, but also at the *distribution level*. Two other significant differences that have taken place during this evolution are the fact that besides large power plants (of several MWs), small-scale generation units (of a few kWs) have been introduced and the fact that some of the sources vary stochastically, like in the case of solar radiation and wind. Due to these differences, the use of power electronic devices and the development of more flexible bi-directional techniques play an important role for a successful integration of new technologies.

This section introduces important aspects related to the recent evolution of power systems. First, a brief summary of some of the main optimization and control techniques used in traditional power systems is presented. Later, a description of three of the main participants in this evolution is provided. Finally, the role of power electronics and the role of information and communication technologies (ICT) is discussed.

1.3.1 Optimization of Traditional Power Systems

The optimization of traditional power systems is based on scheduling and dispatching the power units involved according to the electricity demand. The terms *energy management system (EMS)*, *economic dispatch* and *unit commitment* are described below.

Energy Management Systems

In traditional power systems the transmission and distribution of electrical energy is monitored, coordinated and controlled in a *control center* where an *energy management system* serves as interface between the operator and the power system [15]. In an energy management system, a *Supervisory Control and Data Acquisition* system (SCADA) is in charge of collecting real-time measured data. The data are converted to digital data through a computerized process. By means of a *human-machine interface* (HMI) the human operator has access to the processed data. The processed data can be sent as input to other parallel programs for further computation, for example to an optimal power flow program, a contingency analysis program or a unit commitment program.

Remote terminal units can be connected at several relevant locations. Furthermore a *programmable logic controller* (PLC) can be used to configure and direct the signals and digital data. A communication infrastructure allows the data exchange in the system. The SCADA can be coupled to a control system containing the control algorithms in order to execute further actions. A *state estimator* works in combination with the SCADA system to overcome inconsistencies, for example measurements that may be corrupted, redundant measurements, wrong measurements, etc [15]. Therefore, the state estimator keeps the integrity of the real-time database.

Economic Dispatch

The solution of an *economic dispatch* problem provides the power output that each available generation unit is required to deliver in order to supply a specified load condition in the best economical way [16]. The resulting dispatch is obtained by a program that minimizes the overall cost of fuel that is needed to serve the specified load. In traditional power systems the load considered is the electric load. In this dissertation, the load to be considered can also be of another energy form, for example a heat load.

Unit Commitment

The total power demand varies during the day, for this reason the electricity utility has to decide in advance which generators to start up or shut down, and in which sequence this should be done; this procedure is called *unit commitment* [16]. The unit commitment program schedules the units according to a predicted or forecasted load over a future period of time [16]. Some of the main factors that are taken into account for the optimal scheduling of units are the production costs, the start-up and shut-down costs, the operating fuel costs, the fuel types and the length of the forecasting period.

1.3.2 Control of Traditional Power Systems

In traditional electrical power systems, two main types of control can be identified: *active power control* and *reactive power control*. The term *active power control* is related to performing frequency control, whereas the term *reactive power control* is related to performing voltage control [15, 17]. Frequency and voltage measurements are used to determine the quality of power supply, therefore active and reactive power control are vital to achieving a satisfactory performance [15, 17]. Frequency should remain nearly constant to ensure an almost constant speed at the induction and synchronous motors. A constant speed at the drives is important, since the performance of the generation units depends on the performance of the auxiliary drives associated with the fuel, feed-water and combustion [17].

In traditional power systems, the active power and frequency control is executed at control centers, where data about the system's frequency and about the power flows at interconnecting lines are constantly measured and collected by a SCADA system. Each area is equipped with an automatic generation control, which executes different actions according to the measured control error. In conventional systems, active power control is classified into three different control mechanisms known as *primary control*, *secondary control* and *tertiary control*; all generators that operate above a certain power rate are required to participate in at least the primary control.

Primary Control

Primary control refers to the control actions that take place after a change in the system's frequency has occurred. The frequency of an electrical network depends on the active power balance [17]. A power unbalance occurs when there is a mismatch between the active power that is generated and the active power that is consumed, thus a change in power demand at one point in the network is reflected by a change in frequency in the whole system [17]. In order to compensate for the change in frequency, a speed governor can be set with a *droop* that follows a certain frequency-power characteristic [15]. In this way the mechanical power supplied to the generator is either decreased or increased until the power balance is restored. The per unit droop [p.u.] is given by (1.1):

$$\text{Droop} = \frac{\triangle f / f_{\text{rtd}}}{\triangle P_i / P_{i,\text{rtd}}} \tag{1.1}$$

where $\triangle f$ [Hz] is the frequency change in the system, f_{rtd} [Hz] is the system's nominal rated frequency, $\triangle P_i$ [MW] is the change in active power of generator i and $P_{i,\text{rtd}}$ [MW] is the rated power of generator i.

Secondary Control

After the primary control has been applied, the power balance is restored, but as a consequence, the system operates at a lower or higher frequency than the rated one. *Secondary control* is used to modify the setting of the speed governor in a way that the frequency is brought back to its rated value; this is done by temporarily increasing the prime mover power that raises the kinetic energy of the generation unit [15]. In interconnected systems, there are several areas involved. The *Area Control Error* (ACE) [MW] indicates the surplus or lacking amount of power that has to be generated or injected to a particular area:

$$\text{ACE}_j = \left(P_{j,\text{act}} - P_{j,\text{sch}}\right) + \lambda_j \left(f_{\text{act}} - f_{\text{sch}}\right) \tag{1.2}$$

where $P_{j,\text{act}}$ [MW] is the actual power export of control area j, $P_{j,\text{sch}}$ [MW] is the scheduled power export of control area j, λ_j [MW/Hz] is the network power-frequency characteristic of control area j, f_{act} [Hz] is the actual frequency and f_{sch} [Hz] is the scheduled frequency.

Tertiary Control

Tertiary control is not necessarily applied consecutively after the secondary control actions have been accomplished. Tertiary control is related to the economic dispatch of components: an optimal economic dispatch is calculated for each operating condition. The term economic dispatch was described in Section 1.3.1.

The principles of these three types of control are still used nowadays, however as the participation of (micro-)cogeneration units and the participation of renewable energy sources increase, the control mechanisms will require more flexibility and complexity. In Chapter 4 the hierarchical principle of this traditional control is used, however additional control subsystems are defined in order to allow the control of multiple energy carriers.

1.3.3 Emergent Participants: Cogeneration, District Heating and Renewable Energy Technologies

There are three emergent participants that have played an important role in the evolution of power systems, mainly because of their differences in relation to traditional generation plants. These are: *cogeneration technologies*, *district heating systems* and *renewable energy technologies*. In Section 1.2, potential benefits of integrating cogeneration and renewable technologies were discussed, in the following subsections attention will also be given to the challenges that these participants have created in traditional power system infrastructures.

Cogeneration Technologies

Combined heat and power or *cogeneration* units are defined as generation units that simultaneously generate electricity and useful heat from the same fuel input; the fuel can be coal, biomass, natural gas, nuclear material, sun radiation or heat stored in the earth [18]. Some of the benefits that have been associated with cogeneration technologies are the following [18–20]:

- Cogeneration dramatically increases the energetic efficiency of the system.
- Due to the higher efficiency, reduction of carbon dioxide emissions and other pollutants can be achieved.
- It allows increased energy security through reduced dependence on imported fuel.
- Cogeneration promotes cost savings for the energy consumers.
- Decentralized CHP units reduce the need for transmission and distribution networks.
- Local energy resources can be encouraged, particularly through the use of biomass, waste and geothermal resources in district heating and cooling (DHC) systems.

Due to the resulting combined efficiency (electrical efficiency and thermal efficiency), CHP units allow 75% to 80% of the fuel input to be converted into useful energy, and up to 90% in highly efficient plants, therefore by using fuels in a more efficient way, both energy costs and CO_2 emissions can be reduced [18]. The main difference of a cogeneration plant with respect to a traditional plant is that its useful output is not only electricity, but also heat. Another difference is that domestic CHP (micro-CHP) units may be able to inject power into the electrical grid, for example in the case when more electricity than necessary is produced. These two characteristics increase flexibility in the energy system. Nevertheless, in order to take advantage of this flexibility, new scheduling strategies are necessary, since the control and optimization of the system should not overlook the heat production. This dissertation emerged as a response to filling that gap.

District Heating Technologies

A *district heating system* consists of buildings, pipes, a pump station and a heat production station, where heat can be produced from a geothermal field, combustion and combined heat and power units, among other technologies. Nowadays, the heat demand of some domestic appliances, such as washing machines and dryers is mostly supplied with electricity.

However, this practice is unfavorable since *first class* energy is used for a purpose where a *second class* energy should be used instead, in spite of this, state-of-the-art policies do not encourage district heating supply [21].

Large penetration of district heating systems has taken place particularly in Scandinavian countries, where they occupy over 50% of the heat market; however, district heating comprises a small fraction of the total heat market of the European Union [22]. There is still potential for large penetration in other countries, but national and international policies should be adapted in order to promote it. Some of the main characteristics of district heating are summarized below [23]:

- Existing district heating and cogeneration facilities reduce the global carbon dioxide emissions from fuel combustion by 3-4% annually (in relation to traditional systems). As a reference, the Kyoto Protocol sets a target of 5% average reduction per year in industrialized countries.
- District heating systems are very suitable to be fed by cogeneration plants; this raises the overall efficiency of power and heat production as mentioned above.
- District heating systems can be fed with energy coming from several sources, including industrial waste heat, heat from incinerators, geothermal energy and biomass, among others.

Due to the fact that district heating systems can be fed from several different sources, including CHP units, a multi-carrier scheduling strategy can be beneficial. In Chapter 4 a district heating load is used in the illustrative example.

Renewable Energy Technologies

Renewable energy is energy derived from resources that are not substantially depleted by continuous use. Ideally, these resources do not entail significant pollutant emissions or other environmental problems, and do not involve the perpetuation of substantial health hazards or social injustices [24]. In [15], the structural changes that will occur in existing distribution and transmission networks due to a large-scale implementation of renewable energy sources are attributed to four main differences with respect to traditional systems:

- Most renewable energy generators are connected to the distribution network, in contrast to traditional large-scale generators, which are connected to the transmission network.
- Most renewable energy generators are connected to the electrical grid by means of power electronic interfaces, in contrast to large generation plants which are coupled to the electrical grid directly.
- The output of most renewable energy generators depends on natural and uncontrollable sources, in contrast to traditional plants, which are driven by controllable sources like fossil fuels and hydro power, among others.
- The outputs of several renewable energy generators have an intermittent character, which can lead to power fluctuations in the electrical grid. This does not apply to traditional generators.

As it was mentioned earlier, according to the International Energy Agency, the participation of alternative sources such as geothermal, solar, wind and heat, in the total primary energy supply will increase from 0,8% in 2009 to 11,8% if current policy scenarios are kept unchanged and to 18,6% if a climate policy framework is applied to stabilize the concentration of global greenhouse gases at 450 ppm CO_2 equivalent [6]. This means that transmission and distribution operators should start adapting their monitoring, control and optimization infrastructures in a short term in order to smoothly cope with the changes.

The Clean Energy Progress Report of 2011 shows the results of a sound analysis performed by the Clean Energy Ministerial Secretariat, run by the US Department of Energy in relation to the progress that has been done towards clean energy implementation [25]. Several key findings were published in this report, from which the following were selected due to the relation that can be established with this dissertation:

- *Thanks to favorable policy support, solar PV and wind power are achieving strong growth. However, in order to achieve sustainable energy goals a doubling of all renewable energy use is required by 2020.*

  The fact that a doubling of all renewable energy use is required means that the development and implementation of suitable control systems is crucial. Chapter 4 includes an illustrative example of a control strategy applied to a system with high penetration of wind. Such studies are important to gain insights and be able to cope with the different challenges that stochastically-varying sources bring.

- *Progress has been made to transform the market for some key energy-efficient products, including compact fluorescent light bulbs. However, in the buildings and industry sectors, significant under-investment remains. Much more policy effort is needed to capture the near- term profitable and low cost energy savings opportunities.*

  The scheduling tool described in Chapter 2 is a first step towards the development of tools that can be applied to the building, residential and industry sectors in order to show potential cost/energy saving opportunities and in this way attract investors.

- *Electric vehicles are poised to take off. Major economies have announced targets that together would reach about 7 million vehicle sales per year by 2020. However, this will only account for about 2% of light-duty vehicle stocks worldwide. Fuel economy of conventional light-duty vehicles will need to improve faster to achieve a global target of 50% improvement by 2030 compared to 2005 levels.*

  Even though the topic of electric vehicles is only analyzed by means of an illustrative example in Chapter 5, it shows some insights about the participation of electric vehicles at district level.

- *Increased attention and resources are required to expand smart grid pilot projects on a regional levels.*

  The framework presented in this thesis will be applied to a pilot project during the years 2012 and 2013. The author of this dissertation has been working on this project since January 2012. The results of the pilot project will provide valuable information about further possibilities for implementation at local and regional levels.

1.3.4 Role of Power Electronics in Future Power Systems

In conventional power systems, fully controllable generators are in charge of performing voltage and frequency control. However, due to the increment in the participation of non-controllable units, power electronic devices are taking part in performing these actions. Power electronics allow flexible control of electrical power, they allow DC-to-AC (inverter) conversion, as well as DC-to-DC, AC-to-DC and AC-to-AC conversions.

Decentralized generation units, such as fuel cells and especially the ones powered by renewable energy sources with stochastically varying nature, like photovoltaic systems and wind turbines, are often connected to the distribution network by power electronic interfaces [15]. In distribution systems, like the ones addressed in this dissertation, the main applications are focused on the control of voltage and power flow, but also on the improvement of power quality [26]. Two modes of operation of power electronic interfaces are: *PQ control* and *voltage source control*. These mechanisms are briefly described below. For modeling purposes, the general procedure adopted in the literature is to model converters according to their control functions, this means that fast switching transients, harmonics and inverter losses are neglected [27].

Voltage Source Control

When a power electronic interface operates in *voltage source control* mode, the converter provides power in a way that the voltage level and frequency are kept at a reference level: the converter operates as the master converter of the system. Small-scale power systems that are not connected to the main electrical grid rely on a master converter for their voltage and frequency levels.

PQ Control

When a power electronic interface operates in *PQ control* mode (active power - reactive power control mode), the converter provides active and reactive power according to the respective power set-point. In this case, the converter operates as slave.

1.3.5 Smart Grids: Intelligence in Future Power Systems

In the inaugural edition of the IEEE Smart Grid Newsletter, the term *smart grid* was defined in the following way [28]:

> *. . . a smart grid involves the increased use of digital information and controls technology to improve the reliability, security, and efficiency of the electrical grid . . . (and) dynamic optimization of grid operations and resources, with full cyber-security.*

The infrastructure for *information and communication technology* (ICT) accounts for 3% of the world's electricity usage, but its role in the future energy scenario seems to be far greater than that [29]. Recent and future developments in power systems, such as smart grids and intelligent buildings require ICT infrastructures; this makes energy supply infrastructures dependant on ICT.

The smart grid concept can be applied at any voltage level and the functionalities associated with the term are quite broad. IC technologies will become crucial actors in the smart grid scenario [30]. However many gaps have to be filled before being able to implement smart grids in the current power system infrastructures. A clear description about the current status in relation to ICT and the smart grid concept was found in [31]:

> *. . . currently there are no well-established modeling, analysis, or decision-making paradigms in support of deploying information communications technology (ICT) needed to facilitate new functionalities essential for sustainable energy services. What is available are fragmented coarse models of socio-ecological systems (SESs), climate change energy models, man-made electric power grids, as well as fragmented approaches to ICT developed for other applications and believed to be directly applicable to smart grid design and operations.*

Several authors have already identified difficult challenges that generate from the introduction of smart grids. The ones that were considered most important within the context of this dissertation were selected and summarized below:

- Data might reveal information about the presence of people at their home and about the appliances they use. This might affect their privacy. Therefore, customers might be unwilling to provide their information [32].
- Large amounts of data will be generated with the introduction of smart grid technologies. Techniques for managing, analyzing and acting on this data will need to be developed [30]. Moreover, maintenance, management and storage of data may be a tedious job [32].
- Customer gateways are prone to physical as well as cyber security risks. For this reason, energy meters need proper shelter to be physically secure [32].
- Old power plants will not easily be switched in response to highly variable new plants [31].
- Implementation of smart meter systems involves an investment of several billion dollars for deployment and maintenance [32].
- At the distribution level, it is likely that traditional customers will sell power back to the electrical grid. Depending on the penetration of this kind of loads, the entire distribution system protection and control infrastructure will need to be redesigned to manage different flow patterns. Given that many components have aged, it is a good time to rethink the design of future distribution systems [31].

From the list above, it can be concluded that still many steps need to be taken in order to incorporate the smart grid concept into the current power system's infrastructure. Moreover, as earlier discussed in this chapter, cogeneration and district heating technologies are likely to play an important role in the future due to the higher efficiencies that can be attained with them. These technologies may be coupled to the smart grid optimization and control platform. In most of the papers dealing with smart grids, only electrical flows are taken into account, however in order to make a better use of the synergies provided by the couplings between different energy carriers, smart grid strategies should also take other energy carriers into consideration.

1.4 Problem Definition

Three main concepts serve as platform for the problem definition of this dissertation. These concepts are: *the energy hub approach*, *exergy analysis as assessment tool for energy systems* and *intelligent energy management systems at district level*. A brief discussion of each aspect is given below.

1.4.1 The Energy Hub Approach

The *energy hub* approach was developed as part of the project "Vision of Future Energy Networks - VoFEN" at ETH Zürich. The objective of the VoFEN project is to find optimal structures for energy systems in the future. In the VoFEN project, the interaction and conversion possibilities between different energy carriers are considered to increase the flexibility of energy supply systems. An energy hub is flexible in supply due to the fact that there are different energy carriers available at its inputs and also by the fact that internal conversion and storage are possible [33]. This flexibility allows the use of optimization tools to determine the best way to supply a load, after taking the constraints of the system into account.

An energy hub is a unit where multiple energy carriers are converted, conditioned and stored [34–37]. It can serve as an interface for different energy infrastructures and/or loads [33]. The energy hub shown in Figure 1.2 contains a hybrid input port with electricity and natural gas as energy carriers, and a hybrid output port with electricity and heat as products. The couplings that exist among the inputs and outputs are contained inside the energy hub.

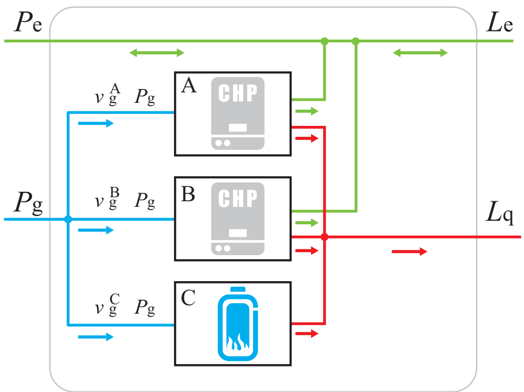

Figure 1.2: Energy hub representation

Depending on its functionality, there are three types of elements that an energy hub can contain: direct connections, converters and storage elements [33]. Direct connections are elements that deliver an input carrier to the output port without converting it into another energy form or changing its quality in a significant way. Converter elements transform energy carriers into different energy forms or qualities. Storage elements are used to represent both direct and indirect storage of energy carriers [33]. The description and mathematical representation of the energy hub is presented in Chapter 2.

The following problems have already been solved using the energy hub approach: *multi-carrier optimal dispatch*, *multi-carrier optimal power flow*, *optimal hub coupling* and *optimal hub layout*. Those problems were covered in the dissertation “Integrated Modeling and Optimization of Multi-Carrier Energy Systems” [33]. The problems of scheduling (unit commitment) and real-time control of such systems also require a flexible framework since the flow interactions in systems with multiple energy carriers create challenges in terms of planning, scheduling and control. Since these problems have not been solved in the literature for systems with multiple energy carriers, the development of a suitable unit commitment framework for these systems was defined as one of the problems to be solved in this dissertation. The energy hub approach is therefore used as platform.

1.4.2 Exergy Analysis as Assessment Tool for Energy Systems

Due to the increasing interest in promoting energy conservation, *exergy analysis* has the potential to become an important tool for the study and design of energy plants and systems. Exergy analysis can be used to evaluate the potential to produce work throughout the system. This can provide a proper measurement of the losses in the system, which is necessary to achieve an effective energy conservation during the system’s design and operation [38].

According to [38], three aspects that have prevented engineers from performing exergy analyses are:

- The analysis presented in books is normally based on the first law of thermodynamics.
- Examples of the second law of thermodynamics are usually limited to simple processes and cycles, where the benefits of using the second law are not apparent.
- The design and operation conditions for energy plants have usually been based on initial costs and not on taking the most advantage of the source, where the second law of thermodynamics plays a role.

During the last decade, the interest in using exergy for the analysis of systems has increased. At Delft University of Technology, several efforts have been made to support activities in the field of exergy. A trigger for the research presented in this dissertation was an example published in the area of built environment [39, 40]. This example is part of the dissertation “Exergy Efficient Building Design” defended at Delft University of Technology, which provides insights about the possibilities of using exergy analysis as assessment tool in the built environment [40]. The author analyzes the effectiveness of using an electricity-driven heat recovery unit in a dwelling ventilation system from an exergy perspective.

The author presented a steady-state energy and exergy analysis for a dwelling ventilation system with and without the use of a heat recovery unit and compared the results. From the results, he concluded that it could make sense to use the heat recovery unit only when the environmental temperature is low enough to compensate for the electricity input, which has a high exergy value [39]. Thus, it can be inferred from the example that from an exergetic point of view, the heat recovery unit has to be scheduled only when the heat demand is high due to low outside temperatures, but from an energetic point of view this is not the case.

As previously claimed by other authors [41, 42], the author stated that an exergy analysis provides a common basis to evaluate systems that contain heat and electricity flows despite their different abilities to produce work in relation to a given environment. The study opened a path for further research. After revising the aforementioned work, the challenge in this dissertation became to provide a tool that would not only be able to schedule the units beforehand (contrary to the case in which the best schedule is selected after having compared the results of selected scenarios), but that could also provide the optimal dispatch of the units involved according to the exergetic/energetic efficiency of the system. Another aspect that was considered important for the optimization tool was to allow the inclusion of several units and multiple energy carriers. The result of the work is condensed in Chapter 3.

As mentioned in Section 1.2, one of the main goals to be reached by including renewable and combined heat and power technologies is to achieve a more efficient and sustainable use of resources. Exergy analysis can be used to calculate the available work throughout a system and to identify losses; this provides valuable information for the planning of the next generation energy supply systems. Due to its potential as assessment tool and because there is very limited literature about the use of exergy analysis in systems with multiple energy carriers, this was defined as one of the problems to be addressed in this dissertation.

1.4.3 Intelligent Energy Management Systems at District Level

Several research institutes, professional societies and governmental agencies have decided to incorporate and promote the development of concepts related to smart grids in their portfolio. The topic of *intelligent energy management systems* falls under the broad coverage of smart grids. As discussed earlier in this chapter, one of the topics that still needs to be explored is the feasibility of developing and implementing an intelligent energy management system for small-scale systems containing multiple energy carriers at district level. Furthermore, special focus must be given to scheduling of the generation units involved. The scheduling tool to be described in Chapter 2 allows the analysis of different load scenarios and system configurations that have arisen in response to several emerging trends in power systems. The trends to be included in the analysis are:

- The growing participation of micro-CHP units
- The application of the *virtual power plant (VPP)* concept, in which several micro generation units are controlled by an aggregator to achieve an optimized operation
- The inclusion of storage
- The inclusion of renewable sources
- The inclusion of electric vehicles.

The application of the scheduling tool for the analysis of these aspects was selected as one of the targets of this dissertation. Additionally, a general control scheme to be applied in systems with multiple energy carriers is presented in Chapter 4. The results of the comparisons among scenarios are presented in Chapter 5. The control scheme is part of the energy management system described in Chapter 6. The examples presented in this dissertation refer to residential loads.

1.5 Research Objective

1.5.1 Main Objective

The main research objective is based on the three concepts discussed in the problem definition. The resulting formulation is:

> *To develop a scheduling tool for small-scale systems that contain multiple energy carriers at district level (residential) by using the energy hub approach and to evaluate the use of an exergy analysis as assessment tool for such systems.*

1.5.2 Research Questions

The following research questions are based on the main research objective. The first research question is the main research question of this work and therefore it is answered throughout all the chapters of this dissertation.

1. What kind of optimization tool can be used for the scheduling and control of systems containing multiple energy carriers in residential areas?

2. What framework can be adopted in order to schedule and optimize the units involved in an energy supply system with multiple energy carriers at district level?

3. What is the potential relevance of using the exergy concept to analyze energy supply systems with multiple energy carriers?

4. What kind of real-time control strategy can be applied in a system containing multiple energy carriers at district level?

5. How can the scheduling tool described in this dissertation be used for the analysis of emerging trends in power systems and what benefits can be obtained from it?

6. What design can be proposed for a multi-carrier energy management system and can it be implemented at DENlab?

Each chapter in this dissertation is dedicated to one of the listed research questions. In order to answer Research Question 6, a partial physical implementation in the renewable energy laboratory DENlab was performed. More information about this laboratory is presented in Chapter 6.

1.6 Overview of this Dissertation

1.6.1 Outline

This dissertation consists of seven chapters. This section concludes Chapter 1, in which the project framework, motivation, problem definition and research questions were introduced. Chapter 2 describes the model behind the scheduling tool that was developed for this PhD project, which is used to optimize systems containing multiple energy carriers. Later in Chapter 3 the optimization tool is adapted to include exergetic efficiency as assessment parameter of such systems. Chapter 4 presents the control architecture that was designed to cope with the dynamic behaviour of the systems under study. The application of the control architecture is shown by means of an example. In Chapter 5 the optimization tool is used to analyze the impact of different emerging trends in district-level power systems, such as the active participation micro-CHP technologies, the incorporation of renewable sources and the application of the virtual power plant concept. Chapter 6 provides insights regarding the implementation of the optimization and control tool in real systems. Finally, Chapter 7 presents the conclusions and recommendations of this dissertation.

1.6.2 Main Contributions

The main contributions of this dissertation are listed below:

- A general *multi-carrier unit commitment* framework for energy systems that contain multiple energy carriers was developed. The framework can be used with any kind of energy carrier and for different possible couplings and power scales (Chapter 2).

- A technique to include storage was developed and implemented as part of the optimization tool. The results show that this technique can be valuable for peak-shaving purposes at the generation side (Chapter 2).

- The *exergy hub* approach was introduced. The exergy hub provides a visual indication of the exergetic efficiency of the units. In Section 3.4 both the energy hub and the exergy hub are depicted next to each other in order to reveal that a unit that is considered to be very efficient from an energy point of view can be considered to be very inefficient from an exergy perspective. Some authors consider that energy efficiencies can be misleading [43], thus the exergy hub representation could serve as a way to avoid this (Chapter 3).

- A comparison between the results for the optimal dispatch obtained from an exergetic efficiency optimization and from an energetic efficiency optimization is performed. In the literature, this kind of comparison has not been performed in the context of energy supply systems containing multiple energy carriers (Chapter 3).

- The results of the scheduling optimization tool are compared to identify which configuration gives the best energy and exergy performances for specific loads. A sensitivity analysis is performed in which the ratio between heat and electricity consumption is varied to observe the influence of the type of load in the scheduling. In the literature, the attempts that have been made to analyze systems containing several generation units from an exergy perspective are very limited and they do not focus on finding an optimal scheduling by means of a mathematical optimization algorithm as done in this dissertation (Chapter 3).

- A two-level control strategy was designed for the application in systems with multiple energy carriers. Most of the control strategies found in the literature only focus on electricity flows, thus the strategy proposed is valuable for multi-carrier systems (Chapter 4).
- Several emergent trends were simulated to provide insights regarding their impact in district-level residential energy supply systems. The optimization tool was extended in order to study the benefits of having an aggregator in charge of the optimization (Chapter 5).
- A comparison among three micro-CHP technologies was presented to show that different benefits can be obtained by using combined heat and power technologies with different electricity-to-heat efficiency ratios (Chapter 5).
- An example was presented in which the influence of incorporating electric vehicles at a neighbourhood was analyzed (Chapter 5).
- A design of a multi-carrier energy management system was presented. A partial implementation in the renewable energy laboratory DENlab was performed, which provides an added value to the theoretical results that were accomplished in this dissertation (Chapter 6).

Chapter 2

The Framework

Multi-Carrier Unit Commitment

This chapter answers Research Question 2. It presents the optimization framework, from now denoted *multi-carrier unit commitment*, that was developed to schedule and optimize controllable units in energy systems with multiple energy carriers. The algorithms were programmed in the optimization software for research applications AIMMS [44].

Section 2.1 contains basic definitions related to the framework. Section 2.2 presents a summary of work that has been done in relation to modeling systems with multiple energy carriers. In Section 2.3, the *multi-carrier unit commitment* framework is modeled and described. Section 2.4 contains simulation results to illustrate the optimization tool. Finally in Section 2.5 the conclusions of this chapter are presented. Parts of this chapter have been published in [1, 45].

2.1 Basic Concepts and Definitions

2.1.1 Energy Hub Element

There are three types of *energy hub elements*: direct connections, converters and storage elements [33]. Direct connections deliver input carrier α to the output port without converting it into another energy form. Conversely, converter elements transform energy carrier α into a different energy carrier β. Finally, storage elements consist of an interface and an internal (ideal) storage. Through the interface, power in the form of energy carrier α may be conditioned and/or converted into energy carrier γ, which is then stored internally. It is assumed that when a storage element exchanges energy carrier α, the element is considered a storage element of energy carrier α, even if energy carrier $\gamma \neq \alpha$ is stored internally [33].

2.1.2 Multi-Carrier Optimal Dispatch

Multi-carrier optimal dispatch is a method to determine an optimal operation policy for a number of converter units processing multiple energy carriers [33]. This term is closely linked to the energy hub concept, which was introduced in Section 1.4.1.

2.1.3 Multi-Carrier Unit Commitment

Multi-carrier unit commitment is introduced in this dissertation as the computational procedure that makes scheduling decisions in advance about the units that must be committed to supply a forecasted load in energy systems containing multiple energy carriers. The procedure determines the sequence in which the start-up and shut-down of the units (energy hub elements) should be executed as well as the optimal dispatch of each committed unit at each time period.

2.2 Modeling of Multi-Carrier Energy Systems

This section introduces the modeling concepts that serve as the base for the development of the multi-carrier unit commitment framework. In the next few pages, the work published in [33, 36, 37] is condensed, thus this section presents a summary of works performed by other authors in relation to modeling systems with multiple energy carriers. Even though the model presented is based on the literature, a modified nomenclature is introduced to describe the model. This modified notation is more consistent and general; this allows the model to be easily extended, as done in Section 2.3, in Chapter 3 and in Chapter 5.

The main constraints, assumptions and equations that are necessary to solve the multi-carrier optimal dispatch problem are included in this section. Moreover, a simple example is added to illustrate the concepts.

2.2.1 Constraints and Assumptions

The following assumptions are considered:

- If not mentioned explicitly, it is assumed that there is a unidirectional power flow from the input to the output ports.
- Losses only occur at the converter elements inside the energy hub. Connecting networks are assumed to be lossless if not mentioned explicitly.
- An energy converter device is represented as a black box characterized by its energetic efficiency or a function representing the input-output dependency.
- Even though the notation is based on the notation presented in [33], several changes were introduced to allow a more precise definition of the variables.

2.2.2 Energy Hub Conversion Model

The energy conversion model proposed in [33] is used in this chapter without significant alterations apart from the notation. For a system with one input energy carrier α and one output energy carrier β, the input and output power flows are coupled by the *coupling factor* $c_{\alpha\beta}$ [-], as shown in (2.1) [33, 36, 37]:

$$L_\beta = c_{\alpha\beta} P_\alpha \tag{2.1}$$

where P_α [kW] is the steady-state input power flow and L_β [kW] is the steady-state output power flow of the energy hub. Due to the conservation of power, the output power of the converter must be equal or smaller than the input power, thus the coupling factor is limited by the following constraint:

$$L_\beta \leq P_\alpha \Rightarrow 0 \leq c_{\alpha\beta} \leq 1. \tag{2.2}$$

In the case of multiple energy carriers, the input energy carriers are denoted by α_1, $\alpha_2, \ldots, \alpha_{n_{\text{in}}}$, while the output energy carriers are denoted by $\beta_1, \beta_2, \ldots, \beta_{n_{\text{out}}}$. In general the following notation will be used for the input and output energy carriers respectively: α_i and β_j, where $i = 1, 2, \ldots, n_{\text{in}}$, $j = 1, 2, \ldots, n_{\text{out}}$, $n_{\text{in}} \in \mathbb{N}$ and $n_{\text{out}} \in \mathbb{N}$. The variables α_i and β_j represent specific energy carriers from the sets $\mathcal{E}_{\text{in}} = \{\text{e}, \text{g}, \text{q}, \ldots\}$ and $\mathcal{E}_{\text{out}} = \{\text{e}, \text{g}, \text{q}, \ldots\}$ that may include electricity 'e', gas 'g', heat 'q', among others energy carriers. The matrix that represents a system with multiple energy carriers is shown in (2.3):

$$\underbrace{\begin{bmatrix} L_{\beta_1} \\ L_{\beta_2} \\ \vdots \\ L_{\beta_{n_{\text{out}}}} \end{bmatrix}}_{\mathbf{L}} = \underbrace{\begin{bmatrix} c_{\alpha_1\beta_1} & c_{\alpha_2\beta_1} & \cdots & c_{\alpha_{n_{\text{in}}}\beta_1} \\ c_{\alpha_1\beta_2} & c_{\alpha_2\beta_2} & \cdots & c_{\alpha_{n_{\text{in}}}\beta_2} \\ \vdots & \vdots & \ddots & \vdots \\ c_{\alpha_1\beta_{n_{\text{out}}}} & c_{\alpha_2\beta_{n_{\text{out}}}} & \cdots & c_{\alpha_{n_{\text{in}}}\beta_{n_{\text{out}}}} \end{bmatrix}}_{\mathbf{C}} \underbrace{\begin{bmatrix} P_{\alpha_1} \\ P_{\alpha_2} \\ \vdots \\ P_{\alpha_{n_{\text{in}}}} \end{bmatrix}}_{\mathbf{P}}. \tag{2.3}$$

When several converters k_p are considered, the set of converters $C_{\alpha_i} = \{A, B, \ldots\}$ is introduced, where $p = 1, 2, \ldots, n_{\text{con}}$ and $n_{\text{con}} \in \mathbb{N}$. Each converter k_p has an energy carrier α_i as input. Therefore, when energy carrier α_i serves as input for several hub elements or converters, *dispatch factors* $\nu_{\alpha_i}^{k_p}$ [-] are introduced. If the total input power P_{α_i} [kW] splits into $N_{C_{\alpha_i}}$ converters, dispatch factor $\nu_{\alpha_i}^{k_p}$ specifies the percentage of input power P_{α_i} that flows into converter k_p [33]. The input power of the converter is denoted by $P_{\alpha_i}^{k_p}$ [kW] and given by:

$$P_{\alpha_i}^{k_p} = \nu_{\alpha_i}^{k_p} P_{\alpha_i}. \tag{2.4}$$

A general expression of coupling factor $c_{\alpha_i\beta_j}$ [-] is given in (2.5). The expression takes into account the participation of each converter k_p, as shown:

$$c_{\alpha_i\beta_j} = \sum_{k_p \in C_{\alpha_i}} \nu_{\alpha_i}^{k_p} \eta_{\alpha_i\beta_j}^{k_p} \tag{2.5}$$

where $\nu_{\alpha_i}^{k_p}$ is the dispatch factor that represents the percentage of input power P_{α_i} that is provided to converter k_p and $\eta_{\alpha_i\beta_j}^{k_p}$ [-] is the efficiency of conversion from energy carrier α_i to β_j of converter k_p. The efficiency of conversion can also be given as a function of the input power flow: $\mathscr{F}_{\beta_j}^{k_p}(P_{\alpha_i})$ [-]. Likewise, the coupling factor $c_{\alpha_i\beta_j}$ results from adding the individual contributions of all converters that produce energy carrier β_j at their output:

$$c_{\alpha_i\beta_j} = \sum_{k_p \in C_{\alpha_i}} \nu_{\alpha_i}^{k_p} \mathscr{F}_{\beta_j}^{k_p}(P_{\alpha_i}). \tag{2.6}$$

The constraints related to the dispatch factor are given by:

$$0 \leq \nu_{\alpha_i}^{k_p} \leq 1 \quad \text{and} \quad \sum_{k_p \in C_{\alpha_i}} \nu_{\alpha_i}^{k_p} = 1. \tag{2.7}$$

Figure 2.1 shows an energy hub in which a single input power P_{α_i} is provided to several converters k_p.

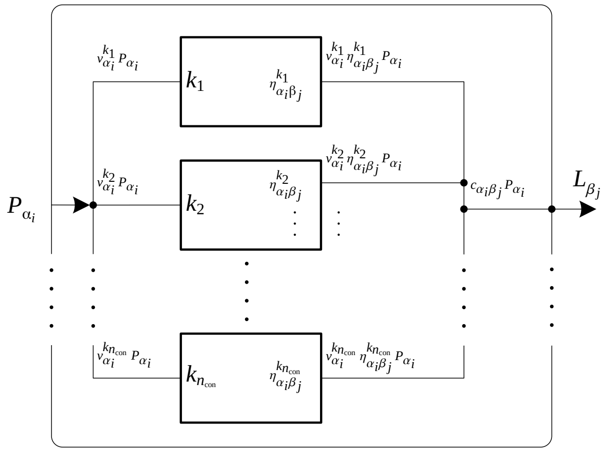

Figure 2.1: Representation of an energy hub with multiple converters

2.2.3 Multi-Carrier Optimal Dispatch Model

This subsection summarizes the problem statement of the multi-carrier optimal dispatch according to [33, 36]. The problem statement includes the objective function to be minimized as well as the equality and inequality constraints.

For an energy hub, the power balance equality constraint states that the output power vector **L** is equal to the coupling matrix **C** multiplied by the respective input power vector **P**. This equality constraint is expressed in (2.8):

$$\mathbf{L} - \mathbf{C}\mathbf{P} = \mathbf{0}. \tag{2.8}$$

The equality constraint for the dispatch factors is shown in (2.9) (derived from (2.7)):

$$1 - \sum_{k_p \in C_{\alpha_i}} v_{\alpha_i}^{k_p} = 0. \tag{2.9}$$

The inequality constraints for the problem statement are given by the lower and upper limits of the hub power inputs ($\underline{P}_{\alpha_i}, \overline{P}_{\alpha_i}$) [kW], the lower and upper limits of the individual converters' power inputs ($\underline{P}_{\alpha_i}^{k_p}, \overline{P}_{\alpha_i}^{k_p}$) [kW] and the limits of the dispatch factors:

$$\underline{P}_{\alpha_i} \leq P_{\alpha_i} \leq \overline{P}_{\alpha_i} \tag{2.10}$$

$$\underline{P}_{\alpha_i}^{k_p} \leq v_{\alpha_i}^{k_p} P_{\alpha_i} \leq \overline{P}_{\alpha_i}^{k_p} \tag{2.11}$$

$$0 \leq v_{\alpha_i}^{k_p} \leq 1. \tag{2.12}$$

The objective function $\mathscr{F}_{\mathrm{obj}}$ [€/(time period)] for the multi-carrier optimal dispatch is a function of the energy hub's variables. For example, when the operational costs are minimized, the objective function can be modeled as a quadratic function of the respective input powers, where K_{1,α_i} [€/(time period)], K_{2,α_i} [€/(time period · kW)] and K_{3,α_i} [€/(time period · kW^2)] are cost coefficients:

$$\mathscr{F}_{\mathrm{obj}} = \sum_{\alpha_i \in \mathscr{E}_{\mathrm{in}}} (\mathrm{K}_{1,\alpha_i} + \mathrm{K}_{2,\alpha_i} P_{\alpha_i} + \mathrm{K}_{3,\alpha_i} P_{\alpha_i}^2). \tag{2.13}$$

Example: Multi-Carrier Optimal Dispatch Coupling Matrix Formulation

The example shows how to obtain the factors of the coupling matrix. The energy hub in the example contains 3 converters and 1 direct connection as shown in Figure 2.2. The hub inputs are natural gas and electricity coming from the electrical grid. The energy hub output consists of an electric load and a heat load. Therefore, the input carrier set is defined as $\mathscr{E}_{\mathrm{in}} = \{\mathrm{e},\mathrm{g}\}$, where 'e' stands for electricity coming from the grid and 'g' stands for natural gas. On the other hand, the output carrier set is defined as $\mathscr{E}_{\mathrm{out}} = \{\mathrm{e},\mathrm{q}\}$ where 'e' stands for electricity and 'q' stands for heat. The set of converters is defined as $C_{\alpha_i} = \{\mathrm{A},\mathrm{B},\mathrm{C}\}$. Converter A and converter B represent two gas-fired CHP units and converter C represents a gas-fired furnace. The direct connection represents the public electrical grid.

From Figure 2.2, it can be observed that there is no gas output L_{g} or any heat input P_{q} at the energy hub under consideration, thus they are not included in the equality constraint matrix shown in (2.14):

$$\begin{bmatrix} L_{\mathrm{e}} \\ L_{\mathrm{q}} \end{bmatrix} - \begin{bmatrix} c_{\mathrm{ee}} & c_{\mathrm{ge}} \\ c_{\mathrm{eq}} & c_{\mathrm{gq}} \end{bmatrix} \begin{bmatrix} P_{\mathrm{e}} \\ P_{\mathrm{g}} \end{bmatrix} = 0. \tag{2.14}$$

There is no conversion from electricity to heat, thus the corresponding coupling factor c_{eq} is equal to zero. There is a direct connection from the electricity input P_{e} to the electricity output L_{e}, for this reason the coupling factor c_{ee} is equal to 1:

$$c_{\mathrm{eq}} = 0, \quad c_{\mathrm{ee}} = 1. \tag{2.15}$$

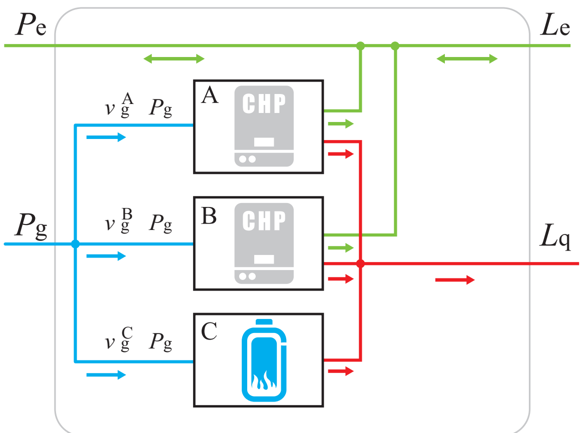

Figure 2.2: Energy hub representation for the example

The conversion from gas to electricity is performed by converter A and converter B. Their individual contributions depend on the dispatch factors $\nu_{\mathrm{g}}^{\mathrm{A}}$ and $\nu_{\mathrm{g}}^{\mathrm{B}}$ and the efficiencies of the converters, given by $\eta_{\mathrm{ge}}^{\mathrm{A}}$ and $\eta_{\mathrm{ge}}^{\mathrm{B}}$ respectively. The coupling factor c_{ge} (gas to electricity) results from the addition of both contributions (see (2.5)):

$$c_{\mathrm{ge}} = \nu_{\mathrm{g}}^{\mathrm{A}}\eta_{\mathrm{ge}}^{\mathrm{A}} + \nu_{\mathrm{g}}^{\mathrm{B}}\eta_{\mathrm{ge}}^{\mathrm{B}}. \tag{2.16}$$

The conversion from gas to heat is performed by converters A, B and C. Similarly, the coupling factor c_{gq} (gas to heat) results from the addition of their individual contributions:

$$c_{\mathrm{gq}} = \nu_{\mathrm{g}}^{\mathrm{A}}\eta_{\mathrm{gq}}^{\mathrm{A}} + \nu_{\mathrm{g}}^{\mathrm{B}}\eta_{\mathrm{gq}}^{\mathrm{B}} + \nu_{\mathrm{g}}^{\mathrm{C}}\eta_{\mathrm{gq}}^{\mathrm{C}}. \tag{2.17}$$

2.2.4 Multi-Carrier Optimal Dispatch Model Including Storage

In accordance to the definition of storage element given in Section 2.1.1, a storage element that exchanges power in the form of energy carrier α_i is considered to be a storage element of α_i, even if another carrier is stored internally. The energy content inside the storage element increases the amount of $\dot{E}_{\alpha_i}\triangle t$ during time period $\triangle t$, where $\dot{E}_{\alpha_i}$ [kW] is the power flowing into the storage element. In order to determine the power $\dot{E}_{\alpha_i}$ that is added or subtracted from the storage element, the power D_{α_i} [kW] flowing to the storage element, is multiplied by the efficiency factor e_{α_i} [-]:

$$\dot{E}_{\alpha_i} = e_{\alpha_i} D_{\alpha_i}. \tag{2.18}$$

The factor e_{α_i} is considered as the charge/discharge efficiency and it depends on the direction of the power flow, i.e., if the storage element is being charged ($e_{\alpha_i}^{+}$) or discharged ($e_{\alpha_i}^{-}$) [33]:

$$e_{\alpha_i} = \begin{cases} e_{\alpha_i}^{+}, & \text{if } D_{\alpha_i} \geq 0 \quad \text{(charging or stand-by)} \\ 1/e_{\alpha_i}^{-}, & \text{otherwise} \quad \text{(discharging).} \end{cases} \tag{2.19}$$

Storage elements can be placed between converters, at the hub's input side or at the hub's output side. The following equations can be obtained from Figure 2.3. From the figure it can be observed that power D_{α_i} flows to a storage element placed at the hub's input side and power M_{β_j} [kW] flows to a storage element placed at the hub's output side. Therefore, the input power $\widetilde{P}_{\alpha_i}$ [kW] and output power $\widetilde{L}_{\beta_j}$ [kW] of the converter cluster (represented by the shaded area) are given by:

$$\widetilde{P}_{\alpha_i} = P_{\alpha_i} - D_{\alpha_i} \tag{2.20}$$

$$\widetilde{L}_{\beta_j} = L_{\beta_j} + M_{\beta_j}. \tag{2.21}$$

In vector form, the balance equation around the converter cluster is:

$$\underbrace{[\mathbf{L} + \mathbf{M}]}_{\widetilde{\mathbf{L}}} = \mathbf{C}\,\underbrace{[\mathbf{P} - \mathbf{D}]}_{\widetilde{\mathbf{P}}} \tag{2.22}$$

which can be rewritten as [33]:

$$\mathbf{L} = \mathbf{CP} - \mathbf{M}^{\mathbf{eq}} \tag{2.23}$$

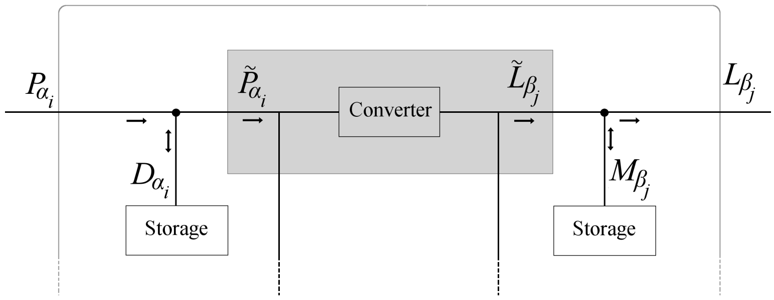

Figure 2.3: Storage elements in an energy hub

where

$$\mathbf{M^{eq}} = \mathbf{CD} + \mathbf{M}. \tag{2.24}$$

In this way all storage devices are mapped to the output side of the energy hub. The *storage coupling matrix* $\mathbf{S}$ contains all the couplings between the equivalent storage vector $\mathbf{M^{eq}}$ and the vector $\dot{\mathbf{E}}$, which contains the changes in energy content of the storage elements. The matrix that results is:

$$\underbrace{\begin{bmatrix} M^{eq}_{\beta_1} \\ M^{eq}_{\beta_2} \\ \vdots \\ M^{eq}_{\beta_{n_{out}}} \end{bmatrix}}_{\mathbf{M}^{eq}} = \underbrace{\begin{bmatrix} s_{\alpha_1\beta_1} & s_{\alpha_2\beta_1} & \cdots & s_{\alpha_{n_{in}}\beta_1} \\ s_{\alpha_1\beta_2} & s_{\alpha_2\beta_2} & \cdots & s_{\alpha_{n_{in}}\beta_2} \\ \vdots & \vdots & \ddots & \vdots \\ s_{\alpha_1\beta_{n_{out}}} & s_{\alpha_2\beta_{n_{out}}} & \cdots & s_{\alpha_{n_{in}}\beta_{n_{out}}} \end{bmatrix}}_{\mathbf{S}} \underbrace{\begin{bmatrix} \dot{E}_{\alpha_1} \\ \dot{E}_{\alpha_2} \\ \vdots \\ \dot{E}_{\alpha_{n_{in}}} \end{bmatrix}}_{\dot{\mathbf{E}}.} \tag{2.25}$$

Thus, after applying (2.25), the power balance equation can be reformulated as follows:

$$\mathbf{L} = \mathbf{CP} - \mathbf{S}\dot{\mathbf{E}} \tag{2.26}$$

where vector $\mathbf{L}$ contains the hub's power outputs, $\mathbf{C}$ contains the coupling factors, $\mathbf{P}$ represents the vector of the energy hub's power inputs, $\mathbf{S}$ is the storage coupling matrix and vector $\dot{\mathbf{E}}$ contains the changes in energy content of the storage elements.

In the case of multi-period problems, time variable t is introduced. The power balance equality becomes:

$$\mathbf{L}^t = \mathbf{C}^t\mathbf{P}^t - \mathbf{S}^t\dot{\mathbf{E}}^t \tag{2.27}$$

where $\dot{\mathbf{E}}^t$ contains the changes in energy content of the storage elements within period t. For a storage element that exchanges energy carrier α_i, the respective equation is [33]:

$$\dot{E}^t_{\alpha_i} = E^t_{\alpha_i} - E^{t-1}_{\alpha_i} + E^{stb}_{\alpha_i} \tag{2.28}$$

where $E^t_{\alpha_i}$ is the stored energy at the end of period t, and $E^{stb}_{\alpha_i}$ represents the stand-by energy losses per period.

In this case, the equality constraint for the dispatch factors is:

$$1 - \sum_{k_p \in C_{\alpha_i}} v^{k_p,t}_{\alpha_i} = 0. \tag{2.29}$$

The inequality constraints for the multi-period multi-carrier optimal power flow that result from adding the storage constraints are:

$$\underline{\mathbf{P}} \leq \mathbf{P}^t \leq \overline{\mathbf{P}} \tag{2.30}$$

$$\underline{P}_{\alpha_i}^{k_p} \leq \nu_{\alpha_i}^{k_p,t} P_{\alpha_i}^t \leq \overline{P}_{\alpha_i}^{k_p} \tag{2.31}$$

$$0 \leq \nu_{\alpha_i}^{k_p,t} \leq 1 \tag{2.32}$$

$$\underline{D}_{\alpha_i} \leq D_{\alpha_i}^t \leq \overline{D}_{\alpha_i} \tag{2.33}$$

$$\underline{M}_{\beta_j} \leq M_{\beta_j}^t \leq \overline{M}_{\beta_j} \tag{2.34}$$

$$\underline{\dot{\mathbf{E}}} \leq \dot{\mathbf{E}}^t \leq \overline{\dot{\mathbf{E}}} \tag{2.35}$$

$$\mathbf{E}^0 - \mathbf{E}^{n_\mathrm{t}} = 0 \tag{2.36}$$

where $t = 1, 2, \ldots, n_\mathrm{t}$, and $n_\mathrm{t} \in \mathbb{N}$. Energy carriers α_i are stored at the input side of the hub, and energy carriers β_j are stored at the output side. The last constraint states that the energy content at the initial time ($t = 0$) must be equal to the energy content at the last time period ($t = n_\mathrm{t}$). This constraint is added in order to bring the storage content at the end of the simulation back to the initial storage content.

2.3 Multi-Carrier Unit Commitment Framework

This section provides an extension to the work presented in the PhD dissertation "Integrated Modeling and Optimization of Multi-Carrier Energy Systems" [33], which was briefly introduced in Section 1.4.1. In this work, the author presented a general steady-state modeling and optimization framework using the energy hub approach for the following problems: multi-carrier optimal dispatch, multi-carrier optimal power flow, optimal hub coupling and optimal hub layout. The main contribution of this chapter is to extend the model in order to solve the multi-carrier unit commitment problem.

2.3.1 Multi-Carrier Unit Commitment Model

The problem statement described in Section 2.2.3 is used to solve a multi-carrier optimal dispatch problem for a defined operating point. An extension is necessary in order to solve the multi-carrier unit commitment problem, where the scheduling of units is involved. One of the main differences in relation to the problem statement presented in Section 2.2.3 is that the multi-carrier unit commitment does not deal with the power inputs of the energy hub, but in fact with the power inputs of the energy hub elements. Therefore, a new binary variable is introduced and the problem statement of the multi-carrier optimal dispatch is modified, as described later in this section.

The new variable specifies the status (on/off) of the energy hub elements; the corresponding symbol is $w_{\alpha_i}^{k_p}$. The new variable is included in the coupling factors as follows:

$$c_{\alpha_i\beta_j} = \sum_{k_p \in C_{\alpha_i}} w_{\alpha_i}^{k_p} \nu_{\alpha_i}^{k_p} \eta_{\alpha_i\beta_j}^{k_p} \quad \text{or} \quad c_{\alpha_i\beta_j} = \sum_{k_p \in C_{\alpha_i}} w_{\alpha_i}^{k_p} \nu_{\alpha_i}^{k_p} \mathscr{F}_{\beta_j}^{k_p}(P_{\alpha_i}). \tag{2.37}$$

The status variable $w_{\alpha_i}^{k_p}$ is equal to 1 when the hub element is turned on and is equal to 0 when the hub element is turned off. The equality constraint that deals with the dispatch factors depends now on the converters that are running, thus it becomes:

$$1 - \sum_{k_p \in C_{\alpha_i}} w_{\alpha_i}^{k_p} \nu_{\alpha_i}^{k_p} = 0. \tag{2.38}$$

Regarding the inequality constraints, the minimum power input limit of converter k_p is now multiplied by the status variable $w_{\alpha_i}^{k_p}$. In this way, the optimization program allows the input power to become zero when the respective energy hub element is turned off, however when it is turned on, the lower limit remains $\underline{P}_{\alpha_i}^{k_p}$:

$$w_{\alpha_i}^{k_p} \underline{P}_{\alpha_i}^{k_p} \leq \nu_{\alpha_i}^{k_p} P_{\alpha_i} \leq \overline{P}_{\alpha_i}^{k_p}. \tag{2.39}$$

The inequality constraint of the hub power input also depends on the status variables. The minimum power input limit of energy carrier α_i is now multiplied by the binary variable w_{α_i}, which is defined in terms of the status variables as follows:

$$w_{\alpha_i} \underline{P}_{\alpha_i} \leq P_{\alpha_i} \leq \overline{P}_{\alpha_i} \tag{2.40}$$

$$\text{where} \quad w_{\alpha_i} = \begin{cases} 0, & \text{if } \sum_{k_p \in C_{\alpha_i}} w_{\alpha_i}^{k_p} = 0 \\ 1, & \text{otherwise.} \end{cases}$$

When all $N_{C_{\alpha_i}}$ converters associated with a specific energy carrier α_i are turned off, $\sum_{k_p \in C_{\alpha_i}} w_{\alpha_i}^{k_p} = 0$, the optimization program allows the input power of this particular energy carrier to be zero. Conversely, when at least one converter associated with this energy carrier is running, $\sum_{k_p \in C_{\alpha_i}} w_{\alpha_i}^{k_p} \neq 0$, the lower limit remains $\underline{P}_{\alpha_i}$.

The objective function must be modified accordingly. For example, in the case of considering economic cost as the objective function, coefficient $\mathrm{K}_{4,\alpha_i}^{k_p}$ can be included to represent costs associated with the individual converters, as for example no-load costs. The resulting equation is:

$$\mathscr{F}_{\text{obj}} = \sum_{\alpha_i \in \mathcal{E}_{\text{in}}} (\mathrm{K}_{1,\alpha_i} + \mathrm{K}_{2,\alpha_i} P_{\alpha_i} + \mathrm{K}_{3,\alpha_i} P_{\alpha_i}^2) + \sum_{\alpha_i \in \mathcal{E}_{\text{in}}, k_p \in C_{\alpha_i}} (\mathrm{K}_{4,\alpha_i}^{k_p} w_{\alpha_i}^{k_p}). \tag{2.41}$$

The recursive algorithm known as *forward dynamic programming* is used to compute the minimum cost in the time interval T_{dp} with combination I_{dp}, as given in (2.42) [46]:

$$F_{\text{cost}}(T_{\text{dp}}, I_{\text{dp}}) = \min[F_{\text{prod}}(T_{\text{dp}}, I_{\text{dp}}) + F_{\text{tran}}((T_{\text{dp}} - 1), J_{\text{dp}} : T_{\text{dp}}, I_{\text{dp}}) + F_{\text{cost}}((T_{\text{dp}} - 1), J_{\text{dp}})] \tag{2.42}$$

where

$(T_{\text{dp}}, I_{\text{dp}})$	combination I_{dp} at time period T_{dp}
$((T_{\text{dp}} - 1), J_{\text{dp}})$	combination J_{dp} at time period $(T_{\text{dp}} - 1)$
$F_{\text{prod}}(T_{\text{dp}}, I_{\text{dp}})$	production cost for state $(T_{\text{dp}}, I_{\text{dp}})$
$F_{\text{cost}}(T_{\text{dp}}, I_{\text{dp}})$	least total cost to arrive at state $(T_{\text{dp}}, I_{\text{dp}})$
$F_{\text{tran}}((T_{\text{dp}} - 1), J_{\text{dp}} : T_{\text{dp}}, I_{\text{dp}})$	transition cost from state $((T_{\text{dp}} - 1), J_{\text{dp}})$ to state $(T_{\text{dp}}, I_{\text{dp}})$.

In the case of 4 units, arbitrary examples of unit combinations can be: $I_{dp} = [1001]$, $I_{dp} = [0011]$, $I_{dp} = [1111]$, etc. The unit is operating (committed) when the digit assigned is 1.

A *strategy* is the transition or path from one state at a given time period to a state at the next time period [46]. Two more variables that are used for the multi-carrier unit commitment are X_{dp} and N_{dp}, where X_{dp} is the number of states that are evaluated within each period and N_{dp} is the number of strategies that are saved at each period. These variables have influence on the computational effort [46]. If fixed costs are considered, they must be included in the equation, but outside the brackets.

Example: Multi-Carrier Unit Commitment Matrix Formulation

The example is based on the energy hub shown in Figure 2.2. It shows the coupling factors and the constraints of the multi-carrier optimal dispatch problem after being adapted to suit the multi-carrier unit commitment problem. In the example, there is no conversion from electricity to heat, thus the corresponding coupling factor c_{eq} is equal to zero. The power balance equality constraint for the example is:

$$\begin{bmatrix} L_e \\ L_q \end{bmatrix} - \begin{bmatrix} c_{ee} & c_{ge} \\ 0 & c_{gq} \end{bmatrix} \begin{bmatrix} P_e \\ P_g \end{bmatrix} = 0. \tag{2.43}$$

The coupling factor c_{ee}, c_{ge} and c_{gq} are now:

$$c_{ee} = w_e \tag{2.44}$$

$$c_{ge} = w_g^A v_g^A \eta_{ge}^A + w_g^B v_g^B \eta_{ge}^B \tag{2.45}$$

$$c_{gq} = w_g^A v_g^A \eta_{gq}^A + w_g^B v_g^B \eta_{gq}^B + w_g^C v_g^C \eta_{gq}^C. \tag{2.46}$$

The dispatch factor equality constraint for the example is:

$$1 - (w_g^A v_g^A + w_g^B v_g^B + w_g^C v_g^C) = 0. \tag{2.47}$$

The constraints in the problem statement are:

$$\begin{bmatrix} w_e \underline{P}_e \\ w_g \underline{P}_g \end{bmatrix} \le \begin{bmatrix} P_e \\ P_g \end{bmatrix} \le \begin{bmatrix} \overline{P}_e \\ \overline{P}_g \end{bmatrix} \tag{2.48}$$

$$\begin{bmatrix} 0 \\ 0 \\ 0 \end{bmatrix} \le \begin{bmatrix} v_g^A \\ v_g^B \\ v_g^C \end{bmatrix} \le \begin{bmatrix} 1 \\ 1 \\ 1 \end{bmatrix} \tag{2.49}$$

$$\begin{bmatrix} w_g^A \underline{P}_g^A \\ w_g^B \underline{P}_g^B \\ w_g^C \underline{P}_g^C \end{bmatrix} \le \begin{bmatrix} v_g^A P_g \\ v_g^B P_g \\ v_g^C P_g \end{bmatrix} \le \begin{bmatrix} \overline{P}_g^A \\ \overline{P}_g^B \\ \overline{P}_g^C \end{bmatrix} \tag{2.50}$$

where the value of the status variable w_e (related to the electric input P_e) is always 1, since it represents the connection to the public electrical grid at all times. The power flow P_e at the input is bidirectional, which means that electricity can be sold back to the grid when the CHPs produce more electricity than required by the load L_e. Other restrictions related to the multi-carrier unit commitment problem that can be considered are the minimum up and minimum down times for the converters. The start-up costs of the converters are included in the optimization under transition costs in (2.42) .

2.3.2 Multi-Carrier Unit Commitment Technique to Include Storage

This section presents a technique to include storage as part of a general unit commitment framework for energy systems with multiple energy carriers. The multi-carrier unit commitment problem is solved using forward dynamic programming.

The technique is depicted in Figure 2.4. Four consecutive steps are involved. At first, a unit schedule is obtained after running the multi-carrier unit commitment problem without considering storage, just as described in Section 2.3.1. This first schedule is considered as the starting point for Step 2.

At Step 2, the storage units are included as part of the system, as described in Section 2.2.4. At this stage, the program assigns a new dispatch to the scheduled generation units and the storage units. Thus, if there are units to be discarded after the inclusion of storage, it is expected that these units will dispatch at (close to) minimum capacity.

At Step 3 a fictitious bidirectional load is included instead of the storage units. This bidirectional load is loaded in accordance to the power values of the storage units that were obtained in Step 2 for each time period. The program runs the multi-carrier unit commitment again and a new schedule is obtained. It is expected that the units that were brought to their minimum capacity at Step 2 will now be turned off, if no minimum up or minimum down constraints are violated.

Step 4 runs a new multi-carrier optimal dispatch, including storage according to Section 2.2.4. This is considered the final solution.

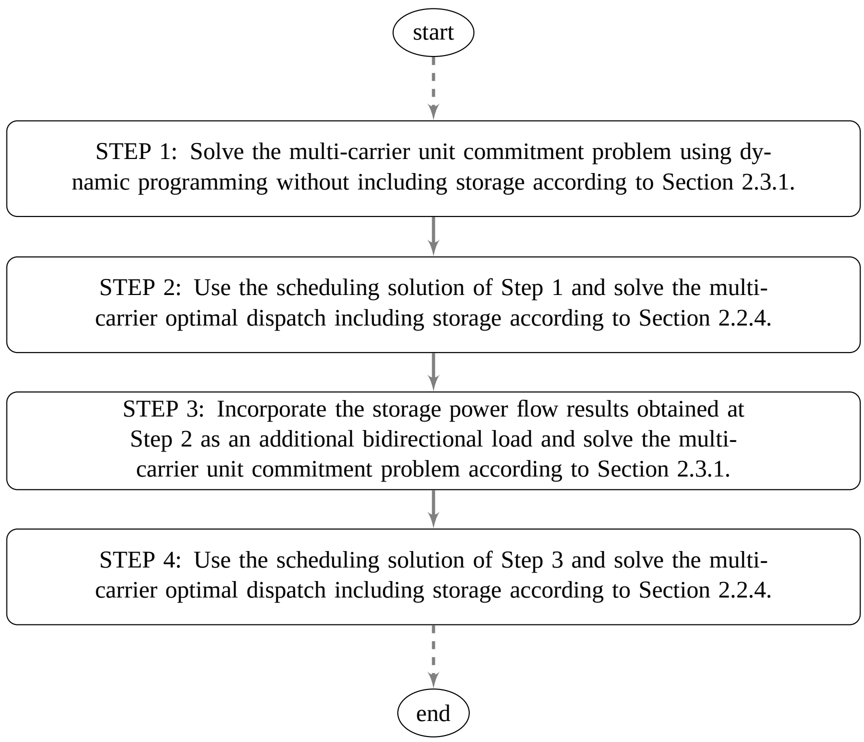

Figure 2.4: Flow chart of the proposed technique

2.4 Simulation Results

This section presents the results of two representative simulations. In the first simulation, no storage is included. In the second simulation, heat storage is considered. All the algorithms used in the simulations follow the descriptions that were presented in this chapter.

2.4.1 Simulation 1: Multi-Carrier Unit Commitment without Storage

In order to keep continuity in this chapter, the energy hub that was used in examples 1 and 2 is also used for the simulations contained in this section. The diagram of the energy hub can be observed in Figure 2.5. The system is connected to the electrical grid through input P_e. The data for electricity and gas costs were obtained from a German website that specifies real prices for small commercial customers [47]. The data can be found in Table 2.1. The multi-carrier unit commitment in this section is specified for time periods of 15 min, for this reason the data found in the website, specified in hours, were adapted to fit the selected time periods, as shown in Table 2.2.

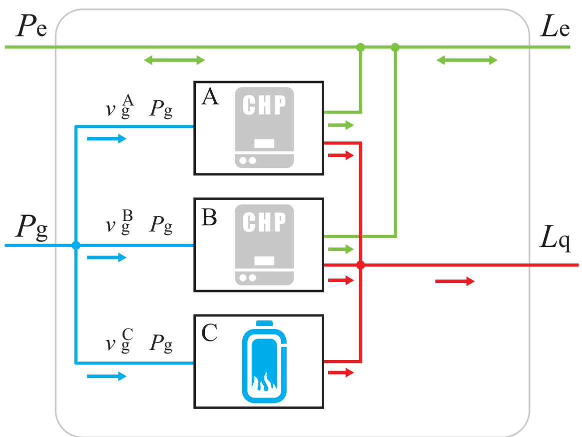

Figure 2.5: Energy hub representation for Simulation 1

Table 2.1: Prices for small commercial costumers at Nordhausen, Germany

Energy		Costs	
Carrier	Use per year (kWh)	Fixed (€)	Consumption (€/kWh)
Electricity	30 001 - 100 000	132,65	0,1897
Gas	2 375 - 12 692	73,50	0,0684
Heat	not specified	30,68	0,0558

Table 2.2: Prices for small commercial costumers used in this case study

Energy		Costs
Carrier	Use per year (kWh)	Consumption $\left(\frac{€}{\text{kW}\cdot(15\text{ min})}\right)$
Electricity	30 001 - 100 000	0,0474
Gas	2 375 - 12 692	0,0171
Heat	not specified	0,0140

Table 2.3: Parameters of the components used in this case study

Parameter	Unit	Component		
		CHP A A	CHP B B	Furnace C
Maximum electrical output	kW	35,00	23,00	-
Minimum electrical output	kW	3,00	2,00	-
Maximum change in power	$\%P_{\alpha_i,\max}$	50,00	50,00	50,00
Start-up duration	min	6,00	6,00	6,00
Minimal down time	min	30,00	30,00	-
Minimal up time	min	60,00	60,00	-
Maximum heat power	kW	45,00	30,00	80,00
Start-up cost	€/start	2,50	1,50	1,00
No-load cost	€/15 min	0,43	0,30	-

In this simulation, the price of electricity that is sold back to the public grid is considered to be 80% of the cost of electricity that is bought from the public grid, since utilities usually buy energy for a lower price than they sell it [34]. Furthermore, the specifications for the CHPs and the furnace were based on data found in [48], which were adapted for this case study. The values that are used in this work are shown in Table 2.3.

The dependency between the inputs and outputs of the converters is represented by the conversion efficiency. The values of the efficiencies were obtained from data of similarly sized components found in [33, 34]. The following values were used:

$$\eta_{\text{gq}}^{\text{A}} = 0,45 \quad \eta_{\text{ge}}^{\text{A}} = 0,35 \tag{2.51}$$

$$\eta_{\text{gq}}^{\text{B}} = 0,40 \quad \eta_{\text{ge}}^{\text{B}} = 0,30 \tag{2.52}$$

$$\eta_{\text{gq}}^{\text{C}} = 0,40. \tag{2.53}$$

The minimum input power is calculated from the minimum electrical power output given in Table 2.3 (the values are given in kW):

$$\underline{P}_{g}^{A} = \frac{\underline{L}_{e}^{A}}{\eta_{ge}^{A}} = \frac{3}{0,35} = 8,6 \tag{2.54}$$

$$\underline{P}_{g}^{B} = \frac{\underline{L}_{e}^{B}}{\eta_{ge}^{B}} = \frac{2}{0,30} = 6,7. \tag{2.55}$$

The maximum gas input of each converter is calculated below:

$$\overline{P}_{g}^{A} = \frac{\underline{L}_{q}^{A}}{\eta_{gq}^{A}} = \frac{45}{0,45} = 100 \tag{2.56}$$

$$\overline{P}_{g}^{B} = \frac{\underline{L}_{q}^{B}}{\eta_{gq}^{B}} = \frac{30}{0,40} = 75 \tag{2.57}$$

$$\overline{P}_{g}^{C} = \frac{\underline{L}_{q}^{C}}{\eta_{gq}^{C}} = \frac{80}{0,40} = 200. \tag{2.58}$$

The maximum gas input to the hub P_g is the sum of the gas input to the converters:

$$\overline{P}_{g} = \overline{P}_{g}^{A} + \overline{P}_{g}^{B} + \overline{P}_{g}^{C} = 375. \tag{2.59}$$

The software program SEPATH [49] is used to obtain the load patterns of 10 households (aggregated). The software randomizes a large selection of data that was obtained through a large survey [49]. After entering some information about the households to be studied, a week load pattern for electricity and heat is generated. In this simulation, the results are depicted for a period of 3 hours in time intervals of 15 minutes. The time range considered starts at 15:45 hours and ends at 18:45 hours. A random Saturday winter day pattern is used. In the Netherlands people habitually have dinner around 18:00 and during winter, sunset occurs somewhere between 16:30 and 18:30. Due to these reasons, an increase in the load pattern takes place during the selected period. The electric and heat load for the 12 intervals is shown in Table 2.4 and in Figure 2.6.

During the simulation, the 4 best strategies are saved by the program at each step. This corresponds to variable N_{dp} (see Section 2.3.1). The best final result is the optimal strategy for the multi-carrier unit commitment, in this case, the lowest total cost for the 12 periods that were considered.

Table 2.4: Electric and heat loads for the period under study in kW

	Time Period											
Load	1	2	3	4	5	6	7	8	9	10	11	12
L_e	10,1	9,9	7,4	8,5	11,9	14,8	14,6	19,2	19,8	16,3	11,0	5,9
L_q	10,6	22,9	26,4	37,6	52,9	54,1	72,3	87,9	88,2	48,1	32,4	33,3

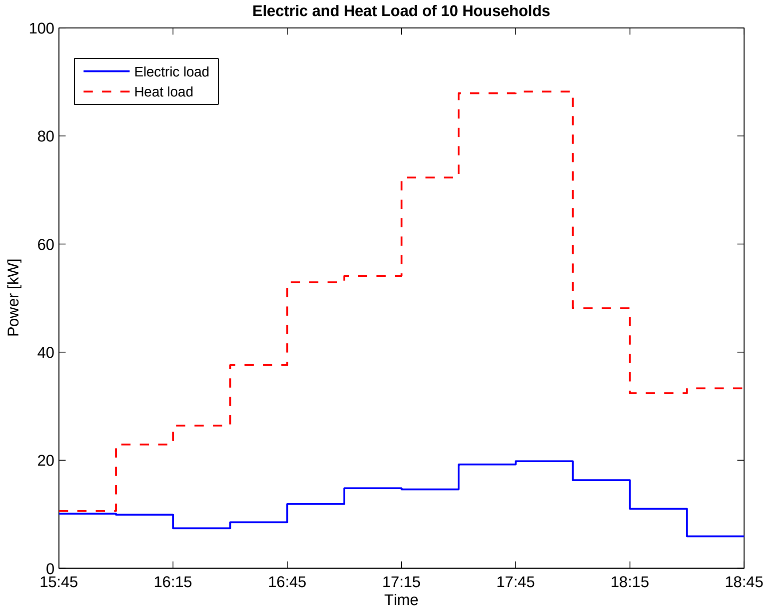

Figure 2.6: Electric and heat loads for the period under study in kW

Four cases are presented in this section:

- Case 1: this is the base case; no-load costs, start-up costs and minimum up and down time constraints are omitted.
- Case 2: this case includes no-load costs.
- Case 3: this case includes no-load costs and start-up costs.
- Case 4: this case includes no-load costs, start-up costs and minimum up and down time constraints.

Case 1

In this case only the operational costs are included. From the results shown in Table 2.5 it can be observed that the multi-carrier unit commitment is ruled by the efficiency of conversion of the components involved. The reason for this is that the costs increase as the efficiency decreases, since more fuel is necessary to provide the same output. CHP A (converter A) has the highest efficiency, followed by CHP B (converter B) and the furnace (converter C). Thus, the furnace operates only when the heat load is above 75 kW, which is the maximum heat power that can be delivered by the CHPs. This occurs in time intervals 8 and 9, which correspond to the time periods that go from 17:30 to 18:00 hours of the selected day. The distribution of load between the converters is the result of the multi-carrier optimal dispatch for each of the commitments shown in Table 2.5. The power values in Table 2.6 correspond to the electricity input P_{e} and the gas power inputs to each converter $P_{\mathrm{g}}^{\mathrm{A}}$, $P_{\mathrm{g}}^{\mathrm{B}}$ and $P_{\mathrm{g}}^{\mathrm{C}}$.

Table 2.5: Simulation 1: Multi-carrier unit commitment - Case 1 (best strategy)

		Time Period											
Converter	Component	1	2	3	4	5	6	7	8	9	10	11	12
	Grid	1	1	1	1	1	1	1	1	1	1	1	1
A	CHP A	1	1	1	1	1	1	1	1	1	1	1	1
B	CHP B	0	0	0	0	1	1	1	1	1	1	0	0
C	Furnace	0	0	0	0	0	0	0	1	1	0	0	0

Table 2.6: Simulation 1: Multi-carrier optimal dispatch - Case 1 (best strategy)

	Time Period											
	1	2	3	4	5	6	7	8	9	10	11	12
P_e	1,9	-7,9	-13,1	-20,7	-29,0	-27,0	-40,9	-38,3	-37,7	-21,0	-14,2	-20,0
P_g^A	23,6	50,9	58,7	83,6	100,0	100,0	100,0	100,0	100,0	100,0	72,0	74,0
P_g^B	0	0	0	0	19,8	22,8	65,3	75,0	75,0	7,8	0	0
P_g^C	0	0	0	0	0	0	0	32,3	33,0	0	0	0

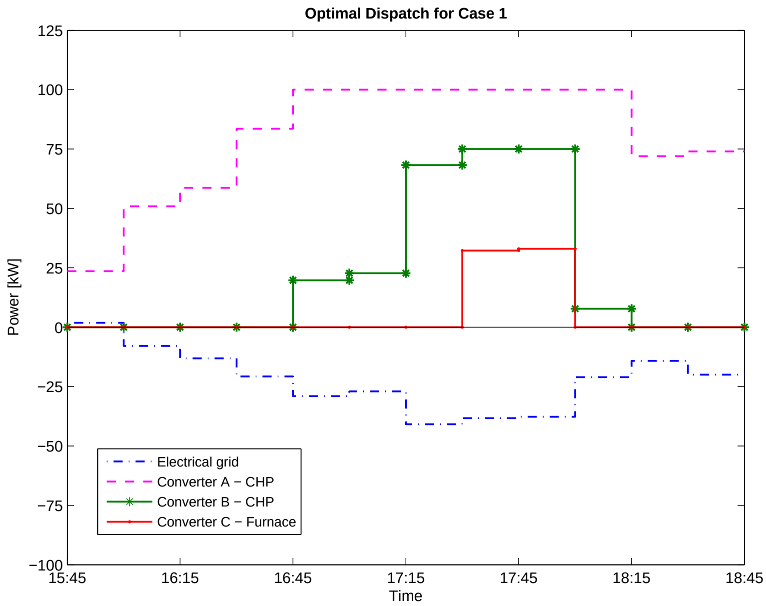

Figure 2.7: Simulation 1: Multi-carrier optimal dispatch - Case 1 (best strategy)

An interesting result can be observed at time period 2, where it is cheaper to sell electricity back to the grid than to use the furnace to produce the difference in the heat demand (Table 2.4 shows that from the first to the second period the electric load varies only 0,2 kW, but the heat demand is more than doubled). This occurs due to the fact that the total efficiency of CHP A is two times higher than the efficiency of the furnace. Moreover, the cost of gas is lower than the cost of electricity and the CHPs are gas-fueled. The total cost for the 12 time intervals is €30.

Case 2

In this case the no-load costs are included. The no-load costs for CHP B are lower than for converter A, as can be observed from Table 2.3. During the first time period this difference in no-load costs appears to be predominant in comparison to the difference in efficiencies. This can be observed in Table 2.7, where CHP B is used instead of CHP A, which has higher efficiency, but higher no-load costs. Similarly, in time periods 5, 6 and 10 it is cheaper to use the furnace, with no-load costs equal to zero, than to use CHP B, which has a higher efficiency. The total cost for the 12 time intervals in this case is €36,58.

Table 2.7: Simulation 1: Multi-carrier unit commitment - Case 2 (best strategy)

	Time Period											
Component	1	2	3	4	5	6	7	8	9	10	11	12
Grid	1	1	1	1	1	1	1	1	1	1	1	1
CHP A	0	1	1	1	1	1	1	1	1	1	1	1
CHP B	1	0	0	0	0	0	1	1	1	0	0	0
Furnace	0	0	0	0	1	1	0	1	1	1	0	0

Case 3

The start-up costs play an important role in this case since they are quite high: €2,5 for CHP A, €1,5 for CHP B and €1 for the furnace, as shown in Table 2.3. It is assumed that only CHP A is committed at the beginning of the simulation. The best strategy found by the program is to use the furnace continuously from time interval 5 to time interval 10, instead of turning it off during period 7, as proposed in the previous case.

Table 2.8 shows the multi-carrier unit commitment for this case. The total cost for the 12 intervals is €39,130. It is important to recall that the program chooses the best feasible path according to the options available for the 12 time periods. Thus, other solutions are possible, which may give a different commitment but with the downside of a higher total cost.

Table 2.8: Simulation 1: Multi-carrier unit commitment - Case 3 (best strategy)

	Time Period											
Component	1	2	3	4	5	6	7	8	9	10	11	12
Grid	1	1	1	1	1	1	1	1	1	1	1	1
CHP A	1	1	1	1	1	1	1	1	1	1	1	1
CHP B	0	0	0	0	0	0	1	1	1	0	0	0
Furnace	0	0	0	0	1	1	1	1	1	1	0	0

Case 4

This case considers the minimum down and up times. The minimum up time for CHP B is 60 min, i.e. 4 time intervals. The solution in Case 3 (which was the cheapest when considering the no-load costs and start-up costs) is not feasible in this case because of the minimum up time limitation. The multi-carrier unit commitment program selects the path that produces the lowest overall cost, which in this case corresponds to the strategy shown in Table 2.9. The total cost for the 12 intervals is €39,212.

Table 2.9: Simulation 1: Multi-carrier unit commitment - Case 4 (best strategy)

	Time Period											
Component	1	2	3	4	5	6	7	8	9	10	11	12
Grid	1	1	1	1	1	1	1	1	1	1	1	1
CHP A	1	1	1	1	1	1	1	1	1	1	1	1
CHP B	0	0	0	0	0	0	0	0	0	0	0	0
Furnace	0	0	0	0	1	1	1	1	1	1	0	0

In Figure 2.8 the optimal dispatch for this case is graphically depicted. It can be observed that CHP B is kept off during the simulation. The furnace is used to supply the heat load that was supplied by CHP B in Case 1. Moreover, the electricity that is sold to the grid is reduced in comparison to Figure 2.7 because CHP B does not participate in this case; as a consequence, the electricity produced is less. Due to the relatively high price that is paid for the electricity that is sold back to the grid (80% of the regular price for electricity), electricity is consumed from the grid only during the first time period, in the rest of the simulation the optimal results are obtained when electricity is injected back to the grid.

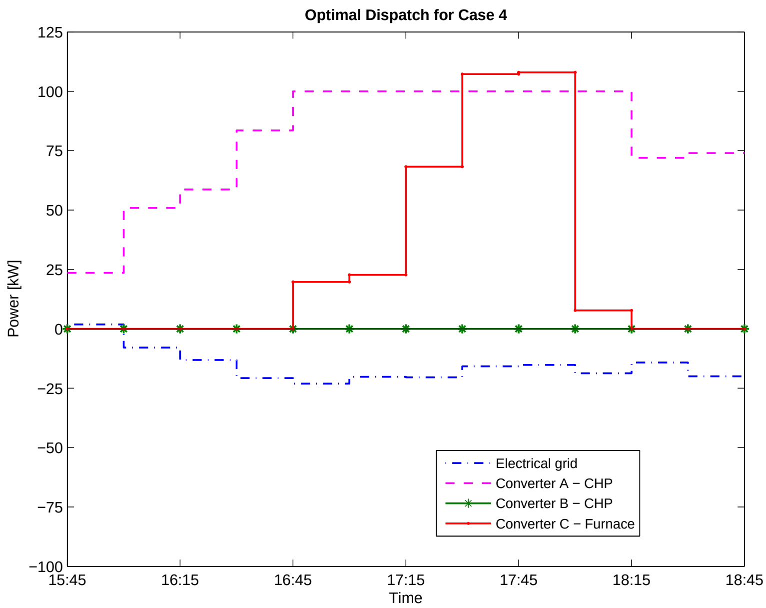

Figure 2.8: Simulation 1: Multi-carrier optimal dispatch - Case 4 (best strategy)

2.4.2 Simulation 2: Multi-Carrier Unit Commitment with Storage

In this simulation, heat storage is added at the output side of the energy hub. Figure 2.9 shows the resulting energy hub. The specifications for the storage unit are based on the data found in [33]. Some intermediate results are shown in this section to illustrate the four-step technique that was described in Section 2.3.2. The program runs and executes the four steps consecutively.

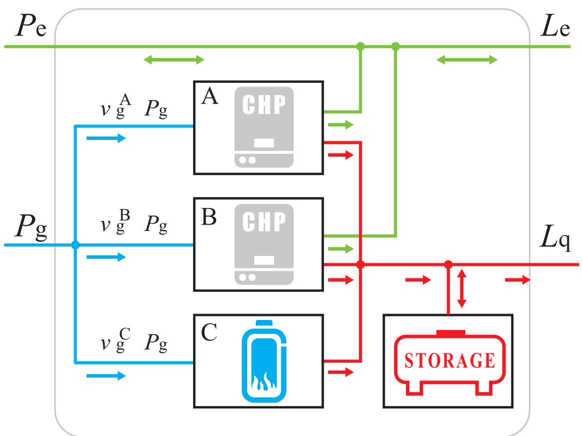

Figure 2.9: Energy hub representation for Simulation 2

The data for the prices, the hub elements and the load are the same that were used in Simulation 1, shown in Table 2.1, Table 2.3 and Table 2.4. The start-up prices are included but the minimum up and down times are set to zero in this simulation in order to show a clear variation in the commitment results due to the inclusion of storage and not to other constraints. Another change with respect to the previous simulation is that the minimum input power for the furnace is considered 1 kW ($\underline{P}_{\mathrm{g}}^{\mathrm{C}} = 1$), instead of zero as in the previous simulation. The data of the storage unit can be found below:

Table 2.10: Parameters of the storage element

Parameter	Unit	Storage
Minimum energy content	kW·(15 min)	68,00
Maximum energy content	kW·(15 min)	100,00
Maximum power (charge)	kW	15,00
Maximum power (discharge)	kW	-15,00
Charging efficiency e_{α_i}	%	0,85
Stand-by losses	kW/step	0,50
Initial energy content	kW·(15 min)	80,00
Final energy content	kW·(15 min)	80,00

In order to understand the results obtained from this simulation, let's first recall the steps included in the technique:

- Step 1: Solve the multi-carrier unit commitment problem using dynamic programming without including storage according to Section 2.3.1.
- Step 2: Use the scheduling solution from Step 1 and solve the multi-carrier optimal dispatch including storage according to Section 2.2.4.
- Step 3: Incorporate the storage power flow results obtained from Step 2 as an additional bidirectional load and solve the multi-carrier unit commitment problem according to Section 2.3.1.
- Step 4: Use the scheduling solution from Step 3 and solve the multi-carrier optimal dispatch including storage according to Section 2.2.4.

Step 1

After Step 1 has been completed, the unit schedule presented in Table 2.11 is obtained. At this step storage is omitted, thus the results are equal to the results obtained at Case 1 in Section 2.4.1. Likewise, the multi-carrier economic dispatch is the same as shown in Table 2.6; they are shown in Figure 2.10. The furnace is turned on at time periods 8 and 9, where the load is the highest.

Table 2.11: Simulation 2: Multi-carrier unit commitment - Step 1 (best strategy)

		Time Period											
Converter	Component	1	2	3	4	5	6	7	8	9	10	11	12
	Grid	1	1	1	1	1	1	1	1	1	1	1	1
A	CHP A	1	1	1	1	1	1	1	1	1	1	1	1
B	CHP B	0	0	0	0	1	1	1	1	1	1	0	0
C	Furnace	0	0	0	0	0	0	0	1	1	0	0	0

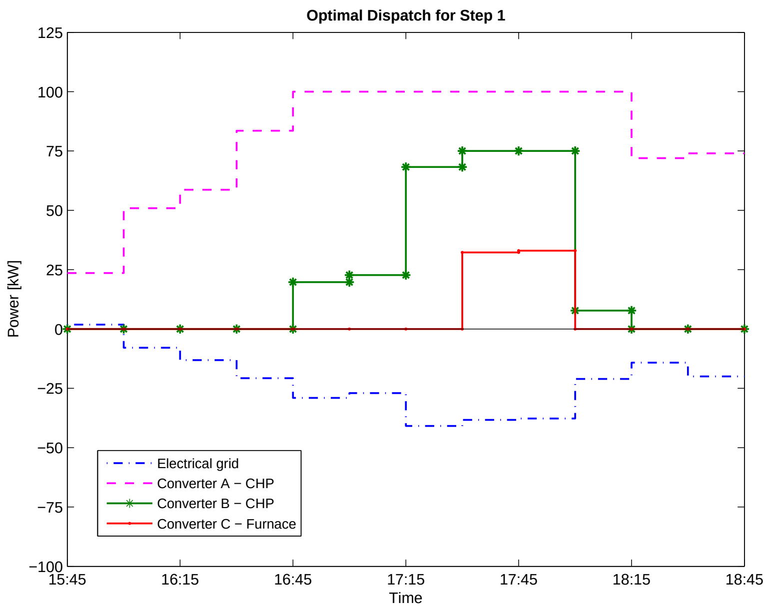

Figure 2.10: Simulation 2: Multi-carrier optimal dispatch - Step 1 (best strategy)

Step 2

At Step 2, the multi-carrier unit commitment shown in Table 2.11 is fixed as a pre-defined parameter. In this case the storage unit is included as part of the system and the multi-carrier optimal dispatch is solved. The results of the optimal dispatch can be observed in Figure 2.11. It can be noted that the furnace works at its minimum capacity ($\underline{P}_{g}^{C} = 1$) when the load is the highest, between 17:30 and 18:00. It is expected that it will be turned off as a result of Step 3, if no constraints are violated.

The storage bulk is charged during the first periods and discharged during the load peak. The energy content of the storage unit can be observed in Figure 2.12. It can be noted that the initial and final energy content is the same, as defined in one of the storage constraints.

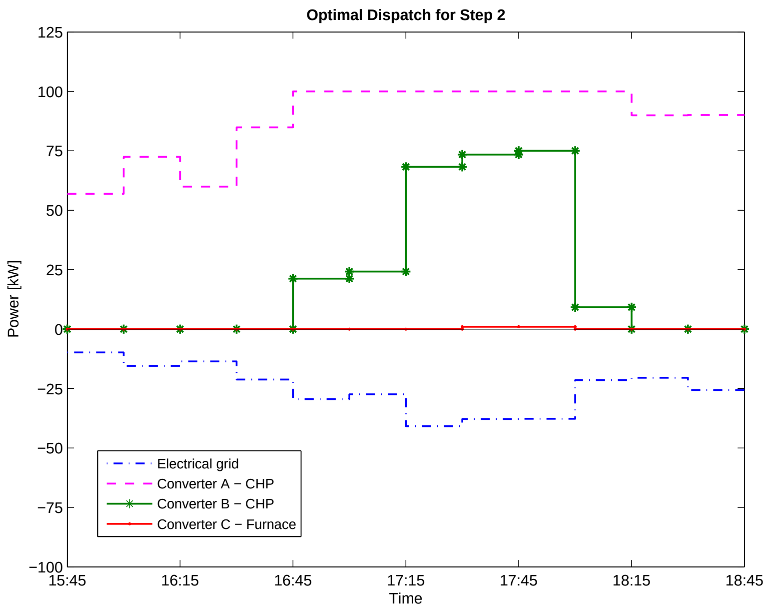

Figure 2.11: Simulation 2: Multi-carrier optimal dispatch - Step 2

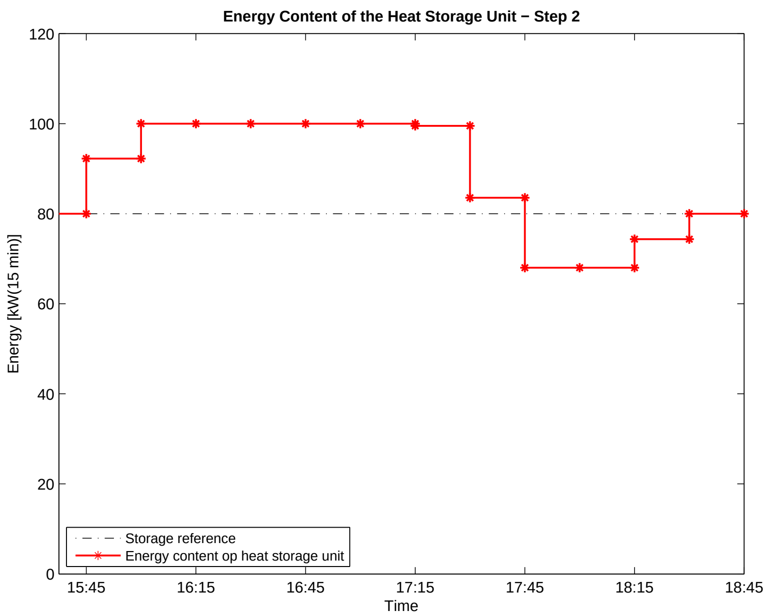

Figure 2.12: Simulation 2: Energy content of the storage element - Step 2

Step 3

In this step the dispatch values obtained from Step 2 for the storage unit are loaded as a fictitious bidirectional load. The program runs the multi-carrier unit commitment again and a new schedule is obtained. It is expected that the units that were brought to the minimum capacity at Step 2, will now be turned off. The results of the multi-carrier unit commitment in Table 2.12 show that the furnace is kept off during the whole simulation now that storage is considered, just as expected. This proves that the use of storage can influence the results of the multi-carrier unit commitment.

Table 2.12: Simulation 2: Multi-carrier unit commitment - Step 3 (best strategy)

		Time Period											
Converter	Component	1	2	3	4	5	6	7	8	9	10	11	12
	Grid	1	1	1	1	1	1	1	1	1	1	1	1
A	CHP A	1	1	1	1	1	1	1	1	1	1	1	1
B	CHP B	0	0	0	0	1	1	1	1	1	1	0	0
C	Furnace	0	0	0	0	0	0	0	0	0	0	0	0

Step 4

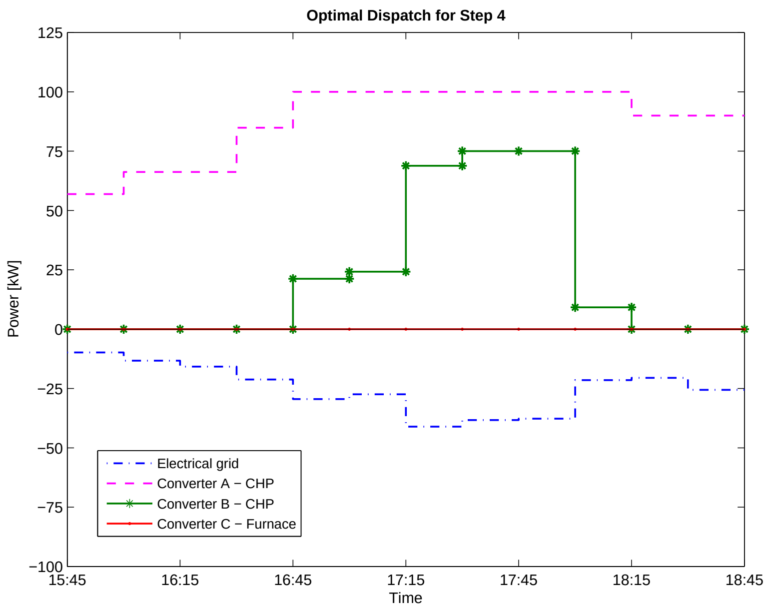

Figure 2.13: Simulation 2: Multi-carrier optimal dispatch - Step 4

Step 4 provides the final solution, shown in Figure 2.13. It can be noticed that CHP A has a higher production during the first periods than in the case where no storage was considered (see Figure 2.10). The extra heat is used to charge the storage tank at the beginning of the simulation. Consequently the storage unit is used to supply the load during the peak that occurs between 17:30 and 18:00. Thus, this technique enables generation peak-saving by the appropriate storage optimization.

With regard to the results of Step 1 (no storage) and Step 4 (with storage), a cost reduction was achieved from €32,5 to €28,5; this represents a 9,2%. In future research, the installation and operation costs of the storage unit can be considered to evaluate if the reduction in operation costs due to the storage optimization can surpass the investment costs. The energy content of the storage unit can be observed in Figure 2.14.

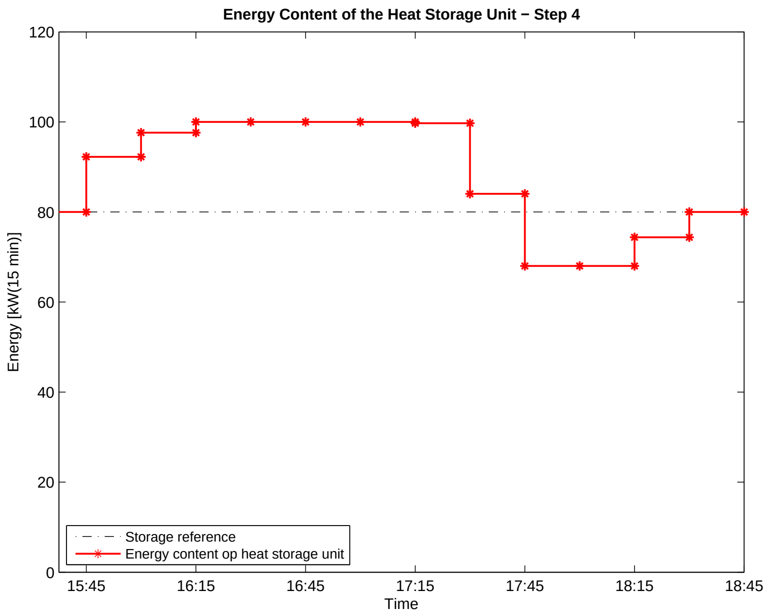

Figure 2.14: Simulation 2: Energy content of the storage element - Step 4

2.5 Conclusions

In this chapter, a general unit commitment framework for energy systems that contain multiple energy carriers was presented. The method was demonstrated with illustrative examples. Electricity and gas were used as input energy carriers due to the fact that the infrastructures for these energy carriers already exist and the prices are available. However, the framework proposed is suitable for any kind of energy carrier and for different possible couplings and power scales.

The use of the energy hub concept proved to be a suitable way to handle the conversion couplings that may exist between carriers. This way of analysis provides flexibility and was successfully applied for the development of the multi-carrier unit commitment framework.

The inclusion of storage proved to be valuable for generation peak-shaving purposes. The technique proposed allows an optimized use of storage in systems with multiple energy carriers. In the example, it was shown that storage has a significant influence on the results of the multi-carrier unit commitment and the optimal dispatch.

Chapter 3

The Approach

Energy or Exergy Optimization?

This chapter deals with Research Question 3 of this dissertation. Section 3.1 includes the main theoretical concepts that are applied. In Section 3.2 a literature review of exergy-related studies is presented. Section 3.3 introduces the optimization framework. Later in Section 3.4 the system under consideration and the component models are described. In Section 3.5 the results of the dispatch optimization and the scheduling optimization are presented. The conclusions of this chapter are presented in Section 3.6. Parts of this chapter have been published in [50].

3.1 Basic Concepts and Definitions

In order to perform an exergy-related study, it is necessary to get familiar with several theoretical concepts. Due to the multi-disciplinary nature of this dissertation, these concepts are included in the following subsections in order to assist the reader with understanding the general approach presented in this chapter.

3.1.1 Energetic Efficiency

The *energetic (or thermal) efficiency* is the ratio between the energy of the product and the energy of the source. It is denoted by η [-].

3.1.2 Exergetic Efficiency

The *exergetic efficiency* is the ratio between the exergy of the product and the exergy of the source. It is denoted by ε [-].

3.1.3 Energy Content of a Fuel

The *energy content of a fuel* is equal to the amount of heat that is produced during combustion and is calculated as the enthalpy difference between the substance and the combustion products, both at 25°C and 1 bar. There are two ways to compute the energy content of a fuel; it can be done in terms of the higher heating value (HHV) or in terms of the lower heating value (LHV). Since water is a product of combustion, HHV is the heat content of water when the water resulting from the combustion process is in liquid form and the LHV is the heat content of water when the water resulting from the combustion process is in gaseous form. The HHV gives an indication of the best possibilities of a fuel.

3.1.4 Specific Internal Energy

Specific internal energy u [J/kg] is the total amount of energy stored in a substance per kg. The change in internal energy is measured by adding or removing energy under constant volume [51].

3.1.5 Entropy Change

Entropy change ΔS [J/K] is associated with the extraction of an amount of heat ΔQ [J] from a reservoir with a given temperature T [K], as shown in (3.1):

$$\Delta S = \frac{\Delta Q}{T}. \tag{3.1}$$

The *increase of entropy principle* states that the entropy creation due to irreversibility is zero for ideal processes and positive for real ones, thus the magnitude of the entropy creation due to irreversibility is a measure of the irreversibility of a process [38, 43].

3.1.6 Specific Enthalpy

Specific enthalpy h [J/kg] can be defined as the total thermomechanical energy content of a mass for a given temperature per kg [38]. The change in enthalpy is measured by adding or removing energy under constant pressure. For solids and liquids, the difference between specific internal energy u [J/kg] and specific enthalpy h [J/kg] is very small, however for gases this difference cannot be neglected [51]. The equation that describes enthalpy is given as follows, where p [Pa] is pressure and v [m^3/kg] is the specific volume:

$$h = u + pv. \tag{3.2}$$

3.1.7 Carnot Cycle

The *Carnot cycle* is the most efficient cycle between any two temperatures [38, 51]. Thus the efficiency of the Carnot cycle (Carnot factor) [-], is the maximum efficiency that can be attained when work is produced out of heat that is extracted from one thermal energy reservoir and transferred to another thermal energy reservoir [51]. It is given by:

$$\text{Carnot factor} = \left(1 - \frac{T_{\text{ref}}}{T}\right) \tag{3.3}$$

where T [K] is the absolute temperature of the thermal energy reservoir and T_{ref} [K] is the reference temperature, for example the temperature of the environment.

3.1.8 First Law and Second Law of Thermodynamics

The *first law of thermodynamics*, also known as the law of conservation of energy states that energy can neither be created nor destroyed, but can be converted from one form to another. The energy content is the amount of energy required to bring a substance from the reference state to the actual state; it depends on conditions as temperature and pressure, and it is determined in relation to a reference state [51]. An energy balance analysis around a process or system accounts for all its energy. Thus, a general energy balance equation considers the energy that enters and leaves the process under study [38].

The *second law of thermodynamics* indicates that heat cannot be fully converted into work. Thus, the most energy-efficient closed cycle to perform the heat-to-work or work-to-heat conversion is the Carnot Cycle under ideal performance conditions [38]. The Kelvin-Planck formulation of the second law states the following [51]:

> *It is impossible for any system to operate in a thermodynamic cycle and deliver a net amount of energy by work to its surroundings while receiving energy by heat transfer from a single thermal energy reservoir.*

Thus, the second law of thermodynamics indicates that heat cannot be fully converted into work. Entropy production must be minimized in order to achieve an efficient energy use [38].

3.1.9 Exergy Definition

Different definitions of exergy can be found in the literature, some of them are:

- Exergy is defined as the work potential that is available in gas, fluid or mass as a result of its non-equilibrium condition relative to some reference condition [38].
- The exergy content of an energy carrier is the maximum amount of work that can be extracted from it, in general [51]:
  - Electricity is work, therefore, the exergy content is equal to the energy content.
  - For fuels, the exergy content is more or less equal to the energy content.
  - The exergy content of heat flows is smaller than the energy content.
- The property exergy defines the maximum amount of work that may theoretically be performed by bringing a resource into equilibrium with its surroundings through a reversible process [52].
- Exergy of a thermodynamic system is the maximum theoretical useful work (shaft work or electrical work) obtainable as the system is brought into complete thermodynamic equilibrium with the thermodynamic environment while the system interacts with this environment only. The total exergy of a system consists of: physical exergy (due to the deviation of the temperature and pressure of the system from those of the environment), chemical exergy (due to the deviation of the chemical composition of the system from that of the environment), kinetic exergy (due to the system velocity measured relative to the environment) and potential exergy (due to the system height measured relative to the environment) [53].

3.1.10 Energy and Exergy General Equations

The *general energy equation* is obtained from the energy balance statement of the first law of thermodynamics, thus for a process or a system under study, the energy entering the system is equal to the energy leaving the system [38]. The equation is divided by mass m [kg] at both sides, thus it contains specific energy values:

$$\underbrace{\underbrace{gz_1}_{\text{Potential energy in}} + \underbrace{\frac{v_1^2}{2}}_{\text{Kinetic energy in}} + \underbrace{u_1}_{\text{Internal energy in}} + \underbrace{p_1 v_1}_{\text{Flow work in}} + \underbrace{w_{in}}_{\text{Work in}}}_{\text{Energy in}}$$
$$= \underbrace{\underbrace{gz_2}_{\text{Potential energy out}} + \underbrace{\frac{v_2^2}{2}}_{\text{Kinetic energy out}} + \underbrace{u_2}_{\text{Internal energy out}} + \underbrace{p_2 v_2}_{\text{Flow work out}} + \underbrace{w_{out}}_{\text{Work out}}}_{\text{Energy out}} \tag{3.4}$$

where g [m/s^2] stands for the gravitational acceleration, z [m] stands for height/altitude, v [m/s] stands for velocity, u [J/kg] stands for specific internal energy, p [Pa] stands for pressure, v [m^3/kg] stands for specific volume, w_{in} [J/kg] stands for the work per kg that goes into the system, w_{out} [J/kg] stands for the work per kg that goes out of the system.

Exergy is an explicit property at steady-state conditions and its value can be calculated at any point of the system relative to a reference condition [38]. The *general specific exergy equation* is:

$$\begin{aligned} a = \underbrace{u - u_0}_{\text{Internal energy}} - \underbrace{T_0(s - s_0)}_{\text{Entropy}} + \underbrace{pv - p_0 v_0}_{\text{Work}} + \\ \underbrace{\frac{v^2}{2}}_{\text{Momentum}} + \underbrace{g(z - z_0)}_{\text{Gravity}} + \underbrace{\sum(\mu_{che} - \mu_0)n_{che}}_{\text{Chemical}} \end{aligned} \tag{3.5}$$

where u [J/kg] stands for specific internal energy, T [K] stands for temperature, s [J/(K·kg)] stands for specific entropy, p [Pa] stands for pressure, v [m^3/kg] stands for specific volume, v [m/s] stands for velocity, g [m/s^2] stands for the gravitational acceleration, z [m] stands for height/altitude, μ_{che} [J/mole] stands for chemical potential and n_{che} [mole/kg] stands for quantity of moles per unit mass. Subscript '0' denotes the reference state. The general specific exergy equation is often used under conditions where the gravitational, chemical and momentum terms can be neglected. In this dissertation, the *work* contribution in (3.5) is already included in the enthalpy definition formulated in (3.2). After using (3.2), in the case of steady flow systems, the resulting specific exergy a [J/kg] is [38]:

$$a = \underbrace{(h - h_0)}_{\text{Enthalpy}} - \underbrace{T_0(s - s_0)}_{\text{Entropy}} \tag{3.6}$$

where subscript '0' denotes the reference state. To compute the available potential work by bringing the system from operational state 1 to operational state 2, the following equation is used:

$$a = (h_2 - h_1) - T_0(s_2 - s_1). \tag{3.7}$$

Equation (3.7) is used for several calculations in Section 3.4. In an exergy analysis the principles of conservation of mass and conservation of energy in combination with the second law of thermodynamics are applied [40]. The conventional definition of energy provides the amount of Joules or British Thermal Units (BTUs) that are involved in the system or process, but does not provide information about the potential to make work of the Joules or BTUs involved. Here is where exergy provides valuable information by indicating the work potential availability in those Joules or BTUs.

3.1.11 Generalities of the Exergy Method

The exergy method answers the question of where, how, why and how much of the available work is lost in the system [38]. This method is based on evaluating the work that is available at different points of the system; in this way, the quantity and location of the lost/useful work can be detected [38]. This method can be used for designing new systems and for evaluating existing ones.

If no useful work is done in the process, the change represents a loss in available work [38]. In [38], the author discusses the importance of choosing a proper reference condition for the system. He argues that using a common reference base like the surrounding environment as the ultimate heat sink is suitable for making valid comparisons between different types of plants. Nevertheless, he points out that there are specific conditions where it is more practical to choose other references according to the characteristics of the system. In this dissertation, different plants are compared; furthermore the surrounding environment can act as the infinite sink. For these reasons the reference condition chosen is the surrounding environment.

A general exergy equation can be obtained by adding up all exergies related to an specific point, as shown in (3.5). Exergy losses are generated by the production of entropy due to non-ideal performance of processes. A high exergy loss in a particular system may indicate that there is a poor match between the quality of energy supplied and the quality of energy required in that specific system, which results in large irreversible losses [38].

3.2 Literature Review

During the last decade, several articles, books and academic documents have promoted exergy analysis as a better tool to assess energy systems than a traditional energy analysis. For example in [43], benefits of using exergy-based rather than energy-based measures for efficiency and losses are presented. The author argues that efficiencies based on energy can often be nonintuitive or misleading, partly because energy efficiencies do not provide a measure of how close a process approaches ideal conditions. The author also states that energy losses can be large in quantity, nevertheless, they may not be that significant thermodynamically due to the low potential to make work of the energy that is lost.

The author M. Rosen has published several papers in the area of exergy [42, 43, 54–58]. One of the main messages given in his work is that exergy analysis provides insights into efficiency improvement and environmental-impact reduction in systems and processes. He argues that in complex systems with multiple products (e.g., cogeneration and trigeneration plants), exergy methods can help evaluate thermodynamic values of different product energy forms, even though they normally exhibit very different characteristics. This statement is closely related to the kind of systems regarded in this dissertation, where multiple energy carriers are involved. Additionally, he indicates that in order to motivate engineers to use exergy, joint efforts must be made to point out the benefits of using exergy methods clearly and unambiguously. This chapter is an effort to show the added value of using exergy to analyze energy supply systems with multiple energy carriers.

The exergy analysis has been introduced to various fields of study, among them, renewable energy, exergoeconomics, industrial ecology, building design and the transportation sector [59–67]. In the area of building design, the topic of exergy has gained attention particularly during the last decade; related works can be found in [40, 68–71].

The following shortcomings were found in the literature that was analyzed:

- Most literature is focused on simple and single processes and not on complex systems with multiple energy carriers.
- In several papers, the term *optimization* is commonly referred to as the improvement of a system with respect to an initial selection of parametric set-points and not as the local or global minimum in a solution.
- Some papers do not provide insight about the benefits of using an exergy analysis with respect to an energy analysis.

In order to overcome these limitations, in this chapter an optimization tool capable of finding the optimal scheduling of units in a system with multiple energy carriers is introduced. In the following paragraphs some examples are discussed in which an exergy optimization of systems was aimed but in which one or more of the listed limitations were found.

In the area of renewable energy, most of the exergy-related papers focus on a single type of energy source. For example, in [59] an energy and exergy analysis of an integrated solar combined cycle system is performed using the design plant data. Moreover, numerous exergy studies have been performed about geothermal energy systems [60–62]. Geothermal energy is to some extent considered a renewable energy source since it usually has a projected life of 30 to 50 years [60].

Another example in the topic of renewable energy can be found in [63], where energy and exergy analyses are performed to four different wind power systems, including horizontal and vertical axis wind turbines. Their work is based on [64], where an efficiency formula based on exergy values for wind energy systems is developed and described. The technique utilizes the wind chill temperature associated with the wind velocity to predict the entropy generation of the process. Their approach is valuable for the design of wind turbines since it quantifies the exergy loss that occurs in the process of generating electricity from the kinetic energy of the wind. Similarly in [65], the exergetic efficiency of a wind turbine is calculated. The authors define the exergetic efficiency as a measure of how well the stream of exergy of the fluid is converted into useful turbine work output or inverter work output. They consider that the availability of the blowing air, in other words the exergy of the blowing air, is simply the kinetic energy it possesses.

In [66] an optimization strategy is proposed where the cost/efficiency ratio is varied and the optimal allocation of renewable energy is determined. One of the limitations in the approach is that it assumes fixed percentages of utilization of the sources for the optimization.

In [72], three different renewable energy systems are studied: solar energy, wind power and geothermal energy. The paper provides the equations to obtain the exergy efficiencies of each system, gives the corresponding results and makes a comparison between renewable and non-renewable sources.

Exergoeconomics is a branch of engineering that combines thermodynamic evaluations based on an exergy analysis with economic principles in order to provide useful information for the design and operation of a cost-effective system [53]. In the literature, a large percentage of exergoeconomic studies have been performed in geothermal systems, as in [73–75]. In [76], prices for energy and exergy of various energy sources along with their CO_2 equivalents are calculated. Detailed tables are provided for the different fuels considered. Even though this kind of studies provides an interesting insight by defining prices and costs based on exergy values of the fuels, an exergoeconomical-oriented approach will not be followed in this dissertation.

The field of industrial ecology emerged from efforts to reduce depletion and to move towards a more sustainable utilization of resources [52, 77]. In [52] an analogy between ecosystem evolution processes and industrial processes is made. By means of this analogy, consumption is interpreted as a process of exergy removal. The authors argue that this approach allows an improved understanding and analysis of the interrelated roles that cycling, cascading, efficiency gains and renewed exergy use may play. This is an example where finding analogies facilitates the use of the exergy analysis in systems where this concept had not been used before.

In the area of building design, the topic of exergy has gained attention particularly during the last decade, related works can be found in [40, 68–71]. Fossil fuels burn at very high temperatures, therefore their work potential is largely wasted when fossil fuels are utilized for hot water heating, space heating or even industrial steam production in building infrastructures, where low-temperature heat is desired [40]. This is also the case in residential district infrastructures, like those considered in this dissertation. The building sector has a very low exergetic efficiency of energy utilization, as a result atmosphere is polluted unnecessarily [40]; likewise, residential district infrastructures, having similar load patterns and heating infrastructures, have a considerable low exergetic efficiency, and thus, have a high potential for improvement.

Only one paper was found in the literature in which the concepts of exergy and the energy hub were combined [67]. In [67] the objective function to be minimized is the inverse equation of the total exergetic efficiency of the system, thus the optimization maximizes the system's exergetic efficiency. Moreover, the interactions between the energy carriers are represented by the energy hub coupling matrix, which contains the energy efficiencies of the units. In the paper, a comparison is made between the optimal dispatch of units obtained by maximizing the exergetic efficiency and the optimal dispatch obtained by minimizing the costs. Even though the results give some insight by stating that the most efficient solution in terms of exergy may not always be the same as the one obtained from the most economical solution, the paper does not give any indication about the results that would be obtained from maximizing the energetic efficiency in relation to maximizing the exergetic efficiency. This comparison would provide insight about differences between the analysis and optimization of systems using energy and exergy, which is a topic of dispute.

In complex systems involving more than one generation unit and multiple energy carriers, the differences that may exist between making an energy or an exergy analysis have not clearly been presented in the literature yet. This chapter provides concrete comparisons between performing an energy and an exergy optimization in a multi-carrier energy supply system.

3.3 Exergy Optimization Approach

3.3.1 Exergy Hub Conversion Model

In the energy hub approach, a coupling matrix is used to represent the interactions among the energy carriers that are contained in the energy hub. In this chapter, the systems to be studied are represented in terms of exergy values, for this reason the term *exergy hub* was selected to refer to the approach presented. The exergy hub model uses a coupling matrix that contains the steady-state exergy efficiencies of each of the hub elements. Just like in the energy hub approach, the input and output exergy flows are coupled by a coupling factor. For a system with one input energy carrier α and one output energy carrier β, the coupling factor $b_{\alpha\beta}$ [-] is used to define the relation between the steady-state input exergy flow $\mathit{\Xi}_\alpha$ [kW] and the steady-state output exergy flow $\mathit{\Gamma}_\beta$ [kW] of the exergy hub:

$$\mathit{\Gamma}_\beta = b_{\alpha\beta}\mathit{\Xi}_\alpha \tag{3.8}$$

where input energy carrier α is converted into the output energy carrier β. For several energy carriers the variables α_i and β_j are used as defined in Chapter 2. The matrix that represents a system with multiple energy carriers is shown in (3.9):

$$\underbrace{\begin{bmatrix} \mathit{\Gamma}_{\beta_1} \\ \mathit{\Gamma}_{\beta_2} \\ \vdots \\ \mathit{\Gamma}_{\beta_{n_\mathrm{out}}} \end{bmatrix}}_{\mathbf{\Gamma}} = \underbrace{\begin{bmatrix} b_{\alpha_1\beta_1} & b_{\alpha_2\beta_1} & \dots & b_{\alpha_{n_\mathrm{in}}\beta_1} \\ b_{\alpha_1\beta_2} & b_{\alpha_2\beta_2} & \dots & b_{\alpha_{n_\mathrm{in}}\beta_2} \\ \vdots & \vdots & \ddots & \vdots \\ b_{\alpha_1\beta_{n_\mathrm{out}}} & b_{\alpha_2\beta_{n_\mathrm{out}}} & \dots & b_{\alpha_{n_\mathrm{in}}\beta_{n_\mathrm{out}}} \end{bmatrix}}_{\mathbf{B}} \underbrace{\begin{bmatrix} \mathit{\Xi}_{\alpha_1} \\ \mathit{\Xi}_{\alpha_2} \\ \vdots \\ \mathit{\Xi}_{\alpha_{n_\mathrm{in}}} \end{bmatrix}}_{\mathbf{\Xi}}. \tag{3.9}$$

When several converters k_p are considered, the coupling factor $b_{\alpha_i\beta_j}$ [-] that takes into account the participation of each converter k_p can be expressed as:

$$b_{\alpha_i\beta_j} = \sum_{k_p \in C_{\alpha_i}} \nu_{\alpha_i}^{k_p} \varepsilon_{\alpha_i\beta_j}^{k_p} \tag{3.10}$$

where $\nu_{\alpha_i}^{k_p}$ [-] is the dispatch factor that represents the percentage of input exergy flow $\mathit{\Xi}_{\alpha_i}$ [kW] that is provided to converter k_p and $\varepsilon_{\alpha_i\beta_j}^{k_p}$ [-] is the exergetic efficiency of conversion from energy carrier α_i to β_j of converter k_p.

3.3.2 Problem Statement

The output exergy flow vector $\mathbf{\Gamma}$ is equal to the coupling matrix $\mathbf{B}$ multiplied by the respective input exergy flow vector $\mathbf{\Xi}$. This represents the exergy balance equality constraint:

$$\mathbf{\Gamma} - \mathbf{B}\mathbf{\Xi} = \mathbf{0}. \tag{3.11}$$

The sum of dispatch factors $\nu_{\alpha_i}^{k_p}$ related to each energy carrier α_i is equal to 1. Thus, the dispatch factor equality constraint is:

$$1 - \sum_{k \in C_{\alpha_i}} \nu_{\alpha_i}^{k_p} = 0. \tag{3.12}$$

The inequality constraints are given by the lower and upper limits of the hub's exergy flow inputs $\left(\underline{\Xi}_{\alpha_i}, \overline{\Xi}_{\alpha_i}\right)$ [kW], of the converter units' power inputs $\left(\underline{\Xi}_{\alpha_i}^{k_p}, \overline{\Xi}_{\alpha_i}^{k_p}\right)$ [kW] and of the dispatch factors:

$$\underline{\Xi}_{\alpha_i} \leq \Xi_{\alpha_i} \leq \overline{\Xi}_{\alpha_i} \tag{3.13}$$

$$\underline{\Xi}_{\alpha_i}^{k_p} \leq \nu_{\alpha_i}^{k_p} \Xi_{\alpha_i} \leq \overline{\Xi}_{\alpha_i}^{k_p} \tag{3.14}$$

$$0 \leq \nu_{\alpha_i}^{k_p} \leq 1. \tag{3.15}$$

Three different objective functions are used for the optimizations presented in this chapter. The first objective function is based on the exergetic efficiency of the system, the second one is based on the energetic efficiency and the third one on the price of the fuels involved.

In the first case, the objective function that is minimized is inversely proportional to the exergetic efficiency of the system under study ε_{tot} [-], in this way the exergetic efficiency of the system is maximized. The corresponding equation is:

$$\mathscr{F}_{\text{obj1}} = \frac{1}{\varepsilon_{\text{tot}}} = \frac{\Xi_{\text{inp}}}{\Gamma_{\text{out}}} \tag{3.16}$$

where ε_{tot} is the total exergetic efficiency of the system, Ξ_{inp} [kW] is equal to the sum of the exergy flow brought to the system by the input fuels and Γ_{out} [kW] is equal to the sum of the exergy flow used by the loads at the output side of the hub.

Analogously, in the second case, the objective function that is minimized is inversely proportional to the energetic efficiency of the system under study η_{tot} [-]. The corresponding equation is:

$$\mathscr{F}_{\text{obj2}} = \frac{1}{\eta_{\text{tot}}} = \frac{P_{\text{inp}}}{L_{\text{out}}} \tag{3.17}$$

where η_{tot} [-] is the total energetic efficiency of the system, P_{inp} [kW] is equal to the sum of the power brought to the system by the input fuels and L_{out} [kW] is equal to the sum of the power used by the loads at the output side of the hub.

Finally, the objective function of the cost minimization [€/(time period)] is a quadratic equation that depends on the energy prices and the input powers of the hub:

$$\mathscr{F}_{\text{obj3}} = \sum_{\alpha_i \in \mathscr{E}_{\text{in}}} (\mathrm{K}_{1,\alpha_i} + \mathrm{K}_{2,\alpha_i} P_{\alpha_i} + \mathrm{K}_{3,\alpha_i} P_{\alpha_i}^2) \tag{3.18}$$

where K_{1,α_i}, K_{2,α_i} and K_{3,α_i} are cost coefficients.

3.4 Exergy Calculation Models and Data

3.4.1 System Representation: Energy Hub versus Exergy Hub

The hub that will be used for the illustrative examples consists of two combined heat and power units, a furnace, a heat pump and a connection to the public electrical grid. The hub's inputs are natural gas, biomass and electricity coming from the grid. The hub's load consists of an electric load and a heat load. The set of input carriers is defined as $\mathcal{E}_{\text{in}} = \{\text{e,g,b}\}$, where 'e' stands for electricity coming from the grid, 'g' stands for natural gas and 'b' stands for biomass. The set of output carriers is defined as $\mathcal{E}_{\text{out}} = \{\text{e,q}\}$ where 'e' stands for electricity and 'q' stands for heat. The selected system serves as an example to demonstrate the tool.

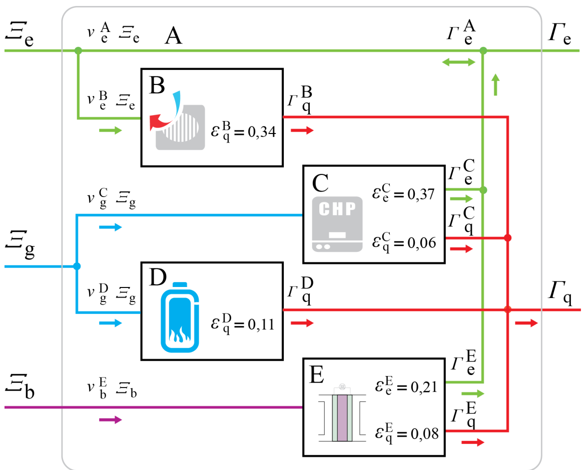

Figure 3.1: Exergy hub representation

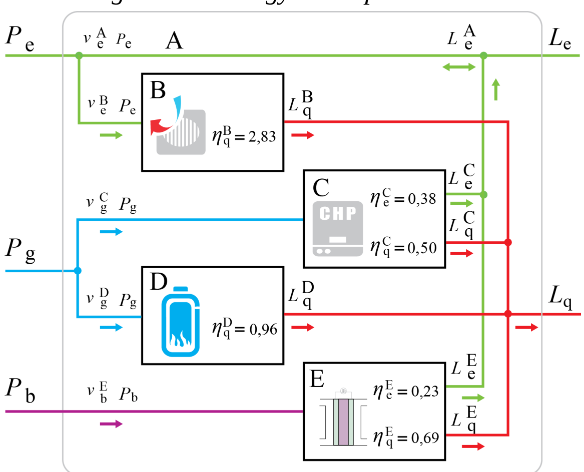

Figure 3.2: Energy hub representation

Direct connection A represents the direct connection with the electrical grid, converter B represents the electricity-driven heat pump, converter C represents the gas turbine (gas-fired CHP), converter D represents the gas-fired furnace and converter E represents the fuel cell system (biomass-fired CHP). Thus, the set of converters is defined as $C_{\alpha_i} = \{A,B,C,D,E\}$.

The exergy hub gives a better representation of what some authors call the *real* efficiency of the units. In the exergy hub, each hub element has an exergetic efficiency associated with it. By comparing Figure 3.1 and Figure 3.2 it is possible to identify which components appear to be very efficient from an energetic point of view, but are not so efficient from an exergetic point of view. A good example is the gas-fired furnace (converter D), which has an energetic efficiency of 96%, whereas an exergetic efficiency of only 11%.

It is interesting to observe that by comparing both the exergy hub and the energy hub representations it is possible to identify that a component may be more efficient from an energetic point of view than another, but less efficient from an exergetic point of view. For example the biomass-fired CHP (converter E) in Figure 3.2 has a total energetic efficiency of 92%, higher than the energetic efficiency of the gas-fired CHP unit (converter C), which has an energetic efficiency of 88%. However, from an exergetic point of view the biomass-fired CHP has an exergetic efficiency of 29%, lower than that of the gas-fired CHP unit, which has an exergetic efficiency of 43%. This difference plays an important role in the optimization results, as will be shown in Section 3.5.

As mentioned in Section 3.1.9, exergy is the maximum theoretical useful work that can be obtained from a source, thus from a sustainable point of view, it is better to look for ways to use the largest amount of exergy that a source can offer than to look only at its energetic performance and be satisfied with a good indicator value.

3.4.2 Energetic and Exergetic Efficiencies of Generation Units

In order to make an exergy analysis, the exergy content of the exergy flows involved is determined. Depending on the energy carrier, different operations are required to calculate the exergy content of the energy flow. The component efficiencies are usually modeled as constants, whereas in reality those will vary over the input range of the component. Ideally, the coupling matrix **B** would include an extensive formula for each component in order to describe the dynamic behavior and its effect on the component efficiency. This formula would be a combination of all the physical processes in the hub elements. Nevertheless, in this chapter constant values are used in order to reduce the complexity of the examples. In the following subsections, the hub elements will be briefly described. The respective data can be found in Table 3.1. The total energetic efficiency of component k_p, denoted by $\eta^{k_p}_{\alpha_i,\mathrm{tot}}$ [-], is given by (3.19), the total exergetic efficiency $\varepsilon^{k_p}_{\alpha_i,\mathrm{tot}}$ [-] is given by (3.20):

$$\eta^{k_p}_{\alpha_i,\mathrm{tot}} = \eta^{k_p}_{\alpha_i\mathrm{e}} + \eta^{k_p}_{\alpha_i\mathrm{q}} \tag{3.19}$$

$$\varepsilon^{k_p}_{\alpha_i,\mathrm{tot}} = \varepsilon^{k_p}_{\alpha_i\mathrm{e}} + \varepsilon^{k_p}_{\alpha_i\mathrm{q}}. \tag{3.20}$$

where $\eta^{k_p}_{\alpha_i\mathrm{e}}$ [-] is equal to the electrical conversion energetic efficiency of converter k_p, $\eta^{k_p}_{\alpha_i\mathrm{q}}$ [-] is equal to the thermal conversion energetic efficiency of converter k_p, $\varepsilon^{k_p}_{\alpha_i\mathrm{e}}$ [-] is equal to the electrical conversion exergetic efficiency of converter k_p and $\varepsilon^{k_p}_{\alpha_i\mathrm{q}}$ [-] is equal to the thermal conversion exergetic efficiency of converter k_p.

3.4.3 Natural Gas Supply and Biomass Supply (Ξ_g, Ξ_b)

The fuel inputs, natural gas and biomass, are chemical energy flows and thus chemical exergy flows. Chemical energy is often calculated using the lower heating value [78], represented in this thesis by $\Upsilon_{\mathrm{LHV},\alpha_i}$ [J/kg] of carrier α_i. In order to calculate the specific exergy a_{α_i} [J/kg] of the fuel input α_i, the exergy factor ζ_{α_i} [-] is introduced. This factor varies per fuel type and is close to unity. The relationship is described in (3.21) and (3.22), where $\phi_{\mathrm{m},\alpha_i}$ [kg/s] is the mass flow and Ξ_{α_i} [kW] is the exergy flow. The exergy factor of natural gas is $\zeta_g = 1,04$ [79], the exergy factor of biomass is $\zeta_b = 1,1069$ (deduced from values in [80]):

$$a_{\alpha_i} = \Upsilon_{\mathrm{LHV},\alpha_i}\zeta_{\alpha_i} \tag{3.21}$$

$$\Xi_{\alpha_i} = \left(a_{\alpha_i}\phi_{\mathrm{m},\alpha_i}\right)\frac{1}{10^3}. \tag{3.22}$$

3.4.4 Electricity Supply (Ξ_e) and Electricity Demand (Γ_e)

An electrical energy flow has an equal exergy content to its energy content (it can be fully converted into work). This is both applicable for the grid input power as for the electrical output power of the CHPs:

$$\Xi_e = P_e \tag{3.23}$$

$$\Gamma_e = L_e. \tag{3.24}$$

In order to calculate the system's efficiency, the electricity that comes from the grid is divided by the exergetic/energetic efficiency of the centralized generation plant with which it is produced. The centralized plants consist of steam generation units fueled by natural gas. These generation units have efficiencies of only 33% to 35% [81]. In this work it is assumed that the energetic efficiency of the centralized generation plant is $\eta_{\mathrm{gen,e}}$ = 33,28% and the exergetic efficiency is $\varepsilon_{\mathrm{gen,e}}$ = 32%. These values were selected arbitrarily.

3.4.5 Heat Load (Γ_q)

The district heating demand represents the heat load in the system under study. The thermal energy flow represents the mass flow $\phi_{\mathrm{m,wat}}$ [kg/s] of water. The heat load decreases the temperature (and thereby the enthalpy) of the working fluid. In the model representing the physical processes, the temperature levels are controlled on reference temperature levels: T_{col} = 53 °C and T_{hot} = 80 °C. Subscript 'hot' represents the hot water flow and subscript 'col' represents the cold water flow of the district heating at 1 atm. The pressure is assumed constant. This gives reference specific enthalpy values $h^{\mathrm{ref}}_{\mathrm{col}}$, $h^{\mathrm{ref}}_{\mathrm{hot}}$ [J/kg] and specific entropies $s^{\mathrm{ref}}_{\mathrm{col}}$, $s^{\mathrm{ref}}_{\mathrm{hot}}$ [J/(K·kg)]. The exergy content of the thermal energy flow is described by (3.26), which is derived from (3.25), where T_0 [K] is the temperature of the reference environment and a_q [J/kg] is the thermal specific exergy. The thermal output exergy Γ_q [kW] is the exergy change of the working fluid:

$$a_q = \left(h - h_0\right) - T_0\left(s - s_0\right) \tag{3.25}$$

$$\Gamma_q = \phi_{\mathrm{m,wat}}\left(\left(h^{\mathrm{ref}}_{\mathrm{hot}} - h^{\mathrm{ref}}_{\mathrm{col}}\right) - T_0\left(s^{\mathrm{ref}}_{\mathrm{hot}} - s^{\mathrm{ref}}_{\mathrm{col}}\right)\right)\frac{1}{10^3}. \tag{3.26}$$

Table 3.1: Component parameters

Parameter	Flow	Unit	Component				
			Electricity Grid A	Heat Pump B	Gas-Fired CHP C	Furnace D	Biom.-Fired CHP E
Input carrier			Electricity	Electricity	Natural gas	Natural gas	Biomass
Maximum input carrier α_i	Power	kW	3000,00	1000,00	1996,00	2255,00	2171,28
Maximum input carrier α_i	Exergy	kW	3000,00	1000,00	2075,84	2345,20	2403,39
Minimum input carrier α_i	Power	kW	-3000,00	75,00	145,00	0,00	151,99
Minimum input carrier α_i	Exergy	kW	-3000,00	75,00	150,80	0,00	168,24
Electrical energetic efficiency $\eta^k_{\alpha_i \mathrm{e}}$		%	100,00	-	38,23	-	23,04
Electrical exergetic efficiency $\varepsilon^k_{\alpha_i \mathrm{e}}$		%	100,00	-	36,76	-	20,81
Thermal energetic efficiency $\eta^k_{\alpha_i \mathrm{q}}$		%	-	283,00	49,76	95,54	69,10
Thermal exergetic efficiency $\varepsilon^k_{\alpha_i \mathrm{q}}$		%	-	34,43	5,82	11,17	7,59
Total energetic efficiency $\eta^k_{\alpha_i,\mathrm{tot}}$		%	100,00	283,00	87,99	95,54	92,14
Total exergetic efficiency $\varepsilon^k_{\alpha_i,\mathrm{tot}}$		%	100,00	34,43	42,58	11,17	28,41
Maximum electrical output	Power, exergy flow	kW	3000,00	-	763,03	-	500,21
Maximum thermal output	Power	kW	-	2830,00	993,16	2154,35	1500,37
Maximum thermal output	Exergy flow	kW	-	344,26	120,82	262,07	182,52

The simulation makes use of time series data of the heat and electric loads. In Section 3.4.4 it was shown that for the electrical flows no further calculations are needed. The load data of the thermal energy requires conversion however.

Combining (3.26) and (3.27) leads to (3.28), which can be used to convert thermal power to a thermal exergy flow:

$$L_{\mathrm{q}} = \phi_{\mathrm{m,wat}} \left(h_{\mathrm{hot}}^{\mathrm{ref}} - h_{\mathrm{col}}^{\mathrm{ref}} \right) \frac{1}{10^3} \tag{3.27}$$

$$\varGamma_{\mathrm{q}} = L_{\mathrm{q}} \left(1 - T_0 \frac{s_{\mathrm{hot}}^{\mathrm{ref}} - s_{\mathrm{col}}^{\mathrm{ref}}}{h_{\mathrm{hot}}^{\mathrm{ref}} - h_{\mathrm{col}}^{\mathrm{ref}}} \right). \tag{3.28}$$

3.4.6 Compression Heat Pump ($\varepsilon_{\mathbf{eq}}^{\mathbf{B}}$)

In order to increase the flexibility of the hub, a compression heat pump is used. The heat pump is electrically driven and uses a ground reservoir as low temperature heat reservoir. The efficiency values are based on [80].

3.4.7 Gas-Fired Combined Heat and Power Unit ($\varepsilon_{\mathbf{ge}}^{\mathbf{C}}$, $\varepsilon_{\mathbf{gq}}^{\mathbf{C}}$)

The values for the gas-fired CHP unit are based on the *GE Jenbacher JMS 312 GS-NL*. The model used in this simulation has a 60% higher rated power than the one found in the data sheet. A fixed efficiency is used from the data sheet [82]. The thermal exergetic efficiency is based on the assumption that heat addition/transfer occurs by the working fluid operating at temperatures between 53 °C and 80 °C.

3.4.8 Gas-Fired Furnace ($\varepsilon_{\mathbf{gq}}^{\mathbf{D}}$)

The gas-fired hot water furnace data are based on the *Byworth FM2500* [83]. The thermal exergetic efficiency is calculated in a similar way as the gas-fired CHP.

3.4.9 Biomass-Fired Combined Heat and Power Unit ($\varepsilon_{\mathbf{be}}^{\mathbf{E}}$, $\varepsilon_{\mathbf{bq}}^{\mathbf{E}}$)

The biomass-fired CHP is a system that converts biomass to electricity and heat. This system consists of 3 subsystems: syngas production, fuel cell system and combustion. The first subsystem converts biomass to synthetic gas, using a *fast internal circulating fluidized bed* gasifier [80]. This process consists of 2 fluidized beds. One is a gasifier to convert the biomass to syngas, the other is a combustor which provides the heat for the gasifier, by combusting the unconverted biomass.

After the gasification the syngas is cleaned and compressed, the syngas is distributed to the fuel cell system, which consists of a solid oxide fuel cell [80]. The unconverted syngas that leaves the fuel cell is combusted, providing heat of which a part is used to preheat the syngas and the air entering the fuel cell.

3.4.10 Cost Data

The data for the cost of electricity and natural gas were obtained from a German website that specifies real prices for small commercial customers [47]. The data for the cost of biomass were found at the website of the Biomass Energy Centre, owned and managed by the UK Forestry Commission [84]. The cost of biomass considered in this work is obtained by multiplying the cost of natural gas found in [47] by the ratio between the cost of biomass and the cost of natural gas given in [84].

The price of biomass considered in this study corresponds to the price of wood pellets. The scheduling computations in this chapter are specified for time periods of 15 min, the data were adapted accordingly, see Table 3.2. The data are used for the cost optimization.

Table 3.2: Fuel costs

Energy		Costs	
Carrier	Use per year (kWh)	Fixed (€)	Consumption $\left(\frac{€}{\text{kW}\cdot(15\text{min})}\right)$
Electricity	30 001 - 100 000	0,0377	0,0474
Natural Gas	2 375 - 12 692	0,0208	0,0171
Biomass (wood pellets)	not specified	not specified	0,0143

3.4.11 Load Data

The load consists of the electricity and heat demand of a district containing 250 houses, for which the components were designed. The software program SEPATH [49] is used to obtain the load patterns. After entering information about the type of households, a load pattern of the electricity and heat demand is generated for a week.

The load data used for the simulations in this chapter were selected from the output data of the program. For the optimal dispatch example, the following data are used:

$$L_\text{e} = 370,00\,\text{kW} \tag{3.29}$$

$$L_\text{q} = 1352,50\,\text{kW} \tag{3.30}$$

$$\Gamma_\text{q} = 164,53\,\text{kW}. \tag{3.31}$$

For the scheduling optimization example, the electric load chosen is $L_\text{e} = 255$ kW, the exergetic and energetic heat loads correspond to the outside temperatures; they are shown in Table 3.3 and Table 3.4.

Table 3.3: Heat loads for the scheduling example

	Environment Temperature (°C)									
	-4	-3	-2	-1	0	1	2	3	4	5
L_q	1157,41	1111,11	1064,81	1018,52	972,22	925,93	879,63	833,33	787,04	740,74
$\mathit{\Gamma}_q$	140,80	135,16	129,53	123,90	118,27	112,64	107,00	101,37	95,74	90,11

Table 3.4: Heat loads for the scheduling example (continued)

	Environment Temperature (°C)										
	6	7	8	9	10	11	12	13	14	15	16
L_q	694,44	648,15	601,85	555,56	509,26	462,96	416,67	370,37	324,07	277,78	231,48
$\mathit{\Gamma}_q$	84,48	78,85	73,21	67,58	61,95	56,32	50,69	45,05	39,42	33,79	28,16

3.5 Simulation Results

In this section the results of the dispatch optimization and the scheduling optimization of the hub elements are presented, depicted in Figure 3.1 . The result of the exergy hub optimization provides the optimal input exergy flows. These results were converted into energy flows to allow the comparison among the evaluated cases.

3.5.1 Simulation 1: Optimal Dispatch - Difference among Optimizing Energetic Efficiency, Exergetic Efficiency and Costs

The optimal dispatch problem is solved applying the exergy hub approach presented in Section 3.3 and using different objective functions for the optimization.

Case 1: Exergetic Efficiency Maximization

In this case, the objective function that is minimized is inversely proportional to the exergetic efficiency of the system under study, in this way the exergetic efficiency of the system is maximized. For the exergy hub under study, electricity, natural gas and biomass are the inputs of the system. The electrical input is divided by the exergetic efficiency of the centralized generation plant $\varepsilon_{\mathrm{gen,e}}$ with which it is produced. The incoming exergy and the exergy used can be calculated with the following equations:

$$\mathit{\Xi}_{\mathrm{inp}} = \sum \left(\frac{\mathit{\Xi}_{\mathrm{e}}}{\varepsilon_{\mathrm{gen,e}}} + \mathit{\Xi}_{\mathrm{g}} + \mathit{\Xi}_{\mathrm{b}} \right) \tag{3.32}$$

$$\mathit{\Gamma}_{\mathrm{out}} = \sum \left(\mathit{\Gamma}_{\mathrm{e}} + \mathit{\Gamma}_{\mathrm{q}} \right) \tag{3.33}$$

where subscript 'e' refers to electricity, subscript 'g' refers to natural gas, subscript 'b' refers to biomass and subscript 'q' refers to heat, Ξ is the input exergy flow and Γ is the output exergy flow of the exergy hub. The resulting objective function is:

$$\mathscr{F}_{\text{obj1}} = \frac{\Xi_{\text{inp}}}{\Gamma_{\text{out}}} = \frac{\sum\left(\frac{\Xi_{\text{e}}}{\varepsilon_{\text{gen,e}}} + \Xi_{\text{g}} + \Xi_{\text{b}}\right)}{\sum\left(\Gamma_{\text{e}} + \Gamma_{\text{q}}\right)}. \tag{3.34}$$

Case 2: Energetic Efficiency Maximization

In this case, the objective function that is minimized is inversely proportional to the energetic efficiency of the system under study, in this way the energetic efficiency of the system is maximized. Here again, the electrical input is divided by the energetic efficiency of the centralized generation plant $\eta_{\text{gen,e}}$:

$$P_{\text{inp}} = \sum\left(\frac{P_{\text{e}}}{\eta_{\text{gen,e}}} + P_{\text{g}} + P_{\text{b}}\right) \tag{3.35}$$

$$L_{\text{out}} = \sum\left(L_{\text{e}} + L_{\text{q}}\right) \tag{3.36}$$

where P is the input power flow and L is the output power flow. The resulting objective function is:

$$\mathscr{F}_{\text{obj2}} = \frac{P_{\text{inp}}}{L_{\text{out}}} = \frac{\sum\left(\frac{P_{\text{e}}}{\eta_{\text{gen,e}}} + P_{\text{g}} + P_{\text{b}}\right)}{\sum\left(L_{\text{e}} + L_{\text{q}}\right)}. \tag{3.37}$$

Case 3: Cost Minimization

In this case a cost minimization is performed. Equation (3.38) shows the objective function with coefficients K_{1,α_i}, K_{2,α_i} and K_{3,α_i}. The coefficient K_{1,α_i} does not affect the optimization results and for this reason it is omitted.

The coefficient K_{2,α_i} for each energy carrier is obtained from the data presented in the last column of Table 3.2, for electricity $\mathrm{K}_{2,\text{e}} = 0,0474$, for natural gas $\mathrm{K}_{2,\text{g}} = 0,0171$ and for biomass $\mathrm{K}_{2,\text{b}} = 0,0143$. The coefficient K_{3,α_i} is considered to be 0,001 for all energy carriers. This value was found acceptable for the electricity coefficient. Due to the fact that no information about this coefficient was readily available for the other energy carriers, the same value was used for all of them. The results that were obtained from the optimization provide enough insight even when using the same coefficient value K_{3,α_i} for all the input carriers, thus this assumption was considered satisfactory for this study. The objective function is shown below:

$$\mathscr{F}_{\text{obj3}} = \sum_{\alpha_i \in \mathcal{E}_{\text{in}}} (\mathrm{K}_{1,\alpha_i} + \mathrm{K}_{2,\alpha_i} P_{\alpha_i} + \mathrm{K}_{3,\alpha_i} P_{\alpha_i}^2). \tag{3.38}$$

Table 3.5: Simulation 1: Optimal dispatch

Optimization	Power input to each hub element					ε_{tot}	η_{tot}	Cost
	Grid (kW)	H. Pump (kW)	Gas-fired CHP (kW)	Furnace (kW)	Biom.-fired CHP (kW)	%	%	€
Input carrier	e	e	g	g	b			
Case 1 - ε_{tot}	0,00	75,00	876,29	627,20	151,99	**27,19**	91,58	150,39
Case 2 - η_{tot}	0,00	75,00	145,00	130,37	1365,48	26,30	**92,30**	218,20
Case 3 - Cost	177,28	351,77	340,57	0,00	271,41	23,16	78,24	**69,18**

Results and Discussion

The results that are shown in Table 3.5 are obtained from a program that was developed by the author of this thesis using the programming software AIMMS. In this program the equations of the problem statement (including equalities and inequalities) presented in Section 3.3 were implemented. The program was used to carry out three different simulations. Each simulation contains a different objective function, namely (3.34), (3.37) and (3.38). The program converges to a solution when the evaluation of the objective function reaches a minimum. Additionally, the program provides the value of the energetic efficiency, the exergetic efficiency and the cost for each simulation so that the results of the three cases can be analyzed and compared.

In this simulation only one load condition is simulated, thus only the optimal dispatch for that specific load is obtained. As mentioned in Section 3.4.11, the electric load is $L_e = \Gamma_e = 370,00$ kW and the heat loads are $L_q = 1352,50$ kW and $\Gamma_q = 164,53$ kW. From Table 3.5 it can be observed that in both Case 1 and in Case 2, the heat pump is used at its minimum capacity, with a power input of 75 kW. This is because its main input is electricity, which has been produced with a relatively inefficient plant, both from an energetic and an exergetic point of view. It is interesting to observe that in Case 1, where exergetic efficiency is maximized, the biomass-fired CHP is used at its minimum capacity, and the gas-fired CHP is the component with the highest dispatch. Conversely, in Case 2, where energetic efficiency is maximized, the biomass-fired CHP has the highest dispatch whereas the gas-fired CHP is working at its minimum capacity. This can be explained by the fact that from an exergetic point of view the gas-fired CHP is the most efficient component and from an energetic point of view the most efficient component is the biomass-fired CHP. In relation to the operating costs it can be observed that for this case, the exergetic efficiency optimization resulted in lower costs than the energetic efficiency optimization.

It can be observed that according to the results of the optimization, the furnace is not used at all in Case 3, and both the electricity input from the grid and the electricity-driven heat pump play an important role in the dispatch, which was not the case in the previous cases. This can be explained by the fact that the optimization looks only at the cost of the input fuels or electricity and not if the electricity was produced with high efficient plants or not. This example shows that the results from a energy optimization can be very different from those of an exergy optimization. As was expected, due to the different nature of the objective function, a cost optimization can give considerably different results with respect to the other two cases.

Table 3.6: Simulation 2: Scheduling for different loads - Case 1

	Environment Temperature (°C)																				
Component	-4	-3	-2	-1	0	1	2	3	4	5	6	7	8	9	10	11	12	13	14	15	16
Grid																				1	1
Heat Pump																					
Gas-Fired CHP	1	1	1	1	1	1	1	1	1	1	1	1	1	1	1	1	1	1	1	1	1
Furnace	1	1	1	1	1	1	1	1	1	1	1	1	1	1	1	1	1	1	1		
Biomass-Fired CHP																					

Table 3.7: Simulation 2: Scheduling for different loads - Case 2

	Environment Temperature (°C)																				
Component	-4	-3	-2	-1	0	1	2	3	4	5	6	7	8	9	10	11	12	13	14	15	16
Grid																				1	1
Heat Pump																					
Gas-Fired CHP												1	1	1	1	1	1	1	1	1	1
Furnace	1	1	1	1	1	1	1	1	1	1	1	1	1						1		
Biomass-Fired CHP	1	1	1	1	1	1	1	1	1	1	1	1	1	1	1	1	1	1			

3.5.2 Simulation 2: Optimal Scheduling - Difference among Optimizing Energetic Efficiency and Exergetic Efficiency

The main objective of this section is to show that in complex systems with several components and multiple energy carriers, the optimal scheduling of units (multi-carrier unit commitment) coming from an exergetic efficiency optimization may vary from an energetic efficiency optimization. In order to solve the scheduling optimization, several algorithms were added to the problem statement described in Section 3.3.2. The multi-carrier unit commitment algorithms were programmed according to the method described in Chapter 2. The optimization is solved with a mixed-integer solver due to the 'on' and 'off' states of the units. The objective functions that were used in Section 3.5.1 are used to obtain the multi-carrier unit commitment.

Results and Discussion

The heat load is varied in order to show the effect on the scheduling of the components with respect to the exergy and energy optimization. The electric load is kept constant at $\Gamma_e = L_e = 255$ kW and the outside temperature is changed in order to increase or decrease the heat demand of the group of houses considered. The heat load values can be found in Table 3.3 and Table 3.4. It can be observed in Table 3.6 and in Table 3.7 that for temperatures equal and below 6 °C in both cases the hub was optimized in a way that the most efficient component delivers the total demand in combination with the furnace (exergetically or energetically efficient respectively).

In Case 1, where exergetic efficiency is optimized, it is the gas-fired CHP the one that is scheduled. Conversely in Case 2, where energetic efficiency is optimized, the biomass-fired CHP, which has the higher energetic efficiency, is the one that is scheduled. It is interesting to observe that at higher temperatures, where the heat demand is lower, both optimization solutions give the same scheduling: the gas-fired CHP and the furnace supply the load. This can be explained because of the load ratio: the electricity demand is equal or higher than the heat demand and thus, the higher electricity conversion efficiency of the gas-fired CHP in relation to the biomass-fired CHP is more important than the overall efficiency of the biomass-fired CHP in comparison to the gas-fired CHP.

This small comparison is just an example of the possibilities of scheduling and analysis that the scheduling tool presented in this chapter provides. Further sensitivity analyses can be performed to evaluate the influence of other conditions or parameters, like for example the efficiency of conversion of the external generation plants.

There are still many disagreements and uncertainties in the scientific community about the influence or advantages that an exergy analysis can provide in relation to an energy analysis and if practical differences can be obtained. This is a valuable example because it shows that the results actually vary: the most energetically efficient solution does not always fit the results of an exergy optimization. This means that depending on the goal of the system designers, different configurations can be believed to be the optimal one. If we were to obtain the maximum potential from the available sources, then we would need to follow the results of an exergy optimization, however this does not necessarily mean that costs will be reduced.

3.6 Conclusions

We are all responsible of finding ways to make a better use of available resources. In this chapter the *exergy hub* approach was introduced. In the exergy hub approach, exergy efficiencies (instead of energy efficiencies) are taken into account for the optimization of systems that contain multiple energy carriers.

A comparison of results obtained by using different objective functions is shown in Section 3.5.1 and Section 3.5.2. From the results it was observed that the dispatch and scheduling of components differ considerably when performing an exergy optimization in relation to an energy optimization. It was observed that the costs were lower for the case in which the exergetic efficiency was maximized, with respect to the case in which the energetic efficiency was maximized. However, this applies only to the case that was analyzed, thus no direct relation between an energy or exergy optimization and a reduction of costs can be established as a conclusion.

Due to its flexibility, the scheduling tool that was presented in this chapter can be used to evaluate different configurations and control strategies of systems with several generation units and multiple energy carriers. The tool can be easily adapted to evaluate configurations designed for the built environment, where research in the topic of exergy has increased during the last years. The strength of the tool is that it can be used in complex systems, like energy hubs with many links between components, or in annual simulations where the calculations become extremely tedious when done by hand.

Exergy analysis is a good tool to determine where the losses of the system are located. Moreover, since exergy is the maximum theoretical work that can be obtained from an energy flow, by choosing the most exergetically efficient configuration we are making the best use of the work potential of the energy sources available. Unfortunately, the existing generation systems were not designed to make the best use of the work potential of the sources and in many cases, sources with high work potential are used to supply low temperature heat; those processes are characterized by having a high entropy production. Thus, in order make a better use of the work potential of the sources, it would be necessary to re-evaluate the existing equipment/machinery and re-design generation units in general according to an exergy-oriented criteria. This is an important challenge for the future.

This dissertation concentrates on the optimization of systems that contain traditional and state-of-the-art equipment, however this equipment was not designed taking exergy into account. Furthermore, the focus of the rest of the dissertation is given to the optimization of total costs and to keep track of the primary energy source utilization, thus even though the tool provided valuable information about how to dispatch and schedule units to attain a higher exergetic efficiency in the system, the *energy hub* was selected as the appropriate approach to be used in the rest of the chapters.

Chapter 4

The Control

Multi-Carrier Hierarchical Control Architecture

This chapter answers Research Question 4 of this dissertation. In Chapter 2 a general unit commitment framework for systems with multiple energy carriers was presented. Nevertheless, the topic of real-time control also deserves to be studied, since mismatches will exist between the forecasted values and the actual ones.

This chapter presents an integrated control architecture for multiple energy carrier systems. The application of the control architecture is illustrated with an example. Section 4.1 contains basic concepts related to the control architecture. Section 4.2 includes a literature review of control strategies for decentralized energy supply systems. In Section 4.3 the integrated control architecture is described. Section 4.4 briefly describes the models that were used and their link to the control architecture. Section 4.5 presents results obtained by applying the control architecture to an example. Finally in Section 4.6 the conclusions of this chapter are included. Parts of this chapter have been published in [85].

4.1 Basic Concepts and Definitions

In this chapter several models of heat components are used, for this reason some basic heat transfer concepts and equations are introduced. Moreover, the definition of *participation factors* is included. Energy can be transferred in three ways: conduction, convection and radiation. In this work only conduction and convection are considered.

4.1.1 Participation Factors

Due to the performance of control actions, when a mismatch exists between the predicted demand and the actual demand, the units involved participate at compensating this mismatch. A *participation factor* defines the percentage in which each of the units has to participate in order to reduce the error due to the mismatch.

4.1.2 Law of conservation of energy in an open system

The total energy change per unit of time [W], or power, is equal to the result of adding the power that flows into the system in the form of γ, given by $\phi_{m,\gamma_{in}} u_{\gamma_{in}}$ [W], the power that goes out of the system, given by $\phi_{m,\gamma_{out}} u_{\gamma_{out}}$ [W]), the power added Φ_{in} [W] and the heat exchanged with the surroundings per unit of time Φ_{out} [W]:

$$\frac{dE}{dt} = \phi_{m,\gamma_{in}} u_{\gamma_{in}} - \phi_{m,\gamma_{out}} u_{\gamma_{out}} + \Phi_{in} - \Phi_{out} \tag{4.1}$$

where $\phi_{m,\gamma_{in}}$ [kg/s] is the mass flowing into the system , $\phi_{m,\gamma_{out}}$ [kg/s] is the mass flowing out of the system, u [J/kg] is the specific internal energy and t [s] is time. The total energy E [J] and the specific internal energy u [J/kg] can be expressed by:

$$E = \rho V c T \tag{4.2}$$

$$u = cT \tag{4.3}$$

where ρ [kg/m^3] is density, V [m^3] is volume, c [J/(K·kg)] is specific heat capacity and T [K] is temperature. Equation (4.4) results from substituting the energy and specific internal energy expressions in (4.1). It is assumed that no mechanical power is being added ($\Phi_{in} = 0$) and that the input and output mass flows are the same ($\phi_{m,\gamma_{in}} = \phi_{m,\gamma_{out}} = \phi_{m,\gamma}$) :

$$mc\frac{dT}{dt} = \phi_{m,\gamma} c_\gamma \left(T_{in} - T_{out}\right) - \Phi_{out} \tag{4.4}$$

where m [kg] stands for mass ($m = \rho V$). If the system is stationary, the heat exchanged with the surroundings Φ_{out}, denoted from now by Φ_q, is equal to the heat transferred by the mass flow $\phi_{m,\gamma}$:

$$\Phi_q = \phi_{m,\gamma} c_\gamma \left(T_{in} - T_{out}\right). \tag{4.5}$$

4.1.3 Heat Conduction

Heat conduction occurs when heat is transferred by interactions between atoms/molecules, but there is no transport of atoms or molecules themselves [51]. The equation that describes the heat conduction process is:

$$\Phi_q = \frac{\kappa}{d} A \Delta T \tag{4.6}$$

where Φ_q [W] is heat transferred per unit of time , κ [W/(m·K)] is the thermal conductivity, d [m] is the thickness of the wall, ΔT [K] is the temperature difference that drives the heat transfer phenomena and A [m^2] is the area of the wall.

4.1.4 Heat Convection

Heat convection occurs when heat is transferred through the transport of material. The equation that represents this process is given by:

$$\Phi_q = UA\Delta T \tag{4.7}$$

where Φ_q [W] is the heat transferred per unit of time, U [W/(m^2·K)] is the heat transfer coefficient, A [m^2] is the area and ΔT [K] is the temperature difference that drives the heat transfer phenomena.

4.2 Literature Review

This section summarizes several papers and reports where control architectures for distributed power systems are proposed. Most of the architectures have two-level hierarchical configurations and only take electrical parameters and electrical interactions into account. For example, in [86] a droop control method is applied on a system that contains renewable energy generators and storage. In [86], the first level is called PQ Droop Control Method and the second level is called Management of the Distributed Power Station. The first level manages the power output of each unit separately, while the second level monitors the whole system and controls the set-points of the units depending on the state of charge of the battery. The control is designed for two operating conditions: normal interconnected mode and emergency mode. In both cases the control unit optimizes the power output of the generators by communicating new droop settings based on the information collected from the inverters, decentralized generation units and battery banks. However, the selection of the suitable droops is a trade-off between the stability margin, dynamic performance and shifts in the droop operating point [86].

Another example can be found in [87], where control and power management strategies based on locally measured signals without communication were proposed under various micro-grid operating conditions. In the paper, the active power of each decentralized generation unit is controlled based on a frequency droop characteristic and a frequency restoration strategy [87].

Apart from the control techniques based on droop mechanisms, other control schemes were also found in the literature. For example in [88] a supervisory hybrid control scheme for a micro-grid system using hybrid control techniques was presented. The hierarchical control consists of a supervisory controller at the top level that interacts with the unit level regulators. The supervisory control regulates the operation of the micro-grid by means of transition management schemes. The predetermined routes for transition to other operating states (i.e on-grid, off-grid, etc) are given by a *finite hybrid automata* representation of the micro-grid system. In their work the micro-grid was partitioned in modules to reduce the complexity of the problem. The control technique is applied to a wind energy conversion and storage system. By means of an example the authors show how a voltage fall higher than 0,7 per unit causes the supervisory controller to initiate a transition from the on-grid operating state to the off-grid operating state.

Additional actions, like the use of storage and load shedding have also been included in the control mechanisms for future power systems and micro-grids. For example, [27] describes and evaluates the feasibility of two control strategies needed for islanded operation of micro-grids. Particular attention is given to storage devices and load shedding strategies. The concept of using a control scheme based on droop concepts to control inverters in an off-grid AC system was studied by using two different control strategies: Single Master Operation and Multi Master Operation, where several inverters are operated with voltage source inverter control. A micro-grid central controller, which is at the top control level, is installed at the medium/low voltage substation. A second hierarchical control level, located at the loads, groups of loads and micro sources, exchanges information with the micro-grid central controller, which provides the respective set-points. In the examples a fuel cell was included, which is a combined heat and power device; however no attention was given to the heat control or heat flows in general in their approach.

Other schemes have been found in which the main objective is to support the grid. For example, in [89] a control strategy is proposed in which inverters are used for grid-forming, grid-supporting and grid-parallel operation. The strategy is applicable to interconnected grids. The control architecture consists of three control levels: *unit control* and *local control* to regulate and maintain voltage and frequency, and a *main supervisory control* to optimize and control power dispatching and load sharing. These controls are based on conventional primary, secondary and tertiary control respectively, described in Section 1.3.2.

From the literature reviewed, it was observed that a two-level architecture can be adjusted to fulfill the needs of future power systems, where decentralized generation will play a more important role. Nevertheless the topic of integrated control for systems with multiple energy carriers like electricity and heat has not been broadly studied yet. For this reason this topic will be addressed in this chapter.

4.3 Integrated Control Architecture

The integrated control architecture that is adopted in this dissertation is hierarchical. It contains two levels, as this was found to be well-accepted in recent literature for distributed energy systems. Nevertheless, it is not limited to electrical parameters but also includes parameters related to the flows of other energy carriers involved. The names given to the two levels are: *unit control* and *main control*. The nomenclature introduced in Chapter 2 is used in this chapter. In Figure 4.1 the two-level architecture is depicted.

4.3.1 Unit Control

The *unit control* is a local control, which can be embedded at each controllable unit. It works independently at each of the units, but it can receive control signals from the *main control*. The parameters required to perform the unit control are monitored locally at the unit. In this context, a unit can be an individual component like a battery, but it can also be a group of components if these components work as a whole and have a common controller. An example can be a fuel cell system equipped with a battery. This fuel cell system can have its own local control, which for example can prevent the fuel cell from suffering sharp current changes by redirecting them to the battery. Since the fuel cell and the battery work as a whole in this example, they are considered to be a single unit.

4.3.2 Main Control

The *main control* regulates the whole system. It is in charge of monitoring the system, allocating the generation output and bringing the system's relevant parameters, or control parameters back to their nominal value. The main control commands the execution of the multi-carrier optimal dispatch and multi-carrier unit commitment. Furthermore, the main control allocates load changes to the controllable units. In the case of applying demand-side management, the main control also regulates the controllable loads. In the case of off-grid electrical systems more considerations must be taken into account than in the case of grid-connected systems, since there should be a master converter in charge of keeping the voltage and frequency of the system within acceptable limits.

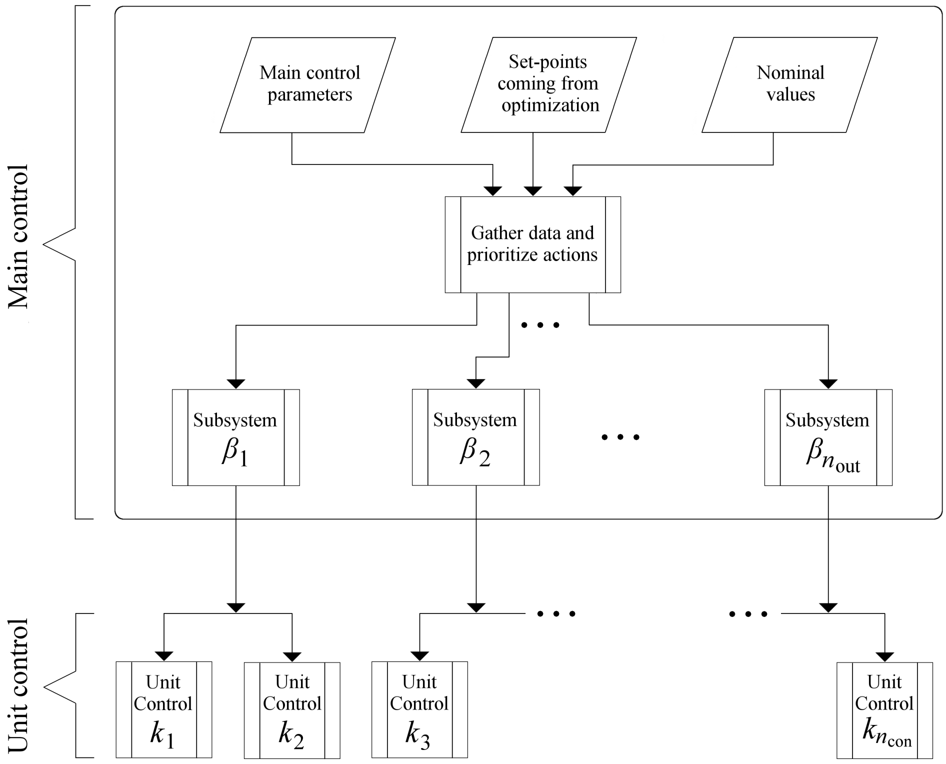

Figure 4.1: Two-level hierarchical control architecture

The power to be generated by each component is calculated through a process that starts by determining the mismatch between the system's control parameter and its nominal value. The sign of the error signal indicates the proper corrective action to be executed, i.e. to increase or decrease the power supply. The error signal can feed a proportional or integral controller in order to determine the power that must be supplied or curtailed to bring the control parameter back to its nominal value.

The main control is divided into control subsystems. Each control subsystem is associated with an energy carrier β_j from the output side of the energy hub. In the case of a hub with two energy carriers at the output side, like electricity and heat, the main control has two control subsystems, one for electricity and another one for heat. Each generation unit is assigned to a particular control subsystem. The particular energy carrier is selected according to the requirements of the system. For example in an off-grid system, a good operation of the electricity control subsystem is crucial for the stability of the entire system; particularly because the frequency and the voltage level are defined by a master converter, and not by the electrical grid. In this case all cogeneration units producing electricity at one of the outputs are assigned to the electricity control subsystem, and therefore, regulated with respect to their electrical output. The main control allocates the power difference between the forecasted and actual values to the units of all control subsystems by means of participation factors. Each controllable unit has its own participation factor, given by:

$$p^{k_p}_{\mathrm{f},\beta_j} = \frac{L^{k_p}_{\beta_j,\mathrm{sch}}/L_{\beta_j,\mathrm{rtd}}}{\sum\limits_{k_p \in C_\alpha} \left(L^{k_p}_{\beta_j,\mathrm{sch}}/L_{\beta_j,\mathrm{rtd}} \right)} + p^{k_p}_{\mathrm{f},\beta_j,\mathrm{min}} \tag{4.8}$$

where $p^{k_p}_{\mathrm{f},\beta_j}$ [-] is the participation factor of unit k_p at control subsystem β_j, variable $L^{k_p}_{\beta_j,\mathrm{sch}}$ is the scheduled power output in the form of energy carrier β_j of controllable unit k_p, $p^{k_p}_{\mathrm{f},\beta_j,\mathrm{min}}$ is the minimum participation of unit k_p (it can be set to zero) and $L_{\beta_j,\mathrm{rtd}}$ is the rated output power. The rated output power can be calculated by adding up the rated power of all the converter units associated with energy carrier β_j, this is equal to: $L_{\beta_j,\mathrm{rtd}} = \sum L^{k_p}_{\beta_j,\mathrm{rtd}}$. Power is given in kW.

The desired power output calculated from the control actions $L^{k_p}_{\beta_j,\mathrm{des}}$ of unit k_p is:

$$L^{k_p}_{\beta_j,\mathrm{des}} = L^{k_p}_{\beta_j,\mathrm{sch}} + p^{k_p}_{\mathrm{f},\beta_j} \Delta L_{\beta_j,\mathrm{dif}} \tag{4.9}$$

where $\Delta L_{\beta,\mathrm{dif}}$ represents the difference between the total scheduled power output and the actual power demand. In the case of storage devices, the following aspects are considered:

- The availability to charge or discharge is evaluated before the main control sends the correction signals. The storage device is available to charge or discharge when the state of charge is lower or higher than the upper or lower state of charge limit respectively. If the requirement is not met, then the storage is set to stand-by. The output power of the storage devices is calculated using magnitudes, not vectors.

- If the scheduled storage action is to charge, but the system requires an increase in supply, the control system passes a zero to (4.9). Likewise, if the scheduled action is to discharge but the system requires a decrease in supply, a zero is passed to (4.9).

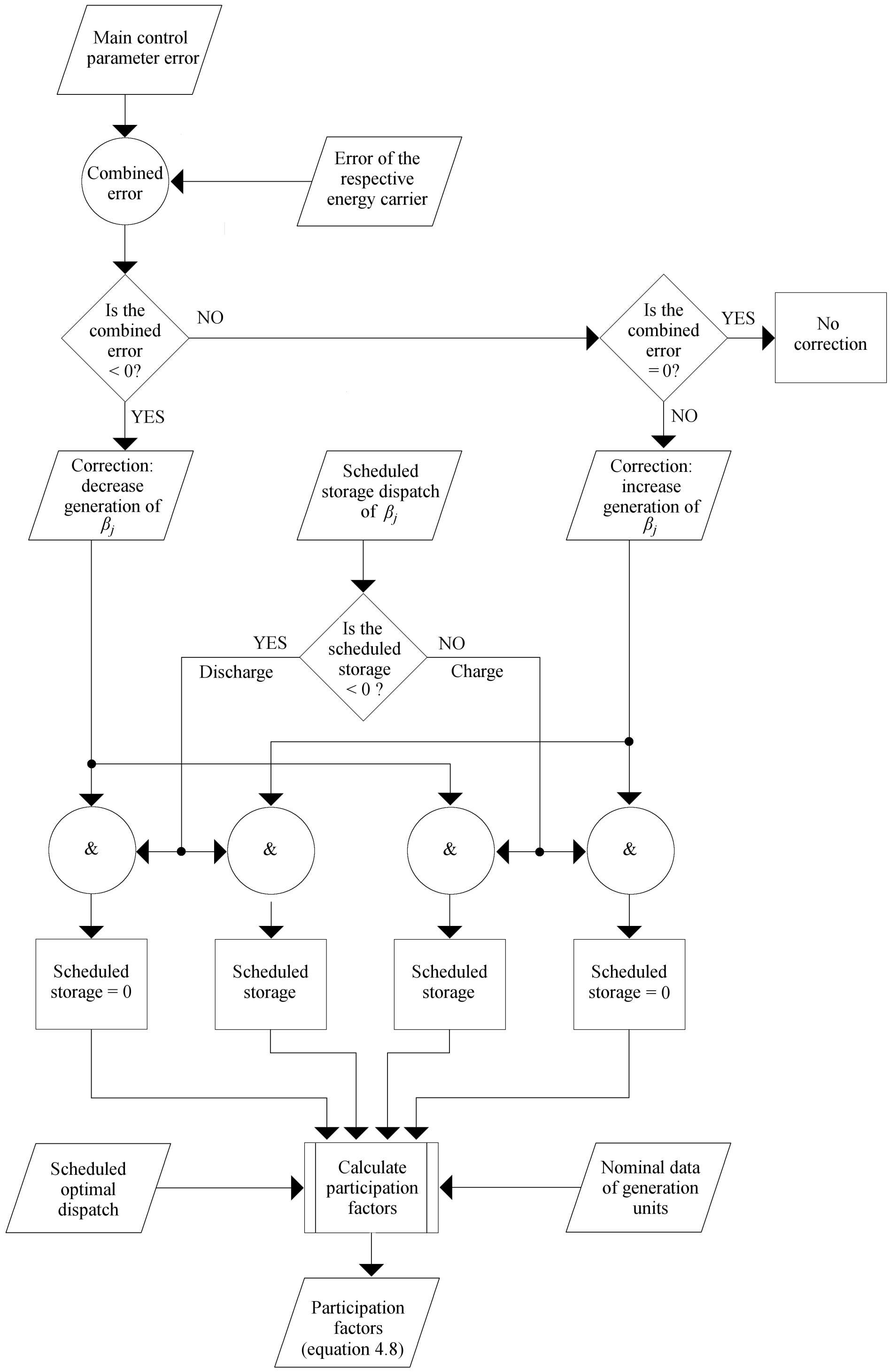

Figure 4.2: Flowchart to compute participation factors

Flowcharts will be used to describe and explain the actions taken by the control subsystems that are part of the main controller. A general flowchart is presented in Figure 4.2, but it can be adapted for any control subsystem considered. Figure 4.2 depicts the first section of the control sequence, which depends on the status of the main control parameter of the control subsystem. The first decision determines if an increase or decrease in the power generation is required. After the total increase or decrease of power generation is determined, the participation of each unit is defined by means of its participation factor, introduced in (4.8), and the storage considerations previously mentioned.

The flowchart that shows how the storage dispatch is executed is shown in Figure 4.3. In this case the actual corrective action required by the system and the scheduled storage charging status are compared. In the case that the charging status does not match, e.g. the system requires generation to be decreased, but discharging is scheduled, the control passes a zero value, otherwise the scheduled storage dispatch is used to compute the participation factors. Moreover the control can identify if the storage device can be charged or discharged according to its state of charge and energy content.

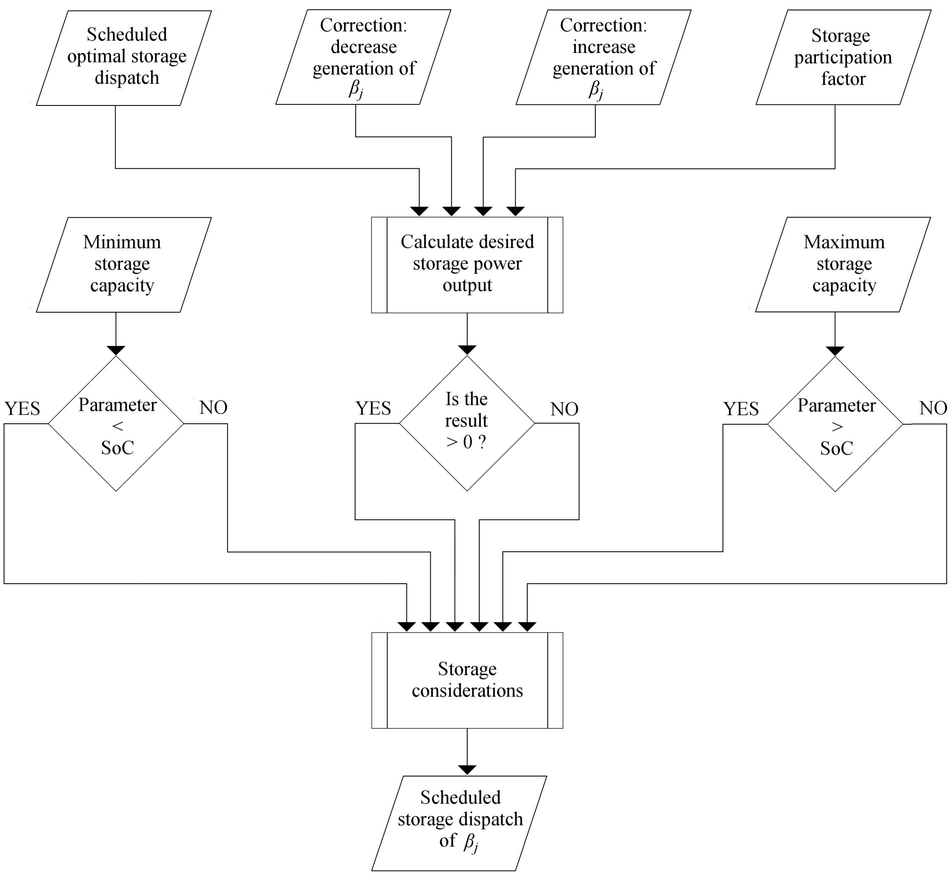

Figure 4.3: Flowchart to define the participation of the storage elements

After the participation factors are calculated, the main control sends the desired set-points to each unit per control subsystem according to (4.9), see Figure 4.4.

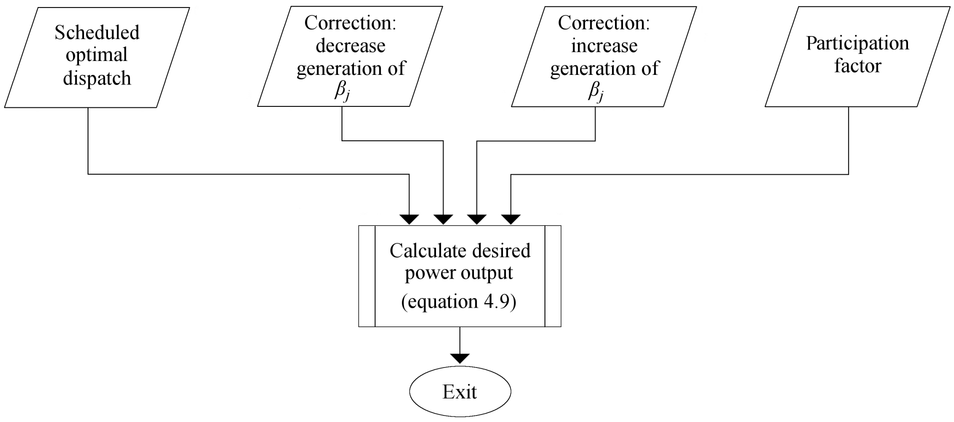

Figure 4.4: Flowchart to calculate the desired power output

4.3.3 Unit Control Applied

The system shown in Figure 4.5 was selected for the application of the integrated control. It consists of 2 gas turbines (CHP), a solid oxide fuel cell (CHP), a furnace, a wind turbine, a battery bank, a heat storage tank and a district heating infrastructure, which is used to model the heat demand. The system operates off-grid.

At first, it is important to identify which units are controllable and what type of *unit control* each of them possesses, since they may vary considerably with respect to each other. A description of each unit control is given in Section 4.4. The description includes the type of control, the aim of the control, the control parameter that serves as trigger and the control actions that are undertaken. The models that are used to represent each of the hub elements in the simulation can also be found in Section 4.4.

4.3.4 Main Control Applied

The *main control* monitors the system and takes actions in order to keep the control parameters at the nominal value. As mentioned in Section 4.3.2, there is a control subsystem for every energy carrier β_j at the output side of the energy hub, in this example they correspond to electricity and heat.

The control parameters are the frequency, which must remain at 50 Hz for the electrical system, and the temperature, which must remain at 100°C at the district heating hot water line. Since the system is not connected to the electrical grid, all components that produce electricity are assigned to the electricity control subsystem, even though they might also produce heat. The rest of the components are assigned to the heat control subsystem. Specific details regarding the control parameters and error signals considered at the main control for both control subsystems are presented in Table 4.1.

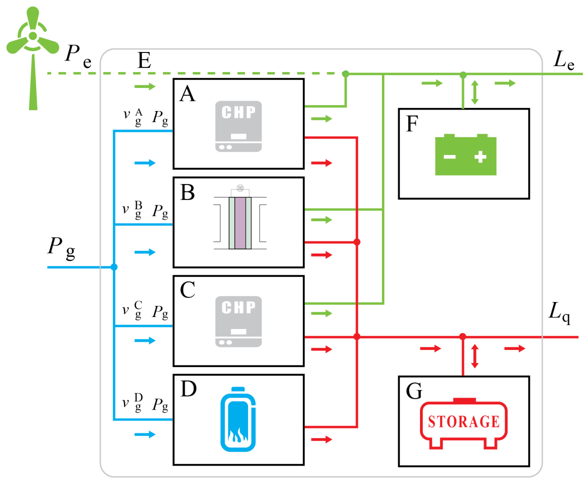

Figure 4.5: Energy hub used in the example

Table 4.1: Main control summary

	Control Subsystems	
Aspect	Heat Subsystem	Electricity Subsystem
Control Type	Proportional controller	Droop-based control
Main control parameters	Hot water pipeline temp. Nominal value: 100 °C	System's frequency Nominal value: 50 Hz
Other variables	Indoor temperature	System's voltage
Error signal	Simple error	Combined error: frequency and load error
Error signal sign	Positive: Increase supply Negative: Decrease supply	Positive: Increase supply Negative: Decrease supply
Storage dispatch	Positive: Charge Negative: Discharge	Positive: Charge Negative: Discharge
Minimum participation factor	Storage: 0,1 Furnace: 0,1	Storage: 0,1 Gas turbine CHP : 0 SOFC CHP : 0

4.4 Dynamic Component Models and Controls

Several of the component models presented in this section were implemented with the help of the MSc project [90], which was performed under the framework of this PhD project and under the guidance of the author of this dissertation. The models are introduced in this section because they are part of the system where the integrated control is tested. Each subsection is dedicated to a particular generation unit, where first some generalities of the unit are given to familiarize the reader, then the model of the unit is presented and finally the unit control and the main control link are described according to the control structure introduced earlier in this chapter. The models to be described in this section are the wind turbine, the battery, the gas-fired turbine (CHP), the gas-fired solid oxide fuel cell (CHP), the gas-fired furnace and the heat components of the district heating system that are used to represent the heat load.

4.4.1 Wind Turbine

Overview

An horizontal axis wind turbine with a nominal power of 120 kW was chosen for the simulations. Horizontal axis wind turbines are by far the most common form of wind turbines manufactured today [24]. It consists of a rotor (containing the blades and the hub), a low-speed rotating shaft, a gearbox, a high speed rotating shaft, a generator and a power converter. A diagram of the wind turbine is shown below, based on [91]:

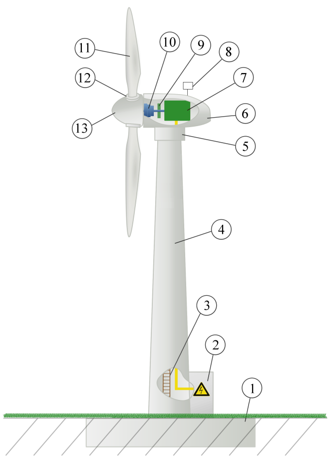

Figure 4.6: Wind turbine

1. Foundation
2. Connection to electrical grid
3. Access ladder
4. Tower
5. Wind orientation control
6. Nacelle
7. Generator
8. Anemometer
9. Brake
10. Gearbox
11. Rotor blade
12. Blade pitch control
13. Rotor hub

The kinetic energy of the wind is captured by the blades and is converted to rotational mechanical energy. This is transmitted to a gearbox that is connected to a high-speed shaft that turns the rotor of the electricity generator. Many of these wind turbines have an embedded control that is linked to the power converter in order to let the wind turbine work in optimal power generation mode.

The kinetic energy contained in the wind is given by the relation:

$$\text{Kinetic Energy} = \frac{1}{2} m_{\mathrm{wnd}} v_{\mathrm{wnd}}^2 \tag{4.10}$$

where m_{wnd} [kg] is the wind mass and v_{wnd} [m/s] is the wind speed.

The mass of air that flows per second $\phi_{\mathrm{m,air}}$ [kg/s] can be obtained by multiplying the air density ρ_{air} [kg/m^3], the wind speed v_{wnd} [m/s] and the area swept by the rotor A_{rot} [m^2]:

$$\phi_{\mathrm{m,air}} = \rho_{\mathrm{air}} A_{\mathrm{rot}} v_{\mathrm{wnd}}. \tag{4.11}$$

After substituting (4.11) in (4.10), the power contained in the wind is obtained. The power in the wind is equal to the kinetic energy per second [J/s] and is given in Watts [W]:

$$P_{\mathrm{wnd}} = \frac{1}{2} \rho_{\mathrm{air}} A_{\mathrm{rot}} v_{\mathrm{wnd}}^3. \tag{4.12}$$

Not all this power can be extracted by a wind turbine due to the losses associated with the energy conversion process. The model that represents the power extracted from the rotor blades is described below.

Model

Low-speed shaft For simplicity and due to the fact that some of the values that were needed are unknown and are not provided by the manufacturer, the stiffness of the shaft is assumed to be infinite.

Rotor The equation used to compute the power extracted from the rotor blades is:

$$P_{\mathrm{wnd}} = \frac{1}{2} c_{\mathrm{p}} \rho_{\mathrm{air}} A_{\mathrm{rot}} v_{\mathrm{wnd}}^3 \tag{4.13}$$

where c_{p} [-] is the performance coefficient of the rotor efficiency and represents the fraction of wind power that is captured by the rotor blades. In practice, this coefficient has a value between 0,4 and 0,5 in the case of high-speed two-blade turbines, and between 0,2 and 0,4 in the case of low-speed turbines. Its maximum theoretical value is 0,59 [92]. The performance coefficient can be expressed as a function of the tip speed ratio λ and the pitch angle θ; $\mathrm{C}_1, \mathrm{C}_2, \mathrm{C}_3, \mathrm{C}_4, \mathrm{C}_5$ and C_6 are constants. The performance coefficient can be expressed by:

$$c_{\mathrm{p}} = \mathrm{C}_1 \left(\frac{\mathrm{C}_2}{\lambda_i} - \mathrm{C}_3 \theta - \mathrm{C}_4 \right) \exp^{-\frac{\mathrm{C}_5}{\lambda_i}} + \mathrm{C}_6 \lambda \tag{4.14}$$

where

$$\frac{1}{\lambda_i} = \frac{1}{\lambda + 0,08\theta} - \frac{0,035}{\theta^3 + 1}. \tag{4.15}$$

Induction Generator In this study, a simple generator model is used. This model is given in per unit. The dynamics of the generator are modeled by the acceleration equation:

$$\frac{d\omega}{dt} = \frac{1}{2J} \left(\tau_{\mathrm{mec}} - \tau_{\mathrm{ele}} \right) \tag{4.16}$$

where ω is the rotational speed, J is the moment of inertia, τ_{mec} represents the mechanical torque and τ_{ele} represents the electrical torque.

Unit Control

Even though the wind turbine is considered to be an uncontrollable unit because its source of energy is the wind, which changes stochastically, there are two parameters that fall into the unit control: the rotor speed and the pitch angle. The description of the unit control is given below.

Rotor Speed Control

Function: keeps the optimal power supply of the wind turbine.

Trigger: responds to a rotor speed error signal.

Action: adjusts the rotor speed by modifying the electromagnetic torque.

Pith Angle Control

Function: performs power limitation by keeping the desired rotor speed.

Trigger: responds to a rotor speed error signal.

Action: adjusts the wind turbine blades.

Main Control Link

There is no control signal sent from the main control, it is assumed that the power contribution of the wind turbine is supplied to the system as it comes.

4.4.2 Lead-Acid Battery

Overview

The electricity storage selected consists of deep-cycle lead-acid batteries. The battery bank has a nominal battery stack capacity of 1250 Ah. Lead-acid batteries are the most commonly used batteries in electrical power system applications, including applications where renewable energy technologies are present. Moreover, this kind of batteries has been widely used in the automotive industry. Lead-acid batteries have a wide range of sizes as well as an acceptable cost in the market. In [93], several advantages and disadvantages of batteries were gathered. Here only a selection is listed from [93–95]. These are some advantages:

- There are many sizes and designs available.
- The technology is well-understood, mature and reliable.
- It is possible to easily determine their state of charge.
- Low self discharge and low maintenance.
- The components are easily recycled.

On the other hand, some disadvantages of lead-acid batteries are:

- Low cycle life.
- Only a limited full discharge cycles are allowed.
- They have low energy density.
- Materials can be toxic when they evaporate, moreover lead and the electrolyte used are environmentally unfriendly.
- No fast charging is allowed.

Model

The battery model available at the library of MATLAB Simulink SimPowerSystems was used in this work.

Unit Control

No unit control is applied. The control signals come directly from the main control.

Main Control Link

The main control sends a control signal to the power converter that indicates if the battery must charge or discharge and how much according to the storage considerations.

4.4.3 Gas-Fired Turbine

Overview

Two gas turbines with a nominal electric power output of 100 kW each were selected for the example. The type of turbine considered in this work has a split-shaft design, which according to [96], can be modeled as a single-shaft turbine. Rowen [97] provided a simplified single-shaft gas turbine model that has been widely used in the literature. A block diagram of this model can be observed in Figure 4.7. In the following subsections each block in the diagram will be described. The PID control and the excitation control are described under unit control. This model is given in per unit.

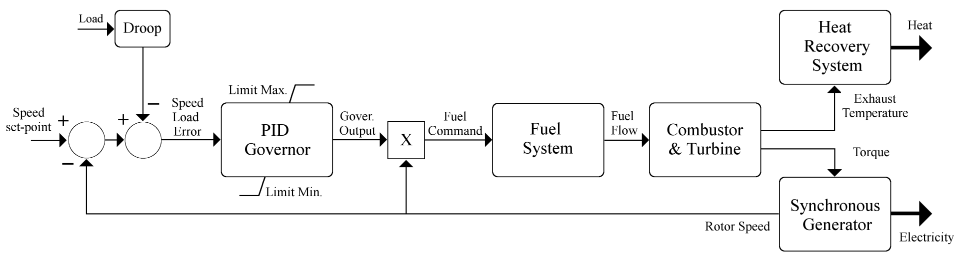

Figure 4.7: Schematic of the micro-CHP gas-fired generator

Model

Fuel System The input to the *fuel system* is the *fuel command*. The fuel command results from multiplying the governor output and the per unit mechanical rotor speed ω. In this study, pressure control may be neglected because of the small volume between these valves [97]. The fuel system consists of two valves in series: one corresponding to the valve positioning system and the other one to the actuator fuel system. Each subsystem has a constant associated with it. The constant τ_V is associated with the valve positioning system, and the constant τ_A is associated with the volumetric time constant related to the downstream piping and fuel gas distribution manifold [97]. The *fuel flow* is the output of this block.

Compressor-Combustor-Turbine Assembly The *fuel flow* is the input for the compressor-combustor-turbine assembly. The model incorporates three transport delays, one associated with the compressor discharge volume τ_{CD}, another associated with the combustion reaction time τ_{CR} and another associated with the gas from the combustion system through the turbine τ_{TD}. The turbine torque τ_{tur} and the turbine exhaust temperature T_{exh} are given by [97]:

$$\tau_{\text{tur}} = 1,3\left(\phi_{\text{m,fue}} - 0,23\right) + 0,5\,(1-\omega) \tag{4.17}$$

$$T_{\text{exh}} = T_{\text{rtd}} - 390(1-\phi_{\text{m,fue}}) + 306(1-\omega) \tag{4.18}$$

where T_{rtd} is the rated exhaust temperature of the turbine and $\phi_{\text{m,fue}}$ is the fuel flow. The subtraction of 0,23 from the fuel flow represents the percentage of fuel needed to keep the gas turbine under operation at a nominal speed, no-load condition.

Synchronous Generator The torque τ_{tur} that results from the compressor-combustor-turbine assembly model is the input for the synchronous generator model. The built-in model of a synchronous generator that is available at the library of MATLAB Simulink SimPowerSystems is used for the simulation.

Exhaust Heat Recovery System The exhaust temperature that results from the compressor-combustor-turbine assembly model T_{exh} is the input for the exhaust heat recovery system, which consists of a recuperator and a shell and tube heat exchanger in countercurrent configuration. The exhaust gases that come from the recuperator are transported to the heat exchanger.

The recuperator exhaust temperature T_{rec} can be calculated using the following equation:

$$T_{\text{rec}} = 0,405(T_{\text{exh}} - T_{\text{amb}}) + T_{\text{amb}} \tag{4.19}$$

where T_{amb} is the ambient temperature and the coefficient 0,405 results from a calculation that involves the inlet and outlet exhaust heat flow at rated values, the turbine exhaust temperature, the recuperator exhaust temperature and the exhaust gases mass flow taken from the micro-CHPs datasheet. The heat transport takes place at the contact area between the hot-side and cold-side exchanger chambers.

The equations that were introduced for the convection and conduction processes in Section 4.1 are used in this section to model the heat recovery heat exchanger. The exhaust gases coming from the recuperator enter the hot chamber of the heat exchanger and warm up the water coming from the return pipe of the district heating system. The hot side of the heat exchanger can be described by the following equation:

$$m_{\mathrm{exh}} c_{\mathrm{exh}} \frac{dT_{\mathrm{out,hot}}}{dt} = \phi_{\mathrm{m,exh}} c_{\mathrm{exh}} \left(T_{\mathrm{in,hot}} - T_{\mathrm{out,hot}}\right) - \Phi_{\mathrm{q,hex}} \tag{4.20}$$

where the incoming temperature at the hot side of the heat exchanger $T_{\mathrm{in,hot}}$ is equal to the recuperator exhaust temperature T_{rec} obtained with (4.19).

The cold side is represented by:

$$m_{\mathrm{wat}} c_{\mathrm{wat}} \frac{dT_{\mathrm{out,col}}}{dt} = \phi_{\mathrm{m,wat}} c_{\mathrm{wat}} \left(T_{\mathrm{in,col}} - T_{\mathrm{out,col}}\right) + \Phi_{\mathrm{q,hex}}. \tag{4.21}$$

In both cases $\Phi_{\mathrm{q,hex}}$ is given by:

$$\Phi_{\mathrm{q,hex}} = U_{\mathrm{hex}} A_{\mathrm{hex}} \Delta T_{\mathrm{LMTD,hex}} \tag{4.22}$$

where subscript ‘hex’ indicates CHP heat exchanger, subscript ‘exh’ represents the exhaust gases coming from the recuperator of the CHP unit, subscript ‘wat’ represents the water flowing through the return pipe of the district heating system, subscript ‘hot’ represents the hot side of the heat exchanger and subscript ‘col’ represents the cold side of the heat exchanger. The equations are based on (4.4) and (4.7). The logarithmic mean temperature difference $\Delta T_{\mathrm{LMTD,hex}}$ is given by:

$$\Delta T_{\mathrm{LMTD,hex}} = \frac{\left(T_{\mathrm{in,hot}} - T_{\mathrm{out,col}}\right) - \left(T_{\mathrm{out,hot}} - T_{\mathrm{in,col}}\right)}{\ln\left(\frac{T_{\mathrm{in,hot}} - T_{\mathrm{out,col}}}{T_{\mathrm{out,hot}} - T_{\mathrm{in,col}}}\right)}. \tag{4.23}$$

Unit Control

This unit is equipped with a PID control and an excitation control. The excitation control is a built-in MATLAB Simulink model.

PID Control

Function: keeps the desired frequency and desired power dispatch.

Trigger: responds to rotor speed error and load error signals.

Action: adjusts the fuel injection.

A Proportional-Derivative-Integral (PID) control that acts on the speed and load errors is selected for the gas turbine. The gains K_P, K_I and K_D are tuned in order to obtain the desired response of the turbine-generator set. In this dissertation, the PID gains that are used are the ones obtained in [90] by using the method suggested in [98] with a step signal as system load input. The value of the governor output is the steady state per unit value of the turbine’s mechanical power.

The speed error and the load error are obtained by subtracting the actual values to the respective assigned reference values. The generators work in droop mode: they share the load changes according to their droop. The droop gain that was selected for the generators is 4%, i.e. a hundred percent change on the output power will result in a four percent change in the frequency. The deviation in the frequency due to droop control is corrected by changing the operating point of the governor. This is done by means of adjusting the load reference set-point. In this way the desired frequency can be recovered. The minimum limit represents the gas turbine's capability of absorbing power from the connected system while maintaining fuel burning in the combustor [97], whereas the maximum limit accounts for the engine temperature control.

Excitation Control

Function: keeps the desired excitation voltage level.

Trigger: responds to a voltage error signal.

Action: adjusts excitation.

The generator is connected to the built-in excitation model to provide field voltage control. The model is available at the library of MATLAB Simulink SimPowerSystems. The model regulates the terminal voltage of the generator at a reference value.

Main Control Link

The set-point of the gas input comes from the main control. The participation of the combined heat and power unit is calculated by the main control as described in Section 4.3.2.

4.4.4 Solid Oxide Fuel Cell

Overview

The interest in fuel cells has increased during the last decade for several reasons, among them: their high efficiency in comparison to heat engines, the very low (or zero) harmful emissions, the low maintenance costs, the lack of vibrations and the very low noise emissions [99]. In this work a solid oxide fuel cell (SOFC) of a rated electric power output of 75 kW is considered. Solid oxide fuel cells are sometimes called the third generation of modern fuel cells [99]. The temperature at their stack ranges between 650°C and 1000°C. Due to their high temperatures, they are intended for stationary applications. Their power output ranges from a few kWs to several MWs. The high quality heat can be used for cogeneration purposes.

One of the main advantages of SOFCs is that because of the high temperatures involved, they do not need expensive catalysts and do not get poisoned by carbon monoxide, allowing fuel flexibility, however sulfur components must be removed before they enter the fuel cell. Furthermore, the high temperatures are linked to their main disadvantages: they have slow start-up times (when starting from cold) and the high temperatures produce corrosion of components. For this reason, research is nowadays focused on lowering the operating temperature down to 600°C in order to reduce the strict material requirements and reduce the start-up times [100].

Fuel cells have a basic structure consisting of an electrolyte and two electrodes. The main functions of the electrolyte are to act as an ion conductor so that ions can migrate from one electrode to another, to act as an electron insulator, so that electrons are forced to flow through the external circuit and to act as a barrier to separate the reactants [99]. On the other hand the main functions of the electrodes are: to provide a place for the electrochemical reaction to occur, to collect the electrons and to provide a flow path for the electron transfer. The fuel cell voltage is equal to the potential difference between the cathode and the anode and the fuel cell's current is defined as the current that flows from the cathode to the anode through the external circuit (opposite to the electron flow), to which the load is connected. Figure 4.8 shows a graphic representation of the SOFC.

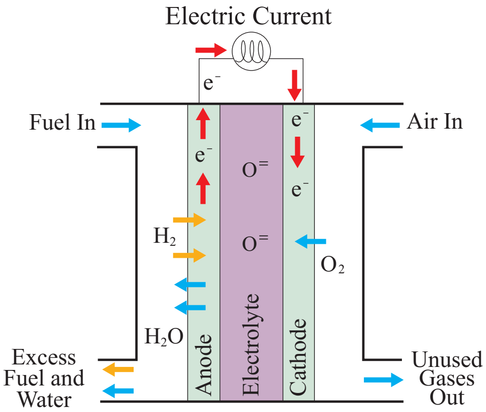

Figure 4.8: Schematic of the solid oxide fuel cell

Model

Fuel Cell Model The fuel cell model available at the library of MATLAB Simulink SimPowerSystems was used in this work.

Heat Recovery System The heat exchanger is modeled using the same equations that were used to model the heat exchanger of the gas turbine. The hot side of the heat exchanger can be described by the following equation:

$$m_{\text{air}} c_{\text{air}} \frac{dT_{\text{out,hot}}}{dt} = \phi_{\text{m,air}} c_{\text{air}} \left(T_{\text{in,hot}} - T_{\text{out,hot}} \right) - \Phi_{\text{q,hex}} \tag{4.24}$$

the air is heated thanks to the fuel cell's stack.

The cold side is represented by:

$$m_{\text{wat}} c_{\text{wat}} \frac{dT_{\text{out,col}}}{dt} = \phi_{\text{m,wat}} c_{\text{wat}} \left(T_{\text{in,col}} - T_{\text{out,col}} \right) + \Phi_{\text{q,hex}}. \tag{4.25}$$

In both cases $\Phi_{\text{q,hex}}$ is given by:

$$\Phi_{\text{q,hex}} = U_{\text{hex}} A_{\text{hex}} \Delta T_{\text{LMTD,hex}} \tag{4.26}$$

where subscript ‘hex’ indicates SOFC heat exchanger, subscript ‘air’ represents the hot air coming from the stack of the SOFC, where the high temperatures are produced, subscript ‘wat’ represents the water flowing through the return pipe of the district heating system, subscript ‘hot’ represents the hot side of the heat exchanger and subscript ‘col’ represents the cold side of the heat exchanger. The equations are based on (4.4) and (4.7). The logarithmic mean temperature difference $\Delta T_{\mathrm{LMTD,hex}}$ is given by:

$$\Delta T_{\mathrm{LMTD,hex}} = \frac{\left(T_{\mathrm{in,hot}} - T_{\mathrm{out,col}}\right) - \left(T_{\mathrm{out,hot}} - T_{\mathrm{in,col}}\right)}{\ln\left(\frac{T_{\mathrm{in,hot}} - T_{\mathrm{out,col}}}{T_{\mathrm{out,hot}} - T_{\mathrm{in,col}}}\right)}. \tag{4.27}$$

Unit Control

A simple delay transfer function is used as unit control for the fuel cell.

Main Control Link

Due to the fact that fuel cells are DC devices, the SOFC is connected to the system by means of an inverter. The inverter receives the power/current settings from the main control.

4.4.5 Furnace

Overview

The furnace model is based on [101] and was implemented and described in [90]. A furnace of a nominal power of 550 kW was selected. The furnace system consists of the furnace and a heat exchanger that transfers heat coming from the flue gases of the furnace to the district heating water.

Model

Furnace The heat that comes from the furnace $\Phi_{\mathrm{q,fur}}$ can be obtained by using (4.5). The factor ξ_{fur} [-] is added to this equation to represent the losses in the furnace:

$$\Phi_{\mathrm{q,fur}} = \phi_{\mathrm{m,flu}} c_{\mathrm{flu}} \left(T_{\mathrm{in,fur}} - T_{\mathrm{out,fur}}\right) \xi_{\mathrm{fur}} \tag{4.28}$$

where $\phi_{\mathrm{m,flu}}$ is the mass flow of the flue gases, c_{flu} represents the specific heat capacity of the flue gases, $T_{\mathrm{in,fur}}$ is the predicted combustion temperature during the fuel combustion adiabatic process, also denoted T_{aft} and $T_{\mathrm{out,fur}}$ represents the temperature of the gases at the exit of the furnace. The equations that are used to calculate the combustion temperature and the temperature of the gases at the exit are given by:

$$T_{\mathrm{in,fur}} = T_{\mathrm{aft}} = \frac{\Upsilon_{\mathrm{LHV,fue}} + r_{\mathrm{afr}} \iota_{\mathrm{exs}} c_{\mathrm{air}} \left(T_{\mathrm{air}} - 80\right)}{\left(1 + r_{\mathrm{afr}} \iota_{\mathrm{exs}}\right) c_{\mathrm{flu}}} \tag{4.29}$$

$$T_{\mathrm{out,fur}} = T_{\mathrm{aft}} \epsilon_{\mathrm{fur}} \tag{4.30}$$

where $\Upsilon_{\text{LHV,fue}}$ is the lower heating value of the fuel, r_{afr} is the stoichiometric air fuel ratio, ι_{fur} [-] is a factor related to the excess air and T_{air} is the temperature of the outside air and ϵ_{fur} [-] is a dimensionless furnace parameter that is based on experimental data. The mass flow of the flue gases $\phi_{\text{m,flu}}$ results from the addition of the fuel mass flow $\phi_{\text{m,fue}}$ and the air mass flow $\phi_{\text{m,air}}$:

$$\phi_{\text{m,flu}} = \phi_{\text{m,fue}} + \phi_{\text{m,air}} \tag{4.31}$$

where the mass flow of the air depends on the stoichiometric air fuel ratio r_{afr} and a factor related to the excess air ι_{exs}:

$$\phi_{\text{m,air}} = \phi_{\text{m,fue}} r_{\text{afr}} \iota_{\text{exs}}. \tag{4.32}$$

Unit Control

No unit control is included. The set-points come directly from the main control.

Main Control Link

The set-point for the gas flow input comes directly from the heat control subsystem of the main control.

4.4.6 District Heating Load

Overview

A brief introduction to district heating systems was already given in Chapter 1. The district heating system considered in this work consists of two types of loads: the service water heat load and the space heating heat load. Each load is supplied with a separate heat exchanger. The district heating considered contains a return pipeline. The temperature is kept at 100°C at the hot water pipeline by the control. A brief description of the model is provided below.

Model

In the model considered, pressure differences are neglected. The equations presented in Section 4.1 are used to represent the different components.

Service Water Heating Load The relation between the service water heat demand $\Phi_{\text{q,swh}}$ and the mass flow $\phi_{\text{m,wat}}$ of the water flowing through the district heating pipelines is obtained by using (4.5). In this case the subscript 'swh' is used to represent the service water heating and 'wat' is used to represent the flowing water.

$$\Phi_{\text{q,swh}} = \phi_{\text{m,wat}} c_{\text{wat}} \left(T_{\text{in,swh}} - T_{\text{out,swh}} \right) \tag{4.33}$$

where $T_{\text{in,swh}}$, given in Kelvin, and is equivalent to 15 °C and $T_{\text{out,swh}}$ is equivalent to 80°C.

Space Heating Load The space heating demand represents the heat load required to keep the indoor temperature at 20°C. The heat $\Phi_{\mathrm{q,rad}}$ is transferred to the rooms by means of radiators. Heat leaves the rooms through walls $\Phi_{\mathrm{q,wal}}$, windows $\Phi_{\mathrm{q,wdw}}$ and the roof $\Phi_{\mathrm{q,rof}}$. The resulting energy balance equation is:

$$m_{\mathrm{air}} c_{\mathrm{air}} \frac{dT_{\mathrm{in,hhd}}}{dt} = \Phi_{\mathrm{q,rad}} - \Phi_{\mathrm{q,wal}} - \Phi_{\mathrm{q,wdw}} - \Phi_{\mathrm{q,rof}} \tag{4.34}$$

where

$$\Phi_{\mathrm{q,wal}} = U_{\mathrm{wal}} A_{\mathrm{wal}} \left(T_{\mathrm{in,hhd}} - T_{\mathrm{out,hhd}}\right) \tag{4.35}$$

$$\Phi_{\mathrm{q,wdw}} = U_{\mathrm{wdw}} A_{\mathrm{wdw}} \left(T_{\mathrm{in,hhd}} - T_{\mathrm{out,hhd}}\right) \tag{4.36}$$

$$\Phi_{\mathrm{q,rof}} = U_{\mathrm{rof}} A_{\mathrm{rof}} \left(T_{\mathrm{in,hhd}} - T_{\mathrm{out,hhd}}\right) \tag{4.37}$$

where Φ_{q} is the heat transferred per unit of time, U is the heat transfer coefficient, A is the area and $\left(T_{\mathrm{in}} - T_{\mathrm{out}}\right)$ is the difference that drives the heat transfer phenomena. Subscript ‘hhd’ means household.

Radiators The radiator is represented by the following equation:

$$m_{\mathrm{wat}} c_{\mathrm{wat}} \frac{dT_{\mathrm{out,rad}}}{dt} = \phi_{\mathrm{m,wat}} c_{\mathrm{wat}} \left(T_{\mathrm{in,rad}} - T_{\mathrm{out,rad}}\right) - \Phi_{\mathrm{q,rad}} \tag{4.38}$$

where:

$$\Phi_{\mathrm{q,rad}} = U_{\mathrm{rad}} A_{\mathrm{rad}} \Delta T_{\mathrm{LMTD,rad}} \tag{4.39}$$

where subscript ‘rad’ indicates radiator and subscript ‘wat’ represents the water flowing through the radiator. The equations are based on (4.4) and (4.7). The logarithmic mean temperature difference $\Delta T_{\mathrm{LMTD,rad}}$ is given by:

$$\Delta T_{\mathrm{LMTD,rad}} = \frac{\left(T_{\mathrm{in,rad}} - T_{\mathrm{out,rad}}\right)}{\ln\left(\frac{T_{\mathrm{in,rad}} - T_{\mathrm{in,hhd}}}{T_{\mathrm{out,rad}} - T_{\mathrm{in,hhd}}}\right)} \tag{4.40}$$

where $T_{\mathrm{in,rad}}$ is the temperature at the entrance of the radiator, $T_{\mathrm{out,rad}}$ is the temperature at the exit of the radiator and T_{hhd} is the household’s indoor temperature.

Heat Exchangers The heat exchangers are modeled in a similar way to those of the CHP units and the SOFC.

Heat Losses The heat losses in the pipes $\Phi_{\mathrm{q,sur}}$ are modeled as heat conduction to the surrounding soil from the pipe insulator. The equation that represents the transfer is:

$$m_{\mathrm{wat}} c_{\mathrm{wat}} \frac{dT_{\mathrm{pip}}}{dt} = \phi_{\mathrm{m,wat}} c_{\mathrm{wat}} \left(T_{\mathrm{sur}} - T_{\mathrm{pip}}\right) - \Phi_{\mathrm{q,sur}} \tag{4.41}$$

where:

$$\Phi_{\mathrm{q,sur}} = U_{\mathrm{pip}} A_{\mathrm{pip}} \Delta T_{\mathrm{LMTD}} \tag{4.42}$$

where subscript ‘pip’ indicates return pipeline, subscript ‘sur’ represents the surroundings and subscript ‘wat’ represents the water flowing through the pipeline. The equations are based on (4.4) and (4.7).

Unit Control

Radiator Control This control keeps the desired indoor temperature by controlling the amount of water mass that flows into the radiator. It consists of a proportional control.

4.4.7 Heat Storage Tank

Overview

The heat storage considered in this work consists of a water tank with a maximum designed capacity of 190 kWh. The tank has a cylindrical shape and is buried in the soil. A heat exchanger is connected between the tank and the hot pipeline of the district heating infrastructure.

Model

In this model the temperature of the storage medium is considered homogeneous.

Tank The storage tank is represented by the following equation:

$$m_{\mathrm{wat}} c_{\mathrm{wat}} \frac{dT_{\mathrm{in,tnk}}}{dt} = \Phi_{\mathrm{in}} - \Phi_{\mathrm{out}} \tag{4.43}$$

where Φ_{out} is equal to the losses to the surroundings:

$$\Phi_{\mathrm{out}} = \Phi_{\mathrm{q,los}} = U_{\mathrm{tnk}} A_{\mathrm{tnk}} (T_{\mathrm{in,tnk}} - T_{\mathrm{out,tnk}}) \tag{4.44}$$

and Φ_{in} is equal to the heat coming from the system $\Phi_{\mathrm{q,sys}}$ times the storage conversion efficiency η_{tnk} [-]:

$$\Phi_{\mathrm{in}} = \Phi_{\mathrm{q,tnk}} = \Phi_{\mathrm{q,sys}} \eta_{\mathrm{tnk}} \tag{4.45}$$

where the storage efficiency η_{tnk} is given by:

$$\eta_{\mathrm{tnk}} = \begin{cases} \eta_{\mathrm{tnk}}, & \text{charging} \\ \frac{1}{\eta_{\mathrm{tnk}}}, & \text{discharging.} \end{cases}$$

Subscript 'tnk' indicates storage tank and subscript 'wat' represents the water contained in the tank. The heat transfer coefficient U_{tnk} depends on heat transfer parameters of the insulator and the soil.

Unit Control

No unit control is applied.

Main Control Link

The main control sends a control signal that indicates if the heat storage must charge or discharge and how much according to the storage considerations.

4.4.8 Summary

In Figure 4.9 the energy hub for the example is presented and Table 4.2 shows the hub elements and their relation to the multi-carrier hierarchical control architecture.

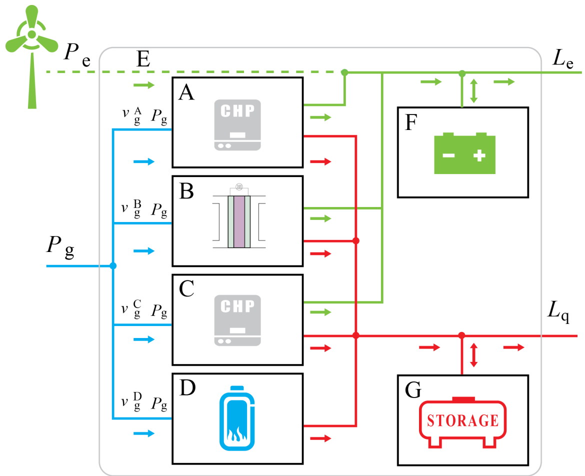

Figure 4.9: Energy hub used in the example

Table 4.2: Components and control subsystems

Hub Element	Hub's Converter	Control Subsystem	Set-point from Main Control	Unit Control
CHP (gas turbine)	A	electricity	gas flow	PID control excitation control
CHP (SOFC)	B	electricity	current	delay transfer function
CHP (gas turbine)	C	electricity	gas flow	PID control excitation control
Boiler	D	heat	gas flow	none
Wind turbine	E	none	none	rotor speed control pitch angle control
Battery bank	F	electricity	current	none
Heat tank	G	heat	gas flow	none

4.5 Simulation Results

The optimal scheduling and power dispatch are obtained from the multi-carrier unit commitment program, however, in the first two simulations the purpose is to show the operation of the hierarchical control architecture, thus the selected dispatch does not correspond to the optimal one. Simulation 1 shows the results of the electricity control subsystem, Simulation 2 shows the results of the heat control subsystem and Simulation 3 presents the results of both subsystems for a simulation period of 24 hours in which the optimal scheduling and optimal power dispatch are determined by the multi-carrier unit commitment program.

4.5.1 Simulation 1: Electricity Control Subsystem Demonstration

This section shows the operation of the electricity control subsystem. The units are working at no-load and the assigned dispatch is set to zero for all units (this is equivalent to assuming that the forecasted electric load is equal to zero). This is done in order to show how the two-level hierarchical control accounts for unpredicted load variations in the system. The electric load pattern and the wind power supply were arbitrarily chosen.

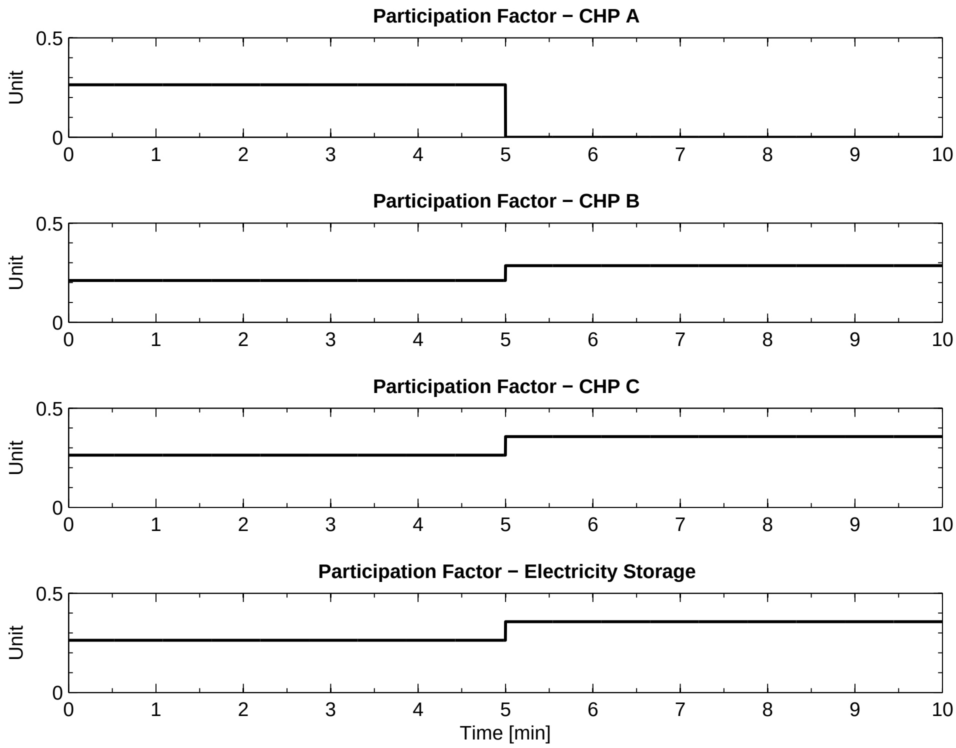

Figure 4.10: Simulation 1: Participation factors of controllable units

As a consequence of having no initial assigned dispatch, the participation factor of each unit is defined according to the unit's rated capacity. At the beginning of the simulation all units are available. At the 5th minute of the simulation CHP A is forced to stop delivering power, thus the main control reassigns the required power demand to the remaining available units. The change in the participation factor of each controllable unit can be observed in Figure 4.10. The rated capacity of CHP A, CHP B, CHP C and the storage are 100 kW, 75 kW, 100 kW and 100 kW respectively. Thus the initial participation factors are 0,26 for CHP A, CHP C and the storage and 0,21 for CHP B. After 5 minutes, the new participation factors are 0,36 for CHP C and the storage and 0,29 for CHP B (the SOFC).

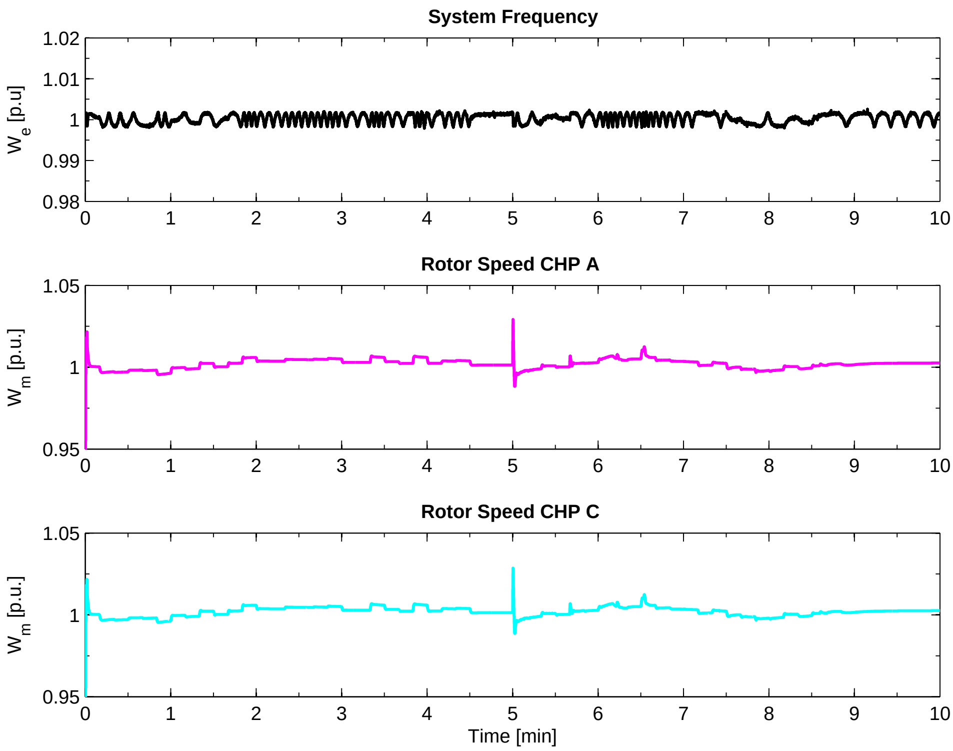

Figure 4.11: Simulation 1: Frequency of the system and rotor speeds

Figure 4.11 shows the control parameter of the electricity control subsystem: the system's frequency. Additionally, the rotor speeds of the gas turbines are depicted (CHP A and CHP C). It can be observed that thanks to the control strategy, the frequency was kept stable. In Figure 4.12 three graphs are presented: the total electricity demand, the wind turbine's supply and the power supply delivered by the gas turbines (CHP A and CHP C) and the fuel cell (CHP B). It can be observed that when the output of the wind turbine increases, the power supplied by the CHPs is reduced accordingly in relation to the participation factors.

Figure 4.13 shows the state of charge of the electricity storage. The total electricity demand and storage supply are also depicted in the upper graph in order to show the correspondence between the state of charge and the power requirements. As it was described in Section 4.3, in order to charge or discharge the storage units, the control system first checks its availability. In the simulation the state of charge remained close to 80%.

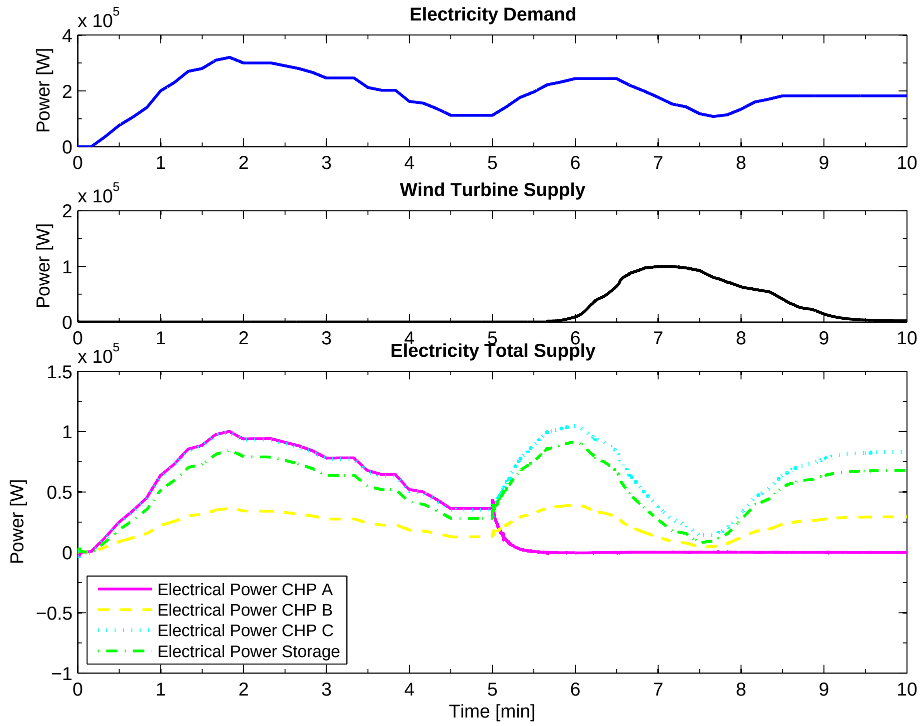

Figure 4.12: Simulation 1: Electricity demand and electricity supply

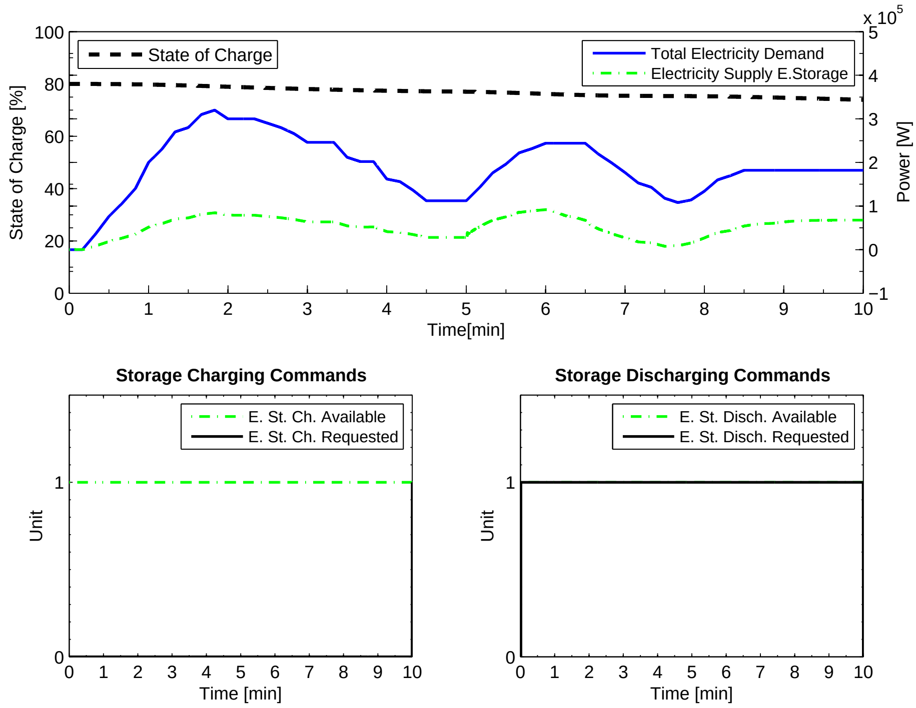

Figure 4.13: Simulation 1: Electricity storage behavior

4.5.2 Simulation 2: Heat Control Subsystem Demonstration

This section shows the heat control subsystem under operation. The space heating and service water loads were arbitrarily chosen and the output of the CHPs is given as an input. Figure 4.14 contains the results of the control parameters: the hot line temperature of the district heating system and the indoor temperature. The return line temperature and the outdoor temperature are also included. It can be observed that the room temperature was kept at 20°C during the whole simulation period and the hot line close to 100°C.

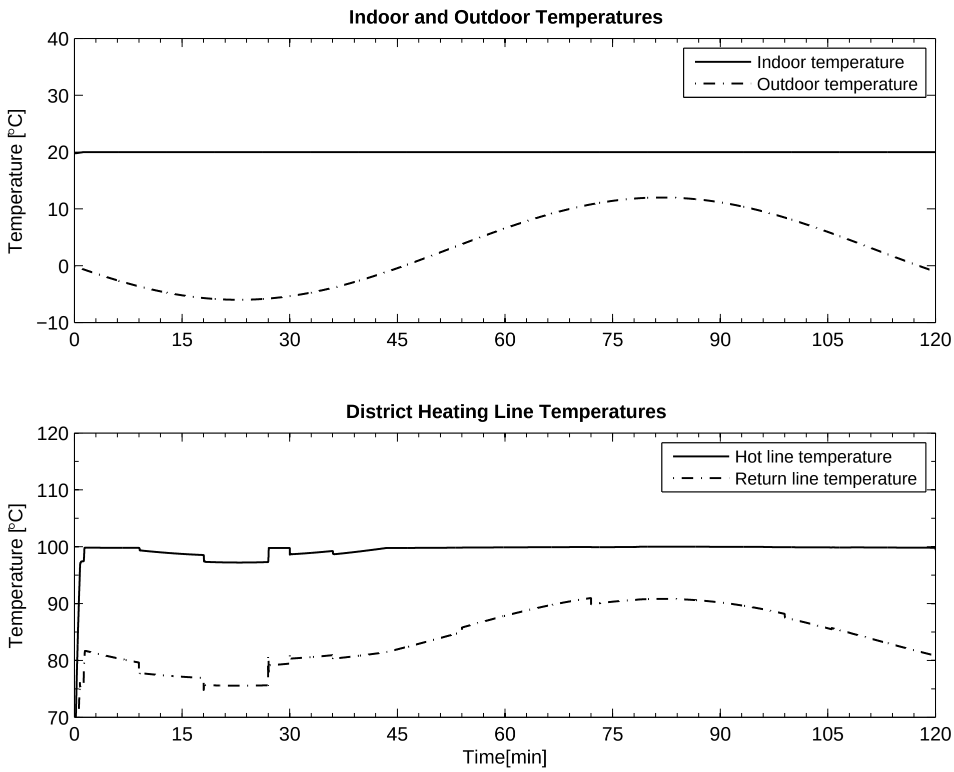

Figure 4.14: Simulation 2: Indoor temperature and DHS line temperatures

Figure 4.15 contains 2 different graphs. The first graph shows the total space heating demand (in correspondence with the outside temperature variation) as well as the space heating demand and the service water demand. In the second graph, the power supplied by the furnace, the CHPs and the heat storage is depicted. It can be observed that the furnace and the storage tank supply heat so that the power balance was accomplished during the whole simulation.

Figure 4.16 shows the total heat demand and storage heat. The temperature of the storage tank, the storage change and discharge commands and the storage availability are also presented to show the correspondence with the heat supplied by the tank.

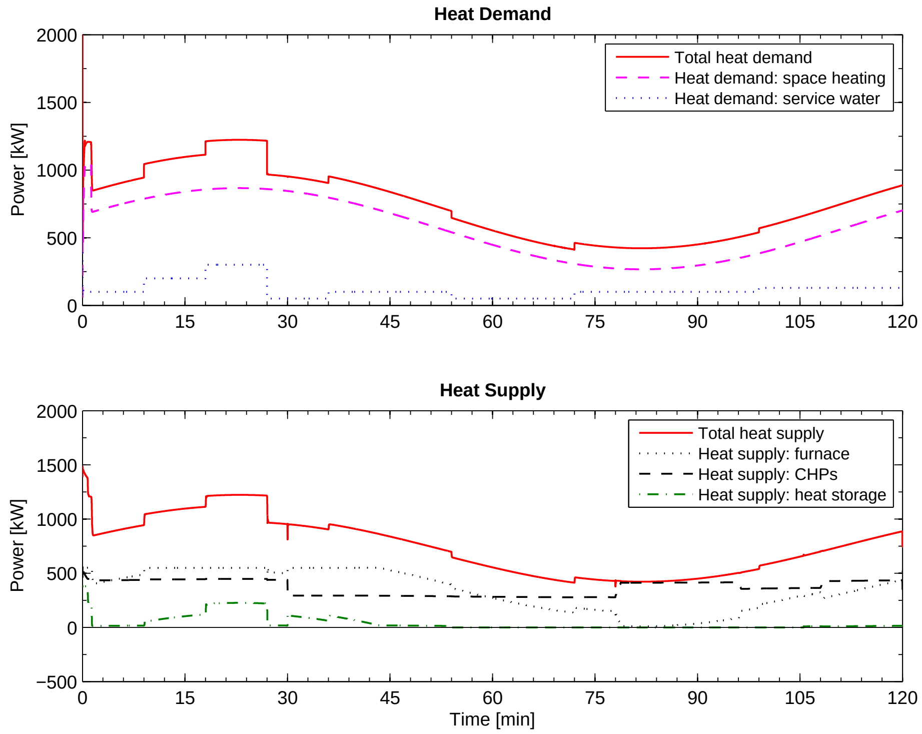

Figure 4.15: Simulation 2: Heat demand and heat supply

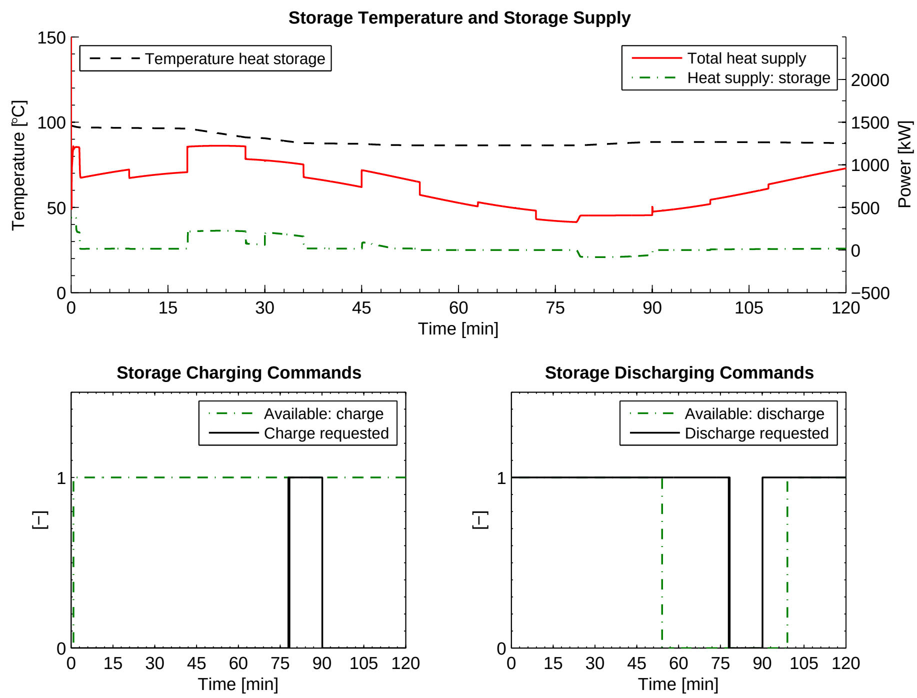

Figure 4.16: Simulation 2: Heat storage behavior

4.5.3 Simulation 3: Complete System Demonstration

In this section a demonstration of the complete system's operation is presented. The simulation was done for 24 hours. The wind speed forecast was obtained from a model that was developed for this project. This forecast model will be described in more detail in Section 6.2.1. Figure 4.17 shows both the forecasted and the actual electric output of the wind turbine and Figure 4.18 shows the forecasted and actual electric load values used in the simulation. It is assumed that the actual heat load values are equal to the predicted ones. Figure 4.19 shows the total heat load, the space heating load and the service water load. As it can be noted in Figure 4.17 and Figure 4.18, the actual values of the wind turbine's power output and electric load differ from the forecasted ones, this gives room for the control system to operate and keep the control parameters within a suitable range of operation.

The forecasted values discussed above are the input to the multi-carrier unit commitment program. Previous to the multi-carrier hierarchical control simulation, the multi-carrier unit commitment program is used to find the optimal solution. In this way the *scheduled* values can be obtained. In Figure 4.1, the *set-points coming from the optimization* shown at the top of the two-level hierarchical control scheme are equal to the results of the multi-carrier unit commitment program.

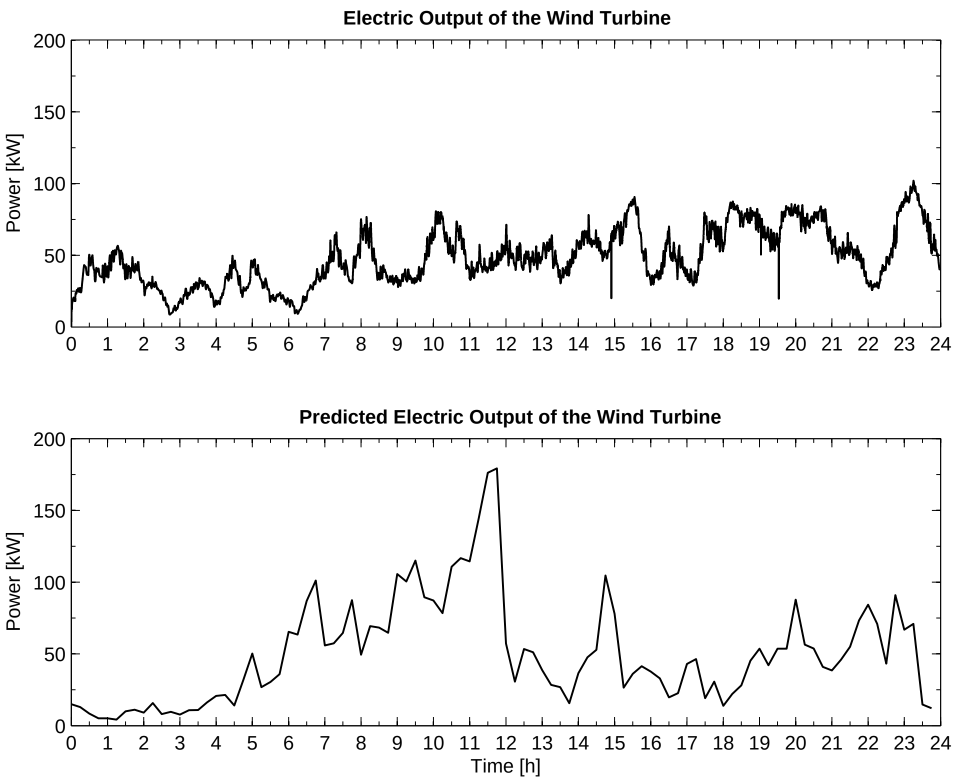

Figure 4.17: Simulation 3: Forecasted and actual output of the wind turbine

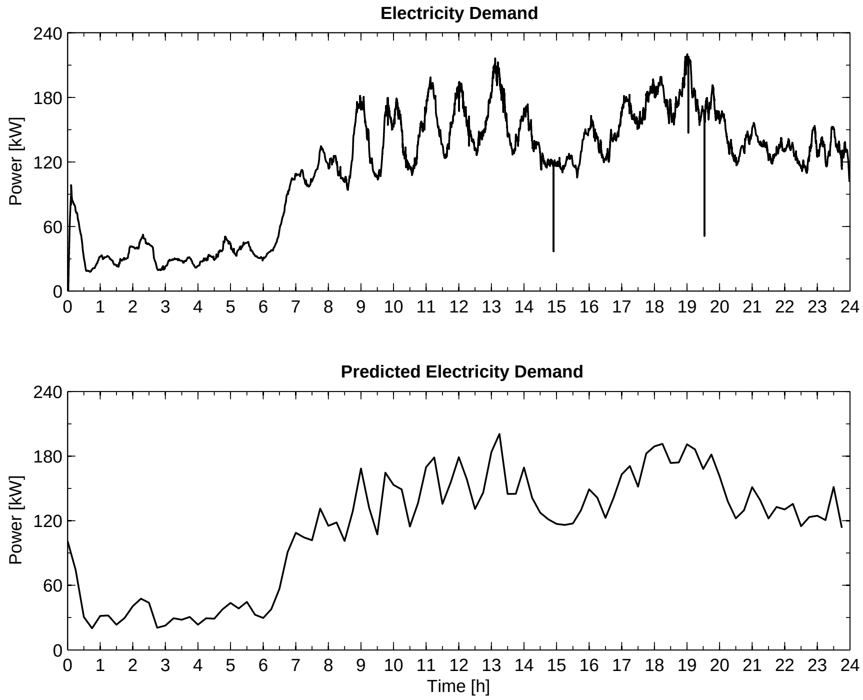

Figure 4.18: Simulation 3: Forecasted and actual electricity load

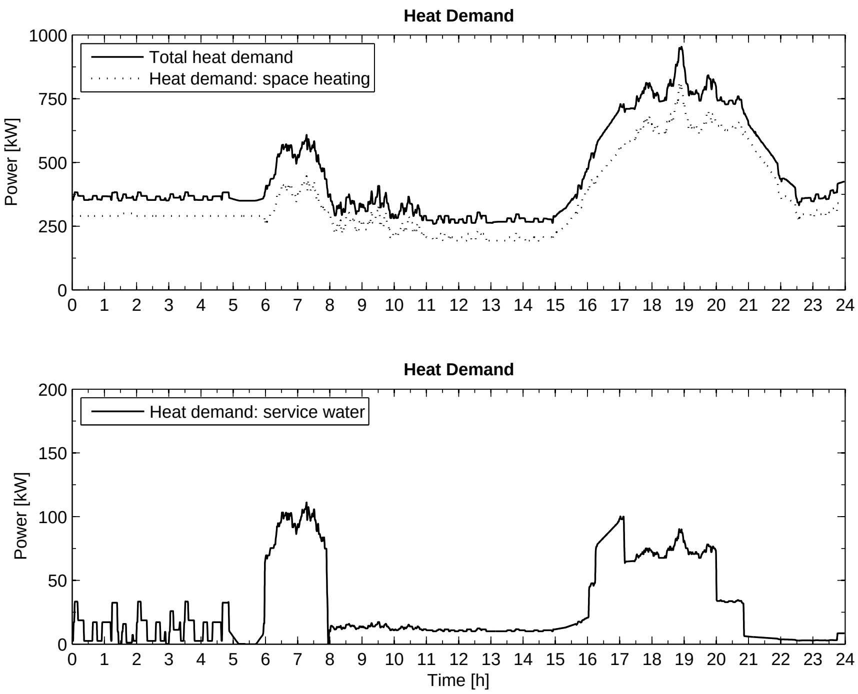

Figure 4.19: Simulation 3: Heat load

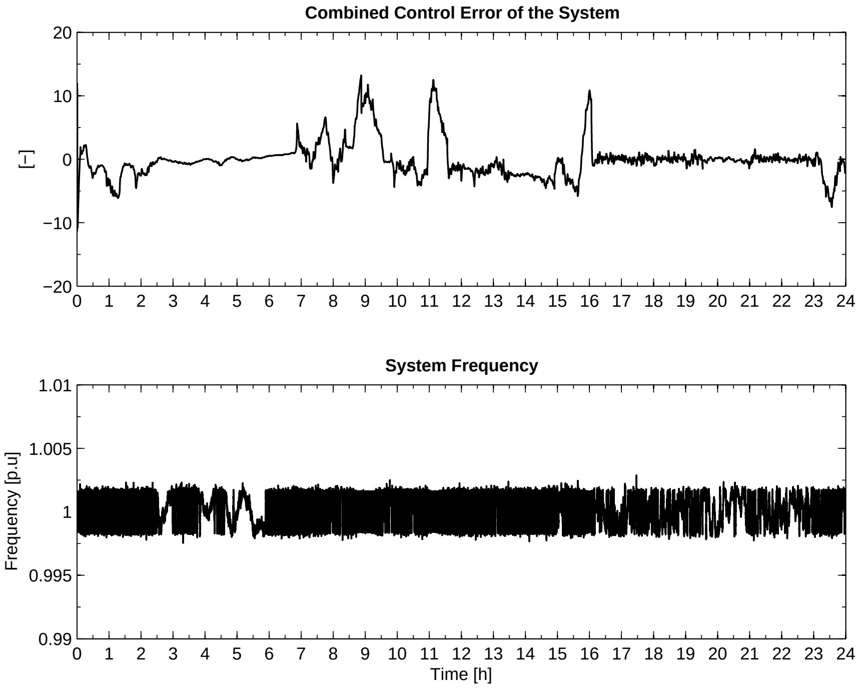

Figure 4.20: Simulation 3: Combined control error and frequency of the system

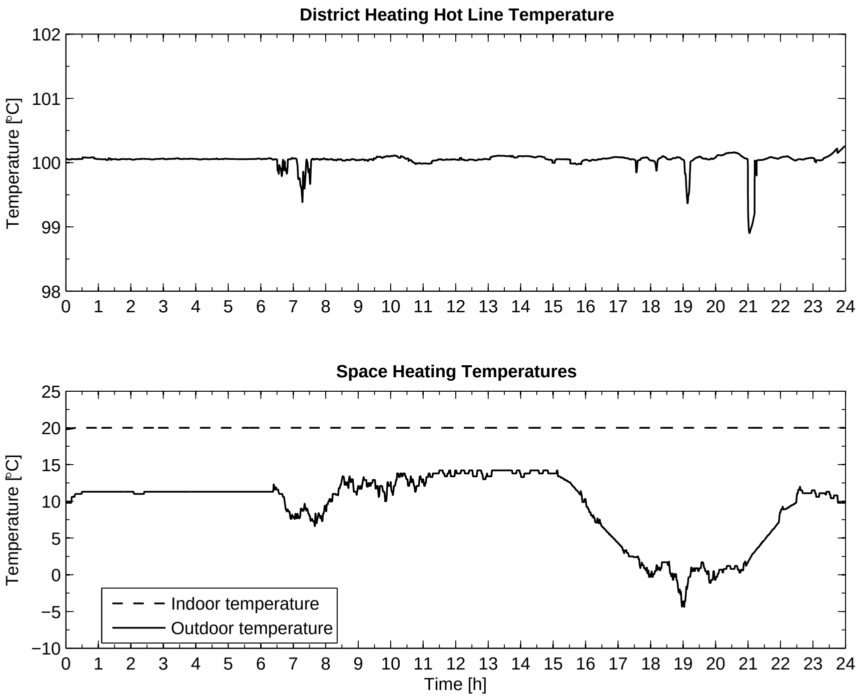

Figure 4.21: Simulation 3: Temperature of the district heating hot line and the space heating

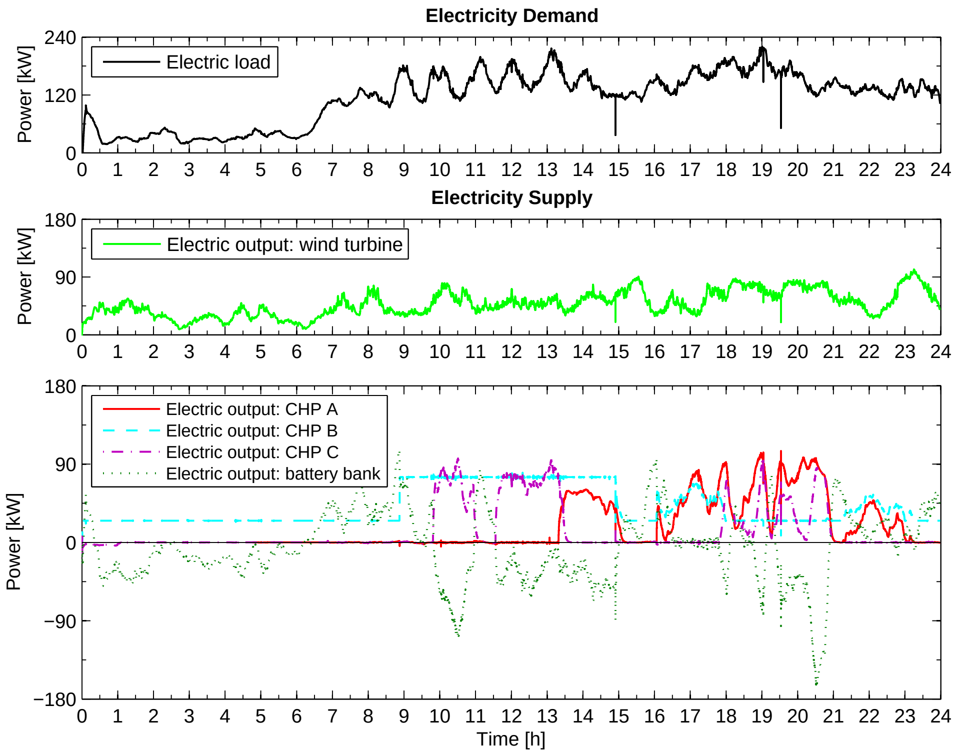

Figure 4.22: Simulation 3: Total electricity demand and electricity supply

In Figure 4.20 and in Figure 4.21 it can be observed that even though there were differences with respect to the forecasted values, the system's frequency, the hot water pipeline temperature and the room temperature were kept within the acceptable boundaries.

Figure 4.22 shows three graphs, the first one shows a curve with the electricity demand, the second one shows the wind turbine's power output and the third one present the power supplied by the CHP units and the storage elements during the 24-hour simulation. CHP B has a minimum operation setting of 25% of its maximum capacity, for this reason it operates during the whole simulation. It can be observed that the storage unit plays an important role in keeping the power balance of the system.

The reader can compare the scheduled values and the actual values in the figures shown in Appendix B. They show the response of the individual units. It can be noted that the overall shape of the actual dispatch is similar to the scheduled one but that the instantaneous values differ from each other due to the influence of the performed control actions. This response coincides with the expectations.

4.6 Conclusions

This chapter presented a two-level hierarchical integrated control architecture for systems that contain multiple energy carriers. In the example electricity and gas were considered as input and electricity and heat as the output. The general architecture was adapted to fit the selected example. In this way the applicability of the control scheme was tested. It showed to be robust and stable for normal operating conditions. Other control actions like load shedding can be applied using the same architecture.

By using an integrated control strategy, the flexibility of having more energy carriers was explored. In future work it would be interesting to include more energy carriers and test the applicability of the control scheme that was designed. Furthermore, the interaction with smart protection algorithms should also be studied.

Chapter 5

The Scenarios

Multi-Carrier Power Applications

This chapter answers Research Question 5 of this dissertation. Section 5.1 presents theoretical concepts that have not been introduced in previous chapters. Section 5.2 presents a brief literature review on works where the concept of aggregating household generation units has been applied. In Section 5.3 the different scenarios to be simulated are described. Section 5.4 includes the input data that are used in the simulations: the prices, the parameters of the storage devices and the parameters of the generation components. Section 5.5 presents the results of the different simulations and includes a discussion based on the comparison of scenarios. Finally in Section 5.6 the conclusions of this chapter are drawn.

5.1 Basic Concepts and Definitions

5.1.1 Virtual Power Plant

In the literature, different definitions of a *virtual power plant* can be found. A definition that fits the scope of this dissertation is the following [102]:

> *A VPP combines different types of renewable and non-renewable generators and storage devices to be able to pose on the electricity market as a single power plant with defined hourly (15 min) output.*

The control of a virtual power plant can be done directly or indirectly. When done directly, the aggregator has control on the signals that are sent to the generation units, whereas when it is done indirectly the aggregator only sends price signals and the household owing the generation unit reacts on them [103]. From this classification it can be inferred that direct control gives the best results, since the aggregator not only sends the prices for the households to react according to their will, but sends the set-points to the micro-generation units itself. Therefore, the aggregator sends and receives information from the users.

5.1.2 Aggregator

The term *aggregator* can be used to refer to different entities, for example retail companies, distribution system operators or integrated utilities, among others. In this dissertation the aggregator will represent an integrated power management node having ICT communication with all houses that have agreed to participate in the group optimization. Therefore, the definition of aggregator used in this dissertation is the following [103]:

> *An aggregator is an actor that trades with aggregate power flows to/from households and/or operates a virtual power plant by controlling micro-CHPs and other controllable units available.*

Several benefits of using an aggregator were found in the literature. Some of the most important ones are the following:

- The controllers at the household level remain simple (only sensing and actuation devices are required) since the optimization control is lifted from the household level to the aggregator level.
- Investments in communication and control equipment become lower when it is done for clusters of households.
- There is higher predictability of aggregated energy demand than that of individual households.

5.2 Literature Review

This literature review comprises articles in which the virtual power plant concept is studied. The articles dealing with the virtual power plant concept can be divided into two categories, those that deal with medium-sized generation plants that are clustered to virtually function as a single power plant and those papers that deal with the aggregation of small-sized generation units placed in households and building infrastructures. Since this chapter pays attention to the latter, papers focusing on micro-generation units of a few kWs are considered in this review.

Several papers focus on the development of virtual power plant optimization frameworks. Some of the methods proposed include *service oriented architecture* [104] and *multi-agent-based control*. For example, in [105] a multi-agent-based control was applied to a test facility consisting of renewable sources and controllable units. The work focused on the implementation of such multi-agent-based control in a real environment. Furthermore, a large percentage of the available papers focus on market-based virtual power plants. In this context, price-signal based control and bidding scenarios are studied [106–109].

The following paragraphs refer to papers that deal with the control of micro-CHPs. They were selected for this review due to their relevance to this research. In [110] a simulation tool based on the software packages Microsoft Excel and Visual Basic is presented. The simulation tool can simulate one day or one year. The input of the tool are electrical and thermal consumption data, given in intervals of 15 minutes. The output data are the thermal and electrical power generated, the content of the heat accumulator, the number of start-ups of the micro-CHP and the electricity supplied from the grid [110]. Even though the paper states the potential benefits of using the VPP concept with several houses, the results shown refer to the output of a single household, thus the interactions between the cluster of houses is not presented. One of the objectives of this chapter is to show the influence that the aggregator has on the interaction among different households.

In [111] each device is represented by an agent that seeks for an economical optimum. In this case no central optimization entity is required. The communication with the auctioneer is very limited since it only exchanges bids between the agents and the agent platform. The agent decides when to start producing according to the bids. The network structure used is the PowerMatcher. The PowerMatcher performs the price-forming process; it coordinates demand and supply of a cluster of devices located directly below it [111]. In this chapter the optimization is shifted to the aggregator due to the reasons mentioned in Section 5.1. In [111] no storage, renewable sources or heat flows were included.

In [112] a methodology of a traceable and modular VPP is presented. The system allows energy trade, network services and balancing. In the paper, some opportunities of using a VPP are listed, for example, to facilitate decentralized energy owners to trade their production, to provide VPP stakeholders with the opportunity of getting benefits from participating in the primary, secondary and tertiary control and to support network operators in congestion and load management. The paper states that further tests are required to execute and evaluate the added value of implementing such system. In this chapter several comparisons are presented in which the added value of having a VPP is shown.

Lastly, [103] presents a VPP control strategy to resolve wind imbalance. Results are shown for a winter week in January. The author focuses of the economic incentives in VPP to invest in micro-CHP units. The simulations were performed using stirling engines placed inside the households. The author concludes that the imbalance volume due to wind and the associated costs can be reduced to 33% and 20% respectively. The research gives good insights about the potential benefits of applying the VPP concept. The author states that further comparisons between other micro-CHP technologies are important. As a response to this argument, this chapter presents a comparison among three different household-level micro-CHP technologies.

5.3 Optimization Scenarios

This section introduces the optimization scenarios that were considered:

Scenario 1 Base Case

Scenario 2 Individual Optimization

Scenario 3 Individual Optimization with Storage

Scenario 4 Collaborative Optimization (Aggregator)

Scenario 5 Collaborative Optimization with Storage (Aggregator)

The inclusion of renewables and electric vehicles is evaluated for different of the aforementioned scenarios in separate simulations. Each scenario is described in the following subsections.

5.3.1 Scenario 1: Base Case

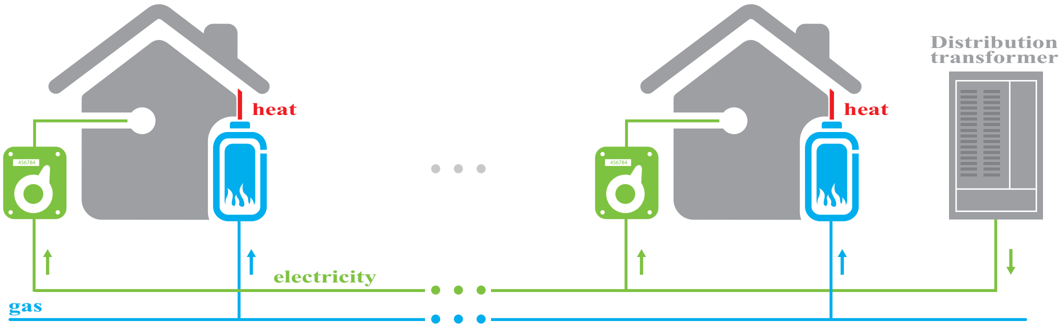

Figure 5.1: Scheme for Scenario 1 - Base case

This scenario is considered the base scenario for comparison. The following assumptions are considered:

- Each household has a furnace to supply its heat load.
- Each household is connected to the electrical grid, from which its electric load is supplied.
- There are no renewable energy technologies or storage elements installed.

5.3.2 Scenario 2: Individual Optimization

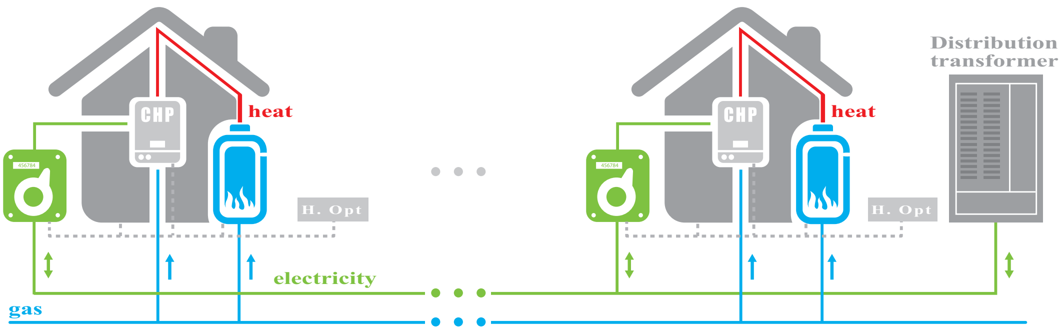

Figure 5.2: Scheme for Scenario 2 - Individual optimization

In this optimization micro-CHP units are placed at each household.

- Each household has a micro-CHP unit to supply (part of) its heat and electricity.
- Each household has a furnace as auxiliary device to supply (part of) its heat load.
- Each household is connected to the electrical grid, from which (part of) its electric load is supplied. Excess electricity produced by the micro-CHP units can be fed back to the grid.
- There are no renewable energy technologies or storage elements installed.
- Each household is optimized individually.
- Each household is represented by an individual energy hub.

The optimization tool developed using the modeling assumptions and algorithms presented in Section 2.3.1 is used to find the solution of this scenario.

5.3.3 Scenario 3: Individual Optimization with Storage

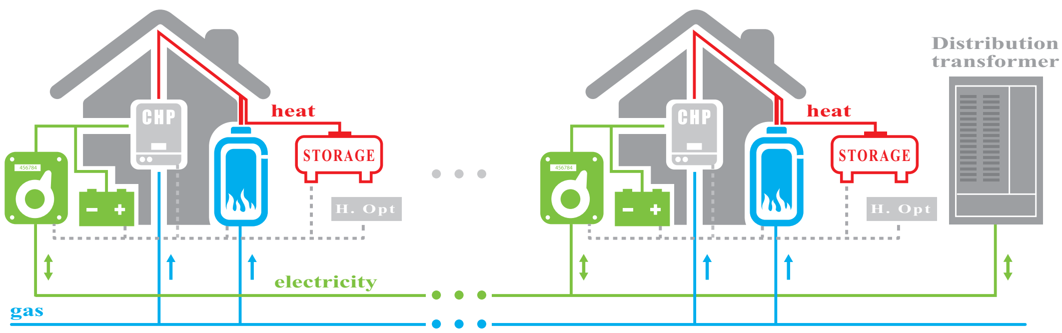

Figure 5.3: Scheme for Scenario 3 - Individual optimization with storage

The only difference with respect to the previous scenario is the addition of storage devices. Each household is provided with a heat storage water tank and/or a battery. In this case the four-step technique introduced in Section 2.3.2 is used for the optimization of each individual household.

5.3.4 Scenario 4: Collaborative Optimization

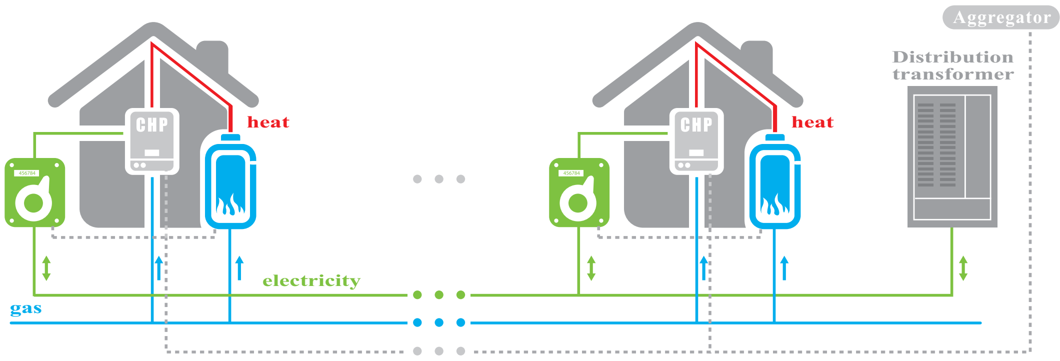

Figure 5.4: Scheme for Scenario 4 - Collaborative optimization

In this optimization, micro-CHP units are placed at each household and an external neighborhood aggregator is in charge of the optimization of the micro-CHP units.

- Each household has a micro-CHP unit to supply (part of) its heat and electricity.
- Each household has a furnace as auxiliary device to supply (part of) its heat load.
- Each household is connected to the electrical grid, from which (part of) its electric load is supplied. Excess electricity produced by the micro-CHP units can be fed back to the grid.
- There are no renewable energy technologies or storage elements installed.
- Each generation unit is operated according to the optimization performed by the aggregator. The aggregator induces exchange among the households; this minimizes the power interaction with the electrical grid and enhances the efficient power utilization within the neighborhood.
- The aggregator determines how much of the power is imported or exported from other households. The respective household will pay or receive money for it according to the price defined for exchanged electricity within the neighborhood.
- Each household is represented by an individual energy hub.

Model Extension

In order to show the influence of an aggregator, additional constraints were implemented in the optimization model that was described in Chapter 2. For each household (represented by an energy hub), the electricity generated by the generation units installed at the household $L^{h_d}_{\mathrm{e,\,hub}}$ is given by the multiplication of the electricity coupling vector and the vector of input carriers delivered to the hub. When several households h_d are considered, where $d = 1, 2, \ldots, n_\mathrm{h}$ and $n_\mathrm{h} \in \mathbb{N}$, the following matrix form is used. Note that in this case the result does not take the contribution of the electricity coming/going to the grid or the electricity exchanged with the neighbors into account (all power values are in kW):

$$L^{h_d}_{\mathrm{e,\,hub}} = \begin{bmatrix} c^{h_d}_{\alpha_i \mathrm{e}} & \ldots & c^{h_d}_{\alpha_{n_\mathrm{in}} \mathrm{e}} \end{bmatrix} \begin{bmatrix} P^{h_d}_{\alpha_i} \\ \vdots \\ P^{h_d}_{\alpha_{n_\mathrm{in}}} \end{bmatrix}_{\mathrm{hub.}} \tag{5.1}$$

The household power unbalance $L^{h_d}_{\mathrm{e,\,unb}}$ is defined as the electricity generated by the generation units of the household $L^{h_d}_{\mathrm{e,\,hub}}$ minus the electricity demand of the household itself $L^{h_d}_{\mathrm{e}}$. At the same time, the power unbalance $L^{h_d}_{\mathrm{e,\,unb}}$ is equal to the power exchanged with other households $P^{h_d}_{\mathrm{e,\,exc}}$ plus the power coming or going to the grid $P^{h_d}_{\mathrm{e,\,grd}}$ (in case that no further exchange is allowed). The constraints associated with this condition are shown below:

$$L^{h_d}_{\mathrm{e,\,unb}} = L^{h_d}_{\mathrm{e,\,hub}} - L^{h_d}_{\mathrm{e}}. \tag{5.2}$$

$$L^{h_d}_{\mathrm{e,\,unb}} = P^{h_d}_{\mathrm{e,\,exc}} + P^{h_d}_{\mathrm{e,\,grd}}. \tag{5.3}$$

The total electricity exchange $P^{h_d}_{\mathrm{e,\,exc}}$ per household is equal to adding the power exported to other households $P^{h_d}_{\mathrm{e,\,exp}}$ minus the power imported from other households $P^{h_d}_{\mathrm{e,\,imp}}$:

$$P^{h_d}_{\mathrm{e,\,exc}} = P^{h_d}_{\mathrm{e,\,exp}} - P^{h_d}_{\mathrm{e,\,imp}}. \tag{5.4}$$

Since it is not expected that a household will import and export electricity at the same time, the following constraint is defined:

$$P^{h_d}_{\mathrm{e,\,exp}} P^{h_d}_{\mathrm{e,\,imp}} = 0. \tag{5.5}$$

The power considered as *exchanged power* only refers to the power exchanged among the households in the neighborhood, thus the sum of the power exchanged by all households in the neighborhood is equal to zero:

$$\sum_{h_d \in \mathcal{H}_{h_d}} P^{h_d}_{\mathrm{e,\,exc}} = 0. \tag{5.6}$$

The power that can be exported to other households is equal or lower than a positive power unbalance and the power that can be imported from other households is equal or lower than the magnitude of a negative power unbalance. This can be accomplished in the optimization program by means of the following constraints:

$$P^{h_d}_{\mathrm{e,\,exc}} P^{h_d}_{\mathrm{e,\,unb}} >= 0 \tag{5.7}$$

$$P^{h_d}_{\mathrm{e,\,exc}} P^{h_d}_{\mathrm{e,\,exc}} <= P^{h_d}_{\mathrm{e,\,unb}} P^{h_d}_{\mathrm{e,\,unb}}. \tag{5.8}$$

5.3.5 Scenario 5: Collaborative Optimization with Storage

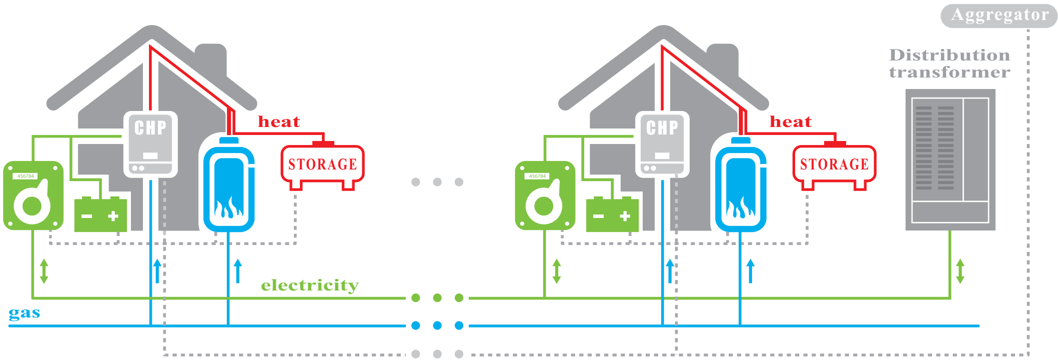

Figure 5.5: Scheme for Scenario 5 - Collaborative optimization with storage

The only difference with respect to the previous scenario is the addition of storage devices. Each household is provided with a heat storage water tank and/or a battery. The four-step technique introduced in Section 2.3.2 is used. The new constraints that were introduced in Scenario 4 are also included in Step 1, Step 2, Step 3 and Step 4 of the optimization technique.

5.3.6 Inclusion of Renewables

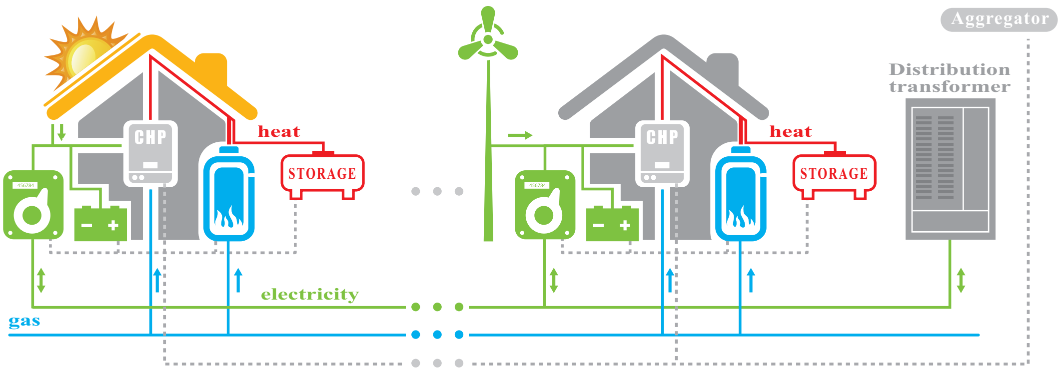

Figure 5.6: Inclusion of renewables in Scenario 5

For modeling purposes, the power coming from uncontrollable renewables ($P^{h_d}_{\text{e, ren}}$) is considered as an extra input at the energy hubs representing each household. In Figure 5.6, the representation of Scenario 5 with renewables is depicted. The equation for the power unbalance can be written as:

$$L^{h_d}_{\text{e, unb}} = P^{h_d}_{\text{e, exc}} + P^{h_d}_{\text{e, grd}} + P^{h_d}_{\text{e, ren}}. \tag{5.9}$$

5.3.7 Inclusion of Electric Vehicles

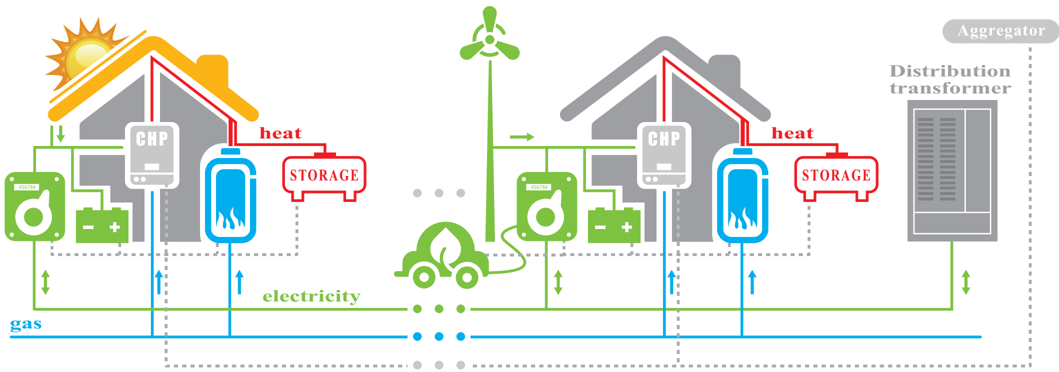

Figure 5.7: Inclusion of electric vehicles in Scenario 5

In Figure 5.7, the representation of Scenario 5 with electric vehicles and renewables is depicted. For modeling purposes, the power demand from the electric vehicles ($L^{h_d}_{\text{e,veh}}$) is added to the electricity demand of each household. The resulting equation for the power unbalance is:

$$L^{h_d}_{\text{e, unb}} = L^{h_d}_{\text{e, hub}} - \left(L^{h_d}_{\text{e}} + L^{h_d}_{\text{e,veh}}\right). \tag{5.10}$$

5.4 Input Data for the Simulations

5.4.1 Prices

Price policies for the electricity that is fed back to the grid are still under development, thus four different price options are analyzed to determine their influence in the optimization, see Table 5.1. In option 1 no reimbursement is regarded, in option 2 the price currently paid in the Netherlands is considered [15]. In the third option, 55% of the price charged for electricity from the grid is considered and in the fourth case the same price for electricity from the grid is taken. To motivate the exchange with other neighbors, the price for the electricity that is imported/exported is 77,5%/72,5% of the price of electricity from the grid.

Table 5.1: Gas and electricity prices

Energy Carrier	Consumption Costs				Source
	Option 1 (€/kWh)	Option 2 (€/kWh)	Option 3 (€/kWh)	Option 4 (€/kWh)	
Gas	0,0684	0,0684	0,0684	0,0684	[47]
Electricity	0,1897	0,1897	0,1897	0,1897	[47]
Electricity back to grid	0,0000	0,0500	0,1897	0,1043	[15]
Electricity exchanged (imported)	-	0,1470	0,1470	0,1470	-
Electricity exchanged (exported)	-	0,1375	0,1375	0,1375	-

5.4.2 Component Parameters

The parameters of the storage devices can be found in Table 5.2. They include the energy content of the storage device, the maximum power that can be withdrawn or delivered to it, the charging efficiency and the stand-by losses. The parameters of the generation devices used in the simulation are shown in Table 5.3. They include the maximum and minimum input carrier boundaries, the electrical and thermal efficiencies, the total energetic efficiency and the source from which the data were taken.

Table 5.2: Parameters of storage devices

Parameter	Unit	Storage		Source
		Electricity	Heat	
Minimum energy content	kWh	1,00	9,60	[113],[103]
Maximum energy content	kWh	5,00	14,00	[113],[103]
Maximum power (charge)	kW	0,80	2,00	[113],assumption
Maximum power (discharge)	kW	-0,50	-2,00	[113],assumption
Charging efficiency e_{α_i}	%	90,00	95,00	[113],[103]
Stand-by losses	kW	4e-3	1e-4	[113],assumption

Table 5.3: Parameters of generation devices

Parameter	Symbol	Unit	Component				
			Grid	CHP 1 Stirling Engine	CHP 2 Gas-Fired CHP	CHP 3 Solid Oxide FC	Furnace
Input carrier	α_i		Electricity	Gas	Gas	Gas	Gas
Minimum input carrier	$\underline{P}_{\alpha_i}$	kW	0,00 or -100,00	0,00	0,00	0,00	0,00
Maximum input carrier	$\overline{P}_{\alpha_i}$	kW	100,00	6,67	10,00	3,33	25,00
Electrical energetic efficiency	$\eta^{k_p}_{\alpha_i \mathrm{e}}$	%	100,00	15,00	30,00	60,00	-
Thermal energetic efficiency	$\eta^{k_p}_{\alpha_i \mathrm{q}}$	%	-	85,00	70,00	25,00	90,00
Total energetic efficiency	$\eta^{k_p}_{\mathrm{tot}}$	%	100,00	100,00	100,00	85,00	90,00
Electrical to thermal efficiency ratio	$\eta^{k_p}_{\alpha_i \mathrm{e}}/\eta^{k_p}_{\alpha_i \mathrm{q}}$	%	-	0,18	0,43	2,40	-
Source			[103]	[103],[113]	[114]	[103]	[103]

5.4.3 Load Patterns

The data of the heat and electric load patterns were obtained from data sets generated in [103]. Individual data sets for 200 houses were provided. Figure 5.8 and Figure 5.11 show average load patterns for one week in winter and one week in summer.

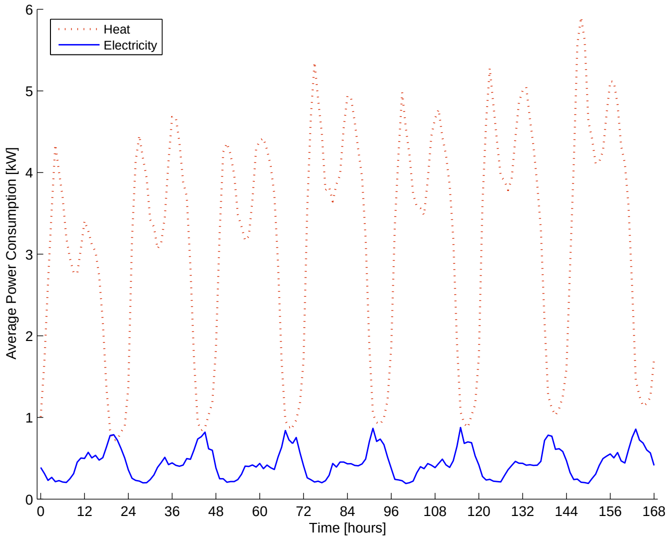

Figure 5.8: Average electricity and heat demand patterns for a week in winter

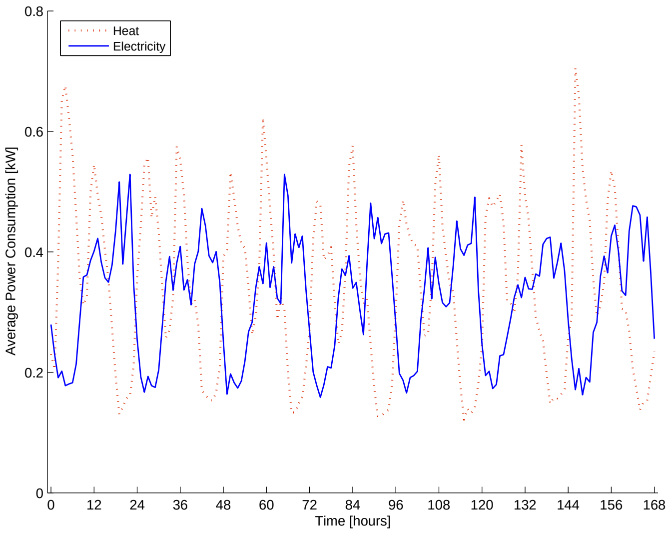

Figure 5.9: Average electricity and heat demand patterns for a week in summer

For illustration purposes, Figure 5.10 and Figure 5.9 show the load patterns of one randomly selected household and the respective average load patterns of four consecutive days in winter and four consecutive days in summer.

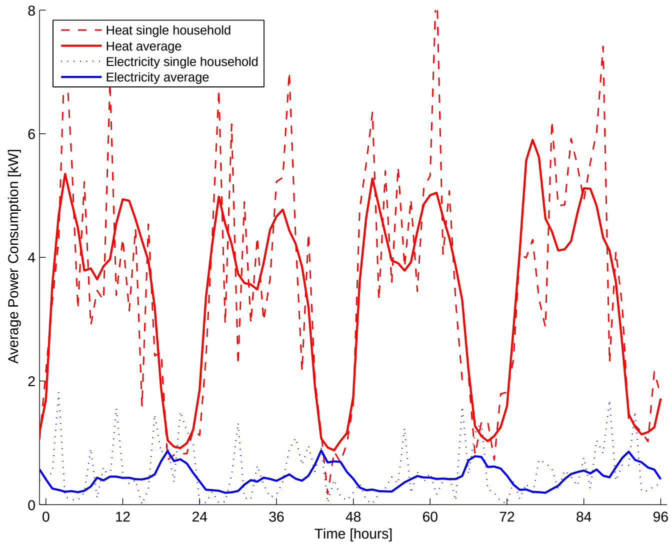

Figure 5.10: Single and average electricity and heat demand patterns for a week in winter

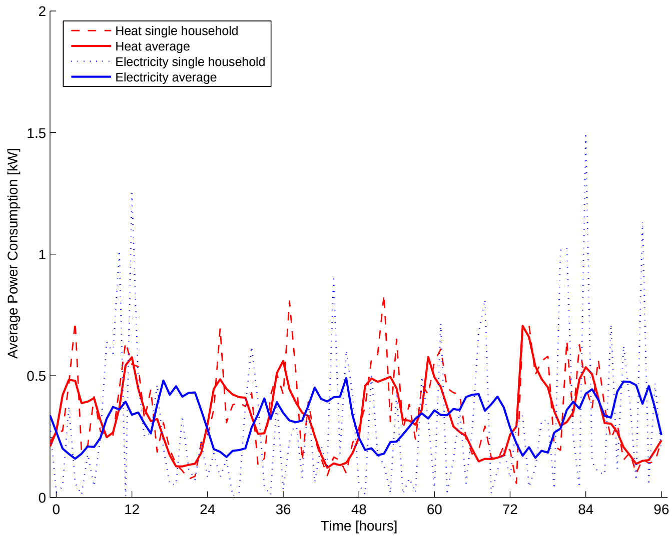

Figure 5.11: Single and average electricity and heat demand patterns for a week in summer

5.5 Simulation Results

In this chapter five simulations are shown. The micro-CHP technologies considered are: a stirling engine, a gas-fired micro-CHP and a solid oxide fuel cell, with an electricity-to-heat efficiency ratio of 0,18, 0,43 and 2,40 respectively; they are referred to as CHP 1, CHP 2, and CHP 3 in the discussions and in the figures. The simulations are described below:

Simulation 1: Comparison of Micro-CHP Technologies and Prices In this simulation, three micro-CHP technologies with different electricity-to-heat efficiency ratios are compared. In order to do so, the electricity and heat demand curves of a single household were selected. Four different price options are considered. The optimization is performed according to Scenario 2 (individual optimization), consequently there is no aggregator involved. The results of the Scenario 1 (base case) are also presented as reference for comparison.

Simulation 2: Introducing an Aggregator The results obtained when an aggregator is introduced are evaluated using the load data of five households. Three micro-CHP technologies with different electricity-to-heat efficiency ratios are considered for comparison. The optimizations are performed according to Scenario 1 (base case), Scenario 2 (individual optimization) and Scenario 4 (collaborative optimization).

Simulation 3: Introducing Storage In this simulation, the influence of introducing storage in a cluster of three households is evaluated. The optimizations are performed according to Scenario 1 (base case), Scenario 2 (individual optimization), Scenario 4 (collaborative optimization) and Scenario 5 (collaborative optimization with storage).

Simulation 4: Introducing Renewables In this simulation the influence of introducing solar panels in a cluster of five households is evaluated. The results of Scenario 5 with several storage combinations was evaluated.

Simulation 5: Introducing Electric Vehicles By means of this simulation it is possible to evaluate the influence of introducing electric vehicles to a district. Two different cases are considered. In the first one, electric vehicles are charged at will, in the second one incentives are given so that the electric vehicles are charged at non-peak periods. In the optimization, a cluster of 200 households is considered. The results correspond to Scenario 2 (individual optimization) with electric vehicles and Scenario 4 with electric vehicles (collaborative optimization).

5.5.1 Simulation 1: Comparison of Micro-CHP Technologies and Prices

Four price options were considered for comparison in this simulation; they are shown in Table 5.1. This is done in order to show how different price policies affect the optimization results. Three micro-CHP technologies are compared: a stirling engine, a gas-fired micro-CHP and a solid oxide fuel cell, with an electricity-to-heat efficiency ratio of 0,18, 0,43 and 2,40 respectively. The parameters can be found in Table 5.3. A single household with average electricity and heat patterns is used for the analysis. The primary energy consumption is calculated in the following way:

$$P_{\text{source}} = \sum \left(\frac{P_{\text{e}}}{\eta_{\text{gen,e}}} + P_{\text{g}} \right) \tag{5.11}$$

where P_{e} is the electricity power consumed from the electrical grid and P_{g} is the gas power input. The primary energy from the electricity that comes from the grid is calculated by dividing the electricity power with the energetic efficiency of a conventional large steam generation unit, which is considered to be 35% [81].

Table 5.4 shows the price policies considered for the simulation and the colors that are used to differentiate the cases in Figure 5.12, Figure 5.13, Figure 5.14 and Figure 5.15.

Table 5.4: Gas and electricity prices

Energy Carrier	Consumption Costs				
	Base Case (€/kWh)	Option 1 (€/kWh)	Option 2 (€/kWh)	Option 3 (€/kWh)	Option 4 (€/kWh)
Gas	0,0684	0,0684	0,0684	0,0684	0,0684
Electricity	0,1897	0,1897	0,1897	0,1897	0,1897
Electricity back to grid	-	0,0000	0,0500	0,1897	0,1043

The optimization in this simulation is based on Scenario 2, in which the household under study is optimized individually. The results of Scenario 1, which corresponds to the base case, are also shown as reference. The total accumulated costs and the primary energy consumption required to supply the load profiles of a chosen week in winter and a chosen week in summer are presented in Figure 5.12 and Figure 5.13 respectively. The gas consumption, reverse energy and grid energy consumption can be observed in Figure 5.14 and Figure 5.15 for winter and summer respectively.

By introducing a *micro-CHP & furnace* configuration instead of the traditional *grid & furnace* configuration (base case), the total operational costs are reduced in all cases considered, regardless of the price option selected or the micro-CHP technology used, see Figure 5.12 and Figure 5.13. It can also be observed that the lowest costs are obtained when CHP 3 is used; this corresponds to the solid oxide fuel cell unit in which the electricity-to-heat efficiency ratio is the highest. This is evident particularly in the summer, where the heat demand is much lower than in winter.

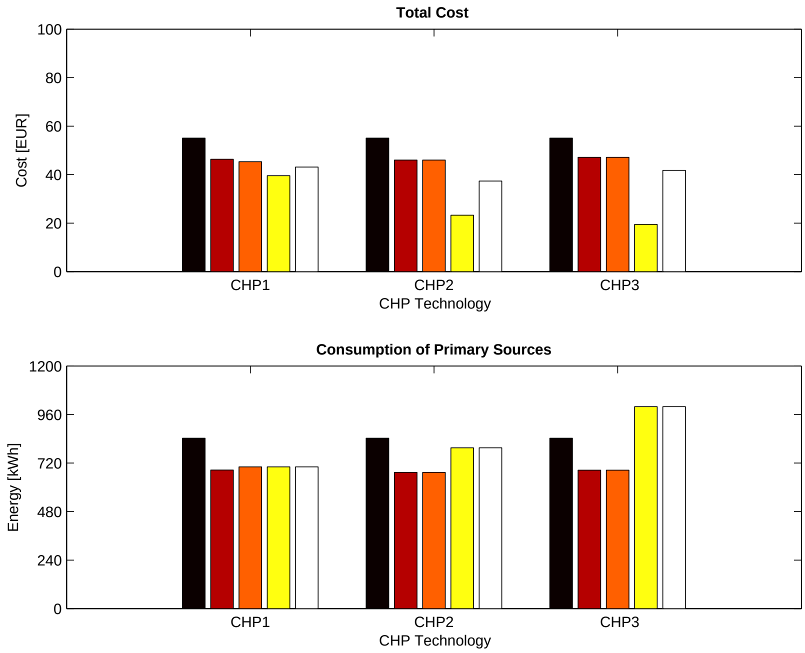

Figure 5.12: Simulation 1: Total costs and primary energy consumption for a week in winter

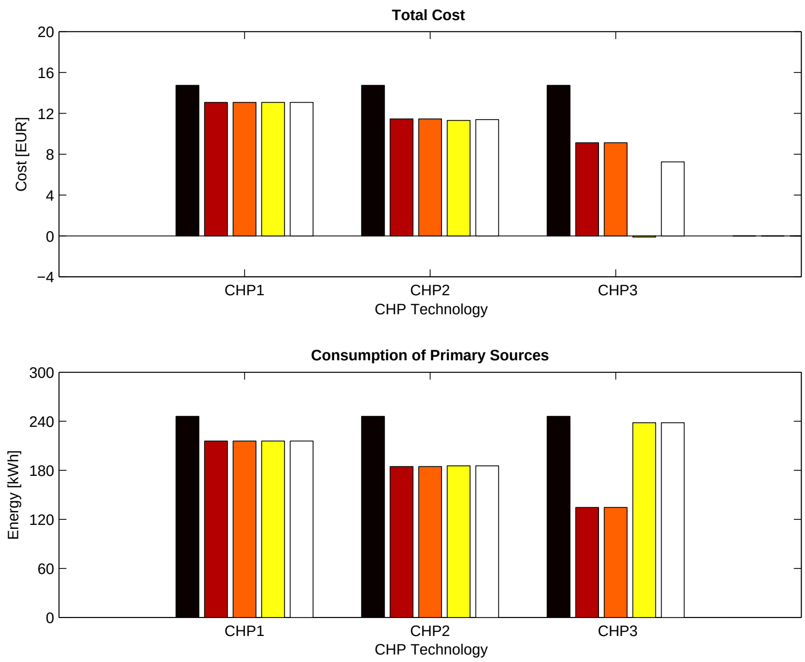

Figure 5.13: Simulation 1: Total costs and primary energy consumption for a week in summer

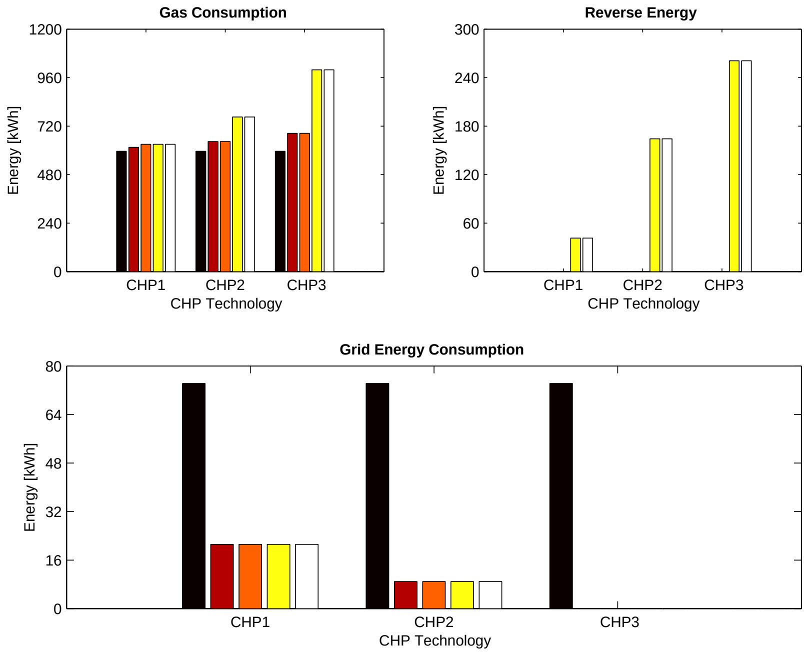

Figure 5.14: Simulation 1: Gas and grid energy consumption for a week in winter

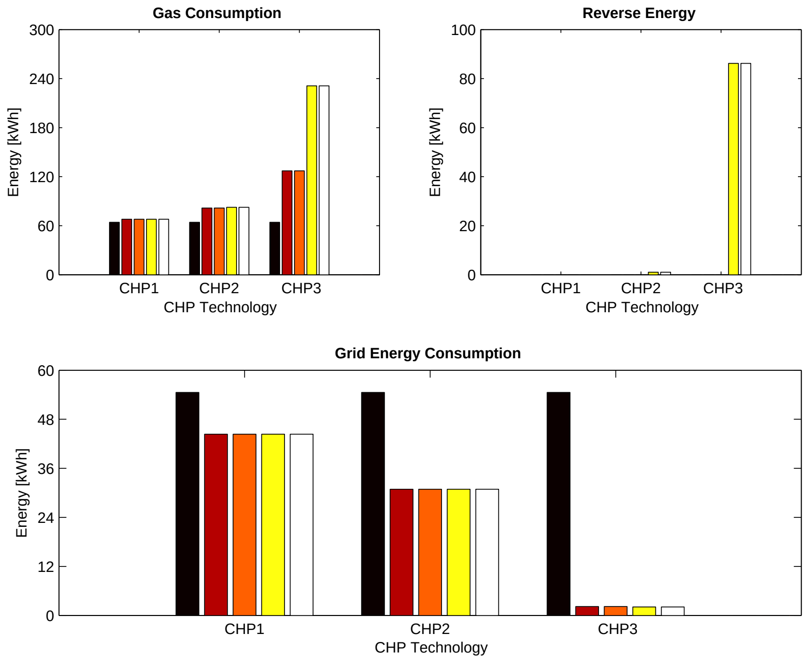

Figure 5.15: Simulation 1: Gas and grid energy consumption for a week in summer

Furthermore, it can be observed in Figure 5.14 and Figure 5.15 that when the reverse power is not economically rewarded (price option 1) and when the currently available reverse power tariff of 0,05 €/kWh is considered (price option 2), there is no incentive for the micro-CHPs to produce more electricity than the one required by the household owing the micro-CHP. When the same price of electricity is paid back (price option 3) and when the price for the reverse power is 0,1043 €/kWh (price option 4), the micro-CHP produces the heat required to match the load without the support of the auxiliary unit and sells all the extra electricity to the grid. The solid oxide fuel cell unit is the technology that takes the most advantage of these two last price options. It can be noted that in the summer the total costs are even negative in the case where the same price is paid back to the micro-CHP owner (price option 3), see Figure 5.13.

With respect to the total primary energy consumed, it can be observed in Figure 5.12 and Figure 5.13 that in the two first cases (price option 1 and price option 2) the total amount is reduced up to a 35% in the case of the CHP 3 (solid oxide fuel cell), and between 10% and 20% in the case of the other two technologies. The reduction is achieved both in summer and winter. This is particularly interesting from a sustainable point of view. The total primary energy is however increased in the case of the solid oxide fuel cell for the other two cases (price option 3 and price option 4). This occurs because the optimization is based on costs, thus the solid oxide fuel cell produces as much electricity as possible to earn the most; this produces the increase. Nevertheless, it is important to recall that the electricity is produced with a higher electrical efficiency, which in the end is better from a sustainable perspective when the complete district is considered as the boundary.

Conclusion

The gas energy consumed is increased in all cases considered, this is expected because the three micro-CHP technologies are fed with gas, see Figure 5.14 and Figure 5.15. As it was mentioned before, the reverse energy increased in the cases where the reverse power was economically rewarded with 0,1897 and 0,1043 €/kWh (price option 3 and price option 4), particularly in the case of the solid oxide fuel cell. Finally, the electricity consumption from the grid is significantly reduced in all cases considered. The minimum exchange with the grid is attained when using a solid oxide fuel cell unit because of its electricity-to-heat ratio.

5.5.2 Simulation 2: Introducing an Aggregator

The influence of introducing an aggregator can be observed in this simulation. By considering only five households it is easier to identify the impact of the control strategy used in each optimization scenario. Five different sets of electric and heat load patterns were arbitrarily chosen for the cluster of households for a period of one week, for both summer and winter. It is assumed that all five households have the same micro-CHP technology installed. Three different cases are compared; in each case a different micro-CHP technology is considered. The micro-CHP technologies considered are: a stirling engine, a gas-fired micro-CHP and a solid oxide fuel cell, with an electricity-to-heat efficiency ratio of 0,18, 0,43 and 2,40 respectively, they are denoted CHP 1, CHP 2, and CHP 3. Price option 2 was selected for the simulation, this means that 0,5 €/kWh is paid for the reverse power.

The optimization is based on Scenario 1, Scenario 2 and Scenario 4, which were described in Section 5.3. The legend associated with the graphs is depicted below.

Scenario 1 Base case - No aggregator

Scenario 2 Individual optimization - No aggregator

Scenario 4 Collaborative optimization - Aggregator

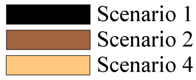

Figure 5.16: Legend

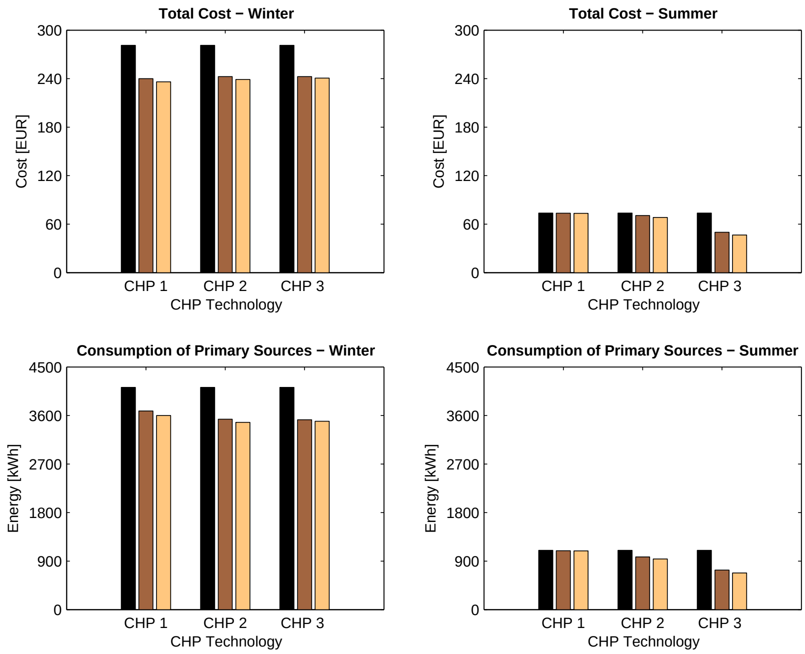

Figure 5.17: Simulation 2: Total costs and primary energy consumption

Figure 5.17 shows the total costs per household and the consumption of energy from primary sources by each of them. It can be observed that for the case in which CHP 3 (solid oxide fuel cell) is installed, the benefits obtained from having an aggregator are the highest, both in summer and winter. Figure 5.18 and Figure 5.19 show the gas consumed by each household, the energy consumed from the grid by each household, the electrical energy injected back to the grid by each household, and the energy exchanged (imported or exported) by each household. It can be noted that the gas consumption is increased in all cases. This is because the micro-CHPs are fed with gas, thus this result was expected. The grid consumption is reduced in all the cases because all these micro-CHPs also produce electricity. However it is important to notice that in the case of CHP 3 for Scenario 4 (after including the aggregator) the electricity consumption from the grid for the week selected in summer becomes almost one tenth of the power consumption of Scenario 1 (the base case) and becomes almost zero for the week selected in winter.

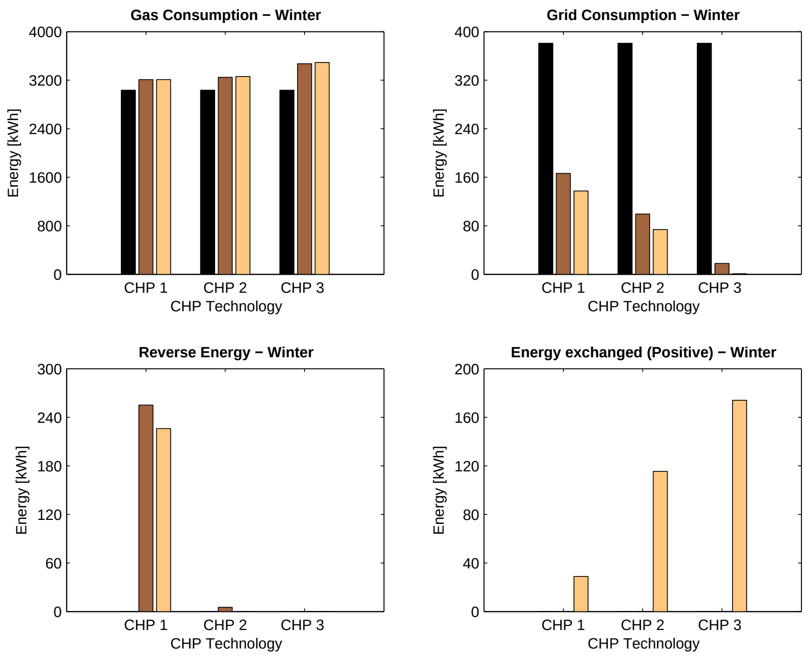

Figure 5.18: Simulation 2: Gas and grid energy consumption for a week in winter

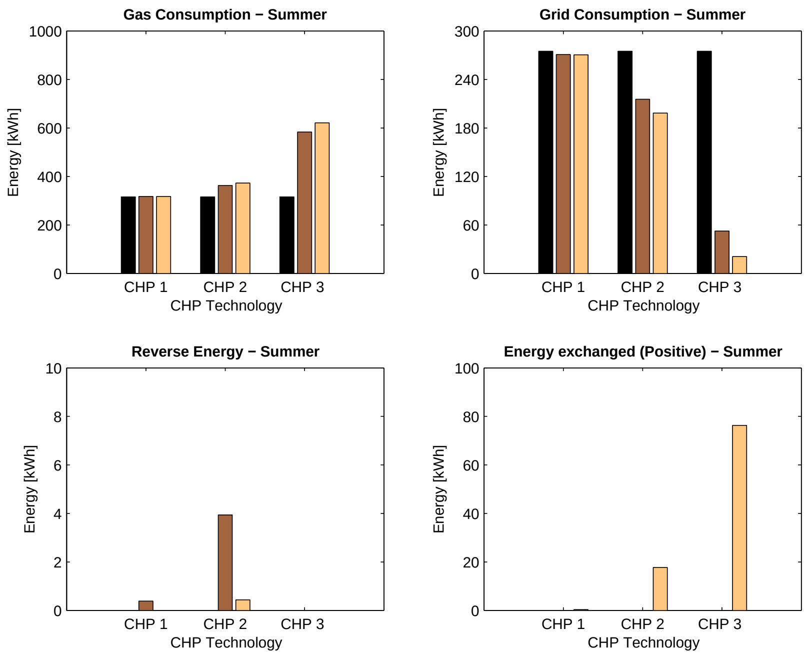

Figure 5.19: Simulation 2: Gas and grid energy consumption for a week in summer

For all cases, i.e. all micro-CHP technologies, the total energy exchange is higher during winter, where both the heat and electric loads are higher than during summer. However, it should be noted that the effect of the aggregator is not always significant. For example, the exchange that takes place in summer for CHP 1 is equal to zero, thus in this case there is no influence of the aggregator in the results of the optimization. Nevertheless, there are cases in which the effect of the aggregator is relevant, for example the highest exchange is performed at the case in which CHP 3 is installed for the selected week in winter, see Figure 5.18.

As mentioned before, the energy consumed from the grid is considerably reduced particularly in the cases of CHP 2 and CHP 3, both in summer and winter, especially when the aggregator is in charge of the cluster optimization. Additionally, it is important to observe that there is no energy injected back to the grid when using CHP 3. These two results show that there is a reduction in the overall energy exchange with the grid when using this particular micro-CHP technology.

Conclusion

After comparing the results for the analyzed cases including different micro-CHP technologies, it can be inferred that for this load by installing a micro-CHP with a high electricity-to-heat efficiency ratio and introducing an aggregator, the energy exchanged with the grid can be reduced significantly for the electric and heat loads considered. This is a very important result that can be taken into account by distribution network operators in charge of the planning of distribution infrastructures.

By doing similar analyses it would be possible to evaluate the response to load patterns of households of different districts and locations. In this way, it would be possible to revise the need for a modification in the distribution infrastructure. For example, after introducing such a micro-CHP technology and an aggregator, it might not be necessary to expand the distribution network anymore; the infrastructure might be kept the same for a longer period of time, even when an increase in the electricity demand is expected. Such an analysis can provide valuable information to be used to perform a more appropriate planning, to establish new policies, to define where to direct investments and to define incentives for consumers that can lead them to pick a micro-CHP technology with a suitable electricity-to-heat efficiency ratio for their particular location.

An aggregator can be used to tackle problems related to reverse energy flows generated from installing generation units at distribution level. By giving incentives to the customers to install suitable micro-CHP generation units to be controlled by a local aggregator, it can be possible to reduce investments intended to increase the capacity and/or to modify the current distribution network infrastructures.

5.5.3 Simulation 3: Introducing Storage

This section shows the influence of introducing storage in the optimization. A cluster of three households is used for the simulation. The optimizations are performed according to Scenario 1 (base case), Scenario 2 (individual optimization), Scenario 4 (collaborative optimization) and Scenario 5 (collaborative optimization with storage) for a period of 24 hours. The micro-CHP technology used for the simulation is the stirling engine.

It is interesting to observe that in this example because of the use of storage, the furnace is no longer used. This can be observed by comparing the multi-carrier unit commitment of Scenario 4 and Scenario 5 in Table 5.5 and Table 5.6.

In Figure 5.20 it can be observed that total cost paid by each household for its electricity and heat consumption in Scenario 2 is lower than in Scenario 1. Furthermore, a reduction is evident in the total energy consumed from primary sources. A reduction of more than 25% is achieved by introducing the micro-CHP units. This means that a significant reduction in cost and energy consumption is obtained after performing an individual optimization per household according to the framework proposed in Chapter 2. This had already been discussed in Simulation 1.

In Scenario 4 an aggregator is introduced. The aggregator controls the output of the connected units and obtains data from the electricity exchange measurements of all households. Due to the presence of an aggregator, the costs associated with each household and consumption of primary energy sources decrease even further. This is because the aggregator takes advantage of forecasts in order to induce an optimal energy exchange among the households. Further savings are achieved by introducing storage, since it allows more flexibility for the optimization.

Figure 5.21 shows the exchanged energy, both imported and exported, for each household. Household 3 imports energy from household 1 and household 2. As a consequence, the energy consumption from the electrical grid and the reverse energy to the grid are significantly reduced when compared to Scenario 2.

Conclusion

These results provide valuable information. Storage is advisable when a significant reduction in the costs and consumption of primary energy is attained. As it was discussed in Chapter 2, the application of storage can affect the multi-carrier unit commitment of the micro-generation units placed at the individual households. It is recommended to use this kind of optimization tools during the planning phase of a district. In this way it can be evaluated if the benefits obtained from using storage overcome the investment and maintenance costs.

Table 5.5: Simulation 3: Multi-carrier unit commitment results for Scenario 4

Multi-Carrier Unit Commitment Solution of Scenario 4 with 3 households																									
		Time Period																							
	Component	1	2	3	4	5	6	7	8	9	10	11	12	13	14	15	16	17	18	19	20	21	22	23	24
1	micro-CHP	1	1	1	1	1	1	1	1	1	1	1	1	1	1	1	1	1	1	1	1	1	1	1	1
	Furnace	0	0	0	0	0	0	0	0	0	0	0	0	0	0	0	0	0	0	0	0	0	0	0	0
2	micro-CHP	1	1	1	1	1	1	1	1	1	1	1	1	1	1	1	1	1	1	1	1	1	1	1	1
	Furnace	0	0	0	0	0	0	0	0	0	0	0	0	0	0	0	0	1	1	0	0	0	0	0	0
3	micro-CHP	1	1	1	1	1	1	1	1	1	1	1	1	1	1	1	1	1	1	1	1	1	1	1	1
	Furnace	0	0	0	0	0	0	0	1	1	0	0	0	0	1	0	0	0	1	0	0	0	0	0	0

Table 5.6: Simulation 3: Multi-carrier unit commitment results for Scenario 5

Multi-Carrier Unit Commitment Solution of Scenario 5 with 3 households																									
		Time Period																							
	Component	1	2	3	4	5	6	7	8	9	10	11	12	13	14	15	16	17	18	19	20	21	22	23	24
1	micro-CHP	1	1	1	1	1	1	1	1	1	1	1	1	1	1	1	1	1	1	1	1	1	1	1	1
	Furnace	0	0	0	0	0	0	0	0	0	0	0	0	0	0	0	0	0	0	0	0	0	0	0	0
2	micro-CHP	1	1	1	1	1	1	1	1	1	1	1	1	1	1	1	1	1	1	1	1	1	1	1	1
	Furnace	0	0	0	0	0	0	0	0	0	0	0	0	0	0	0	0	0	0	0	0	0	0	0	0
3	micro-CHP	1	1	1	1	1	1	1	1	1	1	1	1	1	1	1	1	1	1	1	1	1	1	1	1
	Furnace	0	0	0	0	0	0	0	0	0	0	0	0	0	0	0	0	0	0	0	0	0	0	0	0

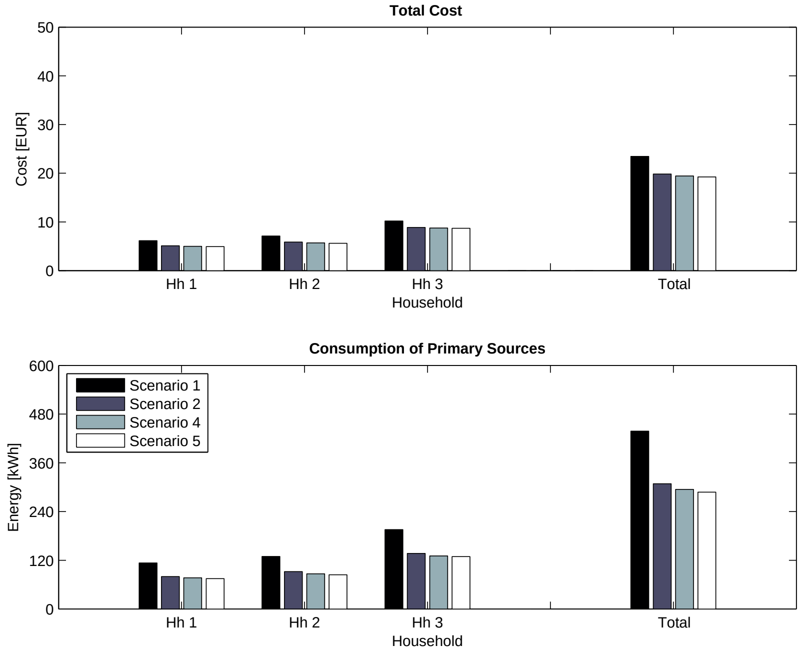

Figure 5.20: Simulation 3: Total costs and primary energy consumption

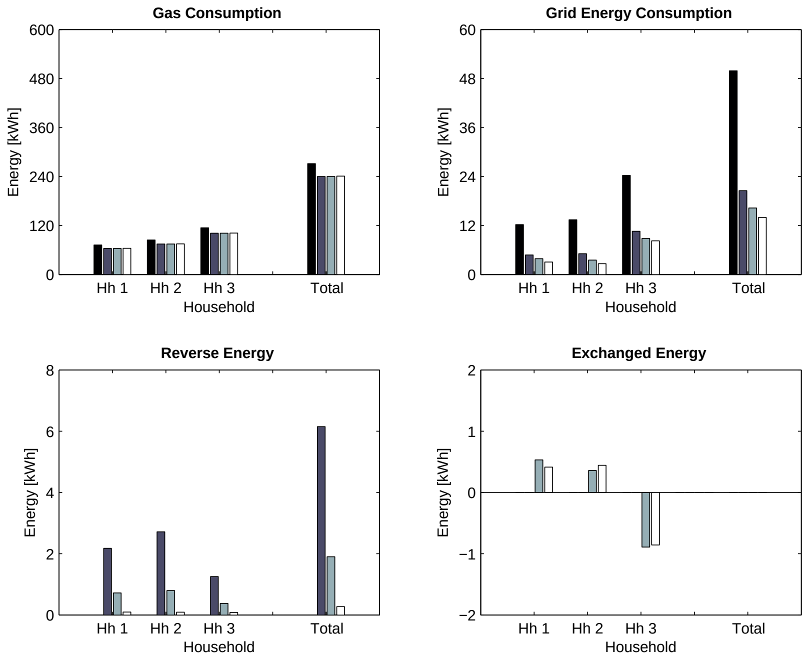

Figure 5.21: Simulation 3: Gas and grid energy consumption

5.5.4 Simulation 4: Introducing Renewables

In this simulation the following cases are evaluated:

- Scenario 4
- Scenario 4 with renewables
- Scenario 5 with renewables and heat and electricity storage
- Scenario 5 with renewables and only heat storage
- Scenario 5 with renewables and only electricity storage

A group of five households is used for a simulation period of 24 hours. It is assumed that each household has 7 solar panels installed on its roof. The patterns for the power coming from the solar panels were based on data available at DENlab. The real data of the power output and solar radiation is logged at the laboratory. Figure 5.22 shows a solar pattern.

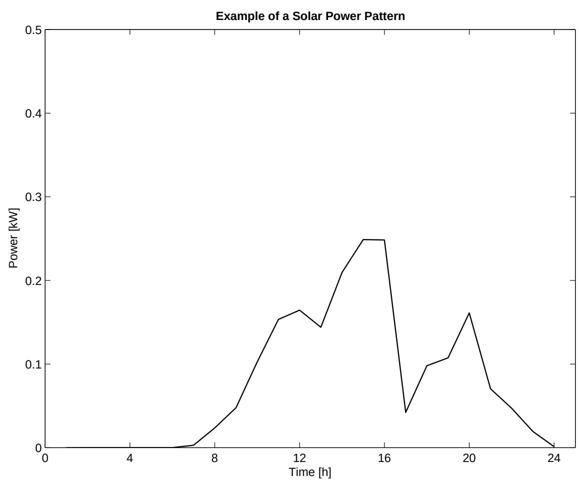

Figure 5.22: Example of a solar power pattern

From the simulation results shown in Figure 5.24 it can be observed that the difference in total costs and primary energy consumption is small for the cases analyzed. A remarkable result is that the power exchange within the neighborhood is reduced when the heat storage is available. The addition of a battery does not produce significant benefits in terms of power exchange.

Conclusion

It can be concluded that due to the low installation capacity and the load profiles considered, the results were not considerably changed by introducing renewables and storage. In such a condition it would be advised to avoid installing batteries. Batteries are disposed after a few years of utilization, which in the end does not represent a sustainable option. This result shows that storage is not necessarily beneficial in a system with renewables.

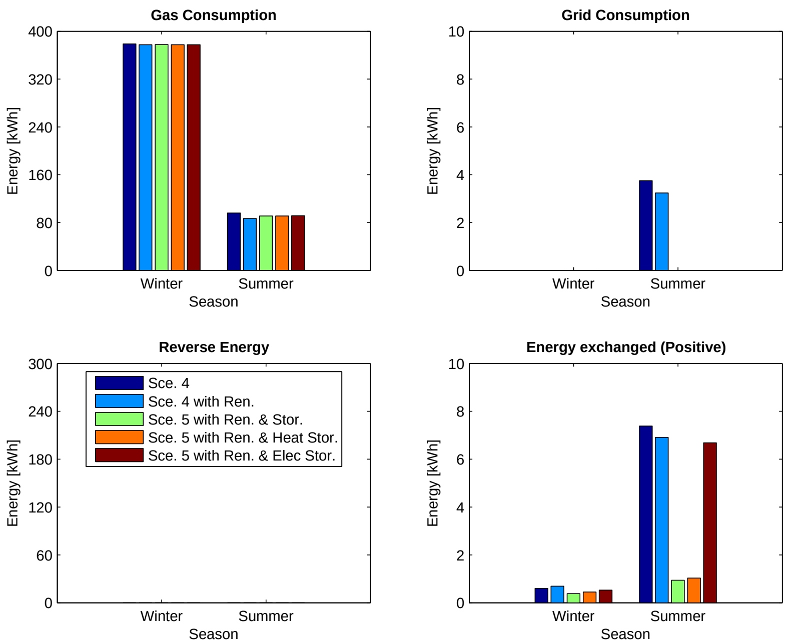

Figure 5.23: Simulation 4: Gas and grid energy consumption

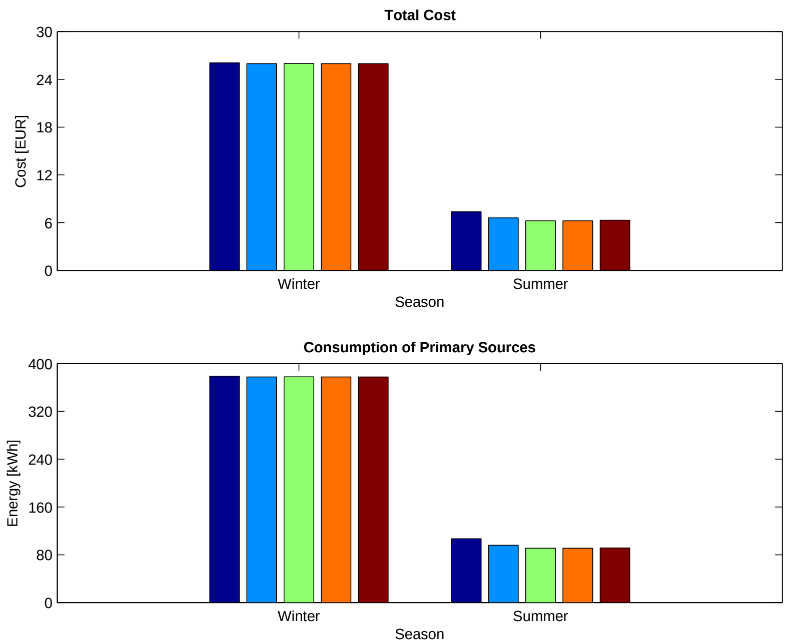

Figure 5.24: Simulation 4: Total costs and primary energy consumption

5.5.5 Simulation 5: Introducing Electric Vehicles

In this section the results after applying two different price policies are compared: in the first one it is assumed that the electric vehicles are charged at will, in the second differentiated price tariffs are provided so that the electric vehicles are charged at non-peak periods. A neighborhood of 200 households is considered for the simulation. Furthermore, an electric vehicle penetration of 20% was considered. Two optimization scenarios were selected for this simulation. In the first one, an individual optimization (Scenario 2) is performed and in the second one, the results of the collaborative optimization (Scenario 4) are shown.

The dataset for the electric vehicle load was obtained from a model developed in the IOP project "Role of Energy Storage in Future Power Systems", where electric vehicle load patterns are obtained based on a Monte Carlo simulation approach. The model variables are characterized by a stochastic behaviour and are correlated; a multivariate distribution function was built by means of copula function and the respective marginal empirical distributions [115].

The original dataset inserted into the model is statistical information obtained from the transportation data of 2008, provided by the Dutch Ministry of Transportation. The dataset includes information about commuting activities like time of departure, time of arrival, address of departure, address of arrival, transport means, trip distance, etc [115]. Only home-to-home trips occurring within one or two consecutive days were considered. The simulated single and double home-to-home trips were combined with a typical electric vehicle charging profile; this allowed the computation of the load patterns. Different electric vehicle penetration levels were modeled. Moreover, by applying price incentives, load shifts towards off-peak hours were also modeled. More information on the mathematical derivation of the model can be found in [115]. Figure 5.25 shows the load curves of the electric vehicles for a random day for illustrative purposes. Both price policies are depicted.

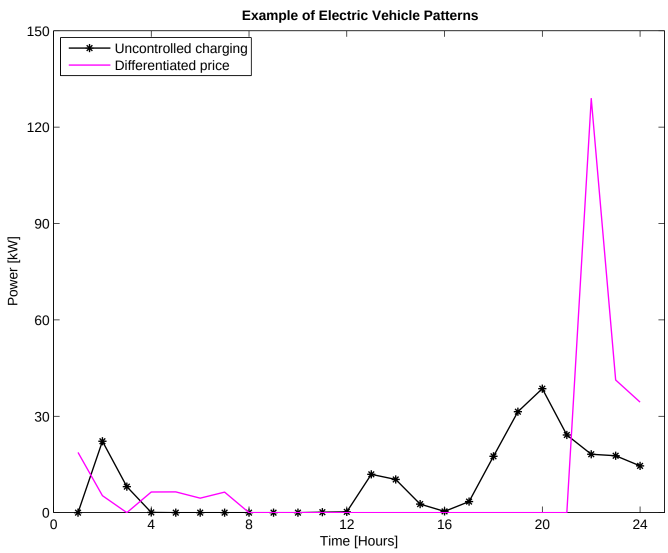

Figure 5.25: Electric vehicle aggregated load pattern for one day

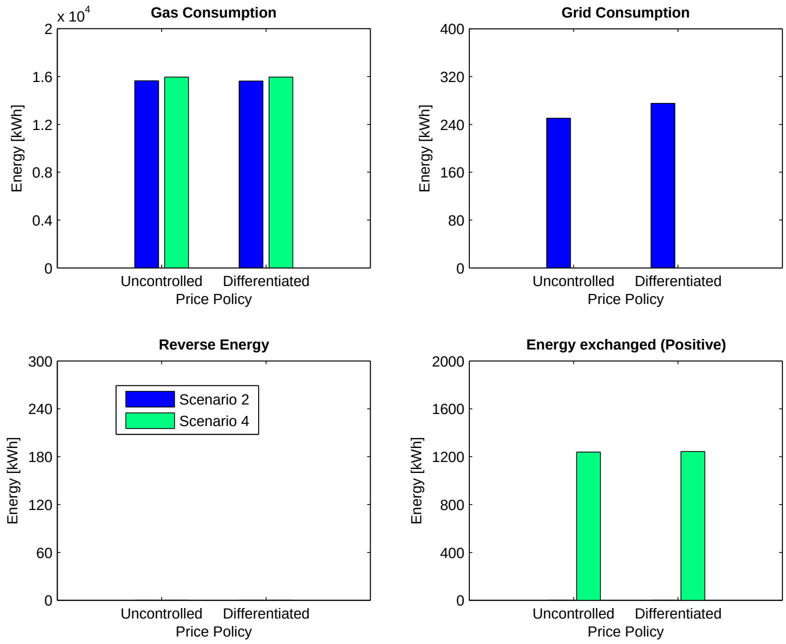

Figure 5.26: Simulation 5: Gas and grid energy consumption

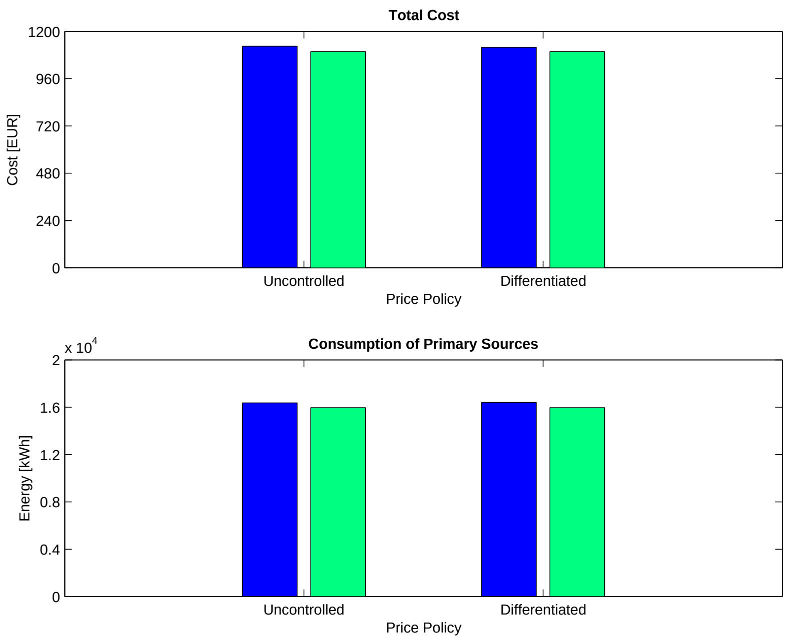

Figure 5.27: Simulation 5: Total costs and primary energy consumption

Individual electric vehicle patterns were added as loads to the individual energy hubs representing the households in the optimization model. In Figure 5.27 it can be observed that there is a very small overall difference in the total costs and primary energy consumption between the uncontrolled case and the case in which the differentiated tariff is applied. Nevertheless, a more evident difference can be observed between the results of Scenario 2 (individual optimization) and Scenario 4 (collaborative optimization). Not only the total costs and the consumption of primary sources is reduced at Scenario 4, but there is no need for grid consumption at Scenario 4, since energy is exchanged within the neighborhood, as shown in Figure 5.26. Therefore, the influence of a collaborative optimization is stronger than the influence of the tariff differentiation.

Conclusion

This section provides valuable information to infer that policies should start focusing more on enabling collaborative optimization channels instead of putting so much effort in coming up with new differentiated tariffs that may not produce such a significant difference in terms of total costs and overall grid consumption and that might bring new local problems due to the additional peak that can occurs when electric vehicles start charging as soon as the differentiated tariff begins.

5.6 Conclusions

Different comparisons were performed in this chapter, from which valuable insights were obtained. For example in the first simulation it was possible to observe that not every micro-CHP technology is capable of providing substantial benefits to a district in terms of cost savings and reduction of energy consumption. For the load patterns that were analyzed, the solid oxide fuel cell provided the best results. In Simulation 2 it was possible to observe the influence of having a collaborative optimization. The use of an aggregator proved to be an effective way to reduce the energy exchange with the grid. As a consequence, by using an aggregator the need for an expansion in the infrastructure can be reduced. Simulation 3 provided results in which the influence of storage was observed. Just like it was previously shown in Chapter 2, by using storage the multi-carrier unit commitment can be altered. In this case, an example of a cluster of 3 houses was selected for illustrative purposes.

When a low capacity of solar panels is installed, like in Simulation 4, the influence on the collaborative optimization is limited. It was observed that storage does not necessarily benefit a system with renewables. Batteries are disposable and their installation should only be performed in cases where a significant benefit can be attained. Heat storage is in that sense a better option, especially when a large amount of heat is produced by the micro-CHP units.

Finally in Simulation 5 the inclusion of electric vehicles was studied. It was concluded that policy makers should focus their effort on enabling the use of local aggregators. This not only reduces the costs and the consumption of primary sources but allows a better way to control possible power peaks. Using differentiated tariffs enhances the risk that all electric vehicles are plugged at the same time, which generates problems related to power capacity of the power distribution network. In conclusion, the scenarios under which a collaborative optimization was performed provided the best results in the analysis.

Chapter 6

The Implementation

Multi-Carrier EMS

This chapter answers Research Question 6 of this dissertation. It is focused on practical aspects related to the implementation of small-scale energy management systems designed for systems with multiple energy carriers. In Section 6.1 a literature review is presented about EMS products available in the market and EMS technologies under development. In Section 6.2 the modules involved in the EMS are described. Section 6.3 presents a description of the laboratory in which the algorithms were tested. Section 6.4 contains the conclusions of this chapter. Parts of this chapter have been already published in [116].

6.1 Literature Review

This section presents a brief literature review on devices and EMS technologies designed for small-scale energy systems that have been developed during recent years. The literature review considers EMS technologies that are available in the market, as well as EMS technologies under development and EMS prototypes. The energy management systems that were taken into account in this section are designed for small-scale applications, some of them are designed for home applications (home energy management systems - HEMS) and others for district applications (district energy management systems - DEMS).

The *Power Router* is focused on the optimization of power flows of individual households. It is in charge of monitoring the power coming from renewable sources like PV panels and in charge of commanding when to charge or discharge the batteries and when to sell electricity to the grid. Moreover, the device can be programmed with feed-in tariffs to schedule and optimize the use of self-generated energy.

The Power Router consists of an inverter that has two DC inputs (150-600V, 15A each string) and independent maximum power point trackers. This allows the maximization of yield. Moreover, there are three power output capacities available: 3kW, 3,7kW and 5kW. The control module decides if it is better to use the power coming from the renewable energy sources to charge the battery, to use it at the household or to feed it into the grid [117]. An important feature is that the Power Router can be used in *island mode* to supply backup power in the case of a grid power interruption. However this option only works if there is sufficient input from the renewable sources. The owner has access to the energy balance, revenue and solar yield via internet. Furthermore, the owner can connect from a computer or mobile phone and retrieve the required information. The Power Router is a product of the Dutch company Nedap. At this moment, the Power Router considers only electricity flows at household-level applications, thus it does not support multiple energy carriers or the coordination with other households.

Plugwise is a platform that can be used to achieve a desired energy consumption pattern by switching home appliances automatically and by monitoring the energy consumption [118]. According to the developers of Plugwise, up to 30% of the electricity consumption can be saved by switching off devices. Some of the main features of the Plugwise platform are: monitoring consumption, remote control and visualization of consumption via charts. The overall optimization is not done automatically by the program, instead, the user makes decisions based on the monitoring results, for example to switch on a washing machine at night to take advantage of the off-peak tariff or to switch off devices when not at home, etc. The switching is performed automatically. The platform is focused on electricity flows, however, the developers are looking forward to including gas consumption data and to operate a thermostat via the Plugwise platform.

The *Energy Guardian* is a smart-metering platform. The system is capable of collecting real-time electricity data and of helping determine how to optimize consumption by automatically switching equipment, such as computers or large energy consumption units like air conditioners and chillers. It can also help regulate the local voltage of the whole installation.

The energy data can be viewed online and can be used to control the switching of certain equipment. Energy consultants can access the data of the site remotely; in this way they can summarize and interpret the findings, but also identify the steps that have to be taken in order to improve the energy usage. The corresponding software provides the following features [119]:

- Real-time display of energy usage (data can be viewed per hour, day, week, month or year).
- It can be used to break down energy data (for example, to monitor a single equipment).
- Remote control of specific devices via the internet.
- Energy alerts by sms or email (to warn if energy usage of a particular device changes unexpectedly).
- Control of electrical appliances individually or in groups.
- It can be used to compare energy use of different groups or individual devices.
- Regression analysis: access real-time or historical data in order to spot trends and opportunities for energy saving.

The Energy Guardian platform focuses on electricity flows. The overall optimization is not done automatically by the program; instead, the energy consultants identify which steps can be taken in order to achieve an improvement. The owner has access to the information, therefore he/she can also participate in the decision-making process.

The *PowerMatcher* is a software platform that was developed by the Energy Research Centre of the Netherlands (ECN). It provides an optimization and coordination protocol of a large number of small units including distributed generation units, electricity storage and demand response loads.

The PowerMatcher takes the electricity price into account to determine when to charge and discharge storage units. It is designed for different power scales, from household-level to areas containing large number of units and several MWs. The system is based on industry standards in both the ICT and energy sectors, thus it can be deployed in existing systems. Moreover, the PowerMatcher is designed to support the virtual power plant concept in which the clustering of units is aimed.

The software is based on agent control, in which a logical tree is used for the optimization. In the tree structure each leave corresponds to an agent that is associated with a unique objective. Moreover, the root of the tree is formed by the auctioneer agent. This is a unique agent in charge of handling the price forming. The different types of agents are described below [120]:

- Local device agent: This agent represents a particular device. This agent coordinates its actions with all other agents in the cluster. The agent communicates its bid to the auctioneer and receives price updates. In this way the amount of power to be produced or consumed is determined.
- Auctioneer agent: This agent performs the process of price-forming. It receives the market bids of the connected agents and searches for the equilibrium price.
- Concentrator agent: This agent represents a sub-cluster.
- Objective agent: This agent is in charge of defining the objective of a cluster.

The last version of the software is now being tested at a real demonstration project. The main focus is given to electricity flows and electrical interactions, not to multiple energy carriers.

Other technologies can be found in the market, however they can only be used to monitor the flows and to display the results. Three of them are listed below:

- *Smart Homes and Cities*: Siemens's IEEE 802.15.4 standard for lighting and climate control management.
- *Wiser Home Energy Management System*: Schneider in-home display connected to smart meter.
- *Panasonic Home Energy Management System*: It monitors and displays the energy flows in the household.

Most of the products that are found in the market are focused on the household-level and on *monitoring* electricity power flows. Considerable efforts still have to be made in order to come with an EMS capable of *coordinating* and *optimizing* several households and multiple energy carriers.

6.2 Implementation of a Multi-Carrier EMS

The energy management system presented in this section incorporates the techniques and methodologies presented in the previous chapters. The multi-carrier EMS consists of three main types of modules: the *forecast module*, the *optimization module* and the *real-time control* module. The multi-carrier EMS is designed to include high penetration of stochastically changing generation as well as multiple energy carriers, such as heat, gas and electricity coming from combined heat and power units. The approach differs from traditional energy management systems, where only electricity flows are taken into account, and from EMS techniques in which the decision is based on data observation from the user and is not done automatically. Figure 6.1 shows a schematic representation of the multi-carrier energy management system. Each module is described in the following subsections. The overall management is accomplished by interactions among the modules.

When only one energy hub is considered, the forecast, optimization and control modules are placed at a local level (for example at the power substation or household that is represented by an energy hub). In the case of multiple hubs (for example, multiple households as in Chapter 5), the forecast and optimization modules are placed at the aggregator level and the control modules are located at the local level (for example at the household level).

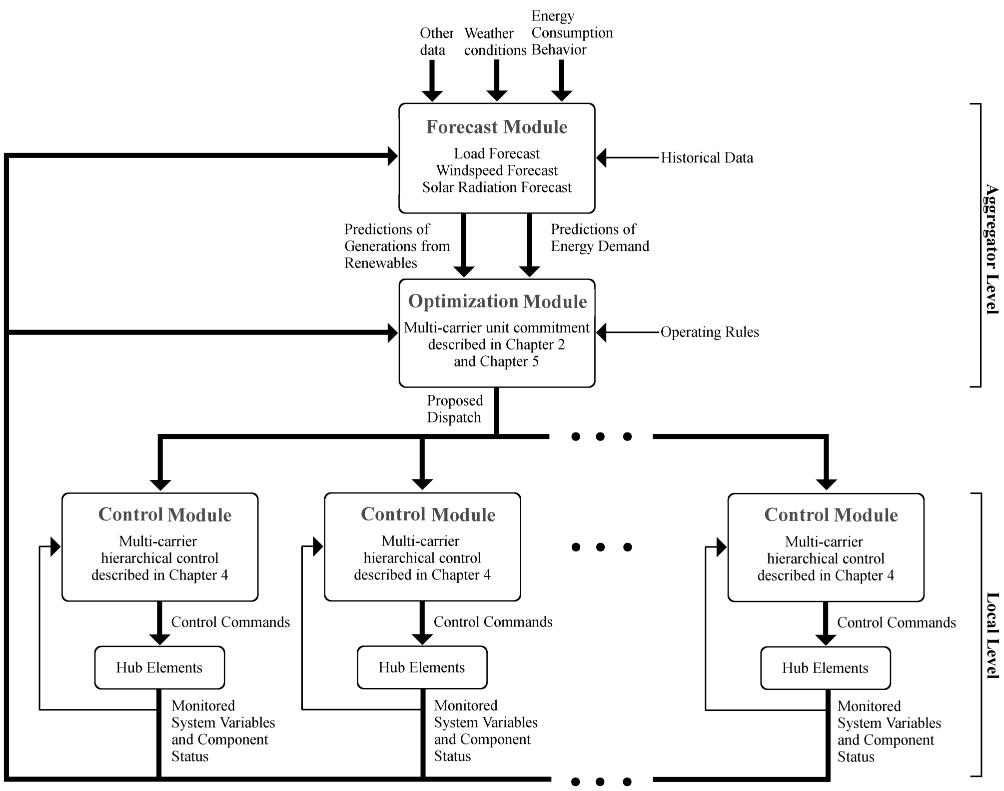

Figure 6.1: Diagram of the multi-carrier energy management system

6.2.1 Forecast Model

The forecast module is in charge of generating forecasts for the time series of the load and the renewable sources, i.e. wind speed and solar radiation. In this project, the *persistence forecast method* was used to determine the load forecast. However a better forecasting method is going to be developed in future work. For the wind speed, a forecasting model was developed using measurements taken by an anemometer that is located at the roof of the Electrical Engineering building of TU Delft. The forecasting model is described below.

The wind power generation for a few hours ahead is characterized by high uncertainty due to the stochastic nature of wind. Due to the influence that the wind power output has on the optimization results, the accuracy of the wind speed forecast has a significant role in the response of the system. For this reason, it is crucial to have reliable information about the future wind speed values. Forecasting in micro-grids is mainly performed in short terms with high temporal resolution, generally for the next 1-4 hours [121]. In this work, forecasts are performed every 15 minutes for a forecast horizon of 4 hours. Moreover, wind speed measurements are regularly made available (at least every 15 minutes). Whenever a wind speed measurement is recorded, the forecasting model is used to predict the wind speed for the next 16 quarters; in this way, the forecasts are regularly updated.

The model presented in this section was developed as part of a joint-collaboration paper between Alicja Lojowska and the author of this dissertation [116]. In order to build the forecasting model, the guidelines for modeling wind speed time series presented in [122] were followed. For this purpose, wind speed time series measurements recorded in October 2006, in DENlab (Delft, the Netherlands) were used. The time series comprises minute-based measurements, thus 15-minute averages were derived so that the new time series complies with the unit scheduling frequency of 15 minutes. First, the time series was transformed to *stationary* by removing features like diurnal seasonality and non-gaussian distribution. Then, by means of statistical tools, a suitable model in the class of ARMA-GARCH models was specified and tested. The model that was found using good statistical practice is the ARMA(1,2)-GARCH(1,1)-T model and it is presented below:

$$v_{\mathrm{w},t} = 0,99 v_{\mathrm{w},t-1} - 0,36\varrho_{t-1} - 0,09\varrho_{t-2} + \varrho_t \tag{6.1}$$

$$\varrho_t = \varsigma_t \sigma_t \tag{6.2}$$

$$\sigma_t^2 = 0,01 + 0,66\sigma_{t-1}^2 + 0,23\varrho_{t-1}^2 \tag{6.3}$$

where $v_{\mathrm{w},t}$ [m/s] denotes the wind speed at time t and ϱ_t denotes the innovations or residuals of the time series. Moreover, σ_t^2 is the conditional variance of ϱ_t and ς_t stands for standardized residuals which are independent, identically Student-T distributed with 5 degrees of freedom. The model was validated with respect to the main features of wind speed: distribution, autocorrelation and persistence and this resulted in a confirmed adequacy of the model. The forecasting model that was built using data from October 2006 can be applied to obtain wind speed predictions for any other October. This is possible because wind speed is characterized by annual seasonality and wind speed behavior does not change significantly from year to year[122]. Figure 6.2 presents measurements recorded in DENlab in October 2007 and the 1-step predictions made using the wind speed time series model. The forecasted values are satisfactory for this study. The forecasts further ahead in the future are associated with higher uncertainty and therefore may deviate more from observations.

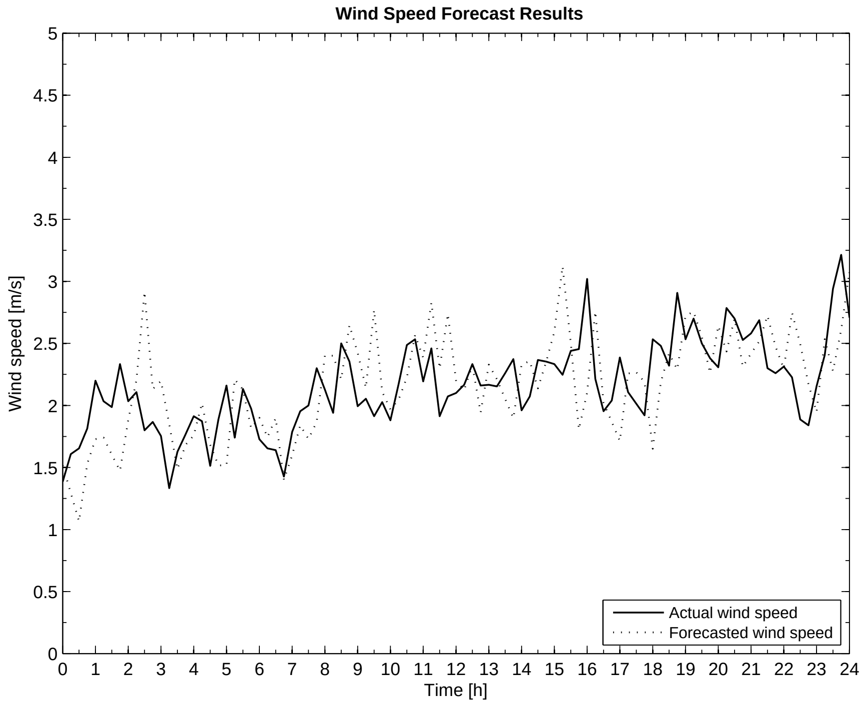

Figure 6.2: Results of the wind forecast model

6.2.2 Optimization Module

The optimization model is based on Chapter 2 and Chapter 5. By using the multi-carrier unit commitment framework and its extension (presented in Chapter 5), the optimization module defines a group of set-points for optimal operation. These set-point are calculated considering the operating rules and constraints of the components as well as the economic, technical and/or environmental objectives that are included in the objective function. The input parameters for the optimization module are the following:

- Load forecast
- Forecast of renewable sources (wind speed, sun radiation, etc)
- Initial status of storage devices
- Fuel prices
- Electricity exchange prices among neighbours in the case that several households are involved.
- Physical constraints of the components
- Other constraints and operating rules of the system.

6.2.3 Real-Time Control Module

The scheduling and dispatch obtained from the optimization module is the input for the real-time control module. This module is based on the hierarchical architecture presented in Chapter 4. The control module makes decisions according to the status of the system's control variables and components. It performs the proposed optimal dispatch and calculates the error in order to define the proper actions to be executed. The control module is placed at the energy hub's local level. This energy hub can be a micro-grid configuration, like the example shown in Chapter 4 or a household containing controllable generation units, like the ones considered in Chapter 5.

The three modules described above make up the multi-carrier energy management system proposed in this dissertation. They are coupled to each other and allow the proper operation of systems with multiple energy carriers. The multi-carrier EMS has the potential to be applied at household level and at district level.

6.3 Implementation at DENlab

6.3.1 Description

DENlab is a renewable energy laboratory located at the Power Systems Group of Delft University of Technology [123]. This laboratory can be used for demonstration projects of micro-grid set-ups containing renewable sources. A Programmable Logic Controller is in charge of the automation of the electromechanical processes in the laboratory. DENlab provides flexibility to emulate different load patterns and generation units by means of 9 power converters, 2 motor-generator-sets of 5,5 kW and 30 kW and profibus communication. The laboratory has 180 solar panels that can be connected to the test facility or redirected to the grid. Figure 6.3 shows the solar panels. The power capacity of the laboratory is 50 kW.

The operational characteristics of the components to be studied at the laboratory can be programmed at the main computer using specialized software. The program can then be downloaded to the PLC. Figure 6.4 shows a picture of the PLC that is used at DENlab. The PLC sends the set-points to nine power converters that are physically placed at the laboratory, in this way the power supplied or consumed by the converters can be controlled, as well as the output of the motor-generator-sets. Therefore, a variety of components can be emulated and the real power flow at DENlab can be monitored. Figure 6.5 shows the motor-generator-sets placed at DENlab.

At the laboratory, the components of the system can be emulated in different ways. In the following paragraphs, three types of components are described to show how this is done: a rotating AC device, an electric load and a DC-operating device. Figure 6.6 shows a diagram of DENlab; this can help the reader to understand the description that is given.

Figure 6.3: Solar panels on the roof

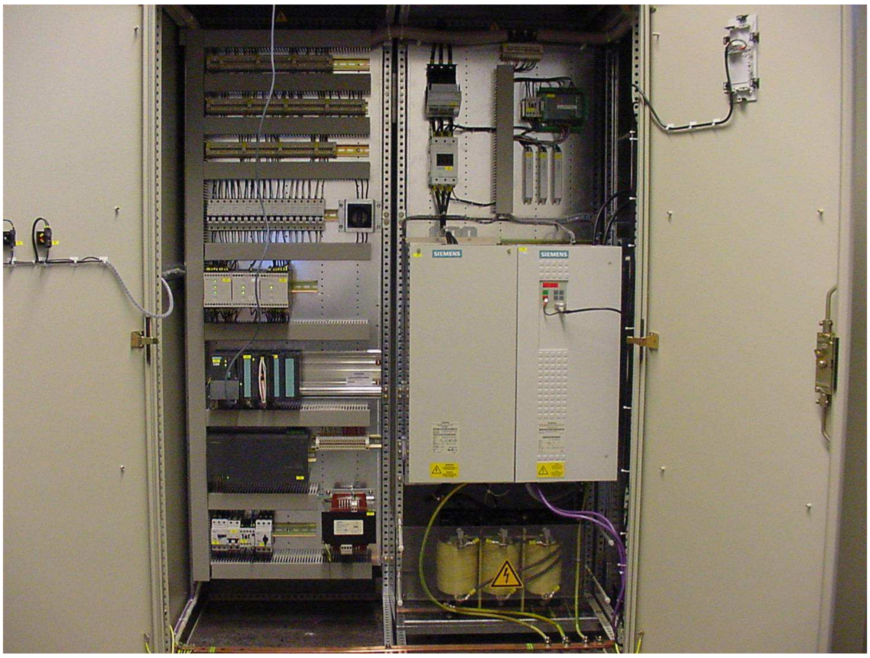

Figure 6.4: PLC and back-to-back converter in DENlab

Figure 6.5: Motor-generator sets used to emulate different components

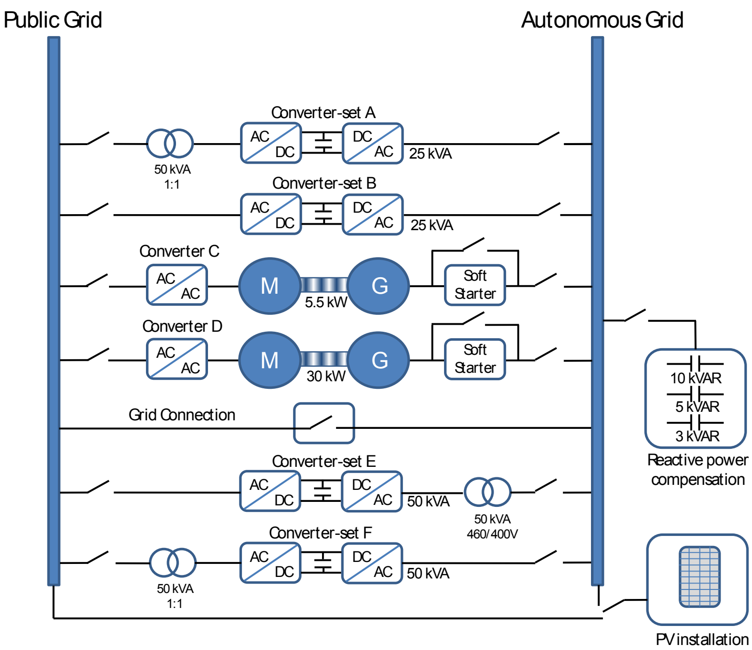

Figure 6.6: DENlab configuration diagram

Firstly, the emulation of a rotating AC machine is done with the help of a power converter and a motor-generator-set. In this case, a wind turbine is chosen for the example. Wind speed data is obtained from an anemometer placed at the roof of the building; this is the input of the wind turbine model. The wind turbine model calculates the power that would be supplied by a wind turbine for the respective wind speeds. The converter's current set-point is calculated from the power output of the model. The converter-sets are connected to the motor-generator-sets, see converter-sets C and D in Figure 6.6. As a consequence, a change in the set-point of the power converter makes the motor-generator-set to turn slower or faster. The currents that flow to the autonomous grid in DENlab represent the currents that would flow in an analogous physical system.

Secondly, the way to emulate an electric load is described. Load profiles are obtained with the software SEPATH [49]. An electric load dataset is used to calculate the set-point of the back-to-back converter that is used to emulate a load of 10 households; this corresponds to converter-set E in Figure 6.6. Due to the fact that in this case a power load is represented, the power flows in the opposite direction to that of the generation units. Therefore, in Figure 6.6 power will flow from the autonomous grid to the public grid and not the other way around, like in the previous case.

Thirdly, a description is given to indicate how to emulate DC-operating devices. In this case back-to-back converters are used. The DC set-points of the current are provided to a AC-to-DC converter and this is transformed back to AC by a DC-to-AC converter. It is possible to define a two-way flow, like in the case of charging or discharging a battery, or a one-way flow like in the case of a fuel cell. Converter-sets A, B and F are used for this purpose.

The activities performed at the laboratory as part of this PhD project include:

- The system configuration was programmed in STEP7, which is the software that is used to control the PLC. This was done in separately organized modules. The input and output ports were mapped to specific memory words and each power electronic converter was assigned a fixed number and a set of memory words to avoid wrong interactions within the program. Due to the modularity introduced, the emulation characteristics of one converter can be easily changed. The new structure allows flexibility in the laboratory for the implementation of different/new components.
- An energy management system based on [123] was implemented to test if the system performed correctly under the new software configuration. This system only considers electricity flows in the system.
- A simple multi-carrier energy management system was implemented in order to test the algorithms designed within this PhD project. The interactions among the forecast module, the optimization module and the real-time control module were analyzed.

The laboratory was originally designed to evaluate only electricity flows, thus it was not possible to implement a real multi-carrier system. Mathematical models were used to represent the heat elements instead.

6.3.2 Example at DENlab

This section shows the results of the most recent tests that were performed at the laboratory. The autonomous energy hub in this example consists of a fuel cell, a furnace and a battery system. The implementation was done during the MSc project [124], guided by the author of this dissertation. The objective of this project was to implement a fuel cell model at converter-set F (which was the last one to be acquired at the laboratory), and integrate it to the multi-carrier EMS.

A partial multi-carrier EMS was implemented at the laboratory, however only simple tests will be shown in this section. Figure 6.7 shows the energy hub representation. The fuel cell was modeled using converter-set F and the battery system was modeled using converter-sets A and B, see Figure 6.6. The electric load represents the consumption of 10 households. The electric load pattern was obtained from the software SEPATH. Every minute a new set-point for the electric load is sent to converter-set E. For this example an artificial heat load was selected in order to show significant load variation within the 20-minutes simulation that is presented.

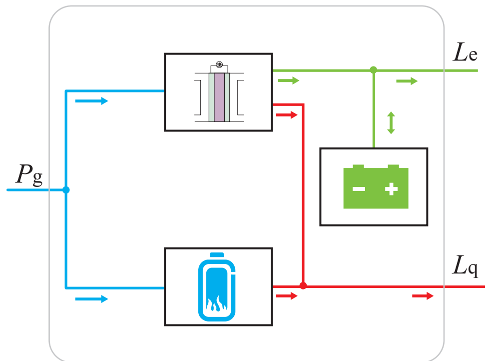

Figure 6.7: Energy hub representation

Table 6.1: Components and control subsystems

Hub Element	Converter in DENlab	Control Subsystem	Set-point from Main Control	Unit Control
Battery Bank 1	A	electricity	current	none
Battery Bank 2	B	electricity	voltage	frequency regulator voltage regulator
Fuel Cell	F	electricity	current	delay transfer function
Boiler	none	heat	gas flow	none

The control module follows the multi-carrier hierarchical control architecture presented in Chapter 4. Due to the fact that there are two energy carrier forms at the output side of the energy hub, two control subsystems were defined: the electricity control subsystem and the heat control subsystem. Table 6.1 shows the components' subsystem assignment.

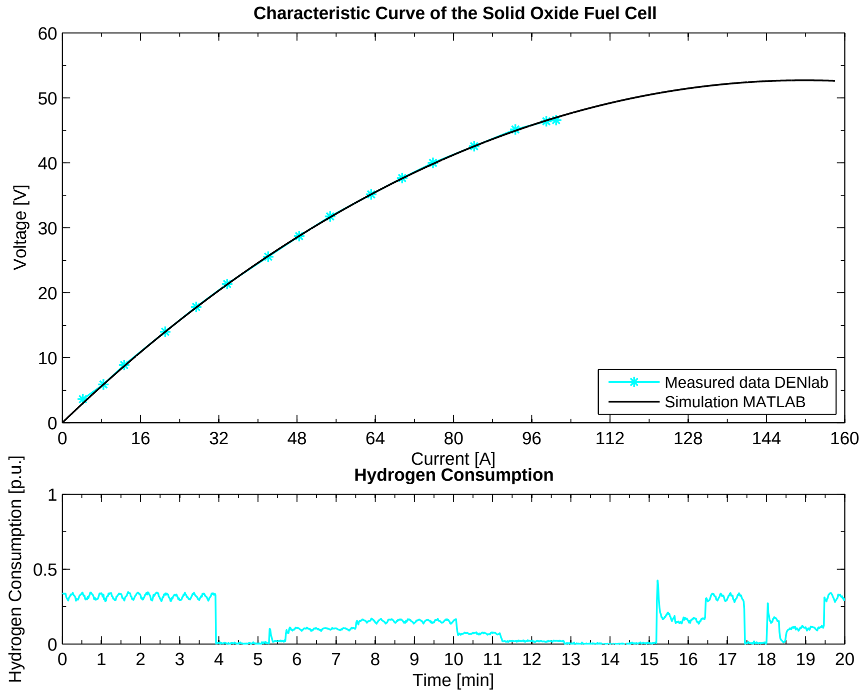

Figure 6.8: Response of the solid oxide fuel cell

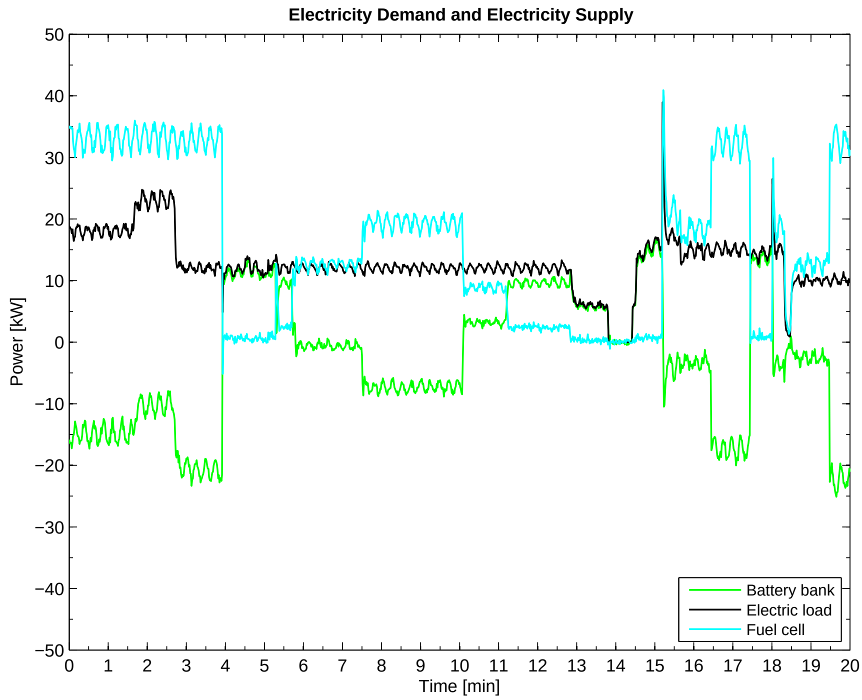

Figure 6.9: Electricity demand and electricity supply

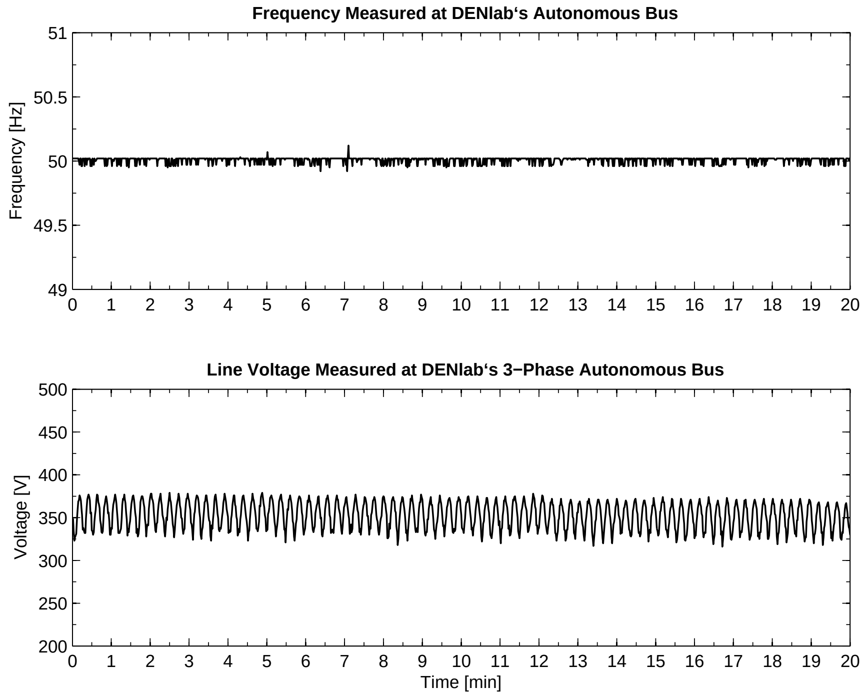

Figure 6.10: Response of the system's frequency and voltage

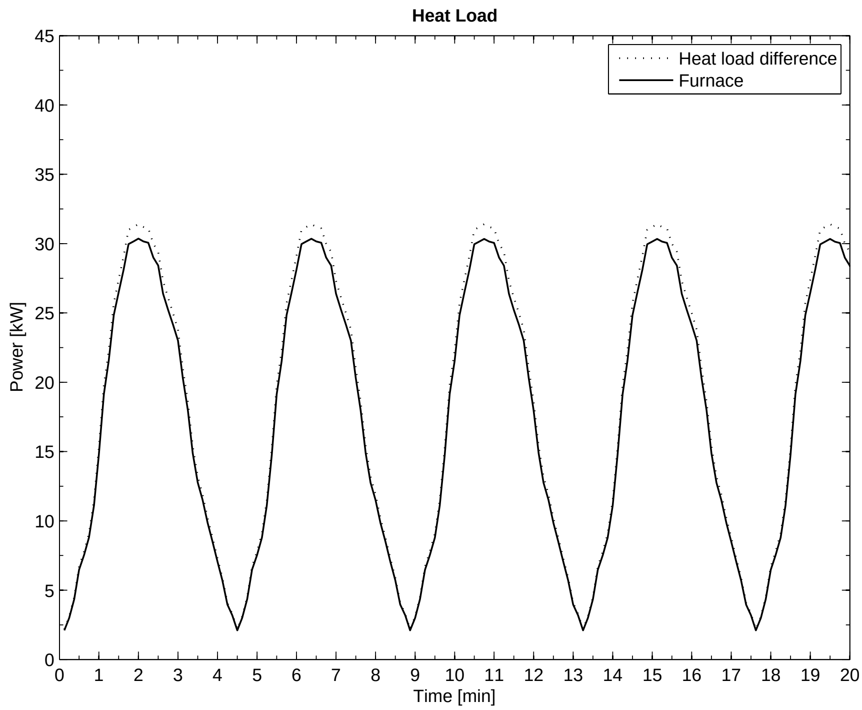

Figure 6.11: Response of the furnace

The following performance criteria for the frequency is considered: the frequency should be kept between 49 and 51 Hz during at least 95% of the time and it should not be less than 42,5 Hz or higher than 57,5 Hz [125]. The voltage and frequency are measured at DENlab's autonomous bus. Converter-set B (battery bank 2) acts as the *master* of the system, thus it operates in a voltage source control mode, whereas converter-sets B and F operate in PQ control mode. These terms were introduced in Section 1.3.4.

The fuel cell model represents a solid oxide fuel cell of 46,5 kW. The model is based on [126]. The fuel cell is assigned to the electricity control subsystem. The main control defines the power that has to be supplied by the fuel cell and sends a current set-point to converter-set F. A delay transfer function is used to make the fuel cell's operation smoother. This transfer function acts as the fuel cell's unit control.

The fuel cell was modeled both in DENlab and MATLAB. A test was made to compare the results of both models. Figure 6.8 shows the current-voltage characteristic curve. As it can be observed, the results are satisfactory. The second figure shows the hydrogen consumption for a period of 20 minutes.

The battery system consists of two battery banks of 25 kW each. The total system's storage capacity is 100 kWh. Each battery bank contributes with half of the power required from the electricity storage. However, due to its unit control for being the master, one of the battery banks (assigned to converter-set B) provides extra compensation if required in order to keep the frequency and voltage stable. Both battery banks are considered as one single hub element and they are assigned to the electricity control subsystem.

In Figure 6.9 the outputs of the fuel cell and the battery system are shown. The battery system and the fuel cell complement each other to supply the load. By keeping the power balance, the system's voltage and frequency are kept within the operating limits. This can be observed in Figure 6.10. In this example the battery set-point was manually changed to observe the reaction of the fuel cell to the change.

In order to test the heat control subsystem it is assumed that the difference between the heat load and the heat supplied by the fuel cell has a sinusoidal shape. Therefore, the furnace (assigned to the heat control subsystem) must supply this difference. In Figure 6.11 the response of the furnace can be observed. The model of the furnace is based on the equations presented un Chapter 4. The main control sends the set-point of the natural gas flow to the furnace model. No unit control is applied in this case.

The following improvements have to be performed in a future study:

- A more detailed model of the heat exchangers is required in order to make a better analysis. At this point only the more representative capabilities of the multi-carrier EMS were tested.
- Renewable energy sources should be included as well as suitable forecasts.
- A more complex hub should be tested in which the motor-generator sets are also included.
- A longer simulation should be performed. For example, a whole week including the solar power input.

6.4 Conclusions

This chapter gives an overview of the design of a multi-carrier energy management system. In Section 6.2.1 the forecasting model used in this dissertation was described for the wind speed time series. Using a similar methodology, the load forecast can be improved as well. This can substitute the persistence load forecast models that are currently being used. In the proposed multi-carrier EMS, the optimization module is based on Chapter 2 and Chapter 5, while the real-time control module is based on Chapter 4.

As a result of the work performed in DENlab, it was possible to program and implement a simple multi-carrier EMS. Moreover, a set of guidelines were defined to introduce new students to the laboratory and to help them start working in new projects without interfering with earlier projects, a separate manual was developed for this. Nevertheless, further work is required in order to attain a proper evaluation and to be able to test more complex configurations that also include renewable sources.

Chapter 7

The Outcome

Conclusions, Recommendations and Further Work

This dissertation provides insights and techniques that can be applied for the optimization of systems with multiple energy carriers. The topics that were presented include the multi-carrier unit commitment framework, the multi-carrier exergy hub approach, a hierarchical multi-carrier control architecture, a comparison of multi-carrier power applications and the implementation of a multi-carrier energy management system in a real infrastructure. Section 7.1 contains the main conclusions of this dissertation, Section 7.2 presents the recommendations for further research and Section 7.3 briefly describes a research project that has been started as a follow-up of this dissertation.

7.1 Conclusions

Multi-Carrier Unit Commitment Framework

Several recent studies analyze the active participation of mini and micro combined heat and power units, but they mostly focus on the electricity outputs of these units and overlook the influence of the heat outputs that are also present. Making this assumption is simplistic and may result in erroneous expectations. For example, a configuration might appear to be adequate to supply a certain electric load, but might produce a heat overload if no heat is required in the system. This kind of mistakes can be avoided by using a general *multi-carrier unit commitment* framework like the one presented in Chapter 2. The framework provides enough flexibility to simulate the various scenarios that were presented in this dissertation, however it can be easily adapted for other power scales and energy carriers.

The inclusion of storage for the balancing of power has traditionally been considered as an independent procedure to be performed only after the unit commitment solution is known, in other words, the unit commitment solution is firstly obtained and the storage is applied afterwards. In this dissertation the inclusion of storage was taken into account during the calculation of the multi-carrier unit commitment solution as part of a four-step technique. By using this technique the multi-carrier unit commitment solution can be influenced by taking the storage availability into account. The technique demonstrated to be valuable for peak-shaving purposes at the generation side as shown in the example of Chapter 2.

Multi-Carrier Exergy Hub Approach

It is valid to say that, since exergy is the maximum theoretical work potential that can be obtained from an energy flow, by choosing the most exergetically efficient configuration we are making the best use of the work potential of the energy source. However, the existing generation systems were not designed to make the best use of the work potential of the sources. Thus, in order to do so, it would be necessary to re-evaluate the existing equipment/machinery and re-design generation units in general. The objectives of this dissertation did not focus on designing or improving individual components, but on optimizing the interaction among several of them. Therefore, the exergy hub approach was introduced in Chapter 3 as an optimization tool for systems with multiple energy carriers. In the exergy hub approach, exergy efficiencies (instead of energy efficiencies) were taken into account for the optimization of systems that contain multiple energy carriers.

Different objective functions were evaluated to show that there is an intrinsic difference between defining the most efficient system from an exergetic point of view and the most efficient system from an energetic point of view. Moreover, an economic optimization does not necessarily correspond to the results of the other two optimization objectives; thus a compromise should be made in order to attain the optimal system.

The tool presented provides flexibility to easily compare different configurations. The maximum exergetic efficiency can be obtained as a result of the optimization. One of the strengths of this tool is that it can perform complex and long-term calculations that would be extremely tedious when done by hand. In the example presented in Chapter 3 it was possible to observe that the scheduling of the generation units was affected by the output temperature. Moreover, the optimal configuration that resulted from maximizing the exergetic efficiency of the system differed from the optimal configuration that resulted from maximizing the energetic efficiency.

Hierarchical Multi-Carrier Control Architecture

Traditional control techniques are no longer suitable to account for the interactions introduced by combined generation units and renewable sources. In Chapter 4 a general hierarchical control architecture was presented for systems with multiple energy carriers. In the chapter, the dynamic behavior of the generation units was considered, thus dynamic models were used for the simulations. The results show that the multi-carrier hierarchical control architecture is capable of dealing with perturbations and load changes in the system. The main control parameters were kept within the defined boundary conditions throughout the simulations.

Comparison of Multi-Carrier Power Applications

The main conclusions of Chapter 5 are enumerated below:

- Not every CHP technology is capable of providing substantial benefits to a district in terms of energy supply. For the load patterns that were analyzed, the solid oxide fuel cell provided the best results due to the electricity-to-heat ratio of the load patterns used in the analysis.

- The use of an aggregator proved to be an effective way to reduce the power exchange with the grid. By using an aggregator the need for further investments to expand the electricity supply infrastructure can be reduced.

- By using storage the unit commitment can be influenced. In this case an example of a cluster of 3 houses was selected for illustrative purposes. If the benefit of having electricity storage is similar to the benefit of having heat storage, it is advisable to opt for heat storage since it is a more sustainable technology, especially when a large amount of heat is produced by the micro-CHP units.

- When a low capacity of renewable sources is installed, like in Simulation 4, their influence in the overall results at the collaborative scenario is limited. If the use of batteries does not significantly change the results, it is recommended to avoid their installation. Batteries are disposable and their installation should only be performed in cases where a significant benefit can be attained.

- Regarding electric vehicles, policy makers should focus their effort on enabling the use of local aggregators. This not only reduces the costs and the consumption of sources but allows a better way to control possible power peaks. The application of differentiated tariffs creates the risk of having all electric vehicles being plugged at the same time, which demands a high power capacity of the energy supply infrastructure.

Multi-Carrier Energy Management System

Chapter 6 provided a global overview of the design of a multi-carrier energy management system and presented a brief description of its parts. Additionally, a partial implementation in the renewable energy laboratory DENlab was performed and guidelines were defined for the future usage of the laboratory, however more tests have to be done to evaluate the robustness of the multi-carrier energy management system that was implemented. This kind of physical installations are very valuable to understand how such a system works and what limitations are likely to be found during the implementation.

7.2 Recommendations for Further Research

Multi-Carrier Unit Commitment Framework

The research presented in this dissertation was focused on the optimization of existing systems with the help of the multi-carrier unit commitment framework. Investment costs were not part of the study because they are important only when choosing a technology at the beginning and not during the optimization of an existing system. The combination of renewable sources, electric vehicles and the way to exchange power between houses is independent of the investment costs. Nevertheless, during the planning stage of an energy system it would be interesting to make a comparison among technologies in which the savings attained by using an optimization tool and/or the intervention of an aggregator can be subtracted from the investment costs. In this way a better decision can be made with respect to the technology to be selected for a certain household or district. Therefore, such an optimization tool can be used to support the planning stage of an energy system.

Multi-Carrier Exergy Hub Approach

The topic of exergy was studied in this thesis, however only one chapter was dedicated to it. This means that still more research can be done particularly to study systems in which the energy sources have a low exergy content like for example heat obtained from a solar thermal system. In this thesis only sources with high exergy content like natural gas, biomass and electricity were evaluated. During the last phase of this PhD project various discussions were carried out with Sabine Jansen from the Architecture Faculty; she researches how to apply exergy studies to improve building design. From the discussions, the following topics were defined as possible research topics to be carried out with the optimization tool in the future:

- Include solar energy: Determine if it is exergetically better to use solar panels or solar collectors under different building scenarios. For example, define the optimal percentage of solar panels and solar collectors that can be placed on a roof given the constraint of the area available for their installation.

- Include storage: Investigate whether the optimization can provide insight on how to further reduce the required input of exergy through the application of storage.

- Include low-exergy sources: Evaluate the optimization results using a combination of sources with low exergy content like geothermal energy and solar collector systems.

Hierarchical Multi-Carrier Control Architecture

The hierarchical multi-carrier control architecture that was presented in Chapter 4 was tested in an off-grid energy system configuration. In order to test the architecture even further the following possibilities are proposed:

- Test the control architecture in a system that is connected to the grid to allow back and forward electricity flows.

- Test the control architecture in a system containing more energy carriers, both at the input side and at the output side of the energy hub.
- Evaluate the control interactions in a system with more that two control subsystems, for example with an electrical control subsystem, a heat control subsystem and a cold control subsystem.

Comparison of Multi-Carrier Power Applications

More simulations can be done in order to make a deeper analysis of the possibilities provided by the optimization tool. For example,

- Make a sensitivity analysis related to the penetration of renewables in which the number of panels per household is different.
- Incorporate the buffer possibilities of including electric vehicles.
- Make longer simulations, for example, for a year, in order to observe the effect of considering longer periods of time, especially in terms of storage utilization.

Multi-Carrier Energy Management System

Further tests need to be performed at DENlab. It is recommended that all the students to be involved in the laboratory follow the guidelines that were defined as part of this PhD project so that their work will not interfere with earlier implemented projects. Regarding the forecasting models, the load forecast can be improved using a similar methodology to the one presented for the wind speed forecast model. In this way a better forecast can be obtained.

7.3 Further Work

Research Project

A research project was started at the beginning of 2012 in which the algorithms and techniques developed during this PhD project are applied at a real office building located in The Hague. The project is being performed by two MSc students of the Power Systems Group of Delft University of Technology with the supervision of the author of this thesis. The results of the project will be published at the end of 2013. The reader is encouraged to contact the author of this thesis for more information of the project.

DENlab

Two students recently started their MSc projects at DENlab. They will continue performing tests related to the implementation of the multi-carrier energy management system described in Chapter 6 in DENlab with the direct supervision of the author of this thesis.

Appendix A

Assumptions and Considerations

- The optimization is solved with a *mixed-integer nonlinear solver* due to the 'on' and 'off' states of the units.

- The BARON solver (Branch-And-Reduce Optimization Navigator) was used to solve the mixed-integer nonlinear problem of the multi-carrier unit commitment. BARON is a global optimization (GO) solver: it is a computational system for solving non-convex optimization problems to global optimality [44]. The solver can solve purely continuous, purely integer, and mixed-integer nonlinear problems, it can also be used to find the k-best solutions.

- The results of the optimization were corroborated using MATLAB 'fmincon' function. Different unit combinations were tested and the results coincided with those obtained by AIMMS. The function 'fmincon' attempts to find a constrained minimum of a scalar function of several variables starting at an initial estimate. This kind of optimization is commonly known as *constrained nonlinear optimization* or *nonlinear programming*.

- The results of the optimal dispatch in Chapter 3 were corroborated with the hand calculations made by exergy researcher Sabine Jansen and the results coincided.

- The algorithms used for the simulations proved to be satisfactory for 250 households or less, which is a quantity of households that can be connected to a distribution transformer.

- A proof of scalability is outside the scope of this research.

- It is recommended to do further research in order to evaluate the performance of the algorithms, especially if larger systems are considered. The objective of this thesis was not to find the algorithm with the best performance, but to evaluate the benefits that could be obtained from a multi-carrier unit commitment optimization and the operation of an aggregator.

- In this work the 4 best solutions were saved at each of the periods of the multi-carrier unit commitment problem. Tests were made in which 6 an 8 solutions were saved, however the results did not improve by increasing the number of saved solutions in the cases that were analyzed.
- A difference is considered *significant* if more than 10% is achieved in relation to the reference case.
- The following performance criteria are considered in the simulations: the frequency should be kept between 49 and 51 Hz during at least 95% of the time and it should not be less than 42,5 Hz or higher than 57,5 Hz [125]. The temperature of the hot line should not be lower than 95 °C and the room temperature should remain between 19 and 21 °C.
- Some of the data that were used for the simulations are classified as confidential. For this reason not all data that are required for the simulations are disclosed, however the reader can contact the author if there is further interest to obtain information about these data.

Appendix B

Complementary Simulation Results

This appendix includes simulation results obtained for the example presented in Section 4.5.3.

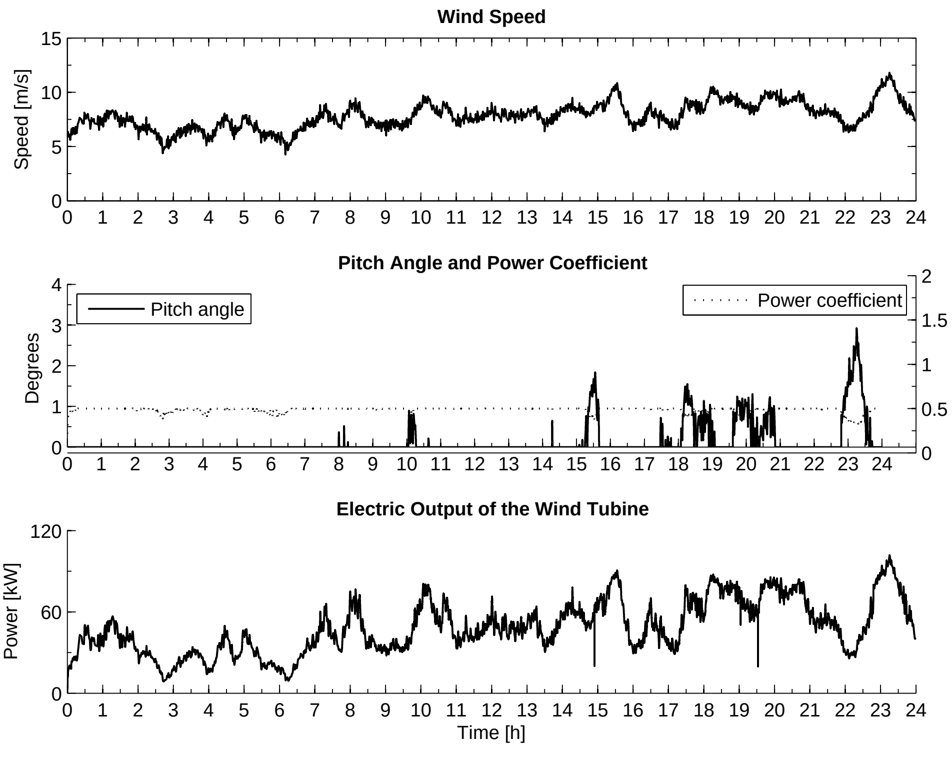

Figure B.1: Simulation 3: Response of the wind turbine

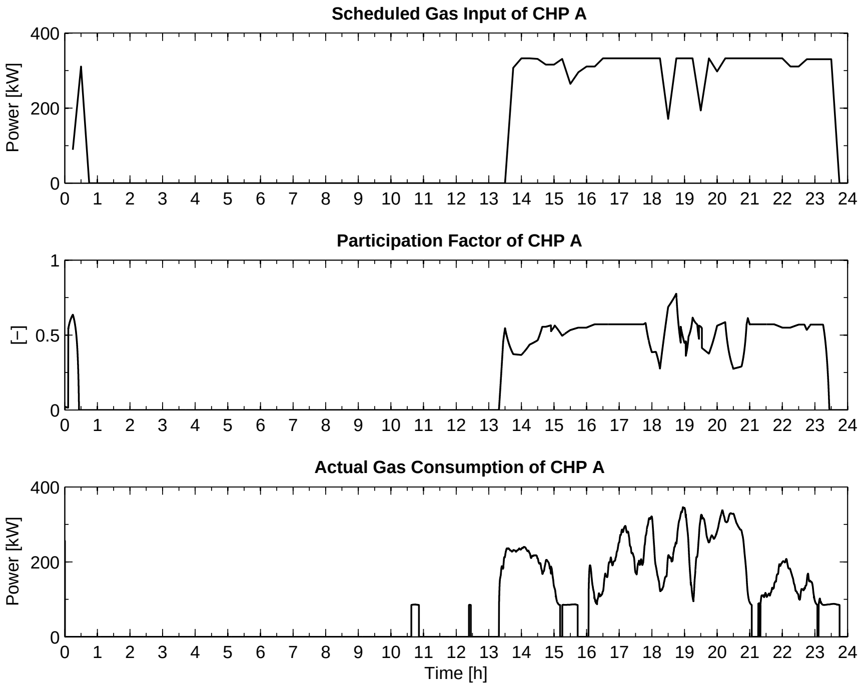

Figure B.2: Simulation 3: Response of CHP A

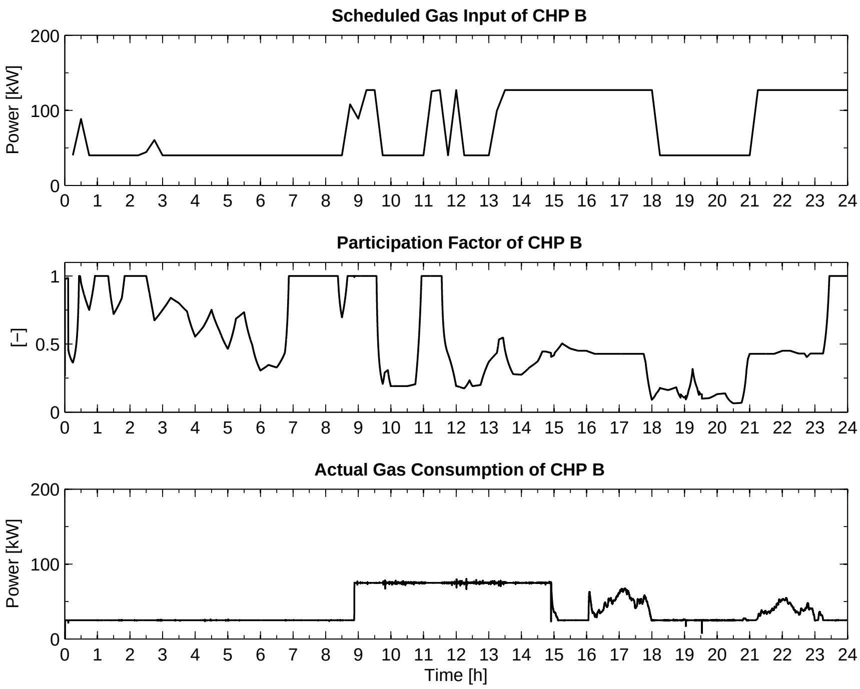

Figure B.3: Simulation 3: Response of CHP B

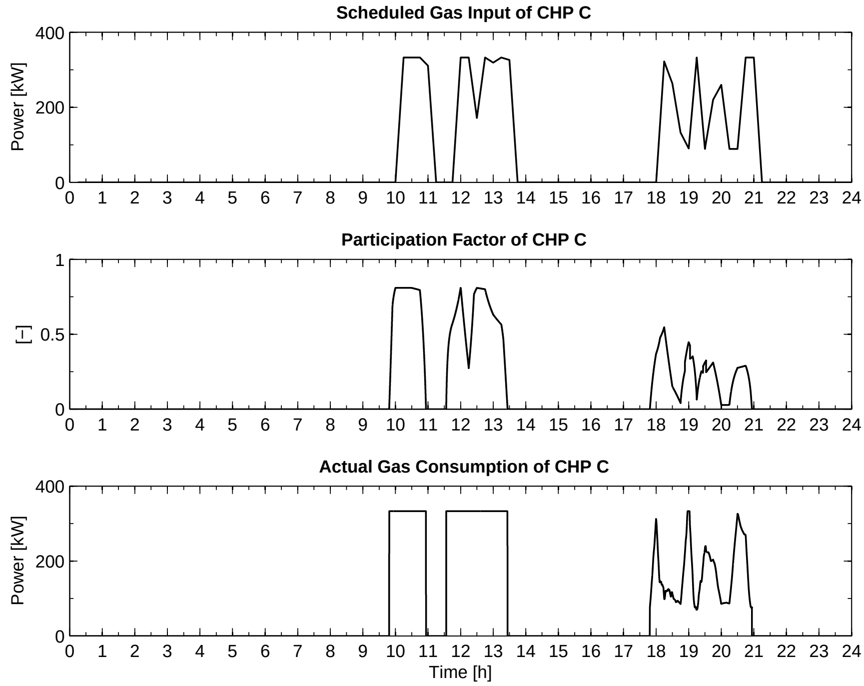

Figure B.4: Simulation 3: Response of CHP C

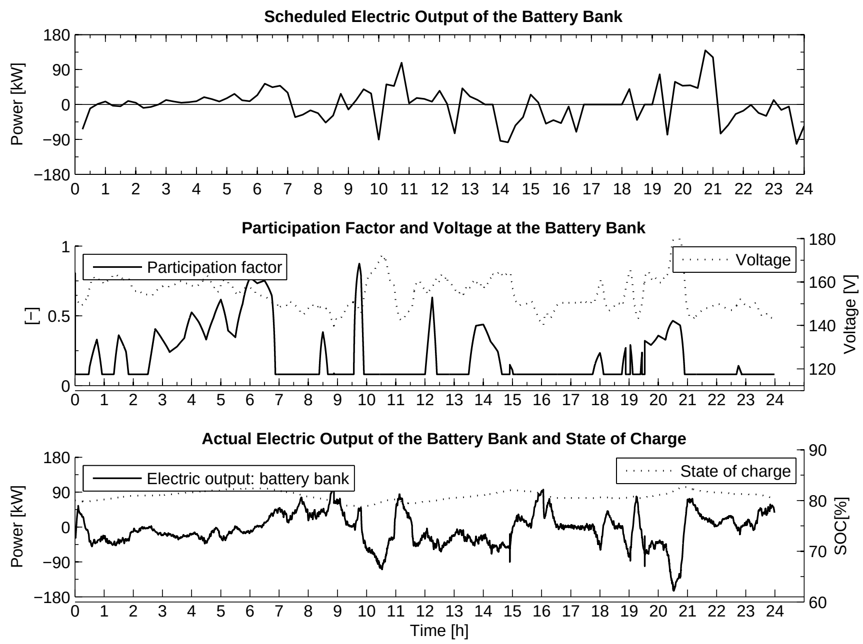

Figure B.5: Simulation 3: Response of the battery bank

Bibliography

[1] L. M. Ramirez-Elizondo and G. C. Paap, "Unit commitment in multiple energy carrier systems," in *Proceedings of the North American Power Symposium (NAPS)*, 2009.

[2] L. M. Ramirez-Elizondo, A. Lojowska, and G. C.Paap, "Design of an energy management system to be implemented at denlab," in *Proceedings of the 6th International Conference Electrical & Power Engineering, Iasi, Romania*, 2010.

[3] L. M. Ramirez-Elizondo, "The increasing importance of small and medium scale renewable energy systems," *Maxwel: Magazine of the Electrotechnische Vereeniging TU Delft*, vol. 12.4, pp. 14–17, 2009.

[4] M. Reza, P. Schavemaker, W. Kling, and L. van der Sluis, "A research program on intelligent power systems: self controlling and self-adapting power systems equipped to deal with the structural changes in the generation and the way of consumption," in *CIRED*, 2003.

[5] The World Alliance for Decentralized Energy, http://www.localpower.org/.

[6] International Energy Agency, *Key World Energy Statistics 2011*, 2011.

[7] European Comission, *Energy 2020: A strategy for competitive, sustainable, and secure energy*, 2011.

[8] European Comission, *Energy Issues: Fieldwork: March - April 2006*, 2006.

[9] International Energy Agency, *Contribution of Renewables to Energy Security*, 2007.

[10] World Alliance for Decentralized Energy, *Security via Decentralized Energy*, 2005.

[11] International Energy Agency, *Energy Security and Climate Policy Assessing Interactions*, 2007.

[12] International Energy Agency, *World Energy Outlook 2006*, 2006.

[13] Intergovernmental Panel on Climate Change, *Mitigation*, 2001.

[14] World Alliance for Decentralized Energy, *Building Integrated Cooling, Heat & Power For Cost-Effective Carbon Mitigation*, 2005.

[15] P. Schavemaker and L. van der Sluis, *Electrical Power System Essentials*. Wiley & Sons, 2008.

[16] J. Grainger and W. Stevenson, *Power System Analysis*. McGraw-Hill, 1994.

[17] P. Kundur, *Power System Stability and Control*. McGraw-Hill Professional, 1994.

[18] International Energy Agency, *Cogeneration and Renewables*, 2011.

[19] International Energy Agency, *Combined Heat and Power: Evaluating the Benefits of Greater Global Investment*, 2008.

[20] International Energy Agency, *Co-generation and District Energy: Sustainable Energy Technologies for Today and Tomorrow*, 2009.

[21] L. Haiyan and P. Valdimarsson, “District heating modelling and simulation,” in *Thirty-Fourth Workshop on Geothermal Reservoir Engineering*, (Stanford, USA), pp. –, Stanford University, 2009.

[22] International Energy Agency, *District Heating and Cooling: Environmental Technology for the 21st Century*, 2002.

[23] International Energy Agency, *Coming from the Cold: Improving District Heating Policy in Transition Economies*, 2004.

[24] G. Boyle, *Renewable Energy: Power for a Sustainable Future*. Oxford University Press, 2004.

[25] International Energy Agency, *Clean Energy Progress Report*, 2011.

[26] R. de Graaff, *Flexible distribution systems through the application of multi back-to-back converters: Concept, implementation and experimental verification*. PhD thesis, Technische Universiteit Eindhoven, 2010.

[27] J. Lopes, C. Moreira, and A. Madureira, “Defining control strategies for microgrids islanded operation,” *IEEE Transactions on Power Systems*, vol. 21, no. 2, pp. 916 – 924, 2006.

[28] IEEE, *Smart Grid Newsletter*, January 2011.

[29] S. Ruth, “Green it more than a three percent solution?,” *IEEE Internet Computing*, vol. 13, pp. 74 –78, july-aug. 2009.

[30] G. Arnold, “Challenges and opportunities in smart grid: A position article,” *Proceedings of the IEEE*, vol. 99, pp. 922 –927, june 2011.

[31] M. D. Ilic, “Dynamic monitoring and decision systems for enabling sustainable energy services,” *Proceedings of the IEEE*, vol. 99, pp. 58 –79, jan. 2011.

[32] S. Depuru, L. Wang, V. Devabhaktuni, and N. Gudi, “Smart meters for power grid: Challenges, issues, advantages and status,” in *Power Systems Conference and Exposition (PSCE)*, pp. 1 –7, March 2011.

[33] M. Geidl, *Integrated Modeling and Optimization of Multi-Carrier Energy Systems*. PhD thesis, Eidgenössische Technische Hochschule ETH Zürich, Nr. 17141, 2007.

[34] M. Geidl and G. Andersson, "Optimal power flow of multiple energy carriers," *IEEE Transactions on Power Systems*, vol. 22, pp. 145 –155, February 2007.

[35] M. Geidl and G. Andersson, "Optimal coupling of energy infrastructures," in *Power Tech, 2007 IEEE Lausanne*, pp. 1398–1403–, 2007.

[36] M. Geidl and G. Andersson, "A modeling and optimization approach for multiple energy carrier power flow," in *Power Tech, Proceedings of the 2005 IEEE, Russia*, pp. 1–7, 2005.

[37] M. Geidl, G. Koeppel, P. Favre-Perrod, B. Klockl, G. Andersson, and K. Frohlich, "Energy hubs for the future," *Power and Energy Magazine, IEEE*, vol. 5, no. 1, pp. 24–30, 2007.

[38] J. Athern, *The Exergy Method of Energy Systems Analysis*. New York: John Wiley & Sons, 1980.

[39] P. Sakulpipatsin, E. Boelman, and J. Cauberg, "Exergy analysis as an assessment tool of heat recovery of dwelling ventilation systems," *International Journal of Ventilation*, vol. 6, pp. 77–86, 2007.

[40] P. Sakulpipatsin, *Exergy efficient building design*. PhD thesis, Technische Universiteit Delft, 2008.

[41] E. Boelman, "Exergy needs for winter ventilation in buildings," *Sustainable Building Conference*, 2002.

[42] M. A. Rosen and I. Dincer, "Exergy as the confluence of energy, environment and sustainable development," *International Journal of Exergy*, vol. 1, no. 1, pp. 3 – 13, 2001.

[43] M. A. Rosen, "Clarifying thermodynamic efficiencies and losses via exergy," *Exergy, An International Journal*, vol. 2, no. 1, pp. 3–5, 2002.

[44] J. Bisshop, *AIMMS, Optimization Modeling*. Paragon Decision Technology: Haarlem, the Netherlands, 1999.

[45] L. M. Ramirez-Elizondo, V. Velez, and G. C. Paap, "A technique for unit commitment in multiple energy carrier systems with storage," in *Proceedings of the 9th International Conference on Environment and Electrical Engineering (EEEIC)*, 2010.

[46] A. J. Wood and B. F. Wollenberg, *Power generation, operation, and control*. New York: J. Wiley & Sons, 1996.

[47] Nordhausen am Harz Tarifinformation, accessed May 1, 2009, http://www.nordhausen.de//wirtschaft_bildung/st_strom_gas.php4.

[48] M. Hable, *Beitrag zur Energieeninsatzoptimierung mit evolutionaeren Algorithmen in lokalen Energiesystemen mit kombinierter Nutzung von Waerme- und Elektroenergie*. PhD thesis, Technische Universitaet Dresden, 2004.

[49] J. Uitzinger, *SEPATH Simulatie van EnergievraagPATronen van Huishoudens*. IVAM, Roetersstraat 33 - 1018 WB Amsterdam - Postbus 18180 - 1001 ZB Amsterdam, July 2003. project: P1999-019.

[50] L. M. Ramirez-Elizondo, G. C. Paap, R. Ammerlaan, R. Negenborn, and R. Toonssen, "On the energy, exergy and cost optimization of multi-energy-carrier power systems," *International Journal of Exergy*, vol. (accepted for publication), 2012.

[51] K. Blok, *Introduction to Energy Analysis*. Amsterdam: Techne Press, 2007.

[52] L. Connelly and C. P. Koshland, "Exergy and industrial ecology–part 1: An exergy-based definition of consumption and a thermodynamic interpretation of ecosystem evolution," *International Journal of Exergy*, vol. 1, no. 3, pp. 146 – 165, 2001.

[53] G. Tsatsaronis, "Definitions and nomenclature in exergy analysis and exergoeconomics," *Energy*, vol. 32, no. 4, pp. 249–253, 2007.

[54] M. A. Rosen, "The exergy of stratified thermal energy storages," *Solar Energy*, vol. 71, no. 3, pp. 173 – 185, 2001.

[55] M. A. Rosen, "Does industry embrace exergy?," *International Journal of Exergy*, vol. 2, no. 4, pp. 221 – 223, 2002.

[56] M. A. Rosen, "Exergy conservation: An alternative to conserving the already conserved quantity energy," *International Journal of Exergy*, vol. 2, no. 2, pp. 59 – 61, 2002.

[57] M. A. Rosen and D. S. Scott, "Entropy production and exergy destruction: Part i–hierarchy of earth's major constituencies," *International Journal of Hydrogen Energy*, vol. 28, no. 12, pp. 1307 – 1313, 2003.

[58] M. A. Rosen and D. S. Scott, "Entropy production and exergy destruction: Part ii–illustrative technologies," *International Journal of Hydrogen Energy*, vol. 28, no. 12, pp. 1315 – 1323, 2003.

[59] A. Baghernejad and M. Yaghoubi, "Exergy analysis of an integrated solar combined cycle system," *Renewable Energy*, vol. 35, no. 10, pp. 2157–2164, 2010.

[60] L. Ozgener, A. Hepbasli, and I. Dincer, "Energy and exergy analysis of geothermal district heating systems: An application," *Building and Environment*, vol. 40, no. 10, pp. 1309–1322, 2005.

[61] L. Ozgener, A. Hepbasli, and I. Dincer, "Exergy analysis of two geothermal district heating systems for building applications," *Energy Conversion and Management*, vol. 48, no. 4, pp. 1185–1192, 2007.

[62] N. Yildirim, M. Toksoy, and G. Gokcen, “Piping network design of geothermal district heating systems: Case study for a university campus,” *Energy*, vol. 35, no. 8, pp. 3256–3262, 2010.

[63] K. Pope, I. Dincer, and G. Naterer, “Energy and exergy efficiency comparison of horizontal and vertical axis wind turbines,” *Renewable Energy*, vol. 35, no. 9, pp. 2102–2113, 2010.

[64] A. D. Aazahin, I. Dincer, and M. A. Rosen, “Thermodynamic analysis of wind energy,” *International Journal of Energy Research*, vol. 30, no. 8, pp. 553–566, 2006.

[65] O. Ozgener and L. Ozgener, “Exergy and reliability analysis of wind turbine systems: A case study,” *Renewable and Sustainable Energy Reviews*, vol. 11, no. 8, pp. 1811–1826, 2007.

[66] L. Suganthi and A. A. Samuel, “Exergy based supply side energy management for sustainable energy development,” *Renewable Energy*, vol. 19, no. 1-2, pp. 285–290, 2000.

[67] T. Krause, F. Kienzle, S. Art, and G. Andersson, “Maximizing exergy efficiency in multi-carrier energy systems,” in *Power and Energy Society General Meeting, 2010 IEEE*, pp. 1 –8, 2010.

[68] C. T. Yucer and A. Hepbasli, “Thermodynamic analysis of a building using exergy analysis method,” *Energy and Buildings*, vol. 43, no. 2-3, pp. 536–542, 2011.

[69] A. Schlueter and F. Thesseling, “Building information model based energy/exergy performance assessment in early design stages,” *Automation in Construction*, vol. 18, no. 2, pp. 153–163, 2009.

[70] L. Tronchin and K. Fabbri, “Analysis of buildings’ energy consumption by means of exergy method,” *International Journal of Exergy*, vol. 5, no. 5-6, pp. 605–625, 2008.

[71] D. Schmidt, “Low exergy systems for high-performance buildings and communities,” *Energy and Buildings*, vol. 41, no. 3, pp. 331 – 336, 2009.

[72] C. Koroneos, T. Spachos, and N. Moussiopoulos, “Exergy analysis of renewable energy sources,” *Renewable Energy*, vol. 28, no. 2, pp. 295 – 310, 2003.

[73] O. Arslan and R. Kose, “Exergoeconomic optimization of integrated geothermal system in simav, kutahya,” *Energy Conversion and Management*, vol. 51, no. 4, pp. 663 – 676, 2010.

[74] L. Ozgener, A. Hepbasli, I. Dincer, and M. A. Rosen, “Exergoeconomic analysis of geothermal district heating systems: A case study,” *Applied Thermal Engineering*, vol. 27, no. 8-9, pp. 1303 – 1310, 2007.

[75] A. Hepbasli, “A review on energetic, exergetic and exergoeconomic aspects of geothermal district heating systems,” *Energy Conversion and Management*, vol. 51, no. 10, pp. 2041 – 2061, 2010.

[76] H. Caliskan and A. Hepbasli, "Energy and exergy prices of various energy sources along with their co2 equivalents," *Energy Policy*, vol. 38, no. 7, pp. 3468 – 3481, 2010.

[77] L. Connelly and C. P. Koshland, "Exergy and industrial ecology. part 2: A non-dimensional analysis of means to reduce resource depletion," *International Journal of Exergy*, vol. 1, no. 4, pp. 234 – 255, 2001.

[78] D. Castorph, M. Kollera, and P. Waas, "Brennwert und heizwert (the high and low heating values)," tech. rep., Fachhochschule Munchen, 1999.

[79] H. Baehr, "Die exergie der brennstoffe," *Brennstoff-Wärme-Kraft*, vol. 31, no. 7, pp. 292 – 297, 1979.

[80] R. Toonssen, *Sustainable Power from Biomass: Comparison of technologies for centralized or de-centralized fuel cell systems*. PhD thesis, Technische Universiteit Delft, 2010.

[81] Natural Gas.org. Accessed August 23, 2011, http://www.naturalgas.org/overview/uses_eletrical.asp.

[82] GE Jenbacher GmbH & Co OHG, *Jenbacher gas engines Technische Beschrijving JMS 312 GS-N.L*, 2010.

[83] Parkwood Boiler Works, Keighley, West Yorkshire BD21 4NW, UK, *Byworth Boilers, Hot water boilers brochure*.

[84] Biomass Energy Centre, accessed August 18, 2011, http://www.biomassenergycentre.org.uk/.

[85] V. Velez, L. M. Ramirez-Elizondo, and G. C. Paap, "Distributed energy management systems control strategy for multiple energy carriers," in *IEEE 16th International Conference on Intelligent Systems Aplications to Power Systems*, 2011.

[86] Y. Zilong, W. Chunsheng, L. Hua, and X. Honghua, "Design of energy management system in distributed power station," in *International Conference on Sustainable Power Generation and Supply*, 2009.

[87] F. Katiraei and M. R. Iravani, "Power management strategies for a microgrid with multiple distributed generation units," vol. 21, no. 4, pp. 1821–1831, 2006.

[88] M. S. Khan and M. R. Iravani, "Supervisory hybrid control of a micro grid system," *IEEE Electrical Power Conference*, pp. 20–24, 2007.

[89] E. Ortjohann, W. Sinsukthavorn, A. Mohd, M. Lingemann, N. Hamsic, and D. Morton, "A hierarchy control strategy of distributed generation systems," in *International Conference on Clean Electrical Power*, pp. 310–315, 2009.

[90] V. Velez, "Design of a control strategy for optimal operation of an autonomous distributed generation system for electricity and heat," Master's thesis, Delft University of Technology, 2010.

[91] A. Nordmann, “Wind turbine illustration.” Wikipedia Commons.

[92] C. Wang, *Modeling and control of hybrid wind/photovoltaic/fuel cell distributed generation systems*. PhD thesis, Montana State University, 2006.

[93] E. Uso, “Energy storage in small-scale power systems,” tech. rep., Delft University of Technology, 2007.

[94] D. Linden and T. Reddy, *Handbook of batteries*. McGraw-Hill, 2002.

[95] I. Buchmann, *Battery University*. Richmond: Cadex Electronics Inc., 2007.

[96] Y. Zhu and K. Tomsovic, “Development of models for analyzing the load-following performance of microturbines and fuel cells,” *Electric Power Systems Research*, vol. 62, no. 1, pp. 1 – 11, 2002.

[97] W. I. Rowen, “Simplified mathematical representations of heavy-duty gas turbines,” *Journal of Engineering for Power*, vol. 105, no. 4, pp. 865–869, 1983.

[98] G. Ellis, *Control System Design Guide: Using Your Computer to Understand and Diagnose Feedback Controllers*. Elsevier Science Inc., 2003.

[99] L. Xianguo, *Principles of Fuel Cells*. Taylor & Francis: New York, 2006.

[100] E. Carlson, Z. R., S. Sriramulu, K. Roth, and J. Brodrick, “Using phosphoric-acid fuel cells for distributed generation,” *ASHRAE*, vol. 49 (1), 2007.

[101] A. Block, *Heat Transfer in Steam Boiler Furnaces*. Leningrad, USSR: Hemisphere Publishing Corporation, 1988.

[102] G. Koeppel, “Distributed generation literature review and outline of the swiss situation,” tech. rep., November 2003.

[103] M. Houwing, *Smart Heat and Power, Utilizing the Flexibility of Micro Cogeneration*. PhD thesis, Technische Universiteit Delft, March 2010.

[104] P. Andersen, B. Poulsen, M. Decker, C. Traeholt, and J. Ostergaard, “Evaluation of a generic virtual power plant framework using service oriented architecture,” in *IEEE 2nd International Power and Energy Conference*, pp. 1212 –1217, 2008.

[105] A. Dimeas and N. Hatziargyriou, “Agent based control of virtual power plants,” in *International Conference on Intelligent Systems Applications to Power Systems*, pp. 1 –6, 2007.

[106] S. You, C. Traeholt, and B. Poulsen, “A market-based virtual power plant,” in *International Conference on Clean Electrical Power*, pp. 460 –465, 2009.

[107] E. Mashhour and S. Moghaddas-Tafreshi, “Bidding strategy of virtual power plant for participating in energy and spinning reserve markets, part i: Problem formulation,” *IEEE Transactions on Power Systems*, vol. 26, no. 2, pp. 949 –956, 2011.

[108] E. Mashhour and S. Moghaddas-Tafreshi, “Bidding strategy of virtual power plant for participating in energy and spinning reserve markets, part ii: Numerical analysis,” *IEEE Transactions on Power Systems*, vol. 26, no. 2, pp. 957 –964, 2011.

[109] E. Mashhour and S. Moghaddas-Tafreshi, “A review on operation of micro grids and virtual power plants in the power markets,” in *2nd International Conference on Adaptive Science Technology*, pp. 273 –277, 2009.

[110] C. Schulz, G. Roder, and M. Kurrat, “Virtual power plants with combined heat and power micro-units,” in *International Conference on Future Power Systems*, pp. 5 pp. –5, 2005.

[111] B. Roossien, M. Hommelberg, C. Warmer, K. Kok, and J.-W. Turkstra, “Virtual power plant field experiment using 10 micro-chp units at consumer premises,” in *CIRED Seminar on Smart Grids for Distribution*, pp. 1 –4, June 2008.

[112] E. Bakari and W. Kling, “Development and operation of virtual power plant system,” *Proceedings of the 2011 IEEE PES Innovative Smart Grid Technologies Conference Europe (ISGT Europe)*, 2011.

[113] F. Adamek, *Demand Response and Energy Storage for a Cost Optimal Residential Energy Supply with Renewable Generation*. PhD thesis, ETH Zurich, 2011.

[114] Bluegen, http://www.bluegen.info/.

[115] A. Lojowska, D. Kurowicka, G. Papaefthymiou, and L. van der Sluis, “Stochastic modeling of power demand due to evs using copula,” 2012.

[116] L. M. Ramirez-Elizondo, A. Lojowska, V. Velez, and G. C. Paap, “Design of a small-scale energy management system to be implemented in denlab,” *Bul. Inst. Polit. Iasi, t. LVII (LXI), f. 4*, 2011.

[117] Nedap Energy Systems, http://powerrouter.com/, *Remote Monitoring and Management*, 2011.

[118] Plugwise, http://www.plugwise.com/nl/idplugtype-f/.

[119] Energy Guardian, http://www.energy-guardian.com/.

[120] PowerMatcher, http://www.powermatcher.net/.

[121] N. D. Hatziargyriou, A. Dimeas, A. G. Tsikalakis, J. A. P. Lopes, G. Karniotakis, and J. Oyarzabal, “Management of microgrids in market environment,” in *International Conference on Future Power Systems*, 2005.

[122] A. Lojowska, D. Kurowicka, G. Papaefthymiou, and L. van der Sluis, “Advantages of arma-garch wind speed time series modeling,” in *IEEE 11th International Conference on Probabilistic Methods Applied to Power Systems (PMAPS)*, 2010.

[123] A. M. van Voorden, G. C. Paap, and L. van der Sluis, “Set-up of a renewable energy laboratory,” in *IEEE Young Researchers Symposium*, 2002.

[124] B. Valladares, “Development of an autonomous distributed energy management system for a diverse energy sources,” *Delft University of Technology, The Netherlands*, 2012.

[125] M. Bollen, J. Zhong, O. Samuelsson, J. Bjornstedt, and L. Striab, “Performance indicators for microgrids during grid-connected and island operation,” in *PowerTech*, 2009.

[126] C. Wang and M. H. Nehrir, “A physically based dynamic model for solid oxide fuel cells,” *IEEE Transaction on energy conversion*, 2007.

List of Publications

L. M. Ramirez-Elizondo et al. *On the Energy, Exergy and Cost Optimization of Multi-Energy-Carrier Power Systems*, International Journal of Exergy. *Journal paper accepted for publication.*

F. S. Melo, A. Sardinha, S. Witwicki, L. M. Ramirez-Elizondo and M. Spaan, *'Decentralized Multiagent Planning for Balance Control in Smart Grids'*, Procs. of the 1st Int'l Workshop on Information Technology for Energy Applications (IT4ENERGY'2012), Lisbon, Portugal, Sep. 6-7th, 2012, Vol. 923 of CEUR Workshop Proceedings, ISSN 1613-0073, online CEUR-WS.org/Vol-923.

B. Asare-Bediako, L. M. Ramirez-Elizondo, P. F. Ribeiro, W. L. Kling, G. C. Paap, *'Analysis and Development of Electricity and Heat Load Profiles for Intelligent Energy Management Systems'*, UPEC 2011.

L. M. Ramirez-Elizondo, A. Lojowska, V. Velez, and G. C. Paap, *'Design of a small-scale energy management system to be implemented in denlab'*, Bulletin of the Inst. Polit. Iasi, t. LVII (LXI), f. 4, 2011.

V. Velez, L. M. Ramirez-Elizondo, and G. C. Paap, *'Distributed energy management systems control strategy for multiple energy carriers'*, in IEEE 16th International Conference on Intelligent Systems Aplications to Power Systems, 2011.

L. M. Ramirez-Elizondo, V. Velez, and G. C. Paap, *'A technique for unit commitment in multiple energy carrier systems with storage'*, in Proceedings of the 9th International Conference on Environment and Electrical Engineering (EEEIC) 2010, pp. 106 109, 16-19 2010.

L. M. Ramirez-Elizondo, A. Lojowska, and G.C. Paap, *'Design of an energy management system to be implemented at DENlab'*, in Proceedings of the 6th International Conference Electrical & Power Engineering, Iasi, Romania, 2010.

L. M. Ramirez-Elizondo, *'The increasing importance of small and medium scale renewable energy systems'*, Maxwel: Magazine of the Electrotechnische Vereeniging TU Delft, vol. 12.4, pp. 1417, 2009.

L. M. Ramirez-Elizondo and G. C. Paap, *‘Unit commitment in multiple energy carrier systems,’* in Proceedings of the North American Power Symposium (NAPS), 2009, pp. 16, 4-6 2009.

L. M. Ramirez-Elizondo, G. C. Paap, Nico Woudstra, *‘The Application of a Fuel Cell Electrolyzer Arrangement as a Power Balancing Set-Up in Autonomous Renewable Energy Systems’*, Proceedings of the 40th IEEE North American Power Symposium, Calgary, Canada, September 28-30, 2008. *(Best paper award)*

L. M. Ramirez Elizondo, G. C. Paap, *‘De Elektriciteitsvoorziening van een Autonoom Systeem d.m.v. een Brandstofcel’*, Poster, Symposium Vermogensconversie IOP-EMVT, April 9, 2008, Arnhem, The Netherlands.

L. M. Ramirez Elizondo, G. C. Paap, *‘Dynamic Modeling and Control of a PEMFC- Supercapacitor Autonomous Power System’*, Proceedings of the 4th IEEE Benelux Young Researchers Symposium in Electrical Power Engineering, February 7-8, 2008 Eindhoven, The Netherlands.

L. M. Ramirez Elizondo, G. C. Paap, *‘Control Strategy for a PEMFC-Supercapacitor Autonomous Power System’*, Proceedings of the Second European Fuel Cell Technology and Applications Conference EFC2007, December 11-14, 2007, Rome, Italy.

Curriculum Vitae

Laura M. Ramírez Elizondo was born in San José, Costa Rica. In 2003, she received her bachelor's degree in Electrical Engineering at the Universidad de Costa Rica. Additionally, on August 2005 she obtained a bachelor's degree in Music with a major in piano at the same institution. She graduated with honors from her M.Sc. studies in Electrical Power Systems at Delft University of Technology in 2007. Laura worked on her PhD project from September 2007 to December 2011. Since January 2012 she has been working as part-time researcher at the Electrical Sustainable Energy Department of Delft University of Technology and as part-time researcher and lecturer at the Amsterdam University of Applied Sciences. Her topics of interest include sustainable development, system integration, music, arts, ashtanga yoga and nutrition.

Recognitions

2008 Best student paper award at the 2008 IEEE North American Power Symposium, Calgary, Canada

2007 Cum Laude graduate (graduated with honours), MSc degree in Electrical Power Systems with a minor in Sustainable Development, Delft University of Technology, the Netherlands

2005 Awarded with a Nuffic (Netherlands Fellowship Program) scholarship to perform MSc studies in the Netherlands

1997 Bronze medal at the National Mathematics Olympics for high school students, Costa Rica

1996 Latin American youth representative at the Young General Assembly, organized for the 50th Anniversary of the United Nations, United Nations Office at Geneva, Switzerland

1995 Costa Rican youth representative at the Young General Assembly, organized for the 50th Anniversary of the United Nations, San Francisco, California, the United States of America

1993 Gold medal at the National Mathematics Olympics for primary school students, Costa Rica